frontiers | Research Topics

“Forentomics”: forest pest and pathogen biology, ecology, and management using omics

Edited by
Amit Roy, Amrita Chakraborty and Quan Lu

Published in
Frontiers in Forests and Global Change

ISSN 1664-8714
ISBN 978-2-8325-6136-2
DOI 10.3389/978-2-8325-6136-2

About Frontiers

Frontiers is more than just an open access publisher of scholarly articles: it is a pioneering approach to the world of academia, radically improving the way scholarly research is managed. The grand vision of Frontiers is a world where all people have an equal opportunity to seek, share and generate knowledge. Frontiers provides immediate and permanent online open access to all its publications, but this alone is not enough to realize our grand goals.

Frontiers journal series

The Frontiers journal series is a multi-tier and interdisciplinary set of open-access, online journals, promising a paradigm shift from the current review, selection and dissemination processes in academic publishing. All Frontiers journals are driven by researchers for researchers; therefore, they constitute a service to the scholarly community. At the same time, the *Frontiers journal series* operates on a revolutionary invention, the tiered publishing system, initially addressing specific communities of scholars, and gradually climbing up to broader public understanding, thus serving the interests of the lay society, too.

Dedication to quality

Each Frontiers article is a landmark of the highest quality, thanks to genuinely collaborative interactions between authors and review editors, who include some of the world's best academicians. Research must be certified by peers before entering a stream of knowledge that may eventually reach the public - and shape society; therefore, Frontiers only applies the most rigorous and unbiased reviews. Frontiers revolutionizes research publishing by freely delivering the most outstanding research, evaluated with no bias from both the academic and social point of view. By applying the most advanced information technologies, Frontiers is catapulting scholarly publishing into a new generation.

What are Frontiers Research Topics?

Frontiers Research Topics are very popular trademarks of the *Frontiers journals series*: they are collections of at least ten articles, all centered on a particular subject. With their unique mix of varied contributions from Original Research to Review Articles, Frontiers Research Topics unify the most influential researchers, the latest key findings and historical advances in a hot research area.

Find out more on how to host your own Frontiers Research Topic or contribute to one as an author by contacting the Frontiers editorial office: frontiersin.org/about/contact

“Forentomics”: forest pest and pathogen biology, ecology, and management using omics

Topic editors

Amit Roy — Czech University of Life Sciences Prague, Czechia

Amrita Chakraborty — Czech University of Life Sciences Prague, Czechia

Quan Lu — Chinese Academy of Forestry, China

Citation

Roy, A., Chakraborty, A., Lu, Q., eds. (2025). *“Forentomics”: forest pest and pathogen biology, ecology, and management using omics*. Lausanne: Frontiers Media SA. doi: 10.3389/978-2-8325-6136-2

Table of contents

frontiers | Frontiers in Forests and Global Change

TYPE Editorial
PUBLISHED 04 March 2025
DOI 10.3389/ffgc.2025.1573774

OPEN ACCESS

EDITED AND REVIEWED BY
Pierluigi Bonello,
The Ohio State University, United States

*CORRESPONDENCE
Amit Roy
roy@fld.czu.cz

RECEIVED 09 February 2025
ACCEPTED 17 February 2025
PUBLISHED 04 March 2025

CITATION
Roy A, Chakraborty A and Lu Q (2025) Editorial: "Forentomics": forest pest and pathogen biology, ecology, and management using omics.
Front. For. Glob. Change 8:1573774.
doi: 10.3389/ffgc.2025.1573774

Editorial: "Forentomics": forest pest and pathogen biology, ecology, and management using omics

Amit Roy[1]*, Amrita Chakraborty[1] and Quan Lu[2]

[1]Faculty of Forestry and Wood Sciences, Czech University of Life Sciences Prague, Prague, Czechia, [2]Key Laboratory of Forest Protection of National Forestry and Grassland Administration, Ecology and Nature Conservation Institute, Chinese Academy of Forestry, Beijing, China

KEYWORDS

forentomics, forest health, forest pest and pathogen, multi-omics, climate change, bark beetles

Editorial on the Research Topic
"Forentomics": forest pest and pathogen biology, ecology, and management using omics

Introduction

Forests are indispensable for ecosystem services such as biodiversity conservation and carbon sequestration. However, forest health is increasingly threatened by climate change, which amplifies pest and pathogen outbreaks, leading to large-scale tree mortality and disruption of forest ecosystems, accelerating the transition of forests from carbon sinks to carbon sources and exacerbating global warming. Mitigating these challenges requires a deeper understanding of forest pests and pathogens and their interaction with hosts at the molecular level to develop sustainable and eco-friendly forest management strategies. The present topic showcases the application of cutting-edge omics tools in tackling forest health under climate change. More specifically, "forentomics" represents research on forest trees, pests, pathogens and their interactions within the forest ecosystem using omics methodologies. Advances in omics technologies, including genomics, transcriptomics, proteomics, and metabolomics, have revolutionized the study of trees, pests and pathogen biology and ecology. These tools can provide detailed insights into the molecular interactions governing forest ecosystems, enabling innovative approaches to help mitigate current forestry challenges.

New frontiers in pest and pathogen detection research

Pathogens pose a significant threat to forest health, and precise detection methods are critical for effective management. Araeinejhad et al. focus on *Brenneria goodwinii*, a

bacterial pathogen responsible for oak and oriental beech decline. By developing a highly specific primer set targeting the *hrpN* gene, the study presented a reliable tool for early detection, enabling timely intervention to mitigate disease spread. Furthermore, Marques et al. reported the taxonomic challenges associated with *Physokermes* species, a group of soft-scale insects damaging conifers. The study resolved species boundaries and identified potential species complexes using nuclear and mitochondrial DNA markers. Accurate taxonomic identification is critical for designing targeted management strategies, especially as climate change influences pest and pathogen distributions.

Unveiling the molecular basis of pest adaptations

Many forest pests are able to exploit complex inherent adaptive mechanisms to respond to a changing climate, contributing to their destructive potential. Naseer et al. analyzed the life-stage, tissue, and sex-specific gene expression dynamics of the Eurasian spruce bark beetle (*Ips typographus*). Their study identified detoxification enzymes and gene related to metabolic regulation that may help bark beetles overcome host defenses, creating a foundation for downstream functional studies on key genes. Ramakrishnan et al. further elucidated the hormonal regulation of *I. typographus* physiology, focusing on juvenile hormone III (JH III). Their research unraveled key genes involved in pheromone biosynthesis and detoxification pathways, highlighting the role of JH III in facilitating adaptive responses. This work emphasized the potential for disrupting aggregation behaviors through hormonal manipulation, a promising avenue for managing bark beetle outbreaks. These findings also offer promising targets for RNA interference (RNAi)-based pest management strategies.

Functional genomics and forest ecosystem impacts

The ecological roles of pests and their interactions with forest ecosystems expand beyond direct tree damage. He et al. conducted a genome-wide analysis of carbohydrate-active enzymes (CAZymes) in termites, highlighting their conserved yet adaptable enzymatic repertoire. Termites, as decomposers, contribute to nutrient cycling and pose economic threats due to their wood-digesting capabilities. This study enhances our understanding of termite symbiosis and its implications for forest ecology.

Singh et al. performed foundational work that identified robust reference genes for real-time quantitative PCR in Norway spruce (*Picea abies*). Their study under diverse stress conditions ensured accurate reference genes for various gene expression studies. This methodological advancement supports future functional genomic research in conifers.

Resilient giants: decoding tree defense mechanisms against biotic stresses

Understanding the molecular defense mechanisms of trees is vital for developing pest-resistant selections. Sun et al. employed proteomics and phosphoproteomics to investigate the responses of Chinese pine (*Pinus tabuliformis*) to caterpillar feeding. This study revealed kinase-mediated phosphorylation networks and identified proteins critical to pine defense responses. These findings provide molecular underpinnings for breeding pest-resistant tree varieties and enhancing forest resilience. Furthermore, Pastierovič et al. studied European aspen (*Populus tremula*) responses to spongy moth feeding. Their analyses revealed that defense mechanisms, including increases in phenolic compounds, were activated within minutes of herbivory, confirming the dynamic nature of tree defenses and the importance of timing in tree-pest interactions. Finally, Stanley et al. explored host-pathogen interactions in green ash (*Fraxinus pennsylvanica*), a species severely impacted by the invasive emerald ash borer (*Agrilus planipennis*). Metabolomic analysis identified biochemical markers associated with host resistance, including induced defensive responses in lingering ash populations. These insights are instrumental for breeding programs aimed at preserving ash genetic diversity.

Leveraging omics for sustainable forest management

Integrating omics tools into forest pest and pathogen management is transforming how we manage forest health. From understanding pest adaptation to variable environmental conditions, to elucidating tree defense mechanisms, these studies collectively provide a roadmap for sustainable forest management strategies under climate change. Researchers can develop eco-friendly interventions, from breeding resistant tree varieties to deploying RNAi-based pest controls and implementing early pathogen detection systems. By disentangling the molecular complexities of forest ecosystems, these studies lay the foundation for innovative solutions to a variety of forest health challenges, both present and yet to come.

Conclusion and future perspectives

"Forentomics" represents a new frontier in forest molecular ecology, offering unprecedented opportunities to dissect the intricate interactions between forest trees, pests, and pathogens. The studies presented here illustrate the power of omics tools to address serious forestry challenges, from pest outbreaks to pathogen-induced tree decline. As climate change reshapes forest ecosystems, integrating molecular and ecological insights will be critical for safeguarding forests and their invaluable ecosystem services for generations to come. Future directions in forest protection will increasingly include precision pest control, AI-based early infection/attack and damage

detection systems, resilient tree breeding using AI-powered phenotypic and genotypic selection, prediction models and climate-responsive strategies.

Author contributions

AR: Conceptualization, Data curation, Writing – original draft, Writing – review & editing. AC: Data curation, Writing – review & editing. QL: Data curation, Writing – review & editing.

Acknowledgments

AR and AC acknowledge "Excellent Team Grants" from FLD, CZU, Prague.

Conflict of interest

The authors declare that the research was conducted in the absence of any commercial or financial relationships that could be construed as a potential conflict of interest.

Publisher's note

frontiers | Frontiers in Forests and Global Change

TYPE Original Research
PUBLISHED 14 March 2023
DOI 10.3389/ffgc.2023.1124754

OPEN ACCESS

EDITED BY
Ari Mikko Hietala,
Norwegian Institute of Bioeconomy Research (NIBIO), Norway

REVIEWED BY
Melissa Hamner Mageroy,
Norwegian Institute of Bioeconomy Research (NIBIO), Norway
Frank Chidawanyika,
International Centre of Insect Physiology and Ecology (ICIPE), Kenya

*CORRESPONDENCE
Amit Roy
✉ Roy@fld.czu.cz

SPECIALTY SECTION
This article was submitted to Pests, Pathogens and Invasions, a section of the journal Frontiers in Forests and Global Change

RECEIVED 15 December 2022
ACCEPTED 13 February 2023
PUBLISHED 14 March 2023

CITATION
Naseer A, Mogilicherla K, Sellamuthu G and Roy A (2023) Age matters: Life-stage, tissue, and sex-specific gene expression dynamics in *Ips typographus* (Coleoptera: Curculionidae: Scolytinae). *Front. For. Glob. Change* 6:1124754. doi: 10.3389/ffgc.2023.1124754

Age matters: Life-stage, tissue, and sex-specific gene expression dynamics in *Ips typographus* (Coleoptera: Curculionidae: Scolytinae)

Aisha Naseer[1], Kanakachari Mogilicherla[2], Gothandapani Sellamuthu[1] and Amit Roy[1,2]*

[1]Excellent Team for Mitigation, Faculty of Forestry and Wood Sciences, Czech University of Life Sciences Prague, Prague, Czechia, [2]EVA 4.0 Unit, Faculty of Forestry and Wood Sciences, Czech University of Life Sciences Prague, Prague, Czechia

The Eurasian spruce bark beetle (ESBB), *Ips typographus*, has recently caused catastrophic damage to Norway spruce (*Picea abies*) forests in Europe, resulting in the loss of more than 100 million cubic meters of wood. Traditional forest management strategies have failed to constrain the growing infestation rate; hence, novel measures must be deployed. A better understanding of ESBB physiology and adaptation to host allelochemicals may provide a platform for future management strategies using molecular tools such as RNA interference. To understand ESBB physiology and adaptation, the current study unraveled the gene expression dynamics of ESBB in different life stages and tissues. We obtained ESBB transcriptomes for different life stages [larvae (L1, L2, and L3), pupa, callow, and sclerotized adult] and male/female tissues (gut, fat body, and head) from callow and sclerotized adult beetles. Differential gene expression analysis (DGE) identified multiple gene families related to detoxification, digestion, resistance, and transport in different life stages and tissues of the beetle. Gene Ontology (GO) enrichment revealed 61 critical metabolic pathways enriched across all DGE comparisons. DGE analysis further pinpointed the differential expression of essential genes involved in detoxification, digestion, transport, and defense in various tissues and life stages. RT-qPCR experiments and enzymatic assays corroborated the findings further. The catalogue of differentially expressed genes identified in ESBB could aid better understanding of ESBB physiology and adaptation to hosts and serve as targets for future RNAi-based ESBB management.

KEYWORDS

Norway spruce, Eurasian spruce bark beetle, DGE analysis, allelochemicals, detoxification, RT-qPCR, enzyme assays, forest pest management

Introduction

Ips typographus, the Eurasian spruce bark beetle, is one of the most destructive forest pests of Norway spruce (*Picea abies*), causing considerable damage throughout Europe (Huang et al., 2020; Fang et al., 2021; Hlásny et al., 2021). They attack trees weakened due to drought or windthrow when the bark beetle population is in an endemic phase

(Jakuš et al., 2011; Biedermann et al., 2019; Hlásny et al., 2019; Netherer and Hammerbacher, 2022). The host selection by ESBB is based on the attraction *via* pheromones and kairomones, viz. 2-methyl-3-buten-2-ol and 4S-(−)-cis-verbenol, and repellence due to non-host volatiles/anti-attractants such as verbenone (Faccoli et al., 2005; Zhang et al., 2012; Unelius et al., 2014; Netherer et al., 2021). Males are the pioneering sex, and after colonizing the host, they release aggregation pheromones to attract conspecifics, resulting in mass attacks. ESBBs infest healthy trees during an epidemic stage and subsequently kill them (Biedermann et al., 2019). The defense mechanism of the conifer trees can be overwhelmed by the detoxification machinery of the beetle and their resident symbionts, such as bacteria and fungi that can metabolize plant defense chemicals to semiochemicals or sequester them to less toxic and more usable carbon resource forms (Krokene and Solheim, 1998; Faldt et al., 2006; Hammerbacher et al., 2013; Davis, 2015; Cale et al., 2019; Chakraborty et al., 2020a,b). Upon encountering a suitable host, the aggressive beetles bore into the intercortical regions where they feed on the phloem tissues, lay eggs, and the emerging larvae develop by feeding on the surrounding tissues, forming characteristic galleries. After completing the development, ESBB adults leave these galleries, swarm around the forest, and attack new trees to start the cycle again (Hlásny et al., 2019).

Conifers have evolved complex constitutive and inducible defenses to protect themselves against herbivores and their associates, including anatomical barriers and secondary metabolites, such as phenolics and terpenes (mono-, sesqui-, and diterpenes) produced *via* phenylpropanoid and terpene synthase pathways (Franceschi et al., 2005; Biedermann et al., 2019; Celedon and Bohlmann, 2019). Herbivore insects counteract these responses by employing various coping strategies, such as avoidance, sequestration, target site mutation, and enhanced metabolism/detoxification (Heckel, 2014; Meng et al., 2015; Gaddelapati et al., 2018; Hilliou et al., 2021; Lu et al., 2021; Bras et al., 2022). During detoxification, insects produce enzymes that convert the toxic allelochemicals to less toxic, easily excretable forms by oxidation, hydroxylation, or glycosylation. Such complex biochemical reactions are carried out by enzymes categorized as phase I, phase II, and, more recently, phase III enzymes (Hilliou et al., 2021). The primary or phase I enzymes target the lipophilic groups *via* oxidation, dihydroxylation, or dealkylation, rendering them water-soluble forms. In contrast, the phase II or secondary enzymes attack the epoxide intermediates of the phase I molecules, which can then be excreted through body fluid. The enzymes involved in phase I detoxification include cytochrome P450s (P450), carboxyl/choline esterases (CCE), and other esterases (i.e., acetylcholinesterase-AChE, JH esterase) that carry out the oxidation, hydrolysis, and reduction of primary toxic molecules. These molecules are then conjugated with glutathione molecules by glutathione S-transferases (GSTs) or glycosylated by UDP-glucuronosyltransferases/UDP-glycosyltransferases (UGTs), which are considered phase II enzymes (Heidel-Fischer and Vogel, 2015; Krempl et al., 2016; Jin et al., 2019). Secondary enzymes also include sulfotransferase and ATP-binding cassette (ABC) transporters. However, ABC transporters have recently been reported as phase III enzymes that obtain energy from the hydrolysis of ATP to transport the substrate across the lipid membrane and facilitate the excretion of entomotoxic compounds (Jin et al., 2019; Hilliou et al., 2021).

Dendroctonus species, close relatives of ESBB, have been well studied regarding their gene expression toward host toxins. In *D. armandii*, sixty-four P450s were identified in different developmental stages (larvae, pupa, and adult) and validated with RT-qPCR; nineteen CYP genes were upregulated upon host feeding (Dai et al., 2015). The role of the CYP4 and CYP9 families in detoxification was also confirmed in *D. rhizophagus* (Cano-Ramirez et al., 2013; Sarabia et al., 2019). In *D. ponderosae*, three CYPs were identified as involved in monoterpene oxidation, and one CYP was implicated in aggregation. Furthermore, transcript levels of several GSTs, ABC transporters, esterases, and dehydrogenases have been reported to increase significantly in mountain pine (*D. ponderosae*) beetles upon host feeding (Robert et al., 2013; Chiu et al., 2019a,b). Various *Ips* species, like *I. paraconfusus* and *I. pini*, are reported to deploy sex-specific expression of CYPs to convert host allelochemicals to *de novo* produced aggregation pheromones (Huber et al., 2007; Song et al., 2013; Tittiger and Blomquist, 2017; Blomquist et al., 2021). For ESBB, the roles of most of the detoxifying enzymes and the related genes upon mass attack have yet to be identified. ESBBs are exposed to various levels of host bark chemicals throughout the life cycle; as a result, the expression or catalytic activity of beetle defense enzymes may fluctuate according to the life stage or phase of the detoxification process. Frequent ESBB outbreaks in the recent past and the projected increased frequency of such outbreaks have created a high demand for target-specific control of ESBBs, as conventional methods have proved inefficient (Hlasny et al., 2021; Joga et al., 2021). Hence, detailed knowledge of the detoxification enzyme expression dynamics in the different life-stages of the ESBB is necessary to obtain the target genes for future species-specific management. Furthermore, the recent release of the ESBB genome has opened such captivating research avenues by giving insights into the ubiquitous presence of phase I, II, and III enzymes (84 P450s, 58 GSTs, 86 UGTs, 75 ABC transporters, and 59 CCE families) in the species (Powell et al., 2021). In the present study, we performed screening of the various developmental stages from larval, callow adults, and fully emerged sclerotized beetles, and different tissues of ESBB to catalogue genes differentially expressed and putatively involved in the processes of detoxification, digestion, and transport. We captured the expression dynamics of detoxification machinery and other physiologically essential genes in ESBB. Our findings have led to a better understanding of ESBB physiology and offer valuable targets for RNAi-based control measures (Joga et al., 2021).

Materials and methods

Sample collection and dissection

All ESBB samples (**Figure 1** and **Supplementary material 1**) were taken directly from beetle-infested logs from Rouchovany in Czechia (49°04′08.0″N 16°06′15.4″ E, 360 m above sea level, a warm and drought-prone area with regular forest management by State Forest Enterprise) during the infestation season in May 2019. The average temperature was around 15°C during collection. The larvae (L1, L2, and L3), pupae, callow, and sclerotized adult beetles were snap-frozen in liquid nitrogen, and the target tissues (gut, head, and fat body) were dissected in sterile conditions

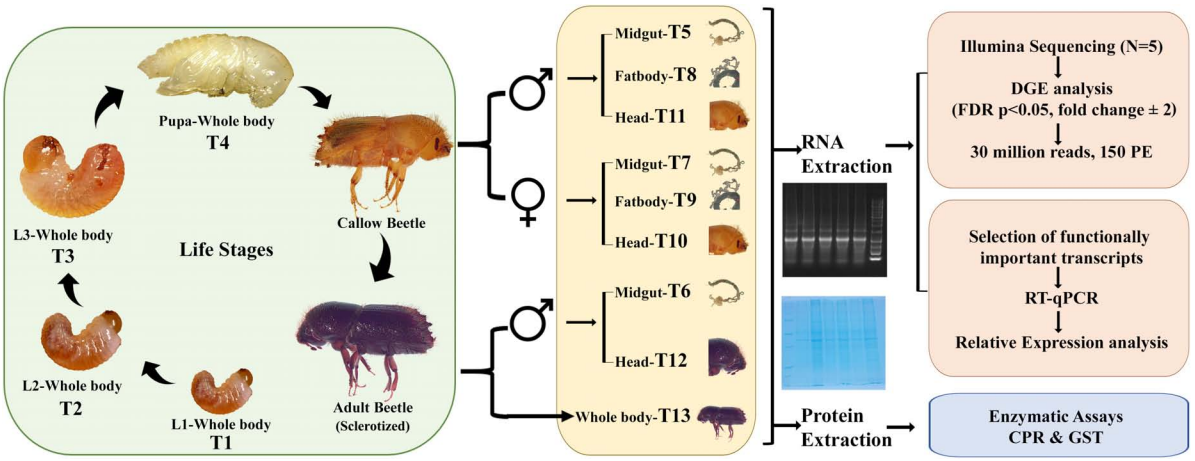

FIGURE 1
Study design. Larvae 1 (L1/T1), Larvae 2 (L2/T2), Larvae 3 (L3/T3), Pupa (T4), Callow male gut (T5), Sclerotized adult gut (T6), Callow female gut (T7), Callow male fat body (T8), Callow female fat body (T9), Callow female head (T10), Callow male head (T11), Sclerotized adult male head (T12), Sclerotized adult whole body (T13) (CPR, Cytochrome P450; GST, Glutathione S-transferase).

and collected in RNAlater™. The sex of the collected beetles was determined by pronotum hair density, as has been described previously (Chakraborty et al., 2020a; Powell et al., 2021). The collected developmental stages and tissues were stored at −80°C until total RNA extraction, as we previously described (Powell et al., 2021). ESBBs were also reared in an insect-rearing chamber with fresh Norway spruce logs at 27 ± 1°C, 70 ± 5% humidity, and a 16:8-h light/dark (L: D) photoperiod. A new set of samples (developmental stages and tissues) was obtained from the F1 generation, and the extracted RNA and protein were used in RT-qPCR and enzymatic experiments, respectively.

Transcriptome sequencing, library preparation, and analysis

Various ESBB life stages and tissues were used to create transcriptome libraries [larval stage 1 (T1), larval stage 2 (T2), larval stage 3 (T3), pupa (T4), callow male gut (T5), sclerotized adult male gut (T6), callow female gut (T7), callow male fat body (T8), callow female fat body (T9), callow female head (T10), callow male head (T11), sclerotized adult male head (T12), and sclerotized adult whole-body (T13)] (**Figure 1** and **Supplementary material 1**) during the *Ips typographus* genome study (Powell et al., 2021). Precisely, mRNA in samples was enriched using oligo (dT) beads, and cDNA libraries were prepared using NEB Next® Ultra™ RNA Library Prep Kit followed by Illumina sequencing (Illumina Novaseq6000) to generate 30 million reads (150 paired-end) for each sample. Five biological replicates were sequenced per sample (Powell et al., 2021). The raw reads were processed using CLC workbench (CLC version 21.0.5, Qiagen, Denmark). The sequence data were submitted to NCBI (PRJNA679450) and reused for the present gene expression study. For differential gene expression analysis (DGE), raw reads were mapped back to the *I. typographus* reference genome (Powell et al., 2021), and the read counts were obtained using CLC workbench (version 21.0.5). Gene expression quantification was obtained by employing standard pre-optimized settings and parameters, such as mapping to exon regions. The TMM-adjusted log CPM counts (similar to the EdgeR approach) were also used to correct biases in the sequence datasets and abundance, resulting in accurate estimations of relative expression levels as described by Robinson et al. (2010). A multi-factorial statistical analysis based on a negative binomial Generalized Linear Model (GLM) was used to identify differentially abundant transcripts between developmental stages and tissues in varied comparisons deploying an FDR corrected p-value < 0.05; fold change ± 2 was used as a threshold for differentially expressed transcripts (DET). Using the GLM model permitted fitting the curves to expression values without presuming that the error on the values was normally distributed. DEGs were functionally annotated using the "cloud blast" feature within the "Blast2GO Plugin" in the CLC Genomic Workbench 21.0.5 (Qiagen, Denmark). A nucleotide blast was done against the NCBI Nr database with an *E*-value cut-off of 1.0E-5. Both annex and GO slim were used to improve the GO term identification further by crossing the three GO categories (biological process, molecular function, and cellular component) to search for name similarities, GO term, and enzyme relationships within KEGG (Kyoto Encyclopedia of Genes and Genomes) pathways (Roy et al., 2017; Powell et al., 2021).

Total RNA extraction, cDNA synthesis, and RT-qPCR analysis

Ribonucleic acid was isolated from each life stage and tissue using the PureLink™ RNA Kit from Ambion (Invitrogen, Carlsbad, CA, USA) following the manufacturer's protocol. For the ESBB tissue samples, 10 guts, 10 fat bodies and 5 heads were dissected and pooled. Eight L1 larvae, eight L2 larvae, five L3 larvae, five pupae, and two adults were used to obtain enough RNA from each developmental phase for downstream processing. The total extracted RNA was then treated with DNase I (TURBO DNase Kit, Ambion, Austin, TX, USA). The integrity of the purified total RNA was checked on 1.2% agarose gel. One μg

of total RNA was used for cDNA synthesis using the High-Capacity cDNA Reverse Transcription kit (Applied Biosystems-Life Technologies, Waltham, MA, USA) and stored at −20°C. The cDNA samples were diluted 10-fold before being used as a template in RT-qPCR experiments. Four biological replicates from each sample were used in each RT-qPCR assay. The IDT PrimerQuest software (IDT, Belgium) was used to design the primers (**Supplementary material 2**). RT-qPCR was carried out for all the samples (T1-T9 and T13). The 10 μL RT-qPCR reactions contained 5.0 μL of SYBR® Green PCR Master Mix (Applied Biosystems), 1.0 μL of cDNA, 1.0 μL of 10 μM forward and reverse primers, and 3.0 μL RNase-free water (Invitrogen). The reactions were performed in an Applied Biosystems™ StepOne™ Real-Time PCR System (Applied Biosystems) with the following conditions: initial denaturation at 95°C for 10 min, followed by 40 cycles of 95°C for 15 s, 60°C for 1 min, and dissociation curve analysis during which temperature was increased from 60 to 95°C. The expression levels of the target genes were calculated using the $2^{-\Delta\Delta Ct}$ method (Livak and Schmittgen, 2001). RPL7 and RPS7 were used as reference genes for expression normalization (Sellamuthu et al., 2022).

Enzyme assays

To consider differences in the enzyme activity levels between the ESBB developmental stages, biochemical assays for Glutathione S-transferase (GST) and Cytochrome P450 Reductase (CYP450) were performed as described previously (Habig and Jakoby, 1981; Ortego et al., 1999; Bosch-Serra et al., 2021). The developmental stages and gut samples of ESBB were collected and homogenized in sodium phosphate buffer (50 mM) solution at pH 7.0. The homogenate was centrifuged at 10,000 rpm for 10 min at 4°C. Precisely, eight L1 larvae (T1), six L2 larvae (T2), four L3 larvae (T3), three pupae (T4), two sclerotized adults, and ten guts were pooled to extract enough protein from each sample category. The extract was collected to serve as a source of the enzyme, and enzyme activities were corrected using the protein concentration as a standard correction factor. The total protein content of the enzyme solution was determined by the Bradford method using bovine serum albumin as the standard (Bradford, 1976).

The activity of glutathione S-transferase (GST) was measured using a spectrophotometric method with 5 mM reduced glutathione (GSH) and 1.5 mM 1-chloro-2, 4-dinitrobenzene (CDNB) as substrates (Habig and Jakoby, 1981; Bosch-Serra et al., 2021). One unit of glutathione S-transferase activity is the amount of enzyme-catalyzing 1 μmol of CDNB -GSH conjugate per minute at 30°C. For the GST activity, the reaction solution contained 20 μl of protein extract (**Supplementary Table 2**), 170 μl of 5 mM GSH in sodium phosphate buffer (pH 7.0), and 10 μL1.5 mM CDNB to make a 200 μl total reaction volume in a transparent micro-plate (96-well Thermo Scientific™ Sterilin™ Clear Microtiter™ Plates). For blanks, 20 μl of sodium phosphate buffer (50 mM pH 7.0) was used instead of protein extracts. After a 1 min incubation period at 30°C, the absorbance of the reaction product [CDNB-glutathione (GSH) conjugate] was measured at 340 nm at intervals of 1 min for up to 10 min using the microplate reader (Agilent BioTek Cytation 5). GST activity was expressed as nmol substrate conjugated·min-1 ·mg-1 protein using a CDNB molar extinction coefficient (9.6 $mM^{-1} \times cm^{-1}$). The final specific activity was expressed in μmol of CDNB-glutathione min^{-1} mg^{-1} of total protein extracted (Habig and Jakoby, 1981).

Cytochrome P450 Reductase (CYP450) activity was measured according to Ortego et al. (1999) and Bosch-Serra et al. (2021). The 200 μl reaction was prepared in a clear micro-plate (96-well Thermo Scientific™ Sterilin™ Clear Microtiter™ Plates). It comprised 20 μl of protein extract or sodium phosphate buffer (blank) (**Supplementary Table 2**) and 160 μl of NADPH-generating system [0.6 mM β-nicotinamide adenine dinucleotide phosphate (NADP), 2.8 mM D-glucose-6-phosphate (G6P), and 0.28 units of glucose-6-phosphate dehydrogenase (G6PD)]. The reaction was initiated by adding 20 μl of 1 mM cytochrome C in sodium phosphate buffer (pH 7.0), and the absorbance was measured at 550 nm at intervals of 1 min for up to 25 min using the microplate reader (Agilent BioTek Cytation 5). CYP450 activity was expressed as nmol substrate conjugated·min^{-1} ·mg^{-1} protein using a cytochrome C molar extinction coefficient (27.6 $mM^{-1} \times cm^{-1}$) (Margoliash and Frohwirt, 1959). The enzymatic activity was measured in cytochrome P450 equivalent unit min^{-1} mg^{-1} of the total protein extracted.

Statistical analysis

First, we conducted pairwise comparisons with Student's *t*-test to consider the differences in RT-qPCR determined gene transcript levels for 19 selected genes related to detoxification. The pairwise comparisons included callow gut vs. sclerotized male gut, and callow female fat body vs. callow male fat body. For multiple comparisons in the relative gene expression of 19 genes between different developmental stages and gut tissues of ESBB, Tukey's HSD was used. Lastly, one-way ANOVA was used to test the significance of differences in enzymatic activities between ESBB developmental stages and tissues. All these analyses were performed in RStudio (version 4.2.2). The statistical analysis deployed for DGE data analysis is described above in the "Transcriptome sequencing, library preparation, and analysis" section.

Results

DGE analysis

From 65 libraries (13 samples × 5 biological replicates), 5,199,150,714 reads were retrieved, and 3,728,549,638 reads were mapped back to the reference genome of *I. typographus* (Powell et al., 2021) to generate the count table (**Supplementary Table 1**). Using CLC workbench 21.0.5 (QIAGEN Aarhus, Denmark), DGE comparisons were performed among the 13 samples (T1 to T13) (**Figure 1**). The number of DEGs, i.e., up- or downregulated genes, were reported based on the cut-off of FDR $p < 0.05$ and fold change ± 2 considered as the threshold for differential expression. We performed DGE for the following perspectives: (A) life-stage comparison: T1, T2, T3, T4, and T13 (from larvae to adult); (B) tissue-specific comparison: (i) T7, T8, and T9, and (ii) T5,

T9, and T11; (C) sex-specific comparison: (i) T7 vs. T5, and (ii) T9 vs. T8; and (D) comparison between gut tissues in different adults stages: T6 vs. T5 (sclerotized vs. callow male guts) (Table 1, Supplementary Figure 1, and Supplementary materials 1, 3–13).

A. DGE in ESBB life stages

A.1. Group-wise comparison between T1-T4 and T13

A group-wise comparison was made between the five samples (three larval stages, pupa, and adult) to explore the differential gene expression across the developmental stages (Supplementary material 3). The principal component analysis (PCA plot) resulted in the segregation of samples from different life stages, indicating life-stage-specific gene expression in ESBB (Figure 2A). The gene expression dynamics in different life stages of ESBB were represented as a heatmap (Figure 2B). We found that detoxifying enzyme families (i.e., cytochrome P450s/CYPs, UDP-glucuronosyltransferases/UGTs, acetylcholinesterase/AchE, hydrolases, dehydrogenases, peroxidases, carboxylesterases, esterases, ABC transporters, and glutathione S-transferases/GSTs) showed differential gene expression (up- and downregulation) in larvae and adult stages (Figures 2C, D). A graph was plotted using mean CPM values (FDR corrected $p < 0.05$) for essential detoxification genes/enzymes (P450s, GSTs, UGTs, carboxylesterases, esterases, and ABC transporters). The expression of detoxification-related genes increased from L1 to L2, decreased in L3 and pupa, and increased in adults (Figure 2D). Some other detoxifying enzymes, such as dehydrogenases, hydrolases, and aminoacylases, also revealed a similar pattern (Supplementary Figure 2).

Most of the cytochrome and esterase family genes showed no variation in gene expression across the life stages of ESBB, indicating their importance for beetle survival under the bark (Figure 3A). The expression of cytochrome P450 genes was high in the larval and adult stages. The present study identified differentially expressed cytochrome P450 genes primarily for family 4, with a few belonging to families 6 and 9 (Figure 3). In the upregulated category, CYP4BH1, CYP6CR2, chorion peroxidase, sphingomyelin phosphodiesterase-like and esterase FE4-like gene were only over-expressed in adults, whereas CYP306A1, CYP6A1-like, cAMP and cAMP-inhibited cGMP 3′,5′-cyclic phosphodiesterase 10A-like, and palmitoleoyl-protein carboxylesterase NOTUM-like were overexpressed only in pupae (Figure 3A). In the downregulated category, most genes were downregulated in pupae compared to other ESBB life stages, with CYP410A1 showing the lowest gene expression level. In adults, the most highly upregulated gene was CYP4G27 (Figure 3A), and the lowest gene expression was recorded for GST 1 isoform D (Figure 3B). The 19 transcripts involved in pheromone biosyntheses, like ipsdienol dehydrogenase, juvenile hormone (JH) epoxide hydrolase, JH esterase, and JH acid O-methyltransferase, were also reported to be primarily overexpressed in adults (T13) and larval stage L2 (T2) and L3 (T3) and were least expressed in pupae (T4) (Supplementary material 3).

A.2. Feeding vs. non-feeding stage comparison (T1, T2, T3, T13 vs. T4)

The effect of bark feeding and encountering the host at different developmental stages was studied by comparing the feeding stages (larva and adult; T1, T2, T3, and T13) against the non-feeding stage (pupae; T4) (Supplementary materials 4–7). This revealed the complete segregation of gene expression between the feeding and non-feeding stages (Figures 4A–D). Compared to T4, the transcript levels of most of the genes of interest were significantly elevated in T1, T2, T3, and T13. The T2 vs. T4 comparison revealed the most differentially expressed gene transcripts, i.e., 8,319 (4,896 downregulated, 3,423 upregulated). We discovered that 1,798 gene transcripts were commonly upregulated, and 1,060 transcripts were commonly downregulated in all feeding stages, including larvae and adults, with the dehydrogenases and cytochromes being the most differentially expressed (Figures 5, 6 and Supplementary materials 36, 37). Two GST transcripts, namely, GST-like isoform X2 and microsomal GST 1-like, had higher expression in the feeding stages (adults and larvae) than the non-feeding pupal stage, indicating their putative involvement in digestion and the detoxification of host allelochemicals.

B. Tissue-specific DGE

We compared tissues from both females and males separately to capture similarities and sex-specific differences in gene expression in different tissues, which are crucial to understand ESBB physiology (Figures 7A, B). In both males and females, the expression of genes related to detoxification, digestion, defense, and metabolism was highest in the gut, followed by in the fat body, and lowest in head tissues.

B.1. Female tissue comparison (T7, T8, and T10)

The callow female head (T10), fat body (T8), and gut (T7) were compared and clustered on a group-by-group basis (Figure 7A, i, ii and Supplementary material 8). There were 6,024 genes upregulated (FDR corrected $p < 0.05$, fold change ≥ 2), including 74 dehydrogenases, 37 CYP/P450s, 20 hydrolases, 9 ABC transporters, 8 sulfotransferases, 5 GSTs, 3 peroxidases, 2 each of the AchE, aminoacylase, and esterase sub-families, and 1 UGT and carboxylesterase (Figure 7A, iii). Among the 4,112 downregulated transcripts (FDR corrected $p < 0.05$, fold change ≤ -2) were 40 dehydrogenases, 15 CYP/P450s, 11 UGTs, 15 hydrolases, 9 ABC transporters, 6 GSTs, 3 of each sulfotransferase and esterase subfamilies, and 1 peroxidase. The upregulated transcripts have molecular functions that relate to defense (21 transcripts), signaling (176 transcripts), growth (22 transcripts), transport (116 transcripts, excluding ABC transporter families), digestion (120 transcripts, excluding esterase sub-families), and metabolism (40 transcripts).

B.2. Male tissue comparison (T5, T9, and T11)

The callow male head (T11), fat body (T9), and gut (T5) were compared and clustered on a group-by-group basis (Figure 7B, i, ii and Supplementary material 9). There were 10,464 transcripts substantially expressed (FDR corrected $p < 0.05$), with 6,178 upregulated (fold change ≥ 2) and 4,287 downregulated (fold change ≤ -2). The upregulated transcripts included 40 CYP/P450s, 1 UGT, 2 AchEs, 7 GSTs, 22 hydrolases, 60 dehydrogenases, 9 sulfotransferases, 3 peroxidases, 1 carboxylesterase, and 2 esterase subfamily genes. The downregulated transcripts included 16 CYP/P450s, 11 UGT, 8 GSTs, 2 aminoacylases, 16 hydrolases, 50 dehydrogenases, 5 sulfotransferases, 1 peroxidase, and 3 esterase subfamily genes (Figure 7B, iii). A total of 17 transcripts had molecular functions associated with defense, 130 with digestion, 30

TABLE 1 The number of differentially expressed genes in various comparisons.

	Comparison		Sample	Life stage or tissues	Sample ID	Downregulated (FDR $p < 0.05$, Fold change ≤ -2)	Upregulated (FDR $p < 0.05$, Fold change ≥ 2)
A	Developmental stages		ITL1, ITL2, ITL3, ITP, ITB	Larval stage 1, 2,3; pupa; sclerotized adult beetle	T1, T2, T3, T14, T13	4,975	7,153
	Feeding vs. non-feeding	(i)	ITL1 vs. ITP	Larval stage 1, Pupa	T1 vs. T4	3,610	3,429
		(ii)	ITL2 vs. ITP	Larval stage 2, Pupa	T2 vs. T4	4,896	3,423
		(iii)	ITL3 vs. ITP	Larval stage 3, Pupa	T3 vs. T4	4,027	3,199
		(iv)	ITB vs. ITP	Sclerotized adult whole body, Pupa	T13 vs. T4	2,473	3,386
B	Tissue-specific	(i)	ITGFG, ITGFF, ITGFH	Callow female gut, callow female fat body, callow female head	T7, T8, T10	4,112	6,024
		(ii)	ITGMG, ITGMF, ITGMH	Callow male gut, callow male fat body, callow male head	T5, T9, T11	4,287	6,177
C	Sex-specific	(ii)	ITGFG vs. ITGMG	Callow female gut, callow male gut	T7 vs. T5	541	99
		(i)	ITGFF vs. ITGMF	Callow female fat body, callow male fat body	T9 vs. T8	3,604	2,847
D	Sclerotized male gut vs. Callow male gut		ITFMG vs. ITGMG	Sclerotized male gut, callow male gut gut	T6 vs. T5	2,767	4,501
E	All gut tissues*		ITGFG, ITGMG, ITFMG	Callow female gut, callow male gut, sclerotized male gut	T5, T6, T7	2,504	5,326

*Supplementary information (Supplementary material 13, 34, 35).

with growth, 170 with signaling, 122 with transport (excluding ABC transporters), and digestion (excluding esterase subfamilies).

C. Sex-specific DGE

We compared the callow male and female ESBB guts (T7 vs. T5) and fat bodies (T9 vs. T8) for gene expression dynamics during maturation feeding (Supplementary Figures 3A, B).

C.1. ESBB gut comparison (T7 vs. T5)

The callow male gut had higher expression levels than the callow female gut for most of the transcripts involved in vital physiological functions, such as detoxification, defense, digestion, transport, metabolism, signaling, and growth (Supplementary Figure 3A, i, ii, iii and Supplementary material 10). Most of the transcripts were upregulated in the male gut (T5), including four cytochrome P450s (301A1, 4G15-like, 4C21-like, CYP410A1), 14 dehydrogenases, 1 ubiquinone oxidoreductase (defense), 6 serine/threonine-protein kinases and 1 phosphatase (signaling), 1 transporter protein and 1 trehalose transporter (transport), 1 serine protease, and 1 phosphodiesterase.

C.2. ESBB fat body comparison (T9 vs. T8)

The callow female and male fat body (T9 vs. T8) comparison showed 7,268 differentially expressed transcripts (FDR-corrected $p < 0.05$); 4,501 were upregulated (fold change ≥ 2), and 2,767 were downregulated (fold change ≤ -2) (Supplementary Figure 3B,i, ii and Supplementary material 11). Most transcripts with molecular functions related to detoxification, defense, digestion, and metabolism had higher expression in the callow male fat body, which is plausibly linked to future host colonization as pioneers (Supplementary Figure 3B iii). Thirteen transcripts related to pheromone biosynthesis were differentially expressed, such as juvenile hormone esterases, epoxide hydrolase, ipsdienol dehydrogenases, juvenile hormone acid O-methyltransferase, and pheromone binding proteins between males and female ESBB fat body. Of these, nine were upregulated in male (T9) and four in female ESBB fat bodies (T8). None of these genes were found to be expressed in the gut comparison.

D. DGE in callow and sclerotized male gut (T6 vs. T5)

The current comparison dealt with the gene expression dynamics in ESBB adults during maturation feeding (callow beetles) and post-maturation feeding (sclerotized). As demonstrated by the PCA plot and heatmap (Figures 8A, B and Supplementary material 12), there was a significant difference in gene expression between sclerotized (black) and callow male gut (T6 vs. T5). A total of 7,268 gene transcripts were significantly expressed (FDR-corrected $p < 0.05$), with 4,501 being upregulated (fold change ≥ 2) and 2,767 being downregulated (fold change ≤ -2). The upregulated gene transcripts include 17 P450s/CYPs, 1 UGT and AchE, 19 hydrolases, 46 dehydrogenases, 6 sulfotransferases, 2 peroxidases, 2 carboxylesterases, and 7 ABC transporters. The downregulated gene transcripts include 26 P450s, 8 UGTs, 12 GSTs, 2 aminoacylases, 14 hydrolases,

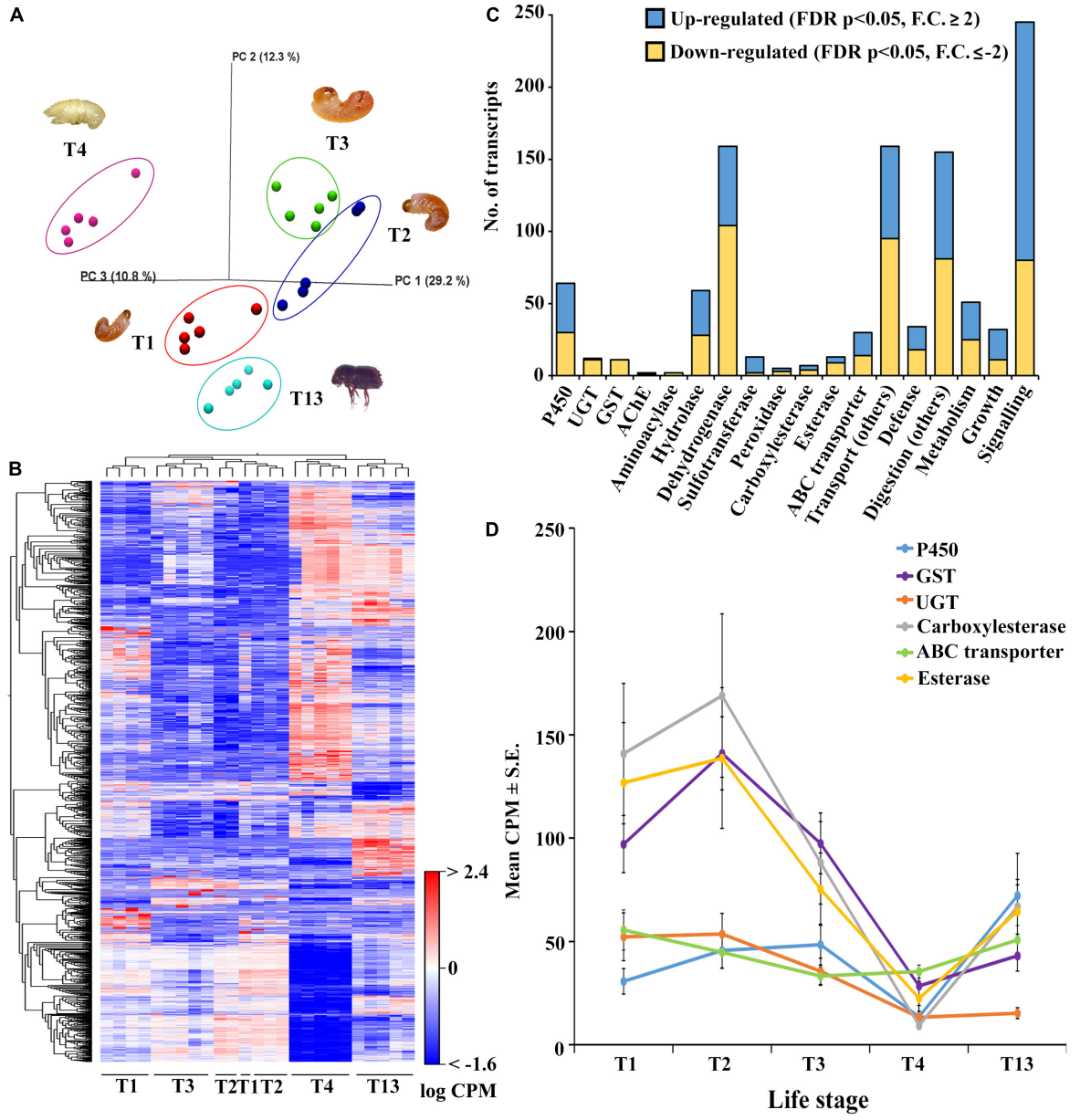

FIGURE 2
Group-wise comparison between different developmental life stages; larvae 1-3 (T1-T3), pupae (T4), and sclerotized adult whole body (T13) (N = 5). **(A)** PCA plot showing sample clustering. **(B)** Heat maps representing gene clustering. The color spectrum, stretching from blue to red, represents TMM-adjusted log CPM expression values obtained after DGE analysis. **(C)** Bar graphs showing the number of transcripts (CPM) for differentially expressed contigs of specific detoxification-related enzyme families and other essential enzymes related to defense, digestion, transport, metabolism, signaling, and growth after group-wise comparison between different developmental life stages. **(D)** Detoxification enzyme dynamics during different life stages. Average CPM ± standard error values of significantly expressed genes are plotted against each enzyme on the x-axis corresponding to the life stages on the y-axis. The total CPM was calculated by taking the average of all the differentially expressed contigs of each gene family. Analysis was done using CLC workbench (21.0.5, Qiagen, Denmark) with FDR $p < 0.05$ and a fold change ± 2 cut-off.

62 dehydrogenases, 3 sulfotransferases, 2 peroxidases, 1 carboxylesterase, 9 esterase subfamilies, and 43 ABC transporters (Figure 8C). A total of 15 gene transcripts had molecular functions predicted to be associated with defense, 145 with signaling, 18 with growth, 103 with transport (excluding ABC transporter families), 107 with digesting (excluding esterase sub-families), and 27 with metabolism. The detoxification-related gene transcripts were plotted based on average CPM values (mean ± STD error) (Figure 8D), and the majority of these were considerably overexpressed in the callow male gut (T6), indicating that callow beetles need those enzymes in high amounts during maturation feeding under the bark before they sclerotize. When comparing the sclerotized male gut, callow male gut, and callow female gut (T6, T5, and T7) (Supplementary material 13, 34, 35), a similar propensity was observed, with the sclerotized male gut (T6) segregating from the other two (T5 and T7), thus indicating the fine-tuning of gene expression for new colony establishment in the pioneer sex (Supplementary Figure 4). The

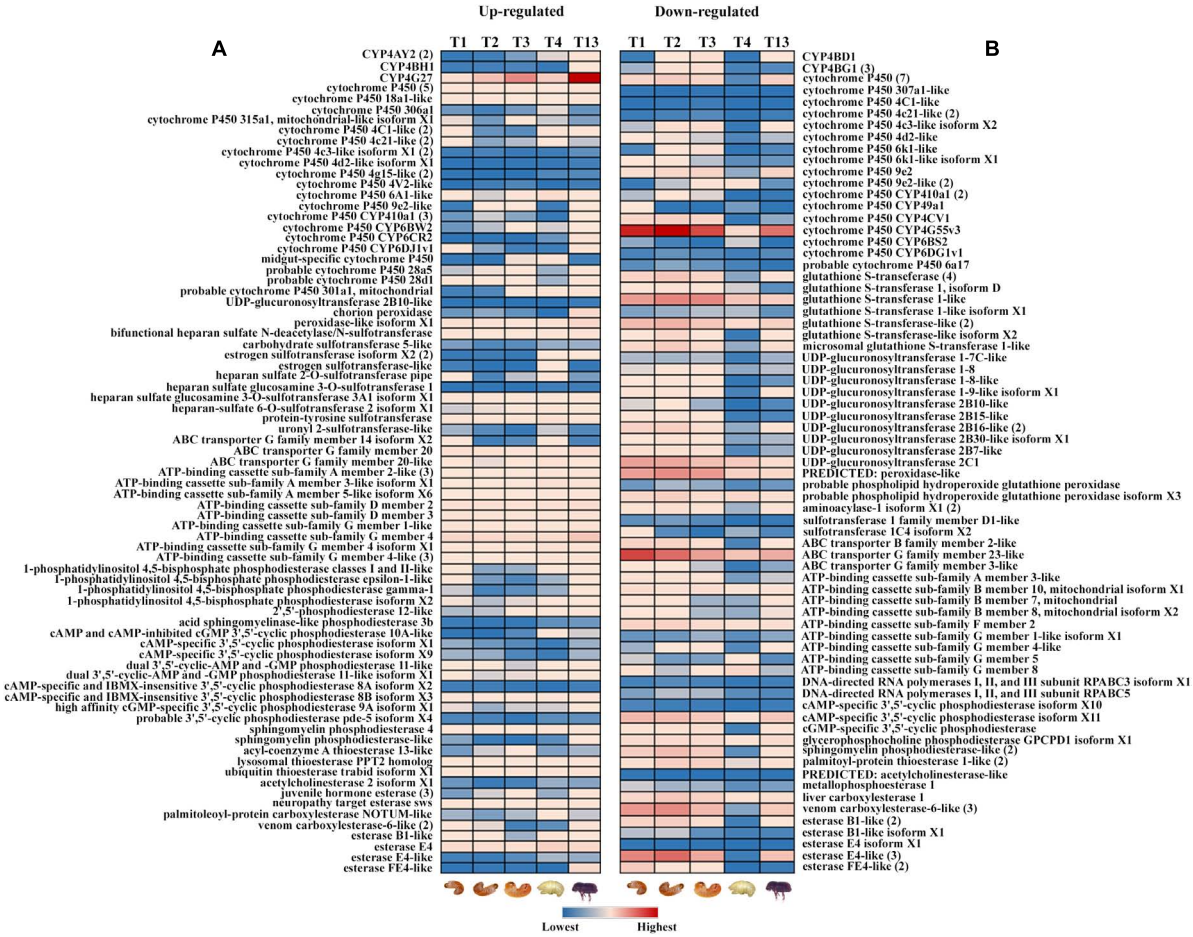

FIGURE 3
Expression profile of detoxification-related genes in different life stages of ESBB. **(A)** Upregulated genes; **(B)** downregulated genes. The details of the genes are given in **Supplementary Excel 3**. The expression level is represented in different colors indicating the TMM-adjusted log CPM expression mean values. Analysis was done with FDR $p < 0.05$ and fold change ± 2 cut-off in CLC workbench (21.0.5, Qiagen, Denmark).

cytochrome P450s expressed substantially in the sclerotized gut (T6) belong to the known detoxification families 4 (5), family 6 (3), and family 9 (1) (**Figure 9A**). However, the downregulated detoxification-related genes had lower mean CPM values or transcript levels in the sclerotized male gut than in the callow one (**Figure 9B**).

Gene ontology enrichment analysis

Gene ontology enrichment analyses for upregulated and downregulated transcripts were performed in all ten comparisons using the FDR-corrected $p < 0.05$ and a fold change threshold of ± 2 (**Supplementary materials 14–33**). According to the GO enrichment, the 62 crucial metabolic pathways enriched across seven comparisons could be involved in detoxification, digestion, and defense. Most of these were related to molecular functions (28) and biological processes (34) in the GO classification system (**Figure 10**). In the comparison of developmental stages (T1, T2, T3, T4, vs. T13), 37 critical pathways were enriched, including acyltransferase activity, hydrolase activity, transferase activity, immune response, stress response, and gene expression regulation. The comparison of callow and sclerotized male gut (T5 vs. T6) showed enrichment of 21 pathways in callow beetles, including catalytic activity, enzyme binding, cellular response to stress, and detection of biotic stress. Concerning specific tissues, 19, 11, 16, and 11 metabolic pathways were enriched in callow male and female fatbody (T8 vs. T9), callow male and female guts (T5 vs. T7), callow male gut, fat body, and head (T5, T9, vs. T11) and callow female gut, fat body, and head (T7, T8, vs. T10), respectively. The pheromone-related activity was only enriched in the callow male fat body vs. callow female fat body (T8 vs. T9), implying that pheromone production occurs in the ESBB fat body (**Figure 10**).

RT-qPCR analysis and enzymatic assay

The RT-qPCR was performed for 19 differentially regulated genes in different life stages, sex-specific guts, and fat body comparisons. Most of these genes revealed strong similarities in transcript levels with respect to expression patterns observed in their respective transcriptome expression (**Figures 11–13**).

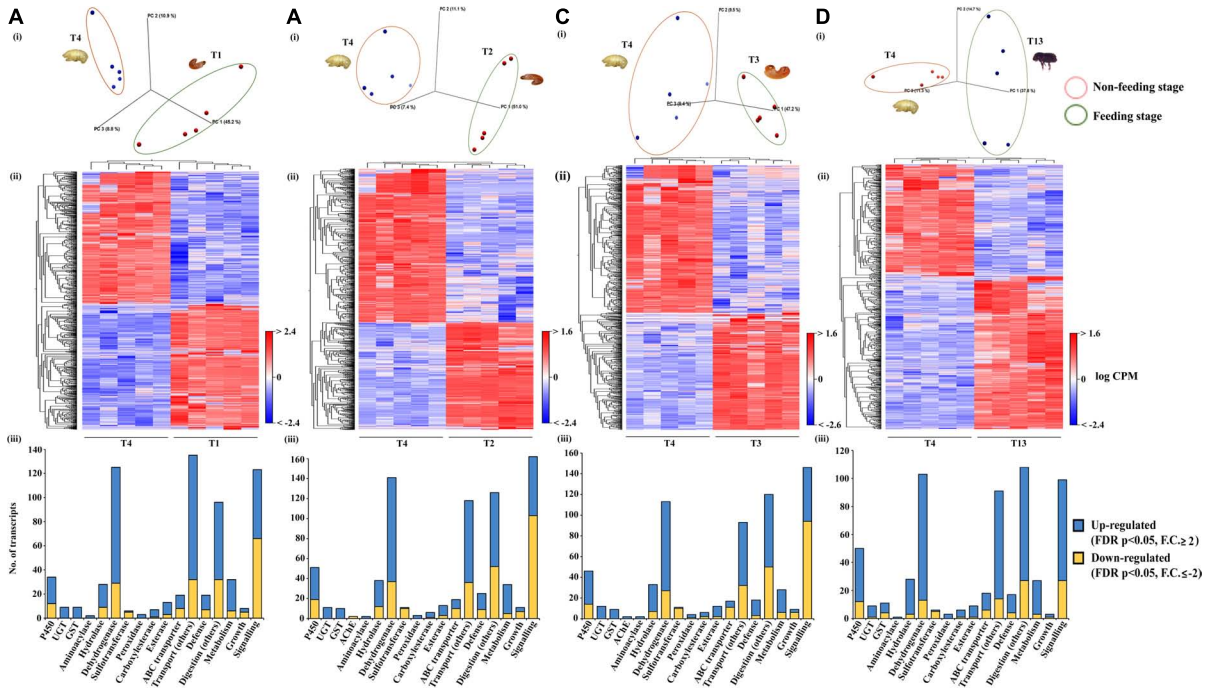

FIGURE 4
Feeding vs. non-feeding stage comparison. Pupa (T4, non-feeding stage) was compared with different feeding stages (T1, T2, T3, and T13) (N = 5). **(A)** PCA plot showing sample clustering. **(B)** Heat maps representing gene clustering. The color spectrum, stretching from blue to red, represents TMM-adjusted log CPM expression values obtained after DGE analysis. **(C,D)** Bar graphs showing differentially expressed contigs of detoxification-related enzyme families and other essential enzymes related to defense, digestion, transport, metabolism, signaling, and growth between the feeding vs. the non-feeding stage. Analysis was done using the CLC workbench using FDR $p < 0.05$ and fold change ± 2 as the threshold for significance.

The enzyme activity assay of cytochrome P450 reductase (CYP450) and glutathione S-transferase (GST) showed stage-specific expression (Figure 14). When compared against the larval stage 1 (T1), the pupa (T4) and sclerotized adult (T13) stages had significantly higher enzyme activities of GST, while the larval stages showed constitutive expression of GST. The activity of CYP450 decreased from T1 stage to T4 and was lowest in the sclerotized adult stage (T13). Similarly, the callow male ESBB gut (T5) had a relatively low expression of CYP450 but a high expression of GST.

Discussion

The family Curculionidae of the order Coleoptera comprises a massive number of bark beetles that colonize tissues of a wide range of tree species. The damage caused by bark beetles has been extensive in recent years, leading to the destruction of more than 100 million m^3 of spruce forest during a single year in Europe and Asia (Hlásny et al., 2019). This included 14.5 (67% forest cover) million m^3 of spruce forest within Czechia in 2021 (Lubojacký et al., 2022). The revenue loss in the timber industry was so huge that the Czechia state had to support it with ca 260 million euros in 2018–2019 (Hlásny et al., 2021). The management of ESBB necessitates a thorough knowledge of its physiology and adaptation to a nutritionally limiting host. ESBB has four main phases in their life cycle: egg, larva, pupa, and adult (callow and sclerotized). The ESBB larvae (L1, L2, and L3), pupa, and adults are developed under the bark upon exposure to the host allelochemicals. When their development is complete, the sclerotized males, being the pioneer sex, attack new host trees displaying constitutive and induced defenses. The shift from callow (early) to sclerotized (black) adult is a critical phase, during which the beetles undergo various physiological and gene-transcript-level changes that prepare them to establish themselves in a new host. The mechanisms that control the growth and development of ESBBs and their resistance toward spruce allelochemicals are still unknown. RNA-seq has always been a standard method for studying complex gene expression and molecular mechanisms in non-model insects. Hence, we used RNA-seq data (PRJNA679450) from developmental stages (larvae to fully emerged sclerotized beetles) and diverse tissues of ESBB produced during the in-house ESBB genome study to evaluate the gene expression dynamics further. RT-qPCR and enzymatic assays further corroborated the transcriptome data.

A. Gene expression dynamics across life stages of ESBB

A.1. Gene family wise comparison

All detoxifying enzyme families were downregulated in the pupae, non-feeding stage, suggesting that the expression of genes related to detoxification was costly and should be optimally expressed as per requirements, for instance, during host feeding. This phase-specific variation (Figure 2D) showed that the

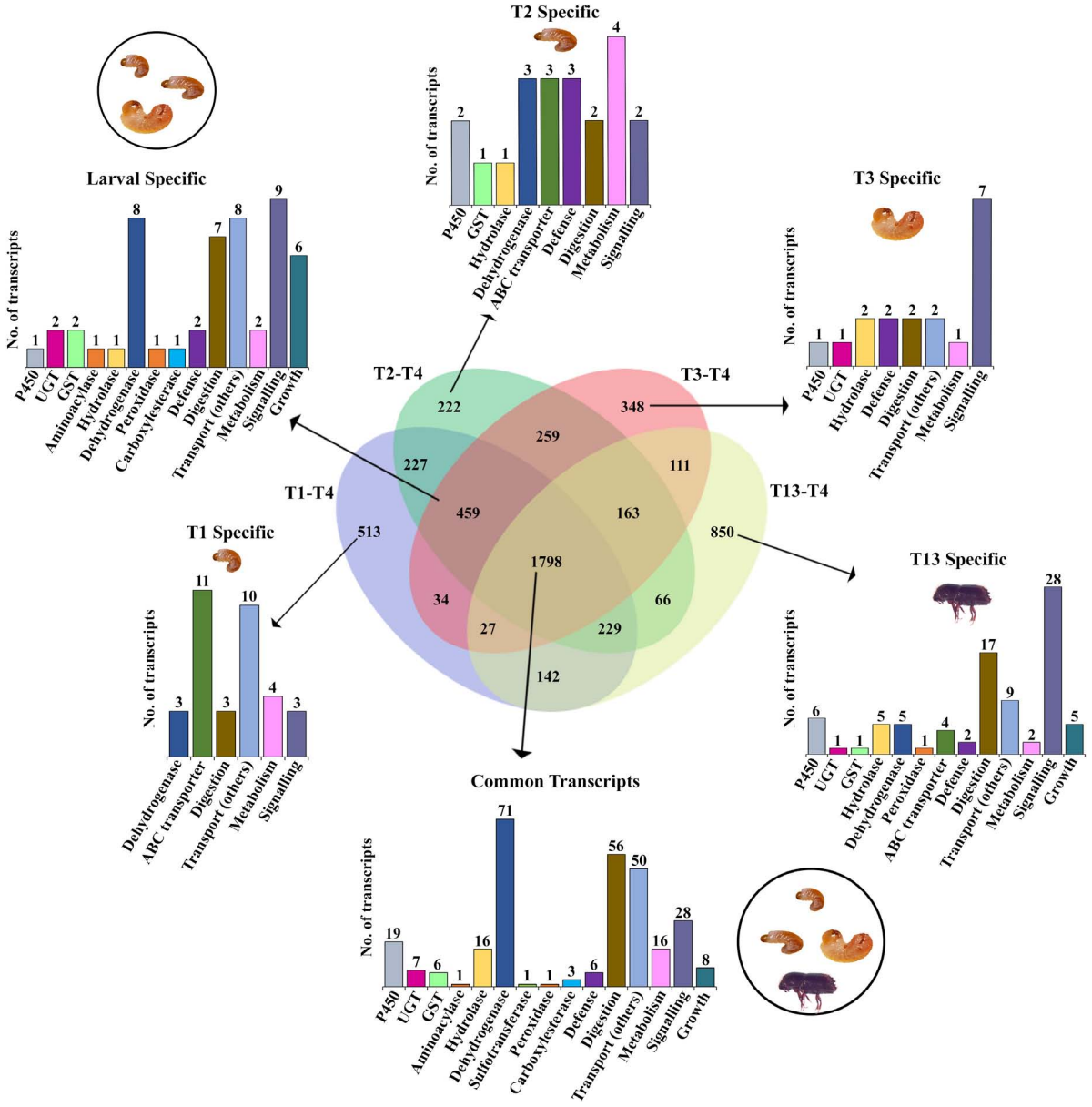

FIGURE 5
Venn diagram representation of feeding vs. non-feeding stage comparison for upregulated enzymes using FDR $p < 0.05$ and fold change ≥ 2 as the threshold for significance. Numbers within the Venn diagram represent the number of contigs found for each group. The bar graph corresponds to the number of contigs of each gene family identified from the list (**Supplementary material 36**).

expression of detoxifying enzymes considerably relies on host encounters and active feeding in ESBB.

A.1.1. Differentially expressed Cytochromes

A.1.1.(a). Cytochromes involved in detoxification

In this study, many detoxification-related cytochrome families (CYP 4, 6, and 9) were overexpressed during the adult life stage. The cytochrome gene expression of the *Dendroctonus* species, close relatives of *I. typographus*, has been extensively researched concerning the detoxification of host allelochemicals. For example, 64 P450s were identified in *D. armandii* at various life stages (larvae, pupae, and adults), and RT-qPCR showed upregulation of 41 of these genes in later life stages as compared to larvae. After host feeding, 19 CYP genes of these 41 genes showed overexpression as compared to the unfed beetles (Dai et al., 2015). *Dendroctonus* bark beetles showed a significant, non-sex-specific change in gene expression of CYP6DG1, CYP6BW5, CYP6DJ2, CYP9Z18, and CYP9Z20 during the early hours of host feeding, implying that cytochrome families 6 and 9 were also involved in the xenobiotic response in beetles as well (Sarabia et al., 2019). In *D. rhizophagus*, the role of CYPs from the CYP4, CYP6, and CYP9 families in detoxification was also confirmed. Recently, three CYPs involved in monoterpene oxidation and one CYP involved in aggregation were identified and characterized in *D. ponderosae* (Chiu et al., 2019a,b). CYP6CR2 is an epoxidase involved in exo-brevicomin

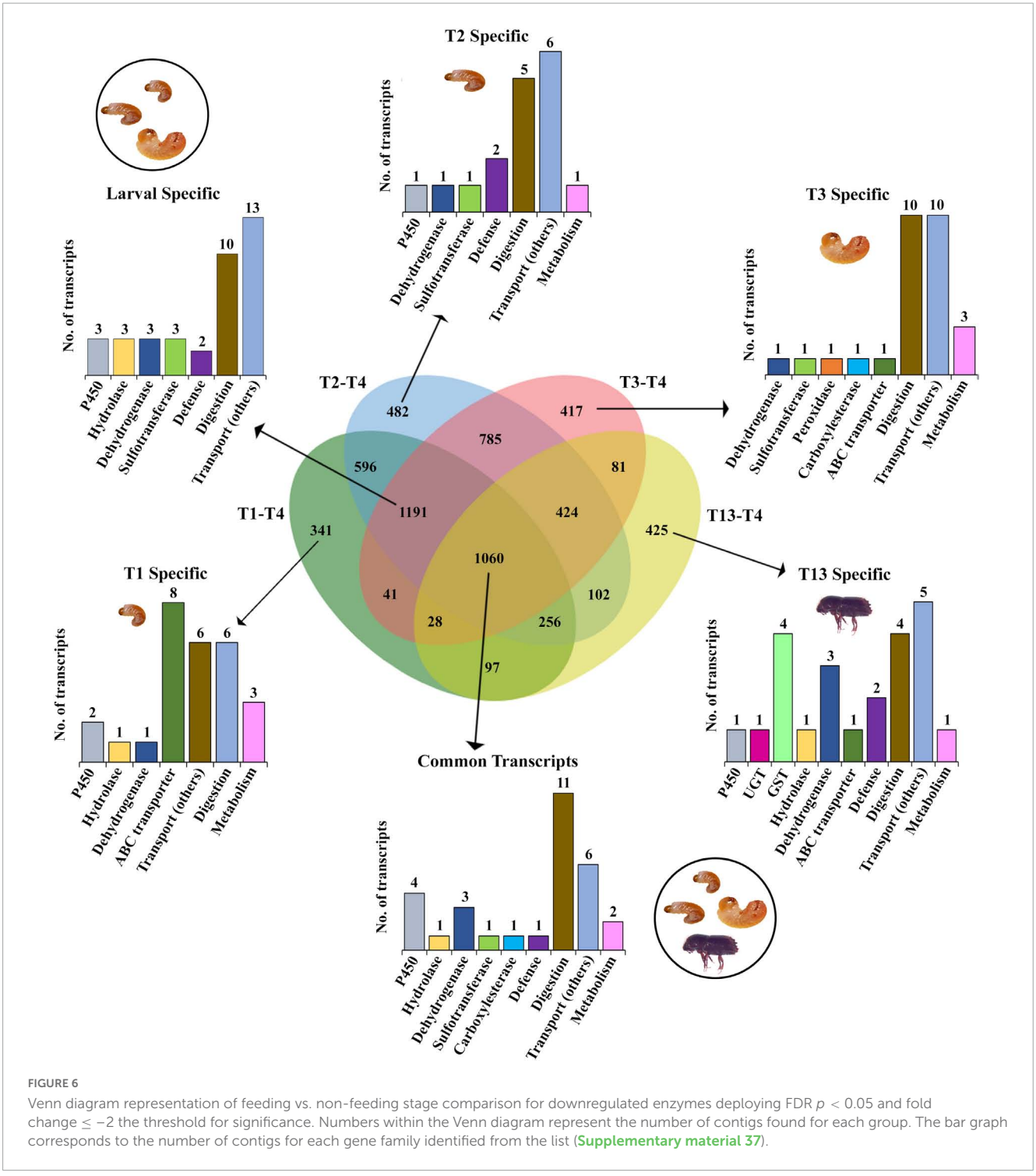

FIGURE 6
Venn diagram representation of feeding vs. non-feeding stage comparison for downregulated enzymes deploying FDR $p < 0.05$ and fold change ≤ -2 the threshold for significance. Numbers within the Venn diagram represent the number of contigs found for each group. The bar graph corresponds to the number of contigs for each gene family identified from the list (**Supplementary material 37**).

biosynthesis and pheromone generation in male mountain pine beetles after they leave the brood tree, but CYP6CR2 decreases during host tree selection and mating (Song et al., 2014). In *Sitophilus zeamais*, terpinen-4-ol fumigation induced differential regulation of cytochrome genes related to detoxification, such as CYP4BH1 (up), CYP6BW2 (up), CYP6DJ1 (up), CYP6DG1 (up), and P450 9E2 (down) (Huang et al., 2018, 2019). Hence, cytochromes are vital components in insect adaptations, including bark beetles.

CYPs, particularly those belonging to the CYP6 gene family, are reported to play a role in detoxification, toxin resistance, and other functions such as pheromone synthesis (Nadeau et al., 2017; Ramakrishnan et al., 2022). In previous investigations, the CYP4 and CYP9 genes have also been reported to have a sex-specific expression when bark beetles are exposed to host tree allelochemicals. For instance, the sex-specific expression of four CYP4 (AY2, G27, BD1, and BG1) and cytochrome P450 9E2 genes were identified in *I. paraconfusus*. The CYP4AY1, CYP4BG1,

10.3389/ffgc.2023.1124754

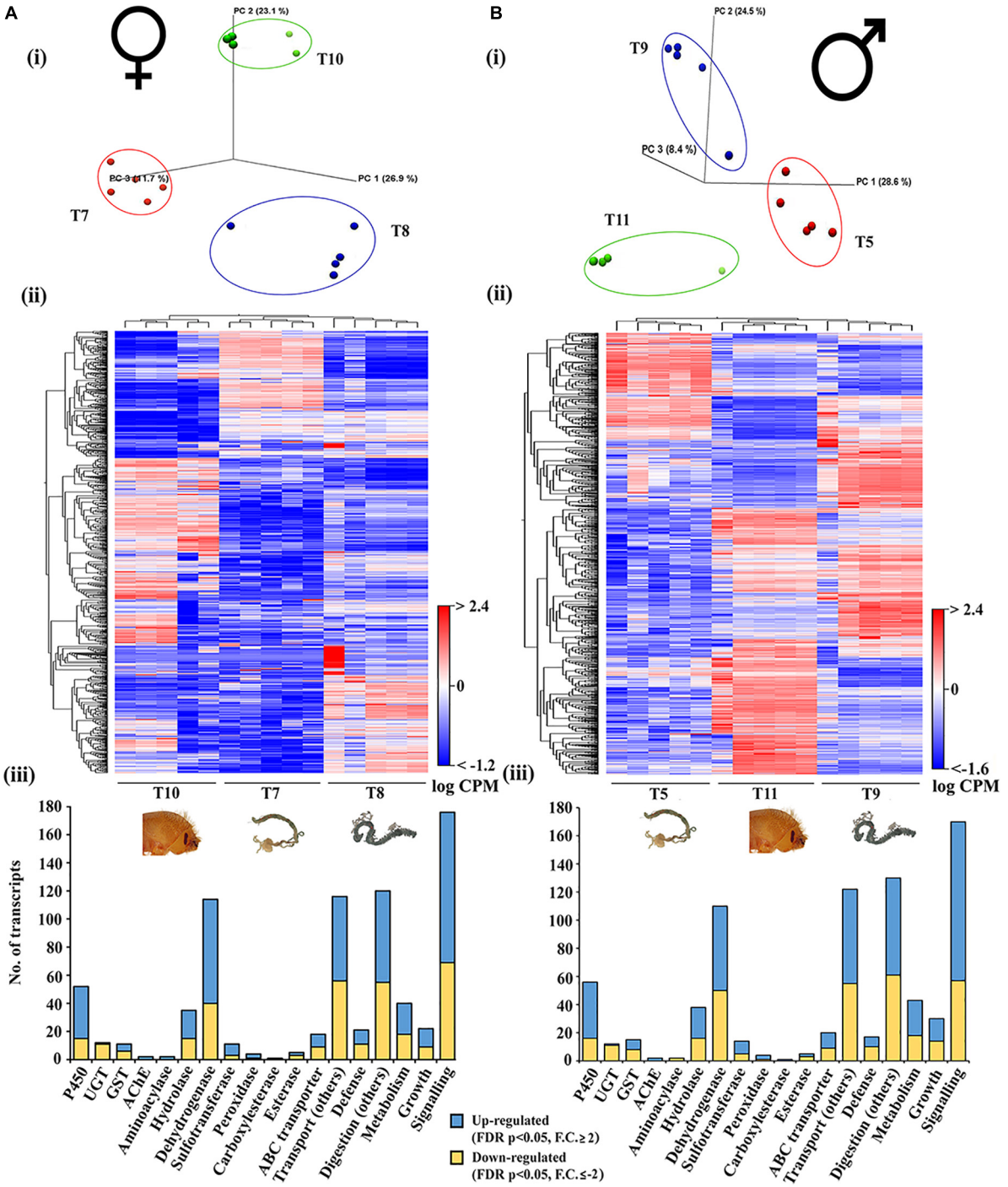

FIGURE 7
Tissue-specific comparison in callow male and female beetles. **(A)** Callow female head (T10), Callow female gut (T7), and Callow female fat body (T8) ($N = 5$). **(B)** Callow male head (T11), Callow male gut (T5), and Callow male fat body (T9) ($N = 5$). (i) PCA plots showing sample clustering. (ii) Heat maps representing gene clustering. The color spectrum, stretching from blue to red, represents TMM-adjusted log CPM expression values obtained after DGE analysis. (iii) Bar graphs showing differentially expressed contigs of detoxification-related enzyme families and other essential enzymes related to defense, digestion, transport, metabolism, signaling, and growth after group-wise comparison between different developmental life stages. Analysis was done using the CLC workbench using FDR $p < 0.05$ and fold change ± 2 as cut-offs for significance.

and CYP9T1 genes are expressed in male *I. paraconfusus*, suggesting their putative involvement in synthesizing male-specific aggregation pheromones (Huber et al., 2007). Similarly, after exposing *D. rhizophagus* to host-tree monoterpenes, differential expression of the CYP4G27, CYP4AY1, and CYP4AY2 genes was observed in the female and male antenna and gut (Cano-Ramirez et al., 2013). In our data, the CYP4BH1 gene was highly expressed in ESBB adults, whereas the CYP4BG1 and CYP4BD1 gene expression were low. The differential expression of these genes suggested that feeding regulates their expression. While we

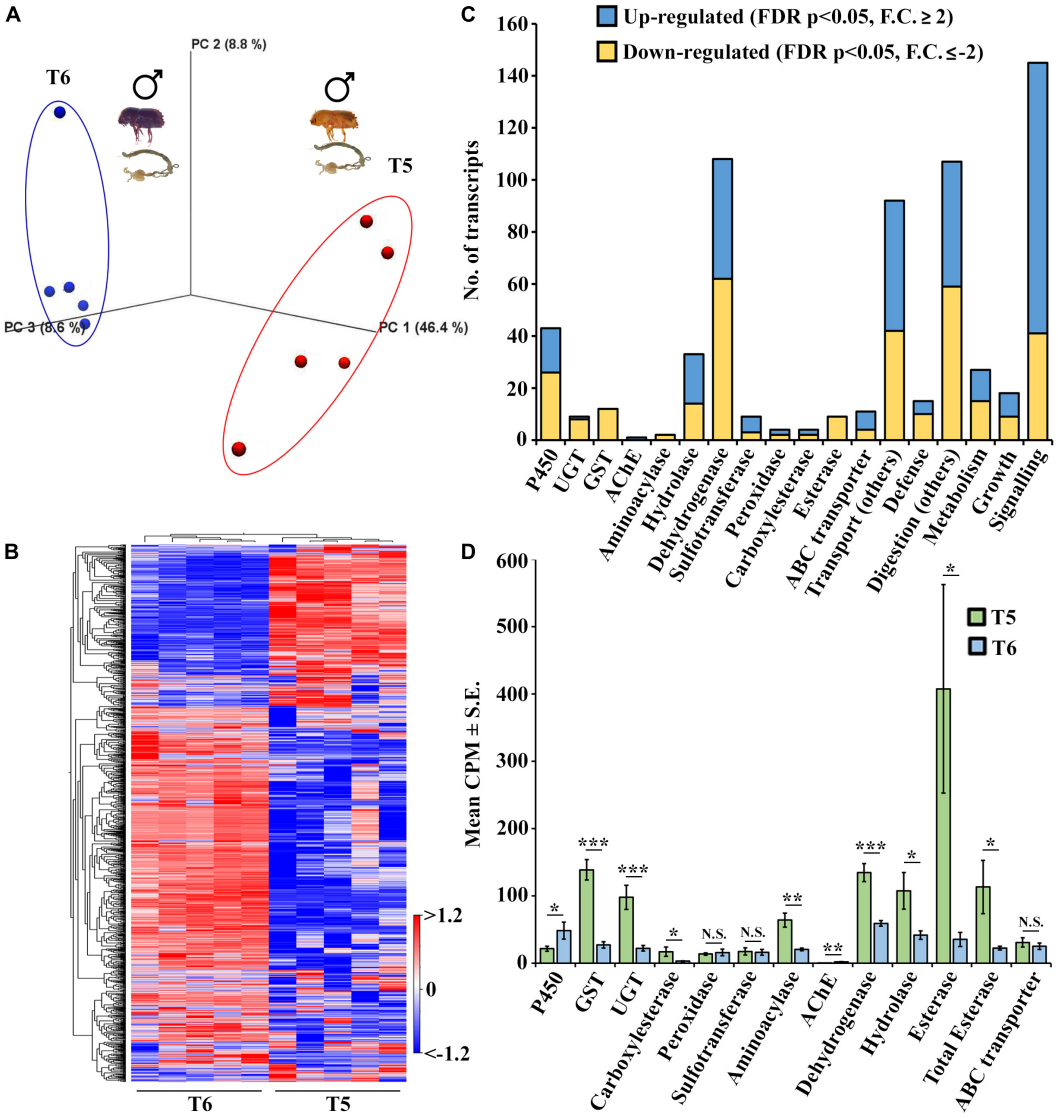

FIGURE 8
Comparison between sclerotized male gut (T6) vs. callow male gut (T5) $N = 5$. **(A)** PCA plots showing sample clustering. **(B)** Heat maps representing gene clustering. The color spectrum, stretching from blue to red, represents TMM-adjusted log CPM expression values obtained after DGE analysis. **(C)** Bar graphs showing the differentially expressed contigs of specific detoxification-related enzyme families and other important enzymes related to defense, digestion, transport, metabolism, signaling, and growth between sclerotized male gut (T6) vs. callow male gut (T5). **(D)** Detoxification genes expressed as the average of total differentially expressed genes in each family between the sclerotized male vs. the callow guts. Gene families on the x-axis plotted against their corresponding mean CPM values ± S.E. One-tailed *T*-test was performed to obtain the significant differences between the two stages. * represents $p < 0.05$, ** represents $p < 0.01$, *** represents $p < 0.001$, and NS represents non-significant difference. DGE analysis was done using CLC workbench with FDR $p < 0.05$ and a fold change ± 2 cut-off.

did not determine the sex of these ESBB adults, the regulation may be sex-specific and related to pheromone biosynthesis pathways, as reported earlier for *Dendroctonus ponderosae* (Nadeau et al., 2017). However, this needs to be functionally validated in ESBB.

Previous research has verified that some of the identified CYP6 family cytochromes (CYP6DJ1, CYP6BW1, and CYP6BW3) in *Dendroctonus* spp. are involved in pheromone biosynthesis pathways during the oxidation of host terpenes (Chiu et al., 2019b). Symbiotic blue-stain fungi vectored by bark beetles synthesize bicyclic ketals, i.e., pheromones and other semiochemicals (exo-brevicomin, endo-brevicomin, and trans-conophthorin) and help the beetles to colonize healthy trees (Lee et al., 2006; Zhao et al., 2019). A recent study showed that the CYP6CR2 and CYP6DE5 genes were highly expressed under the treatment of terpenoids, whereas silencing of these genes significantly reduced the activity of P450 and increased the mortality of adults after exposure to terpenoids. CYP6CR2 expression was considerably higher in larvae and sclerotized adults, with lower expression in starving adult mountain pine beetles (Robert et al., 2013, 2016; Liu et al., 2022). A transcriptome study of the imidacloprid resistance (IR) and isogenic susceptible (IGS) strains of *Aphis gossypii* revealed that the resistant strain had high gene expression of cytochrome P450 4G15-like (Kim et al., 2015). We found that the CYP6CR2 gene was expressed 400-fold higher in sclerotized adult beetles than in the other stages. Cytochrome P450 4G15-like gene expression

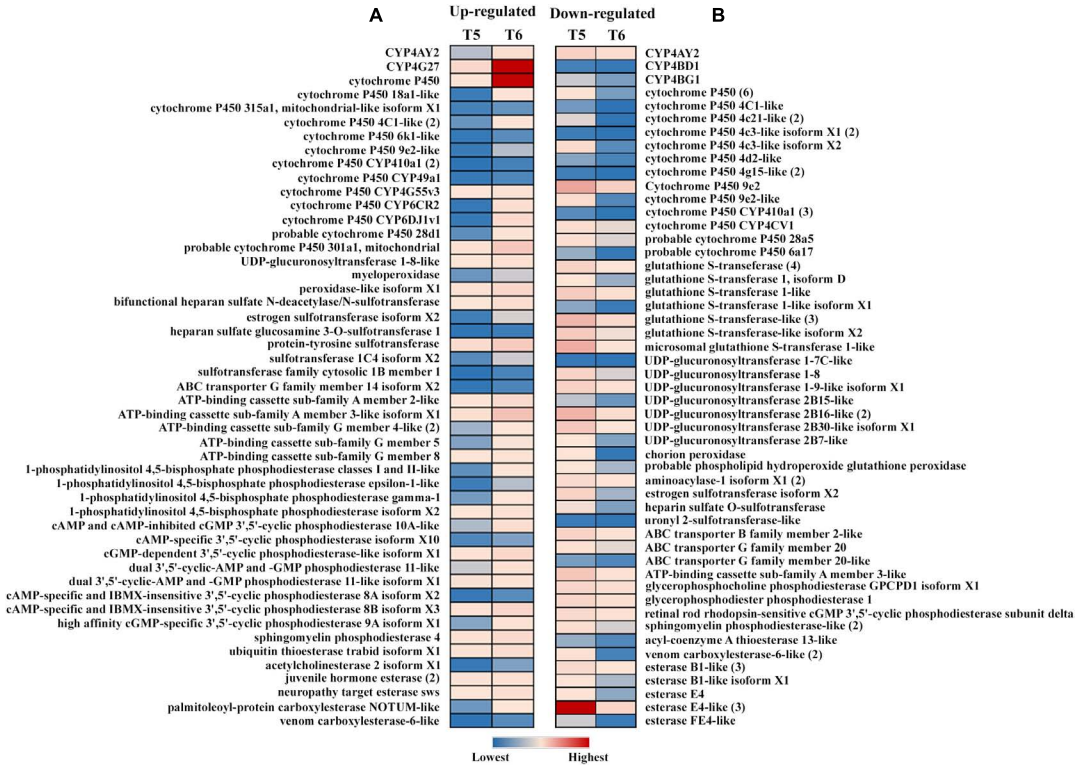

FIGURE 9
Expression profiles of detoxification-related genes in the sclerotized male gut (T6) vs. callow male gut (T5) (N = 5). **(A)** Upregulated genes FDR corrected $p < 0.05$ and equal or above the threshold of fold change of 2; **(B)** downregulated genes FDR corrected $p < 0.05$ and equal or below the threshold of fold change of −2. The expression level is represented in different colors indicating the TMM-adjusted log CPM expression mean values.

was also higher in adult ESBB, suggesting that both genes may play a role in detoxifying plant-allelochemicals.

A.1.1.(b). Cytochromes involved in other physiological functions

In general, cytochrome genes are involved in many critical physiological functions in addition to detoxification. For instance, ecdysteroid 26-hydroxylase encoded by CYP18A1 is a key hormone inactivation enzyme. CYP18A1 is expressed in many of the target tissues of ecdysteroid (20E) in *Drosophila* larvae, and CYP18A1 inactivation slows the larval development and causes pupal mortality, while CYP18A1 overexpression causes late embryonic lethality. According to these findings, the inactivation of 20E is required for proper growth, and CYP18A1 is a crucial enzyme in this process (Guittard et al., 2011). In the current study, the CYP18A1-like gene was constitutively expressed from the initial larvae to the adult, which showed that uniform expression of this gene may aid larval development and pupal formation and adult development (**Figure 3B**). The enzyme Cytochrome P450 306A1 is involved in the metabolism of insect hormones, such as ecdysteroid C25-hydroxylase activity, and the breakdown of synthetic pesticides. The effective conversion of keto-diol to keto-triol in CYP306A1 transfected S2 cells *via* carbon 25 hydroxylation suggests that CYP306A1 works as a carbon 25 hydroxylase and plays an essential role in ecdysteroid production during insect development (Niwa et al., 2004). Cytochrome P450 306A1 gene was highly expressed in the pupal stage, suggesting that it may aid in the pupal transition into an adult. The enzyme CYP4C1 is involved in abiotic stress tolerance. For instance, silencing of CYP4C1 causes *B. tabaci* to have much lower heat resistance and higher cold tolerance, implying that CYP4C1 is a significant regulator in temperature adaptation and geographical distribution (Shen et al., 2021). The CYP4C1-like gene was highly expressed in the sclerotized adult ESBB, suggesting its putative involvement in winter survival, range expansion, and adaptability to different environments. Chalkbrood is the most common fungal disease in honeybees, and transcriptome investigation of the immunological defenses of *A. cerana* larvae to *A. apis* infection revealed that the fungal-infected strain had a high expression of the cytochrome P450 6A1-like gene (Guo et al., 2019). The cytochrome P450 6A1-like gene was significantly expressed in the ESBB pupal stage, suggesting that it may aid pupal resistance to fungal infection (**Figure 3B**). Interestingly, CYP4BD1 was expressed in all larval stages and sclerotized adults but not in the pupa (**Figure 3B**). CYP4BD1 expression was higher in males and did not differ significantly in females compared to unfed individuals; it might be required for male-specific physiological activities such as pheromone production and/or juvenile hormone biosynthesis (Tillman et al., 1998, 2004; Helvig et al., 2004; Huber et al., 2007).

A.1.2. Differentially expressed UGTs and GSTs

We found UGTs and GSTs expressed in various life stages and gut tissues of ESBB (**Figure 3**). UGTs are endoplasmic reticulum-associated enzymes that perform glycosylation using

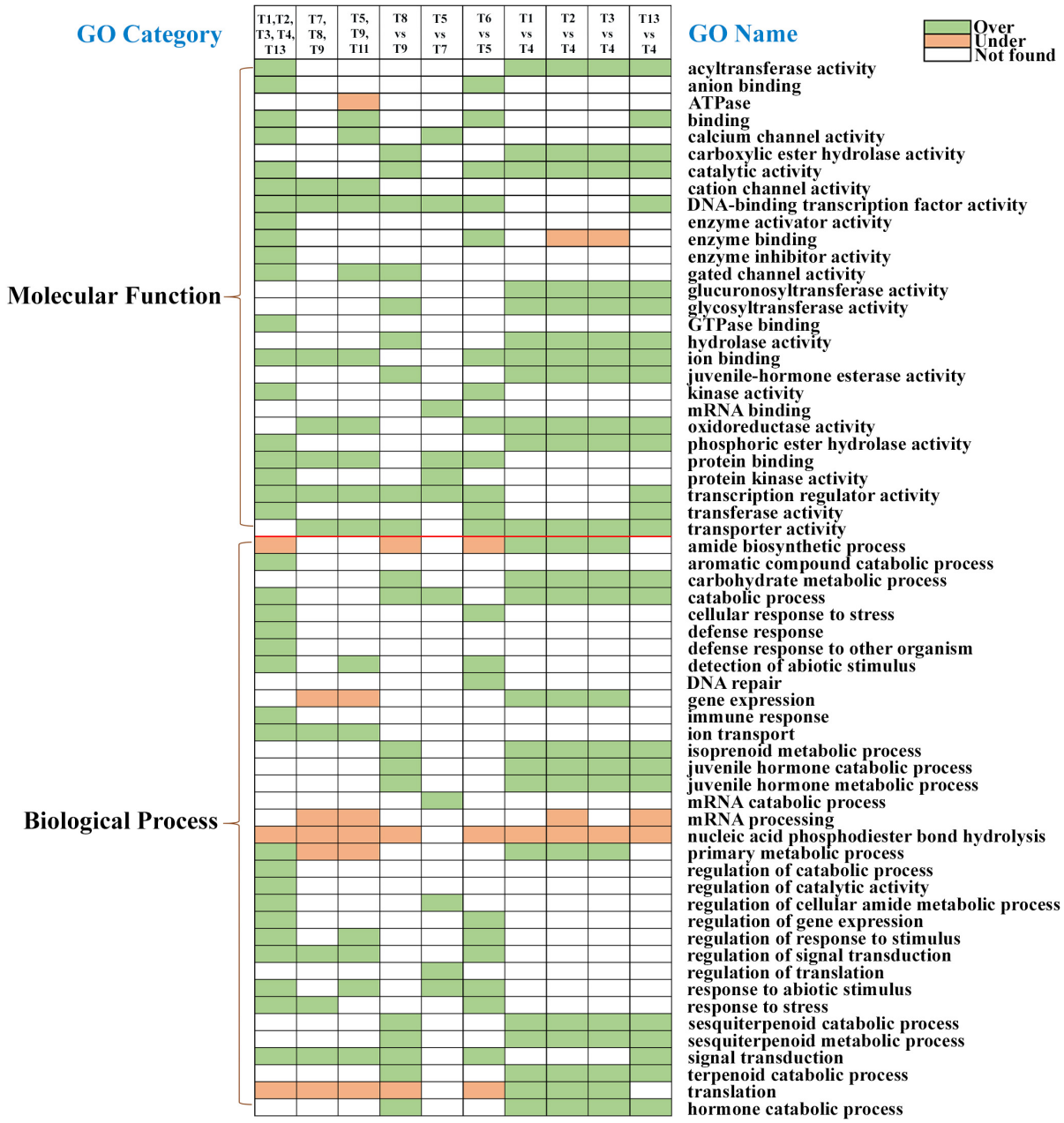

FIGURE 10
Critical physiological processes in different ESBB sample comparisons after GO enrichment analysis (FDR $p < 0.05$, fold change ≥ 2). Green boxes are over-enriched, orange boxes are under-enriched, and white boxes represent processes not occurring in a particular comparison.

UDP-glucose as an active sugar source. The protein structures are composed of N-terminal aglycone substrate-binding and C-terminal UDP-glycoside binding domains. About 40 UGTs in *H. armigera* and 44 UGTs in *Bombyx mori* were identified, and two UGT genes, UGT41B3 and UGT40D1, have been linked to metabolizing gossypol *via* glycosylation in *H. armigera* (Ahn et al., 2012; Krempl et al., 2016). Ecdysteroid UDP-glycosyltransferase (EGT), a baculovirus-encoded protein, activates and regulates insect molting by ecdysteroid hormones (Shen et al., 2018). UGTs were reported to aid host plant allelochemical detoxification in *Spodoptera* (Roy et al., 2016). The UDP-glucuronosyltransferase 2B10 (UGT2B10) is a detoxifying enzyme specializing in the N-linked glucuronidation of numerous drugs and xenobiotics. In our investigation, the UDP-glucuronosyltransferase 2B10-like gene was significantly expressed in sclerotized adults, suggesting that it may play a role in detoxification (**Figure 3B**). The UDP-glucuronosyltransferase 1-8 (UGT1A8) is an enzyme that participates in the glucuronidation pathway, which converts small lipophilic compounds into water-soluble, excretable metabolites (Wang et al., 2013). UDP-glucuronosyltransferase 1-8 and UDP-glucuronosyltransferase 1-8-like genes were expressed in ESBB larvae, probably facilitating food digestion and excretion.

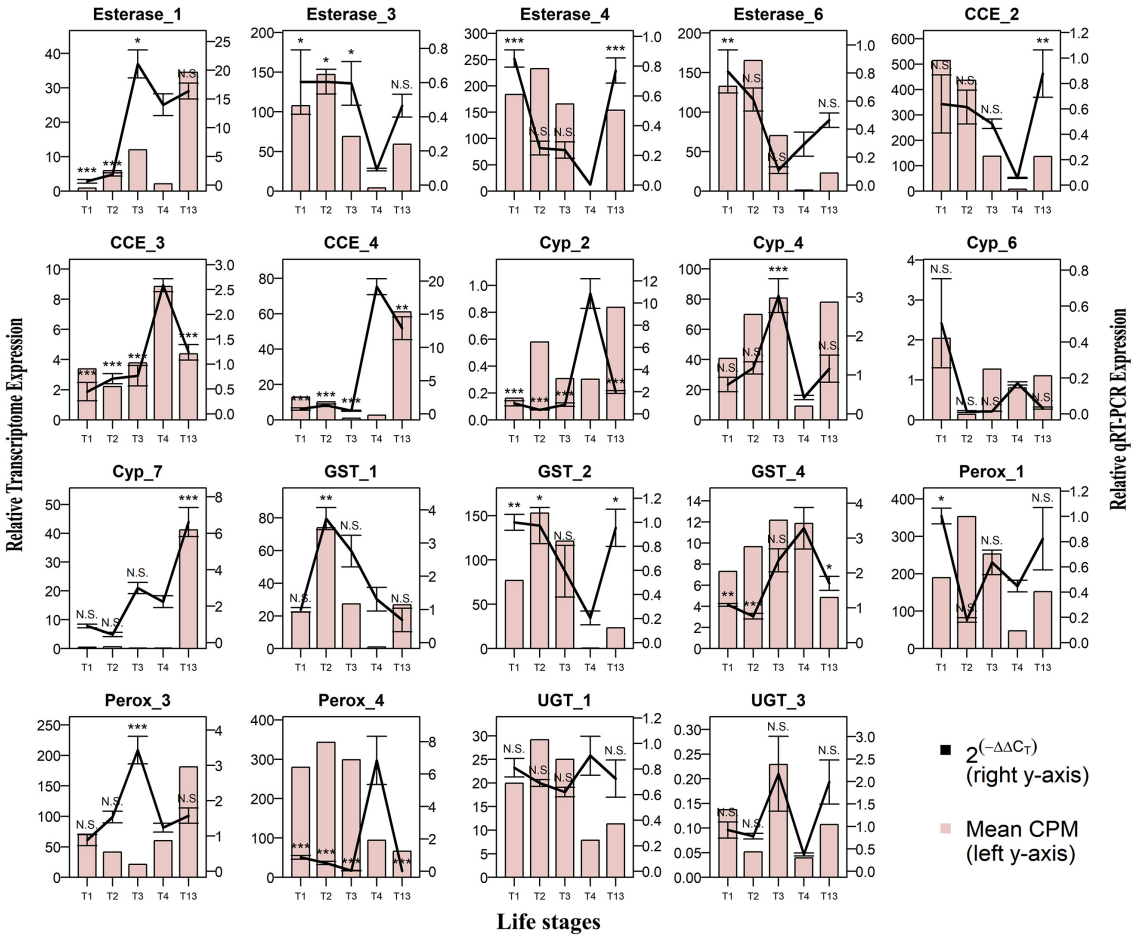

FIGURE 11
Comparison of RNA-seq and RT-qPCR data for the relative expression of 19 genes in developmental life stages. Life stages: 1st instar larvae (T1), 2nd instar larvae (T2), 3rd instar larvae (T3), pupae (T4), and sclerotized adult beetles (T13) on the *x*-axis plotted against relative expression in RNA seq ($N = 5$) represented as mean CPM on the left *y*-axis, and relative expression in RT-qPCR ($N = 4$) represented as mean 2^{-}-($\Delta\Delta$Ct) ± S.E. on the right y-axis. The bar graph represents CPM-based expression from RNA-seq, and the solid line represents RT-qPCR expression. Tukey's HSD was performed with a 95% confidence level with T4 as the control group, and *p*-values were generated as per the fit model. * represents $p < 0.05$, ** represents $p < 0.01$, *** represents $p < 0.001$, and *N.S.* represents non-significant difference.

Glutathione S-transferases are well-known for mediating insecticide resistance by reductive dehydrochlorination or conjugation reactions (Kostaropoulos et al., 2001; Enayati et al., 2005; Song et al., 2022). In *S. litura*, RNA-seq-based DGE studies were used to identify 8 GSTs and verify the involvement of GSTS1 in tomatine metabolism (Li et al., 2019). Previous studies have reported 16 GSTs from four different groups (delta, epsilon, sigma, and theta) in the Chinese white pine beetle, and these GSTs were expressed in all developmental stages and tissues (antennae, gut, and reproductive tissues) (Gao et al., 2020). Similarly, the present study observed GSTs expression during the different life stages and tissues of ESBB, implying its physiological importance in bark beetles (**Figure 3**).

A.1.3. Differentially expressed esterases

The overexpression of esterases (ESTs), particularly those belonging to class I (clade A-C), aids detoxification, while class III (clade I-M), containing CCE and AChEs (clade I-M), works primarily through target site mutation-based resistance to pyrethroids, organophosphates, and carbamates, but their role in detoxification has also been documented concerning malathion detoxification (Wei et al., 2020). The NOTUM gene encodes a palmitoleoyl-protein carboxylesterase that works as a negative regulator of the Wnt signaling pathway. NOTUM knockdown lentivirus inhibits colon adenocarcinoma development *in vitro* and *in vivo* by reducing tumor proliferation, shrinking tumor size, and enhancing apoptosis (Gong et al., 2021). The palmitoleoyl-protein carboxylesterase NOTUM-like gene was significantly expressed in ESBB pupae, implying that it regulates apoptosis in the non-feeding stage. Carboxylesterase 6 has the highest expression level in the social wasp *P. varia*, while solitary wasps have little or no expression, suggesting that this protein may play a defensive role in social wasps (Yoon et al., 2020). The venom carboxylesterase-6-like gene was highly expressed in ESBB sclerotized adults, suggesting its putative involvement in the ESBB defense mechanism (**Figure 3A**). In insects, chorion peroxidase (pxt) has a role in the formation of a rigid and insoluble egg chorion by catalyzing chorion protein crosslinking through dityrosine formation and phenol oxidase-catalyzed chorion melanization (Li et al., 2004). Chorion peroxidase and peroxidase-like isoform X1 were highly expressed in sclerotized

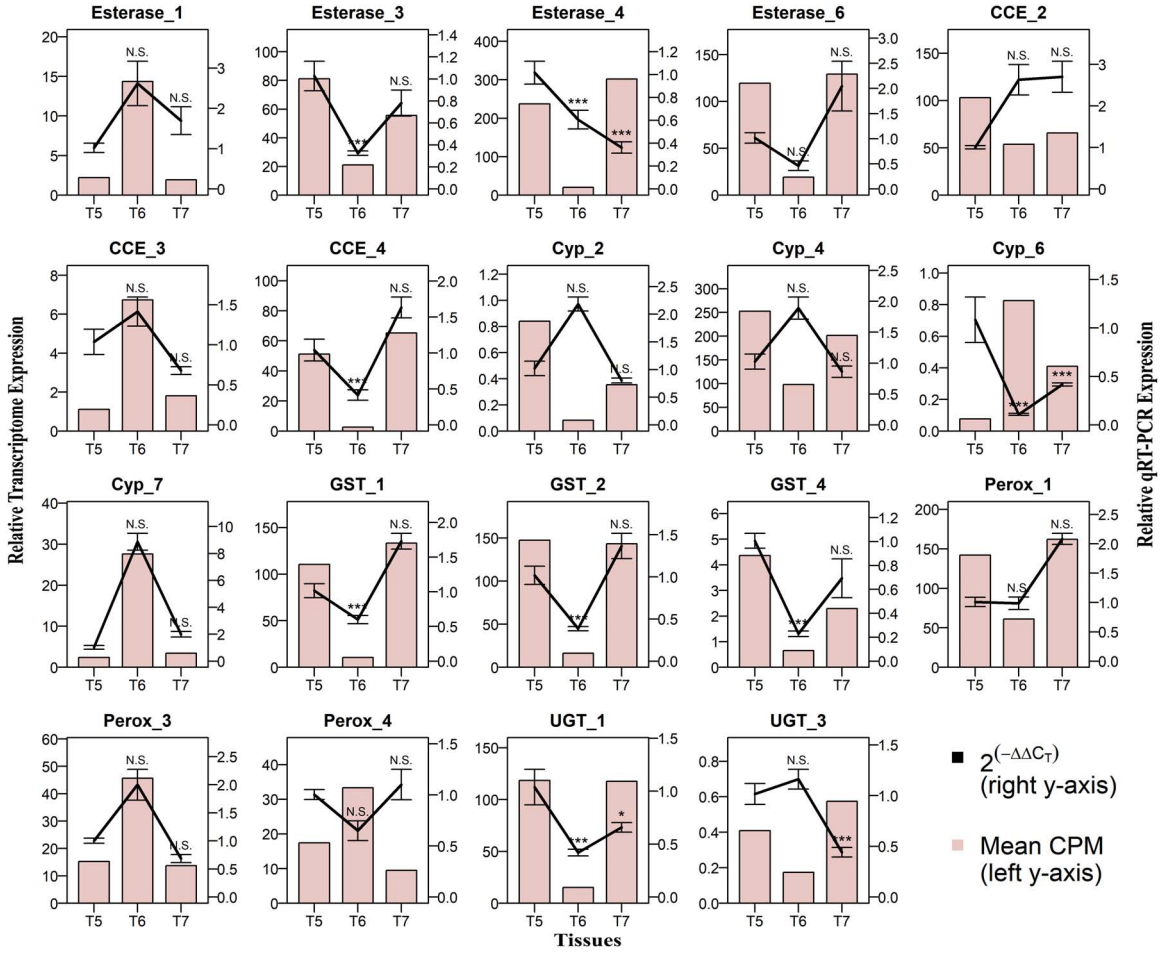

FIGURE 12
Comparison of RNA-seq and RT-qPCR data for the relative expression of 19 genes in gut tissues. Callow male gut (T5), sclerotized adult male gut (T6), and callow female gut (T7) on the *x*-axis plotted against relative expression in RNA seq (N = 5) represented as mean CPM on the left *y*-axis and relative expression in RT-qPCR (N = 4) represented as mean 2^{-}-(ΔΔCt) ± S.E. on the right *y*-axis. The bar graph represents the mean CPM-based expression from RNA-seq transcriptome data, and the solid line represents RT-qPCR expression. Relative expressions in T6 and T7 were compared against those in T5 using Tukey's HSD with a 95% confidence level, and *p*-values were generated as per the fit model. * represents $p < 0.05$, *** represents $p < 0.001$, and *N.S.* represents non-significant difference.

adults, suggesting that they may function in egg production and development (**Figure 3A**). In *Myzus persicae*, the overexpression of E4 and FE4 genes have a role in insecticide resistance (Field and Devonshire, 1998). In our study, the esterase FE4-like gene was expressed in all larval and sclerotized adult stages but not in the pupae, suggesting that it may influence the detoxification of host allelochemicals during feeding (**Figures 3A, B**). However, esterase B1-like and esterase E4 genes were expressed in pupae, suggesting that they may be involved in fat consumption for energy production during pupa-to-adult development. However, our observations need further experimental validation.

A.1.4. Differentially expressed hydrolases

The phospholipase activity of the mitochondrial cardiolipin hydrolase gene is essential for mitochondrial fusion and fission, allowing cells to cope with the increased nucleotide demand during DNA synthesis (Huang et al., 2011). In the current study, the mitochondrial cardiolipin hydrolase-like gene was highly expressed in late larval and adult stages, suggesting its involvement in larvae-to-pupae conversion and adult development. The protein deubiquitination carried by the ubiquitin C-terminal hydrolase (UCH) and ubiquitin-specific processing protease (UBP) protein families is involved in various biological activities in animals, fungi, and plants (Wang et al., 2018). Ubiquitin carboxyl-terminal hydrolase 1-like gene was significantly expressed in pupae and adult ESBB stages compared to the larvae, suggesting its putative role in later stages of ESBB development.

A.1.5. Differentially expressed transporter enzymes

ATP-binding cassette transporter proteins transport a variety of molecules across cell membranes. ATP binding cassette subfamily A member 12 (ABCA12) protein is essential for transporting fats (lipids) and enzymes in the cells and maintaining the layers of lipids within the epidermis to prevent water loss (dehydration) and to allow normal skin development (Fukuda et al., 2012; Akiyama, 2014). The expression of ABC transporters remained primarily constant throughout development, suggesting their importance

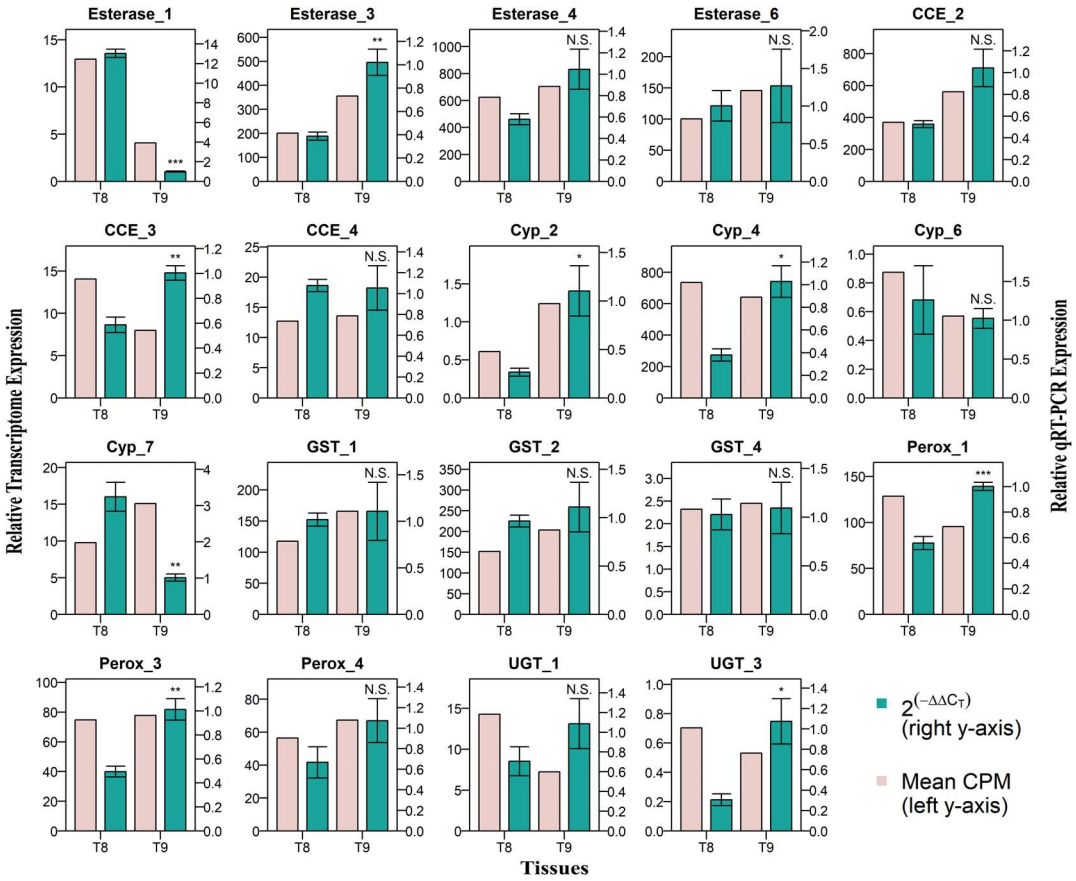

FIGURE 13
Comparison of RNA-seq and RT-qPCR data for the relative expression of 19 genes during RT-qPCR in the fat body tissues. Callow female fat body (T8) and callow male fat body (T9) on the *x*-axis plotted against relative expression in RNA seq ($N = 5$) represented as mean CPM on the left *y*-axis, and relative expression in RT-qPCR ($N = 4$) represented as mean 2^{-}-($\Delta\Delta$Ct) ± S.E. on the right y-axis. Light brown bars represent mean transcriptome expression, and dark green bars represent RT-qPCR expression. Student's *T*-test was performed with a 95% confidence level, and *p*-values were generated after comparing RT-qPCR expression between T9 vs. T8. * represents $p < 0.05$, ** represents $p < 0.01$, *** represents $p < 0.001$, and *N.S.* represents the non-significant difference.

throughout the life cycle of ESBB. In the larval and adult stages, the ABC transporter subfamily genes (D member 3, G member 1-like, and G member 4) exhibited higher expression than in the pupal stage (**Figure 3**). Interestingly, ABC transporter expression dropped dramatically during the early ESBB larval stage, but increased again in the pupal and adult stages, demonstrating its role in later developmental stages in ESBB. Interestingly, all ABC transporter subfamily A genes had higher expression in pupae, suggesting that these genes might play an essential role during the pupal stage. The ABC transporter subfamilies D and G genes expressed in other ESBB life stages may be involved in detoxification during feeding. Furthermore, ATP-binding cassette sub-family A member 2-like and ATP-binding cassette sub-family A member 3-like isoform X1 were highly expressed in ESBB pupae, suggesting that they may facilitate proper epidermis formation in ESBB. The ATP-binding cassette sub-family G member 4 (ABCG4) subunit of heterodimeric precursor transporters for eye-pigment synthesis was identified in *Drosophila's* brain and eye (Oldfield et al., 2002). In the current study, the ATP-binding cassette sub-family G member 4, ATP-binding cassette sub-family G member 4-like, and ATP-binding cassette sub-family G member 4 isoform X1 genes were significantly expressed in ESBB sclerotized adults as compared to larvae and pupae, indicating that they may play a similar role in eye pigment synthesis. The ATP binding cassette subfamily G member 8 (ABCG8) and member 5 (ABCG5) genes produced sterolin-1 and sterolin-2, respectively, and combinedly formed sterolin protein (Calandra et al., 2011). Sterolin is a plant sterol transporter protein that moves substances across cell membranes and is found mainly in intestines and liver cells. Sterolin also helps cholesterol regulation; typically, about 50 percent of the cholesterol in the diet is absorbed by the body (Calandra et al., 2011). The ATP-binding cassette sub-family G member 8 and ATP-binding cassette sub-family G member 5 genes were significantly expressed in ESBB pupae, implying that they may be involved in fat absorption and accumulation to provide energy for adult conversion.

A.1.6. Differentially expressed dehydrogenases

The mitochondrial glutamate dehydrogenase catalyzes the conversion of L-glutamate into alpha-ketoglutarate, an essential intermediate in the tricarboxylic acid cycle. It plays a role in insulin homeostasis and is also involved in learning and memory reactions by increasing the turnover of the excitatory neurotransmitter glutamate (Plaitakis et al., 2000, 2017). In this

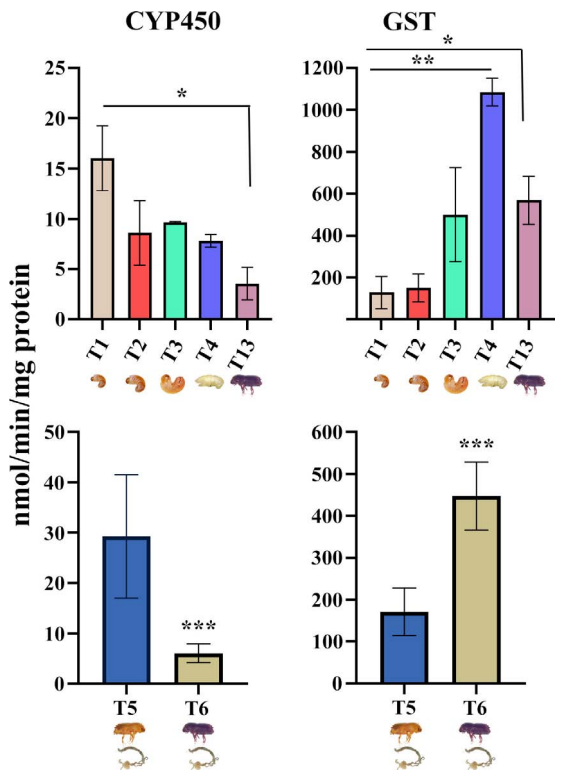

FIGURE 14
The activities of selected enzymes, glutathione S-transferase (GST) and cytochrome P450 (CYP450), measured in the developmental and tissue-specific stages. The bars represent mean values and whiskers standard deviations in four biological replicates. One-way ANOVA was performed between the life stages (T1, T2, T3, T4, and T13) and Student's *t*-test between guts of callow and sclerotized males (T6 vs. T5). * indicates that values are significantly different from each other at * $p < 0.05$, ** $p < 0.01$, ***$p < 0.001$. GST, and CYP450 activity are expressed as nmol/min/mg protein.

study, glutamate dehydrogenase mitochondrial-like protein and glutamate dehydrogenase mitochondrial-like isoform X2 genes were highly expressed from late larvae to adults, suggesting that they may be involved in energy production and ESBB development (**Supplementary material 3**). In the glycolytic pathway, the glyceraldehyde-3-phosphate dehydrogenase (GAPDH) is a highly conserved enzyme that catalyzes the transformation of glyceraldehyde-3-phosphate to glycerate-1, 3-biphosphate, and produces NADH. In the *Mortierella alpina* fungus, the overexpression or knockdown of GAPDH1 and GAPDH2 genes significantly accumulated or reduced lipid content, respectively (Wang et al., 2020). In the current study, the glyceraldehyde-3-phosphate dehydrogenase-like and glyceraldehyde-3-phosphate dehydrogenase 2-like genes were highly expressed from late larvae to adults. Fungi and insects share common metabolic pathways, and our data implied that these genes may have a role in lipid accumulation to satisfy the energy requirement for ESBB while searching for a suitable host. The glucose dehydrogenase genes are expressed at all stages of *Drosophila* development and play an essential role in the eclosion process and cuticular remodeling (Krasney et al., 1990). Similarly, the glucose dehydrogenase (FAD, quinone)-like gene was expressed in all ESBB developmental stages, suggesting its involvement in the eclosion process and cuticular remodeling in ESBB. In *Ips pini*, the short-chain oxidoreductase ipsdienol dehydrogenase (IDOLDH) converts (-)-ipsdienol to ipsdienone and plays a role in determining pheromone composition (Figueroa-Teran et al., 2016). In the current study, ipsdienol dehydrogenase transcripts were expressed from initial larvae to adults, suggesting that they may have a similar role in pheromone biosynthesis and composition in ESBB (Ramakrishnan et al., 2022). The glutaryl-CoA dehydrogenase (GCDH) is an enzyme found in mitochondria and involved in the breakdown of amino acids like lysine, hydroxylysine, and tryptophan, which are building blocks of proteins (Basinger et al., 2006). The glutaryl-CoA dehydrogenase mitochondrial gene was expressed in all larval and adult stages in our study but not in the pupae, implying a function in protein formation during ESBB feeding stages. However, such observations need to be further empirically validated.

B. Tissue-specific comparison

We observed tissue-specific regulation of many genes; for instance, CYP6K1-like and CYP410A1 had higher expression in the head and lower expression in the gut and fat body, respectively, implying a role in olfaction as odorant degrading enzymes (ODEs) (Baldwin et al., 2021). Similarly, juvenile hormone epoxide hydrolase 1-like (JHEH 1-like) gene transcripts were more abundant in the gut and fat body than in the head, as these two tissues are the site of production and metabolism of aggregation pheromone in ESBB (Ramakrishnan et al., 2022). Our findings (**Figure 7**) were consistent with earlier research showing the upregulation of detoxification-related genes and pheromone genes in the gut and fat body (Keeling et al., 2016; Li et al., 2019; Ramakrishnan et al., 2022). Cytochrome P450 4C1 (CYP4C1) transcripts are mainly engaged in the metabolism of insect hormones and the breakdown of synthetic insecticides. Whiteflies, after silencing CYP4C1, showed significantly lower heat resistance and higher cold tolerance, which indicates that CYP4C1 is a critical regulator in temperature adaptation and influences the geographical distribution and dispersal of whiteflies (Shen et al., 2021). In the present study, the cytochrome P450 4C1-like gene transcripts showed high levels in male and female fat bodies and heads of callow ESBB, suggesting a putative role in thermal adaptation during new host finding. In bark beetles, the CYP9T2 (gut-specific cytochrome P450) gene hydroxylates myrcene to ipsdienol and functions toward the end of the pheromone biosynthesis pathway (Sandstrom et al., 2006). Gut-specific cytochrome P450 transcript was expressed in both male and female callow ESBB fat body, suggesting a putative role in pheromone biosynthesis and odor degradation.

The glutathione S-transferases (GSTs) play an essential role in detoxifying xenobiotic toxins in insects, including insecticides (Balakrishnan et al., 2018). Most GSTs, such as glutathione S-transferase-like, glutathione S-transferase-like isoform X2, and microsomal glutathione S-transferase 1-like transcripts, are expressed in the callow beetle's gut, suggesting roles in food digestion and detoxification of plant xenobiotics. UDP-glucuronosyltransferases (UGTs) are significant phase II drug metabolism and multifunctional detoxification enzymes that play an essential role in insect resistance to various plant allelochemicals and pesticides (Neumann et al., 2016; Roy et al., 2016; Cui

et al., 2020). Most UGTs, such as UDP-glucuronosyltransferase 1-8, UDP-glucuronosyltransferase 1-9-like isoform X1, UDP-glucuronosyltransferase 2B10-like, UDP-glucuronosyltransferase 2B16-like, UDP-glucuronosyltransferase 2B30-like isoform X1, and UDP-glucuronosyltransferase 2C1, are expressed in the male and female callow ESBB gut, implying a role in multifunctional detoxification during maturation feeding of ESBB. Aminoacylase 1 (ACY1) was found in many tissues and organs, where it may be involved in breaking down proteins that are no longer needed. A novel aminoacylase isolated from *Burkholderia* sp. strain LP5_18B effectively catalyzes N-lauroyl-L-amino acids synthesis (Takakura and Asano, 2019). In the current study, aminoacylase-1 isoform X1 was expressed in both callow ESBB male and female guts, suggesting a role in dietary protein breakdown. Epoxide hydrolases (EH) are essential regulators of lipid epoxides and play a role in detoxification processes, and their inhibition can have a physiological and pathological impact (Morisseau, 2013). Epoxide hydrolase 4-like gene was expressed highly in the fat bodies of both male and female callow ESBB, suggesting that it may be required for lipid regulation and detoxification and also help in the physiological process upon conversion of immature callow to mature sclerotized (black) beetles. Glycosyl hydrolases hydrolyze the glycosidic bond between two or more carbohydrates or between a carbohydrate and a non-carbohydrate moiety. The enzymatic activity and ancestral origin suggest that glycoside hydrolase families 45 (GH45s) were likely essential for the adaptation of phytophagous beetles to feed on plants (Busch et al., 2019). GH45 transcript was highly expressed in both the gut and fat bodies of males and females of callow ESBB, suggesting roles in food digestion, detoxification, and host adaptation. The juvenile hormone epoxide hydrolase (JHEH) is an essential enzyme in the breakdown pathways of juvenile hormone (JH) in insects; it converts JH to JH-diol and hydrolyzes JH acid to JH acid-diol, and JHEH titers regulate the entire process of insect development. In the gypsy moth *Lymantria dispar*, the knockdown of JHEH1 slightly delayed larval development (Wen et al., 2018). The juvenile hormone epoxide hydrolase 1-like transcripts were highly expressed in the male and female guts and fat bodies of callow ESBB, suggesting that they may be involved in JH pathway regulation. The genome-wide microarray study in gut tissue of Indian silkworm *Bombyx mori* Sarupat race resistant against BmNPV infection of gut showed upregulation of the lactase-phlorizin hydrolase-like gene, indicating that the gene plays a role in the antiviral immune response (Lekha et al., 2015). The lactase-phlorizin hydrolase-like transcript was highly expressed in the gut of callow ESBB, probably performing a similar role by protecting the beetles from getting infected with pathogenic viruses during maturation feeding.

Sulfotransferase catalyzes the sulfate conjugation of catecholamines such as dopamine, prostaglandins, leukotriene E4, drugs, and xenobiotic substances by using 3'-phospho-5'-adenylyl sulfate (PAPS) as a sulfonate donor. Sulfonation enhances the water solubility of most chemicals and facilitates their excretion, but it can also lead to bioactivation and the formation of active metabolites (Shimada et al., 2004). In the present study, the sulfotransferase 1 family member D1-like transcript was highly expressed in the gut of callow ESBB, pointing toward similar xenobiotic catabolism. The chorion peroxidase is expressed in mature eggs of *Aedes aegypti* mosquitoes and is involved in forming a rigid and insoluble chorion (egg shell) by catalyzing chorion protein cross-linking (Han et al., 2000). Esterases are often present in antennae and help in odor desensitization (Guo and Smith, 2022). Esterase E4 transcripts were expressed in the head of callow ESBB, possibly performing a similar function. The ABCB subfamily contains both full-transporters and half-transporters; ABCB2 and ABCB10 are half-transporters with evolutionarily conserved roles and protect arthropods from oxidative stress (Wang et al., 2019). ABC transporter B family member 2-like and ATP-binding cassette sub-family B member 10 mitochondrial isoform X1 transcripts were expressed in both the gut and fat body of callow ESBB, suggesting that they may be involved in the transport and subsequent excretion of entomotoxic substances during maturation feeding.

C. Sex-specific comparison

C.1. Sex-specific gene expression dynamics in callow ESBB gut

Most of the upregulated genes were linked to cytochromes and peroxidases in the male gut, indicating roles in establishing an attack on the new host tree as the pioneer sex and capacity to aid digestion and detoxification of dietary material. Other key genes expressed in the gut, such as UGTs, GSTs, esterase sub-families, hydrolases, and peroxidases, were not differentially regulated, indicating conserved expression requirements. Cytochrome P450s are essential for insecticide tolerance in the endoparasitoid wasp *Meteorus pulchricornis*; the cytochrome P450 301A1 (mitochondrial) gene was expressed highly after insecticide exposure compared to control (Xing et al., 2021). In the current study, a probable cytochrome P450 301A1 (mitochondrial) transcript was highly expressed in a callow male gut and fat body of ESBB, suggesting a role in supporting male beetles to deal with host allelochemicals during host colonization (**Supplementary Figure 3**).

C.2. Sex-specific gene expression dynamics in callow ESBB fat bodies

Apart from the detoxification-, digestion-, and defense-related genes, we observed that the genes related to pheromone biosynthesis were expressed in the fat body tissues, which are the site of pheromone production in ESBB. Our finding was coherent with the copulation and infestation mechanism where ESBB male, the pioneer sex, releases sex aggregation pheromones to attract the conspecifics during new host colonization (Ramakrishnan et al., 2022). Various *Ips* species, including *I. paraconfusus* and *I. pini*, have been observed to use the sex-specific expression of CYPs to convert host allelochemicals into aggregation pheromones (Huber et al., 2007; Song et al., 2013; Tittiger and Blomquist, 2017; Blomquist et al., 2021). However, the function of these genes is yet to be confirmed in *I. typographus*. Furthermore, additional validation of the pheromone biosynthesis pathway genes of ESBB may reveal sex-specific roles. All stages of ESBB are exposed to the chemical defenses of the trees to varying degrees. These enzymes are produced at different times in different tissues throughout life, and it is believed that variations in their expression or catalytic activity are related to the need for compound detoxification. The transcriptome of the sex pheromone gland of the sandfly, *Lutzomyia longipalpis,* revealed the expression of NADP + dependent farnesol dehydrogenase, which is implicated in the isoprenoid pathway (Gonzalez-Caballero et al., 2013).

Furthermore, a farnesol dehydrogenase-like transcript was highly expressed in callow male ESBB fat body, implying its involvement in pheromone synthesis.

D. Gene expression differences between callow and sclerotized male gut (T6 vs. T5)

As the gene expression in the gut reflects the feeding behavior, differences in gene expression between callow and sclerotized adult guts have additional adaptive significance. Many physiologically important genes are differentially regulated in these tissues. For instance, the cytochrome P450 9E2-like gene showed higher gene expression in the sclerotized male gut of *Ips typographus* than in the callow male gut (Ramakrishnan et al., 2022). In the current study, the cytochrome P450 9E2-like was extensively expressed in the larval and adult stages, suggesting a role in ESBB feeding and aggregation pheromone production (**Figure 9**). In *Aedes aegypti*, transcriptome comparison between an insecticide-susceptible strain (Bora7) and insecticide-resistant strain (KhanhHoa7) showed upregulation of cytochrome P450 4C1, 4C3, 4C21, 4D1, 4D1 isoform X2, 4D2, 4D2 isoform X2, 4G15, 6A2, 6A8, 6D3, and 9E2 in the resistant strain (Lien et al., 2019). The comparative genome-wide analysis of single-base nucleotide polymorphisms between insecticide-resistant MED whitefly lines and insecticide-susceptible MED whitefly lines showed potential resistance markers (SNP) in cytochrome P450 4C21-like transcripts (Wang et al., 2022). In the current study, the cytochrome P450 4C1-like, cytochrome P450 4C21-like, cytochrome P450 4C3-like isoform X1, cytochrome P450 4C3-like isoform X2, cytochrome P450 4D2-like, cytochrome P450 4G15-like, cytochrome P450 6K1-like, Cytochrome P450 9E2, and cytochrome P450 9E2-like transcripts were expressed in the callow male gut, suggesting that they may have a role in detoxification mechanism during maturation feeding.

Furthermore, glutathione S-transferase, glutathione S-transferase 1, isoform D, glutathione S-transferase 1-like, glutathione S-transferase 1-like isoform X1, glutathione S-transferase-like, glutathione S-transferase-like isoform X2, and microsomal glutathione S-transferase 1-like transcripts were highly expressed in the callow male gut, suggesting that they may help freshly emerged callow beetles to detoxify plant allelochemicals. UDP-glucuronosyltransferase 1-8, UDP-glucuronosyltransferase 1-9-like isoform X1, UDP-glucuronosyltransferase 2B15-like, UDP-glucuronosyltransferase 2B16-like, UDP-glucuronosyltransferase 2B16-like, UDP-glucuronosyltransferase 2B30-like isoform X1, and UDP-glucuronosyltransferase 2B7-like transcripts were highly expressed in the callow male gut, suggesting roles in detoxification.

In the mosquito, *Culex pipiens*, the evolution of overproduced esterases is implicated in organophosphate pesticide resistance (Raymond et al., 1998). Esterase B1-like, esterase B1-like isoform X1, esterase E4, and esterase E4-like transcripts were highly expressed in the callow male gut, implying a role in ESBB digestion and detoxification. The mitochondrially encoded NADH: ubiquinone oxidoreductase core subunit 1 (MT-ND1) gene encodes a protein called NADH dehydrogenase 1. This protein is part of a large enzyme complex known as complex I, active in mitochondria that convert the energy from food to power the biochemical reactions in the cell (Valentino et al., 2004). NADH dehydrogenase [ubiquinone] 1 alpha subcomplex subunit 9 (mitochondrial), NADH dehydrogenase [ubiquinone] 1 beta subcomplex subunit 11 (mitochondrial), subunit 5 (mitochondrial), subunit 8 (mitochondrial), NADH dehydrogenase [ubiquinone] 1 subunit C2 and NADH dehydrogenase [ubiquinone] flavoprotein 1 (mitochondrial), and NADH dehydrogenase [ubiquinone] iron-sulfur protein 6 (mitochondrial) transcripts were highly expressed in the callow male gut, possibly to aid food digestion and energy metabolism.

In summary, many physiologically essential genes, such as cytochromes, GSTs, UGTs, esterases, and dehydrogenases, were differentially expressed in the callow or sclerotized ESBB gut, probably supporting different behavioral traits (i.e., such as maturation feeding, host finding, and new colony establishments). The ecological relevance of such fine-tuned gene expression demands further functional corroboration.

Enzymatic assay endorsing the RNA-seq findings

The enzymatic assay results drew attention toward fine-tuned protein expressions that reflect the feeding and non-feeding behavior of ESBB. The larvae are in an intense feeding and growth stage, which involves detoxification and digestion of host materials. During the pupal stage, the beetle becomes sedentary and non-feeding, and most of its energy reserves are deployed in ecdysis and metamorphosis. The pupae develop into the callow stage and again start feeding and become sclerotized, as they require energy to fly out, start a new attack, and aggregate the conspecifics (by male ESBB). Our assay results pinpointed that most GST proteins are abundant in pupae and have putative functions in body development and overwintering (for pupae). In contrast, cytochromes were expressed more in both larvae and adult ESBB and participate primarily in detoxification and digestion during host feeding. These results were in accordance with the previous studies suggesting life stage-specific expression of various genes in different insect groups (Perkin and Oppert, 2019; Oppert et al., 2020; Ernst and Westerman, 2021).

Study limitations

The science of insect physiology has dramatically benefited from RNA-seq-based studies. This trend will continue as omics technology becomes more accessible and less expensive. However, there are some limitations in transcriptomics studies. Regulatory proteins are more likely to influence physiological response than mRNAs with short half-lives, i.e., an increase or decrease in mRNA may not always equate to a corresponding change in protein abundance or activity. Such limitations also exist in the current study. To alleviate some of these limitations, we performed RT-qPCR to validate the most crucial DEGs with independently collected fresh samples. Furthermore, we used an enzymatic assay to cross-check the protein expression and activity of two key proteins in ESBB, namely, cytochromes and GSTs. The results of the enzymatic and RT-qPCR assays correlated positively with the transcriptome findings, with minor exceptions. The physiological

functions of several crucial genes discussed in the present study need additional validation.

Conclusion

Overall, the current transcriptome study combined with RT-qPCR validation and enzymatic assays reveals gene expression dynamics specific to ESBB life stages, sex, and tissues. Our findings indicated that ESBB has allelochemical resistance mechanisms that are an essential precondition for the hormetic response in larval and adult ESBB growth, ultimately contributing to the widespread successful colonization of coniferous trees. The physiologically essential genes identified in this work should be functionally validated to better understand ESBB physiology and adaptation to a nutritionally challenging diet containing host defense allelochemicals. Furthermore, the RNAi-based approach can target key genes for survival and adaptation, identified in the present study, for ESBB management as described in detail by Joga et al. (2021).

Data availability statement

The datasets presented in this study can be found in online repositories. The names of the repository/repositories and accession number(s) can be found below: https://www.ncbi.nlm.nih.gov/- PRJNA679450.

Author contributions

AR conceptualized the study and performed the RNA-seq analysis. AN and GS did the lab work. AR, AN, and KM interpreted the data. AN and AR prepared the figures. AN wrote the first draft. AR, KM, AN, and GS prepared the final draft. All authors read and approved the final draft.

Funding

This research was supported by grant no. CZ.02.1.01/0.0/0.0/15_003/0000433, "EXTEMIT–K project," financed by the Operational Program Research, Development and Education (OP RDE), and Internal Grant Agency (A_06_22, AISHA NASEER) at the Faculty of Forestry and Wood Sciences, Czech University of Life Sciences, Prague, Czechia. AR and KM are supported by grant no. CZ.02. 1.01/0.0/0.0/16_019/0000803 financed by OP RDE.

Acknowledgments

We acknowledge the support from Faculty for Forestry and Wood Sciences (FLD), CZU, for conducting the present study. We also acknowledge Dr. Roman Modlinger and Dr. Jiri Synek, FLD, CZU, for assistance in beetle collection and maintenance. We acknowledge the *Ips typographus* genome manuscript team's contribution in generating the valuable RNA-seq data. We appreciate the helpful feedback provided by the reviewers and especially the handling editor. Special thanks to Prof. Fredrik Schlyter for his constructive comments and encouragement.

Conflict of interest

The authors declare that the research was conducted in the absence of any commercial or financial relationships that could be construed as a potential conflict of interest.

Publisher's note

All claims expressed in this article are solely those of the authors and do not necessarily represent those of their affiliated organizations, or those of the publisher, the editors and the reviewers. Any product that may be evaluated in this article, or claim that may be made by its manufacturer, is not guaranteed or endorsed by the publisher.

Supplementary material

The Supplementary Material for this article can be found online at: https://www.frontiersin.org/articles/10.3389/ffgc.2023.1124754/full#supplementary-material

SUPPLEMENTARY FIGURE 1
Volcano plots of different comparisons were made for the study with the number of differentially expressed contigs (FDR $p < 0.05$, fold change $\pm$ 2). **(A)** Group-wise comparison between L1-L3 (T1-T3), pupa (T4), and sclerotized adult whole-body (T13); **(B)** T1 vs. T4; **(C)** T2 vs. T4; **(D)** T3 vs. T4; **(E)** T13 vs. T4; **(F)** tissue-specific group-wise comparison between the callow female head (T10), gut (T7) and fat body (T8); **(G)** tissue-specific group-wise comparison between the callow male head (T11), gut (T5) and fat body (T9); **(H)** sex-specific comparison between callow male gut (T5) vs. callow female gut (T7); **(I)** sex-specific comparison between callow female fat body (T8) vs. callow male fat body (T9); **(J)** comparison between sclerotized male gut (T6) vs. callow male gut (T5); and **(K)** group-wise comparison between all gut tissues sclerotized male gut (T6), callow male gut (T5), and callow female gut (T7). $N = 5$. Up-head arrows represent upregulation (fold change ≥ 2), and down-head arrows represent downregulation (fold change ≤ -2). Red dots represent significantly expressed contigs (FDR $p < 0.05$), and blue dots represent non-significantly expressed contigs (FDR $p > 0.05$). The X-axis represents the $\log_2$ fold-change plotted against $-\log_{10}$ (p-values).

SUPPLEMENTARY FIGURE 2
Dynamics of other detoxification-related genes. Different life stages of ESBB on the x-axis are plotted against the average CPM values of all the contigs of a gene family on the y-axis. Different line colors represent individual gene families. The total CPM was calculated by taking the average of all the differentially expressed contigs (FDR $p < 0.05$, fold change $\pm$ 2) of each gene family. T1, T2, and T3 represent the first, second, and third larval stage, respectively, T4 represent pupal stage, and T13 represent the sclerotized adult stage of *I. typographus*.

SUPPLEMENTARY FIGURE 3
Sex-specific comparison. **(A)** Callow male gut (T5) vs. Callow female gut (T7) ($N = 5$). **(B)** Callow female fat body (T8) vs. Callow male fat body

(T9) (N = 5). (i) PCA plot showing sample clustering. (ii) Heatmaps representing gene clustering. The color spectrum, stretching from blue to red, represents TMM-adjusted log CPM expression values obtained after DGE analysis. (iii) Bar graphs showing differentially expressed contigs of specific detoxification-related enzyme families and other essential enzymes related to defense, digestion, transport, metabolism, signaling, and growth. Analysis was done using the CLC workbench (FDR $p < 0.05$ and fold change ± 2).

SUPPLEMENTARY FIGURE 4
Group-wise comparison between sclerotized male gut (T6), callow male gut (T5), and callow female gut (T7) (N = 5). (i) PCA plot showing sample clustering. (ii) Heatmaps representing gene clustering. The color spectrum, stretching from blue to red, represents TMM-adjusted log CPM expression values obtained after DGE analysis. (iii) Bar graphs showing differentially expressed contigs of specific detoxification-related enzyme families and other essential enzymes related to defense, digestion, transport, metabolism, signaling, and growth after group-wise comparison between the three tissues. Analysis was done using CLC workbench with FDR $p < 0.05$ and fold change ± 2 cut off.

SUPPLEMENTARY TABLE 1
RNA-seq statistics for ESBB life stage and tissue transcriptomes (T1-T13).

SUPPLEMENTARY TABLE 2
Protein concentrations for four replicates used in enzymatic assays (T1-T6 and T13).

SUPPLEMENTARY MATERIAL 1
Metadata file for all the life stages and tissues used for the study.

SUPPLEMENTARY MATERIAL 2
Functional information about the genes used for designing primer for RT-qPCR and their functional information in NCBI BLASTn.

SUPPLEMENTARY MATERIAL 3
Expression browser for group-wise comparison between all life stages (T1, T2, T3, T4, and T13) containing all the differentially expressed genes (FDR $p < 0.05$, fold change ± 2) and their mean CPM values for each stage (N = 5).

SUPPLEMENTARY MATERIAL 4
Expression browser for all the differentially expressed genes in T1 compared against T4 as control (FDR $p < 0.05$, fold change ± 2) and their mean CPM values for each stage (N = 5).

SUPPLEMENTARY MATERIAL 5
Expression browser for all the differentially expressed genes in T2 compared against T4 as control (FDR $p < 0.05$, fold change ± 2) and their mean CPM values for each stage (N = 5).

SUPPLEMENTARY MATERIAL 6
Expression browser for all the differentially expressed genes in T3 compared against T4 as control (FDR $p < 0.05$, fold change ± 2) and their mean CPM values for each stage (N = 5).

SUPPLEMENTARY MATERIAL 7
Expression browser for all the differentially expressed genes in T13 compared against T4 as control (FDR $p < 0.05$, fold change ± 2) and their mean CPM values for each stage (N = 5).

SUPPLEMENTARY MATERIAL 8
Expression browser for group-wise comparison for tissue-specific female comparison between callow female gut (T7), callow female fat body (T8), and callow female head (T10) containing all the differentially expressed genes (FDR $p < 0.05$, fold change ± 2) and their mean CPM values for each stage (N = 5).

SUPPLEMENTARY MATERIAL 9
Expression browser for group-wise comparison for tissue-specific male comparison between callow male gut (T5), callow male fat body (T9), and callow male head (T11) containing all the differentially expressed genes (FDR $p < 0.05$, fold change ± 2) and their mean CPM values for each stage (N = 5).

SUPPLEMENTARY MATERIAL 10
Expression browser for all the differentially expressed genes in the callow female gut (T7) compared against callow male gut (T5) as control (FDR $p < 0.05$, fold change ± 2) and their mean CPM values for each stage (N = 5).

SUPPLEMENTARY MATERIAL 11
Expression browser for all the differentially expressed genes in callow female fat body (T8) compared against callow male fat body (T9) as control (FDR $p < 0.05$, fold change ± 2) and their mean CPM values for each stage (N = 5).

SUPPLEMENTARY MATERIAL 12
Expression browser for all the differentially expressed genes in the sclerotized male gut (T6) compared against callow male gut (T5) as control (FDR $p < 0.05$, fold change ± 2) and their mean CPM values for each stage (N = 5).

SUPPLEMENTARY MATERIAL 13
Expression browser for group-wise comparison for tissue-specific male comparison between callow male gut (T5), sclerotized male gut (T6), and callow female gut (T7) containing all the differentially expressed genes (FDR $p < 0.05$, fold change ± 2) and their mean CPM values for each stage (N = 5).

SUPPLEMENTARY MATERIAL 14
Fisher extract test result for all life stages (T1, T2, T3, T4, and T13) comparison for differentially upregulated transcript IDs (FDR $p < 0.05$, fold change ≥ 2).

SUPPLEMENTARY MATERIAL 15
Fisher extract result for all life stage (T1, T2, T3, T4, and T13) comparison for differentially downregulated transcript IDs (FDR $p < 0.05$, fold change ≤ -2).

SUPPLEMENTARY MATERIAL 16
Fisher extract test result for T1 vs. T4 comparison for differentially upregulated transcript IDs (FDR $p < 0.05$, fold change ≥ 2).

SUPPLEMENTARY MATERIAL 17
Fisher extract test result for T1 vs. T4 comparison for differentially downregulated transcript IDs (FDR $p < 0.05$, fold change ≤ -2).

SUPPLEMENTARY MATERIAL 18
Fisher extract test result for T2 vs. T4 comparison for differentially upregulated transcript IDs (FDR $p < 0.05$, fold change ≥ 2).

SUPPLEMENTARY MATERIAL 19
Fisher extract test result for T2 vs. T4 comparison for differentially downregulated transcript IDs (FDR $p < 0.05$, fold change ≤ -2).

SUPPLEMENTARY MATERIAL 20
Fisher extract test result for T3 vs. T4 comparison for differentially upregulated transcript IDs (FDR $p < 0.05$, fold change ≥ 2).

SUPPLEMENTARY MATERIAL 21
Fisher extract test result for T3 vs. T4 comparison for differentially downregulated transcript IDs (FDR $p < 0.05$, fold change ≤ -2).

SUPPLEMENTARY MATERIAL 22
Fisher extract test result for T13 vs. T4 comparison for differentially upregulated transcript IDs (FDR $p < 0.05$, fold change ≥ 2).

SUPPLEMENTARY MATERIAL 23
Fisher extract test result for T13 vs. T4 comparison for differentially downregulated transcript IDs (FDR $p < 0.05$, fold change ≤ -2).

SUPPLEMENTARY MATERIAL 24
Fisher extract test result for T7, T8, and T10 comparison for differentially upregulated transcript IDs (FDR $p < 0.05$, fold change ≥ 2).

SUPPLEMENTARY MATERIAL 25
Fisher extract test result T7, T8, and T10 comparison for differentially downregulated transcript IDs (FDR $p < 0.05$, fold change ≤ -2).

SUPPLEMENTARY MATERIAL 26
Fisher extract test result for T5, T9, and T11 comparison for differentially upregulated transcript IDs (FDR $p < 0.05$, fold change ≥ 2).

SUPPLEMENTARY MATERIAL 27
Fisher extract test result T5, T9, and T11 comparison for differentially downregulated transcript IDs (FDR $p < 0.05$, fold change ≤ -2).

SUPPLEMENTARY MATERIAL 28
Fisher extract test result for T7 vs. T5 comparison for differentially upregulated transcript IDs (FDR $p < 0.05$, fold change ≥ 2).

SUPPLEMENTARY MATERIAL 29
Fisher extract test result for T7 vs. T5 comparison for differentially downregulated transcript IDs (FDR $p < 0.05$, fold change ≤ -2).

SUPPLEMENTARY MATERIAL 30
Fisher extract test result for T8 vs. T9 comparison for differentially upregulated transcript IDs (FDR $p < 0.05$, fold change ≥ 2).

SUPPLEMENTARY MATERIAL 31
Fisher extract test result for T8 vs. T9 comparison for differentially downregulated transcript IDs (FDR $p < 0.05$, fold change ≤ -2).

SUPPLEMENTARY MATERIAL 32
Fisher extract test result for T6 vs. T5 comparison for differentially upregulated transcript IDs (FDR $p < 0.05$, fold change ≥ 2).

SUPPLEMENTARY MATERIAL 33
Fisher extract test result for T6 vs. T5 comparison for differentially downregulated transcript IDs (FDR $p < 0.05$, fold change ≤ -2).

SUPPLEMENTARY MATERIAL 34
Fisher extract test result for T5, T6, and T7 comparison for differentially upregulated transcript IDs (FDR $p < 0.05$, fold change ≥ 2).

SUPPLEMENTARY MATERIAL 35
Fisher extract test result T5, T6, and T7 comparison for differentially downregulated transcript IDs (FDR $p < 0.05$, fold change ≤ -2).

SUPPLEMENTARY MATERIAL 36
List of common and unique differentially upregulated (FDR $p < 0.05$, fold change ≥ 2) transcript IDs between life stages (T1, T2, T3, T4, and T5) described in **Figure 5**.

SUPPLEMENTARY MATERIAL 37
List of common and unique differentially downregulated (FDR $p < 0.05$, fold change ≤ -2) transcript IDs between life stages (T1, T2, T3, T4, and T5) described in **Figure 6**.

References

Ahn, S. J., Vogel, H., and Heckel, D. G. (2012). Comparative analysis of the UDP-glycosyltransferase multigene family in insects. *Insect Biochem. Mol. Biol.* 42, 133–147. doi: 10.1016/j.ibmb.2011.11.006

Akiyama, M. (2014). The roles of ABCA12 in epidermal lipid barrier formation and keratinocyte differentiation. *Biochim. Biophys. Acta Mol. Cell Biol. Lipids* 1841, 435–440. doi: 10.1016/j.bbalip.2013.08.009

Balakrishnan, B., Su, S., Wang, K., Tian, R. Z., and Chen, M. H. (2018). Identification, Expression, and regulation of an omega class glutathione S-transferase in *Rhopalosiphum padi* (L.) (Hemiptera: Aphididae) under insecticide stress. *Front. Physiol.* 9:427. doi: 10.3389/fphys.2018.00427

Baldwin, S. R., Mohapatra, P., Nagalla, M., Sindvani, R., Amaya, D., Dickson, H. A., et al. (2021). Identification and characterization of CYPs induced in the *Drosophila* antenna by exposure to a plant odorant. *Sci. Rep.* 11:20530. doi: 10.1038/s41598-021-99910-9

Basinger, A. A., Booker, J. K., Frazier, D. M., Koeberl, D. D., Sullivan, J. A., and Muenzer, J. (2006). Glutaric acidemia type 1 in patients of Lumbee heritage from North Carolina. *Mol. Genet. Metab.* 88, 90–92. doi: 10.1016/j.ymgme.2005.12.008

Biedermann, P. H. W., Muller, J., Gregoire, J. C., Gruppe, A., Hagge, J., Hammerbacher, A., et al. (2019). Bark beetle population dynamics in the Anthropocene: Challenges and solutions. *Trends Ecol. Evol.* 34, 914–924. doi: 10.1016/j.tree.2019.06.002

Blomquist, G. J., Tittiger, C., MacLean, M., and Keeling, C. I. (2021). Cytochromes P450: Terpene detoxification and pheromone production in bark beetles. *Curr. Opin. Insect Sci.* 43, 97–102. doi: 10.1016/j.cois.2020.11.010

Bosch-Serra, D., Rodríguez, M. A., Avilla, J., Sarasúa, M. J., and Miarnau, X. (2021). Esterase, glutathione s-transferase and NADPH-cytochrome P450 reductase activity evaluation in *Cacopsylla pyri* L.(Hemiptera: Psyllidae) individual adults. *Insects* 12:329. doi: 10.3390/insects12040329

Bradford, M. M. (1976). A rapid and sensitive method for the quantitation of microgram quantities of protein utilizing the principle of protein-dye binding. *Anal. Biochem.* 72, 248–254.

Bras, A., Roy, A., Heckel, D. G., Anderson, P., and Karlsson Green, K. (2022). Pesticide resistance in arthropods: Ecology matters too. *Ecol. Lett.* 25, 1746–1759. doi: 10.1111/ele.14030

Busch, A., Danchin, E. G. J., and Pauchet, Y. (2019). Functional diversification of horizontally acquired glycoside hydrolase family 45 (GH45) proteins in phytophaga beetles. *BMC Evol. Biol.* 19:100. doi: 10.1186/s12862-019-1429-9

Calandra, S., Tarugi, P., Speedy, H. E., Dean, A. F., Bertolini, S., and Shoulders, C. C. (2011). Mechanisms and genetic determinants regulating sterol absorption, circulating LDL levels, and sterol elimination: Implications for classification and disease risk. *J. Lipid Res.* 52, 1885–1926. doi: 10.1194/jlr.R017855

Cale, J. A., Ding, R. S., Wang, F. A., Rajabzadeh, R., and Erbilgin, N. (2019). Ophiostomatoid fungi can emit the bark beetle pheromone verbenone and other semiochemicals in media amended with various pine chemicals and beetle-released compounds. *Fungal Ecol.* 39, 285–295. doi: 10.1016/j.funeco.2019.01.003

Cano-Ramirez, C., Lopez, M. F., Cesar-Ayala, A. K., Pineda-Martinez, V., Sullivan, B. T., and Zuniga, G. (2013). Isolation and expression of cytochrome P450 genes in the antennae and gut of pine beetle *Dendroctonus rhizophagus* (Curculionidae: Scolytinae) following exposure to host monoterpenes. *Gene* 520, 47–63. doi: 10.1016/j.gene.2012.11.059

Celedon, J. M., and Bohlmann, J. (2019). Oleoresin defenses in conifers: Chemical diversity, terpene synthases and limitations of oleoresin defense under climate change. *New Phytol.* 224, 1444–1463. doi: 10.1111/nph.15984

Chakraborty, A., Ashraf, M. Z., Modlinger, R., Synek, J., Schlyter, F., and Roy, A. (2020a). Unravelling the gut bacteriome of Ips (Coleoptera: Curculionidae: Scolytinae): Identifying core bacterial assemblage and their ecological relevance. *Sci. Rep.* 10:18572. doi: 10.1038/s41598-020-75203-5

Chakraborty, A., Modlinger, R., Ashraf, M. Z., Synek, J., Schlyter, F., and Roy, A. (2020b). Core mycobiome and their ecological relevance in the gut of five Ips bark beetles (Coleoptera: Curculionidae: Scolytinae). *Front. Microbiol.* 11:568853. doi: 10.3389/fmicb.2020.568853

Chiu, C. C., Keeling, C. I., and Bohlmann, J. (2019a). The cytochrome P450 CYP6DE1 catalyzes the conversion of α-pinene into the mountain pine beetle aggregation pheromone *trans*-verbenol. *Sci. Rep.* 9:1477. doi: 10.1038/s41598-018-38047-8

Chiu, C. C., Keeling, C. I., Henderson, H. M., and Bohlmann, J. (2019b). Functions of mountain pine beetle cytochromes P450 CYP6DJ1, CYP6BW1 and CYP6BW3 in the oxidation of pine monoterpenes and diterpene resin acids. *PLoS One* 14:e0216753. doi: 10.1371/journal.pone.0216753

Cui, X. P., Wang, C., Wang, X. X., Li, G. L., Liu, Z. G., Wang, H. F., et al. (2020). Molecular mechanism of the UDP-glucuronosyltransferase 2b20-like gene (*AccUGT2B20-like*) in pesticide resistance of *Apis cerana cerana*. *Front. Genet.* 11:592595. doi: 10.3389/fgene.2020.592595

Dai, L. L., Ma, M. Y., Wang, C. Y., Shi, Q., Zhang, R. R., and Chen, H. (2015). Cytochrome P450s from the Chinese white pine beetle, *Dendroctonus armandi* (Curculionidae: Scolytinae): Expression profiles of different stages and responses to host allelochemicals. *Insect Biochem. Mol. Biol.* 65, 35–46. doi: 10.1016/j.ibmb.2015.08.004

Davis, T. S. (2015). The ecology of yeasts in the bark beetle holobiont: A century of research revisited. *Microb. Ecol.* 69, 723–732. doi: 10.1007/s00248-014-0479-1

Enayati, A. A., Ranson, H., and Hemingway, J. (2005). Insect glutathione transferases and insecticide resistance. *Insect Mol. Biol.* 14, 3–8. doi: 10.1111/j.1365-2583.2004.00529.x

Ernst, D. A., and Westerman, E. L. (2021). Stage-and sex-specific transcriptome analyses reveal distinctive sensory gene expression patterns in a butterfly. *BMC Genomics* 22:584. doi: 10.1186/s12864-021-07819-4

Faccoli, M., Blazenec, M., and Schlyter, F. (2005). Feeding response to host and nonhost compounds by males and females of the spruce bark beetle *Ips typographus* in a tunneling microassay. *J. Chem. Ecol.* 31, 745–759. doi: 10.1007/s10886-005-3542-z

Faldt, J., Solheim, H., Langstrom, B., and Borg-Karlson, A. K. (2006). Influence of fungal infection and wounding on contents and enantiomeric compositions of monoterpenes in phloem of *Pinus sylvestris*. *J. Chem. Ecol.* 32, 1779–1795. doi: 10.1007/s10886-006-9109-9

Fang, J. X., Zhang, S. F., Liu, F., Cheng, B., Zhang, Z., Zhang, Q. H., et al. (2021). Functional investigation of monoterpenes for improved understanding of the relationship between hosts and bark beetles. *J. Appl. Entomol.* 145, 303–311. doi: 10.1111/jen.12850

Field, L. M., and Devonshire, A. L. (1998). Evidence that the E4 and FE4 esterase genes responsible for insecticide resistance in the aphid *Myzus persicae* (Sulzer) are part of a gene family. *Biochem. J.* 330, 169–173. doi: 10.1042/bj3300169

Figueroa-Teran, R., Pak, H., Blomquist, G. J., and Tittiger, C. (2016). High substrate specificity of ipsdienol dehydrogenase (IDOLDH), a short-chain dehydrogenase from *Ips pini* bark beetles. *J. Biochem.* 160, 141–151. doi: 10.1093/jb/mvw019

Franceschi, V. R., Krokene, P., Christiansen, E., and Krekling, T. (2005). Anatomical and chemical defenses of conifer bark against bark beetles and other pests. *New Phytol.* 167, 353–375. doi: 10.1111/j.1469-8137.2005.01436.x

Fukuda, S., Hamada, T., Ishii, N., Sakaguchi, S., Sakai, K., Akiyama, M., et al. (2012). Novel adenosine triphosphate (ATP)-binding cassette, subfamily A, member 12 (ABCA12) mutations associated with congenital ichthyosiform erythroderma. *Br. J. Dermatol.* 166, 218–221. doi: 10.1111/j.1365-2133.2011.10516.x

Gaddelapati, S. C., Kalsi, M., Roy, A., and Palli, S. R. (2018). Cap 'n' collar C regulates genes responsible for imidacloprid resistance in the Colorado potato beetle, *Leptinotarsa decemlineata*. *Insect Biochem. Mol. Biol.* 99, 54–62. doi: 10.1016/j.ibmb.2018.05.006

Gao, H. M., Dai, L. L., Fu, D. Y., Sun, Y. Y., and Chen, H. (2020). Isolation, expression profiling, and regulation via host allelochemicals of 16 glutathione S-transferases in the Chinese white pine beetle, *Dendroctonus armandi*. *Front. Physiol.* 11:546592. doi: 10.3389/fphys.2020.546592

Gong, H., Niu, Q., Zhou, Y., Wang, Y. X., Xu, X. F., and Hou, K. Z. (2021). Notum palmitoleoyl-protein carboxylesterase regulates Fas cell surface death receptor-mediated apoptosis via the Wnt signaling pathway in colon adenocarcinoma. *Bioengineered* 12, 5241–5252. doi: 10.1080/21655979.2021.1961657

Gonzalez-Caballero, N., Valenzuela, J. G., Mc Ribeiro, J., Cuervo, P., and Brazil, R. P. (2013). Transcriptome exploration of the sex pheromone gland of *Lutzomyia longipalpis* (Diptera: Psychodidae: Phlebotominae). *Parasit. Vectors* 6, 56. doi: 10.1186/1756-3305-6-56

Guittard, E., Blais, C., Maria, A., Parvy, J. P., Pasricha, S., Lumb, C., et al. (2011). CYP18A1, a key enzyme of *Drosophila* steroid hormone inactivation, is essential for metamorphosis. *Dev. Biol.* 349, 35–45. doi: 10.1016/j.ydbio.2010.09.023

Guo, H., and Smith, D. P. (2022). Time-Dependent Odorant Sensitivity Modulation in Insects. *Insects* 13:354.

Guo, R., Chen, D. F., Diao, Q. Y., Xiong, C. L., Zheng, Y. Z., and Hou, C. S. (2019). Transcriptomic investigation of immune responses of the *Apis cerana cerana* larval gut infected by *Ascosphaera apis*. *J. Invertebr. Pathol.* 166:107210. doi: 10.1016/j.jip.2019.107210

Habig, W. H., and Jakoby, W. B. (1981). [51] Assays for differentiation of glutathione S-transferases. *Methods Enzymol.* 77, 398–405.

Hammerbacher, A., Schmidt, A., Wadke, N., Wright, L. P., Schneider, B., Bohlmann, J., et al. (2013). A common fungal associate of the spruce bark beetle metabolizes the stilbene defenses of Norway spruce. *Plant Physiol.* 162, 1324–1336. doi: 10.1104/pp.113.218610

Han, Q., Li, G., and Li, J. (2000). Purification and characterization of chorion peroxidase from *Aedes aegypti* eggs. *Arch. Biochem. Biophys.* 378, 107–115. doi: 10.1006/abbi.2000.1821

Heckel, D. G. (2014). Insect detoxification and sequestration strategies. *Annu. Plant Rev. Online* 47, 77–114.

Heidel-Fischer, H. M., and Vogel, H. (2015). Molecular mechanisms of insect adaptation to plant secondary compounds. *Curr. Opin. Insect Sci.* 8, 8–14. doi: 10.1016/j.cois.2015.02.004

Helvig, C., Koener, J., Unnithan, G., and Feyereisen, R. (2004). CYP15A1, the cytochrome P450 that catalyzes epoxidation of methyl farnesoate to juvenile hormone III in cockroach corpora allata. *Proc. Natl. Acad. Sci. U.S.A.* 101, 4024–4029. doi: 10.1073/pnas.0306980101

Hilliou, F., Chertemps, T., Maibeche, M., and Le Goff, G. (2021). Resistance in the genus *Spodoptera*: Key insect detoxification genes. *Insects* 12:544. doi: 10.3390/insects12060544

Hlásny, T., Krokene, P., Liebhold, A., Montagné-Huck, C., Müller, J., Qin, H., et al. (2019). *Living with bark beetles: Impacts, outlook and management options*. Joensuu: European Forest Institute.

Hlasny, T., Zimova, S., and Bentz, B. (2021). Scientific response to intensifying bark beetle outbreaks in Europe and North America. *For. Ecol. Manag.* 499:119599. doi: 10.1016/j.foreco.2021.119599

Hlásny, T., Zimová, S., Merganičová, K., Štěpánek, P., Modlinger, R., and Turčáni, M. (2021). Devastating outbreak of bark beetles in the Czech republic: Drivers, impacts, and management implications. *For. Ecol. Manag.* 490:119075.

Huang, H. Y., Gao, Q., Peng, X. X., Choi, S. Y., Sarma, K., Ren, H. M., et al. (2011). piRNA-associated germline nuage formation and spermatogenesis require MitoPLD profusogenic mitochondrial-surface lipid signaling. *Dev. Cell* 20, 376–387. doi: 10.1016/j.devcel.2011.01.004

Huang, J. B., Kautz, M., Trowbridge, A. M., Hammerbacher, A., Raffa, K. F., Adams, H. D., et al. (2020). Tree defence and bark beetles in a drying world: Carbon partitioning, functioning and modelling. *New Phytol.* 225, 26–36. doi: 10.1111/nph.16173

Huang, Y., Liao, M., Yang, Q., Xiao, J., Hu, Z., and Cao, H. (2019). iTRAQ-based quantitative proteome revealed metabolic changes of *Sitophilus zeamais* in response to terpinen-4-ol fumigation. *Pest Manag. Sci.* 75, 444–451. doi: 10.1002/ps.5135

Huang, Y., Liao, M., Yang, Q., Xiao, J., Hu, Z., Zhou, L., et al. (2018). Transcriptome profiling reveals differential gene expression of detoxification enzymes in *Sitophilus zeamais* responding to terpinen-4-ol fumigation. *Pestic. Biochem. Physiol.* 149, 44–53. doi: 10.1016/j.pestbp.2018.05.008

Huber, D. P., Erickson, M. L., Leutenegger, C. M., Bohlmann, J., and Seybold, S. J. (2007). Isolation and extreme sex-specific expression of cytochrome P450 genes in the bark beetle, *Ips paraconfusus*, following feeding on the phloem of host ponderosa pine, *Pinus ponderosa*. *Insect Mol. Biol.* 16, 335–349. doi: 10.1111/j.1365-2583.2007.00731.x

Jakuš, R., Edwards-Jonášová, M., Cudlín, P., Blaženec, M., Ježík, M., Havlíèek, F., et al. (2011). Characteristics of Norway spruce trees (*Picea abies*) surviving a spruce bark beetle (*Ips typographus* L.) outbreak. *Trees* 25, 965–973.

Jin, M., Liao, C., Fu, X., Holdbrook, R., Wu, K., and Xiao, Y. (2019). Adaptive regulation of detoxification enzymes in *Helicoverpa armigera* to different host plants. *Insect Mol. Biol.* 28, 628–636. doi: 10.1111/imb.12578

Joga, M. R., Mogilicherla, K., Smagghe, G., and Roy, A. (2021). RNA interference-based forest protection products (FPPs) against wood-boring coleopterans: Hope or hype? *Front. Plant Sci.* 12:733608. doi: 10.3389/fpls.2021.733608

Keeling, C. I., Li, M., Sandhu, H. K., Henderson, H., Saint Yuen, M. M., and Bohlmann, J. (2016). Quantitative metabolome, proteome and transcriptome analysis of midgut and fat body tissues in the mountain pine beetle, *Dendroctonus ponderosae* Hopkins, and insights into pheromone biosynthesis. *Insect Biochem. Mol. Biol.* 70, 170–183. doi: 10.1016/j.ibmb.2016.01.002

Kim, J. I., Kwon, M., Kim, G.-H., Kim, S. Y., and Lee, S. H. (2015). Two mutations in nAChR beta subunit is associated with imidacloprid resistance in the *Aphis gossypii*. *J. Asia Pac. Entomol.* 18, 291–296.

Kostaropoulos, I., Papadopoulos, A. I., Metaxakis, A., Boukouvala, E., and Papadopoulou-Mourkidou, E. (2001). The role of glutathione S-transferases in the detoxification of some organophosphorus insecticides in larvae and pupae of the yellow mealworm, *Tenebrio molitor* (Coleoptera: Tenebrionidae). *Pest Manag. Sci.* 57, 501–508. doi: 10.1002/ps.323

Krasney, P. A., Carr, C., and Cavener, D. R. (1990). Evolution of the glucose-dehydrogenase gene in *Drosophila*. *Mol. Biol. Evol.* 7, 155–177.

Krempl, C., Sporer, T., Reichelt, M., Ahn, S.-J., Heidel-Fischer, H., Vogel, H., et al. (2016). Potential detoxification of gossypol by UDP-glycosyltransferases in the two Heliothine moth species *Helicoverpa armigera* and *Heliothis virescens*. *Insect Biochem. Mol. Biol.* 71, 49–57. doi: 10.1016/j.ibmb.2016.02.005

Krokene, P., and Solheim, H. (1998). Pathogenicity of four blue-stain fungi associated with aggressive and nonaggressive bark beetles. *Phytopathology* 88, 39–44. doi: 10.1094/phyto.1998.88.1.39

Lee, S., Kim, J. J., and Breuil, C. (2006). Diversity of fungi associated with the mountain pine beetle, *Dendroctonus ponderosae* and infested Lodgepole pines in British Columbia. *Fungal Divers.* 22, 91–105.

Lekha, G., Gupta, T., Awasthi, A. K., Murthy, G. N., Trivedy, K., and Ponnuvel, K. M. (2015). Genome wide microarray based expression profiles associated with BmNPV resistance and susceptibility in Indian silkworm races of *Bombyx mori*. *Genomics* 106, 393–403. doi: 10.1016/j.ygeno.2015.09.002

Li, J. S., Kim, S. R., and Li, J. Y. (2004). Molecular characterization of a novel peroxidase involved in *Aedes aegypti* chorion protein crosslinking. *Insect Biochem. Mol. Biol.* 34, 1195–1203. doi: 10.1016/j.ibmb.2004.08.001

Li, Q. L., Sun, Z. X., Shi, Q., Wang, R. M., Xu, C. C., Wang, H. H., et al. (2019). RNA-Seq analyses of midgut and fat body tissues reveal the molecular mechanism underlying *Spodoptera litura* resistance to tomatine. *Front. Physiol.* 10:8. doi: 10.3389/fphys.2019.00008

Lien, N. T. K., Ngoc, N. T. H., Lan, N. N., Hien, N. T., Tung, N. V., Ngan, N. T. T., et al. (2019). Transcriptome sequencing and analysis of changes associated with insecticide resistance in the dengue mosquito (*Aedes aegypti*) in Vietnam. *Am. J. Trop. Med. Hyg.* 100, 1240–1248. doi: 10.4269/ajtmh.18-0607

Liu, B., Fu, D., Ning, H., Tang, M., and Chen, H. (2022). Knockdown of CYP6CR2 and CYP6DE5 reduces tolerance to host plant allelochemicals in the Chinese white pine beetle *Dendroctonus armandi*. *Pestic. Biochem. Physiol.* 187:105180. doi: 10.1016/j.pestbp.2022.105180

Livak, K. J., and Schmittgen, T. D. (2001). Analysis of relative gene expression data using real-time quantitative PCR and the 2- ΔΔCT method. *Methods* 25, 402–408.

Lu, K., Song, Y. Y., and Zeng, R. S. (2021). The role of cytochrome P450-mediated detoxification in insect adaptation to xenobiotics. *Curr. Opin. Insect Sci.* 43, 103–107. doi: 10.1016/j.cois.2020.11.004

Lubojacký, J., Lorenc, F., Samek, M., Knížek, M., and Liška J. (2022). "Hlavní problémy v ochraně lesa v Česku v roce 2021 a prognóza na rok 2022," in *Škodliví činitelé v lesích Česka 2021/2022 – Škody zvěří. Sborník referátů z celostátního semináře s mezinárodní účastí. Průhonice*, April 28, 2022, ed. F. Lorenc (Průhonice: Zpravodaj Ochrany Lesa), 17–26.

Margoliash, E., and Frohwirt, N. (1959). Spectrum of horse-heart cytochrome c. *Biochem. J.* 71, 570–572.

Meng, X. K., Zhang, Y. X., Bao, H. B., and Liu, Z. W. (2015). Sequence analysis of insecticide action and detoxification-related genes in the insect pest natural enemy *Pardosa pseudoannulata*. *PLoS One* 10:e0125242. doi: 10.1371/journal.pone.0125242

Morisseau, C. (2013). Role of epoxide hydrolases in lipid metabolism. *Biochimie* 95, 91–95. doi: 10.1016/j.biochi.2012.06.011

Nadeau, J. A., Petereit, J., Tillett, R. L., Jung, K., Fotoohi, M., MacLean, M., et al. (2017). Comparative transcriptomics of mountain pine beetle pheromone-biosynthetic tissues and functional analysis of CYP6DE3. *BMC Genomics* 18:311. doi: 10.1186/s12864-017-3696-4

Netherer, S., and Hammerbacher, A. (2022). "The Eurasian spruce bark beetle in a warming climate: Phenology, behavior, and biotic interactions," in *Bark beetle*

management, ecology, and climate change, eds R. W. Hofstetter and K. J. K. Gandhi (Amsterdam: Elsevier), 89–131.

Netherer, S., Kandasamy, D., Jirosova, A., Kalinova, B., Schebeck, M., and Schlyter, F. (2021). Interactions among Norway spruce, the bark beetle *Ips typographus* and its fungal symbionts in times of drought. *J. Pest Sci.* 94, 591–614. doi: 10.1007/s10340-021-01341-y

Neumann, E., Mehboob, H., Ramirez, J., Mirkov, S., Zhang, M., and Liu, W. Q. (2016). Age-dependent hepatic UDP-glucuronosyltransferase gene expression and activity in children. *Front. Pharmacol.* 7:437. doi: 10.3389/fphar.2016.00437

Niwa, R., Matsuda, T., Yoshiyama, T., Namiki, T., Mita, K., Fujimoto, Y., et al. (2004). CYP306A1, a cytochrome P450 enzyme, is essential for ecdysteroid biosynthesis in the prothoracic glands of *Bombyx* and *Drosophila*. *J. Biol. Chem.* 279, 35942–35949. doi: 10.1074/jbc.M404514200

Oldfield, S., Lowry, C. A., Ruddick, J., and Lightman, S. L. (2002). ABCG4: A novel human white family ABC-transporter expressed in the brain and eye. *Biochim. Biophys. Acta Mol. Cell Res.* 1591, 175–179. doi: 10.1016/s0167-4889(02)00269-0

Oppert, B., Perkin, L. C., Lorenzen, M., and Dossey, A. T. (2020). Transcriptome analysis of life stages of the house cricket, *Acheta domesticus*, to improve insect crop production. *Sci. Rep.* 10:3471. doi: 10.1038/s41598-020-59087-z

Ortego, F., López-Olguìn, J., Ruız, M., and Castañera, P. (1999). Effects of toxic and deterrent terpenoids on digestive protease and detoxication enzyme activities of Colorado potato beetle larvae. *Pestic. Biochem. Physiol.* 63, 76–84.

Perkin, L. C., and Oppert, B. (2019). Gene expression in *Tribolium castaneum* life stages: Identifying a species-specific target for pest control applications. *PeerJ* 7:e6946.

Plaitakis, A., Kalef-Ezra, E., Kotzamani, D., Zaganas, I., and Spanaki, C. (2017). The glutamate dehydrogenase pathway and its roles in cell and tissue biology in health and disease. *Biology* 6:11. doi: 10.3390/biology6010011

Plaitakis, A., Metaxari, M., and Shashidharan, P. (2000). Nerve tissue-specific (GLUD2) and housekeeping (GLUD1) human glutamate dehydrogenases are regulated by distinct allosteric mechanisms: Implications for biologic function. *J. Neurochem.* 75, 1862–1869. doi: 10.1046/j.1471-4159.2000.0751862.x

Powell, D., Grosse-Wilde, E., Krokene, P., Roy, A., Chakraborty, A., Lofstedt, C., et al. (2021). A highly-contiguous genome assembly of the Eurasian spruce bark beetle, *Ips typographus*, provides insight into a major forest pest. *Commun. Biol.* 4:1059. doi: 10.1038/s42003-021-02602-3

Ramakrishnan, R., Hradecky, J., Roy, A., Kalinova, B., Mendezes, R. C., Synek, J., et al. (2022). Metabolomics and transcriptomics of pheromone biosynthesis in an aggressive forest pest *Ips typographus*. *Insect Biochem. Mol. Biol.* 140:103680. doi: 10.1016/j.ibmb.2021.103680

Raymond, M., Chevillon, C., Guillemaud, T., Lenormand, T., and Pasteur, N. (1998). An overview of the evolution of overproduced esterases in the mosquito *Culex pipiens*. *Philos. Trans. R. Soc. B Biol. Sci.* 353, 1707–1711. doi: 10.1098/rstb.1998.0322

Robert, J. A., Bonnett, T., Pitt, C., Spooner, L. J., Fraser, J., Yuen, M. M. S., et al. (2016). Gene expression analysis of overwintering mountain pine beetle larvae suggests multiple systems involved in overwintering stress, cold hardiness, and preparation for spring development. *PeerJ* 4:e2109. doi: 10.7717/peerj.2109

Robert, J. A., Pitt, C., Bonnett, T. R., Yuen, M. M. S., Keeling, C. I., Bohlmann, J., et al. (2013). Disentangling detoxification: Gene expression analysis of feeding mountain pine beetle illuminates molecular-level host chemical defense detoxification mechanisms. *PLoS One* 8:e77777. doi: 10.1371/journal.pone.0077777

Robinson, M. D., McCarthy, D. J., and Smyth, G. K. (2010). edgeR: A bioconductor package for differential expression analysis of digital gene expression data. *Bioinformatics* 26, 139–140.

Roy, A., George, S., and Palli, S. R. (2017). Multiple functions of CREB-binding protein during postembryonic development: Identification of target genes. *BMC Genomics* 18:996. doi: 10.1186/s12864-017-4373-3

Roy, A., Walker, I. W., Vogel, H., Chattington, S., Larsson, M., Anderson, P., et al. (2016). Diet dependent metabolic responses in three generalist insect herbivores *Spodoptera* spp. *Insect Biochem. Mol. Biol.* 71, 91–105. doi: 10.1016/j.ibmb.2016.02.006

Sandstrom, P., Welch, W. H., Blomquist, G. J., and Tittiger, C. (2006). Functional expression of a bark beetle cytochrome P450 that hydroxylates myrcene to ipsdienol. *Insect Biochem. Mol. Biol.* 36, 835–845. doi: 10.1016/j.ibmb.2006.08.004

Sarabia, L. E., Lopez, M. F., Pineda-Mendoza, R. M., Obregon-Molina, G., Gonzalez-Escobedo, R., Albores-Medina, A., et al. (2019). Time-course of CYP450 genes expression from *Dendroctonus rhizophagus* (Curculionidae: Scolytinae) during early hours of drilling bark and settling into the host tree. *J. Insect Sci.* 19:7. doi: 10.1093/jisesa/iez046

Sellamuthu, G., Bílý, J., Joga, M. R., Synek, J., and Roy, A. (2022). Identifying optimal reference genes for gene expression studies in Eurasian spruce bark beetle, *Ips typographus* (Coleoptera: Curculionidae: Scolytinae). *Sci. Rep.* 12:4671. doi: 10.1038/s41598-022-08434-3

Shen, G. W., Wu, J. X., Wang, Y., Liu, H. L., Zhang, H. Y., Ma, S. Y., et al. (2018). The expression of ecdysteroid UDP-glucosyltransferase enhances cocoon shell ratio by reducing ecdysteroid titre in last-instar larvae of silkworm, *Bombyx mori*. *Sci. Rep.* 8:17710. doi: 10.1038/s41598-018-36261-y

Shen, X. A., Liu, W. X., Wan, F. H., Lv, Z. C., and Guo, J. Y. (2021). The role of cytochrome P450 4C1 and carbonic anhydrase 3 in response to temperature stress in *Bemisia tabaci*. *Insects* 12:1071. doi: 10.3390/insects12121071

Shimada, M., Terazawa, R., Kamiyama, Y., Honma, W., Nagata, K., and Yamazoe, Y. (2004). Unique properties of a renal sulfotransferase, st1d1, in dopamine metabolism. *J. Pharmacol. Exp. Ther.* 310, 808–814. doi: 10.1124/jpet.104.065532

Song, M., Gorzalski, A., Nguyen, T. T., Liu, X., Jeffrey, C., Blomquist, G. J., et al. (2014). exo-Brevicomin biosynthesis in the fat body of the mountain pine beetle, *Dendroctonus ponderosae*. *J. Chem. Ecol.* 40, 181–189. doi: 10.1007/s10886-014-0381-9

Song, M. M., Kim, A. C., Gorzalski, A. J., MacLean, M., Young, S., Ginzel, M. D., et al. (2013). Functional characterization of myrcene hydroxylases from two geographically distinct *Ips pini* populations. *Insect Biochem. Mol. Biol.* 43, 336–343. doi: 10.1016/j.ibmb.2013.01.003

Song, X. W., Zhong, Q. S., Ji, Y. H., Zhang, Y. M., Tang, J., Feng, F., et al. (2022). Characterization of a sigma class GST (GSTS6) required for cellular detoxification and embryogenesis in *Tribolium castaneum*. *Insect Sci.* 29, 215–229. doi: 10.1111/1744-7917.12930

Takakura, Y., and Asano, Y. (2019). Purification, characterization, and gene cloning of a novel aminoacylase from *Burkholderia* sp. strain LP5_18B that efficiently catalyzes the synthesis of *N*-lauroyl-l-amino acids. *Biosci. Biotechnol. Biochem.* 83, 1964–1973. doi: 10.1080/09168451.2019.1630255

Tillman, J. A., Holbrook, G. L., Dallara, P. L., Schal, C., Wood, D. L., Blomquist, G. J., et al. (1998). Endocrine regulation of de novo aggregation pheromone biosynthesis in the pine engraver, *Ips pini* (Say)(Coleoptera: Scolytidae). *Insect Biochem. Mol. Biol.* 28, 705–715.

Tillman, J. A., Lu, F., Goddard, L. M., Donaldson, Z. R., Dwinell, S. C., Tittiger, C., et al. (2004). Juvenile hormone regulates de novo isoprenoid aggregation pheromone biosynthesis in pine bark beetles, Ips spp., through transcriptional control of HMG-CoA reductase. *J. Chem. Ecol.* 30, 2459–2494. doi: 10.1007/s10886-004-7945-z

Tittiger, C., and Blomquist, G. J. (2017). Pheromone biosynthesis in bark beetles. *Curr. Opin. Insect Sci.* 24, 68–74.

Unelius, C. R., Schiebe, C., Bohman, B., Andersson, M. N., and Schlyter, F. (2014). Non-host volatile blend optimization for forest protection against the European spruce bark beetle, *Ips typographus*. *PLoS One* 9:e85381. doi: 10.1371/journal.pone.0085381

Valentino, M. L., Barboni, P., Ghelli, A., Bucchi, L., Rengo, C., Achilli, A., et al. (2004). The ND1 gene of complex I is a mutational hot spot for Leber's hereditary optic neuropathy. *Ann. Neurol.* 56, 631–641. doi: 10.1002/ana.20236

Wang, D. H., Song, W., Wei, S. W., Zheng, Y. F., Chen, Z. S., Han, J. D., et al. (2018). Characterization of the ubiquitin C-terminal hydrolase and ubiquitin-specific protease families in rice (*Oryza sativa*). *Front. Plant Sci.* 9:1636. doi: 10.3389/fpls.2018.01636

Wang, H.-L., Rao, Q., Chen, Z.-Z., and Navas-Castillo, J. (2022). *Identifying potential insecticide resistance markers through genomic-level comparison of Bemisia tabaci (Gennadius) lines*. Available online at: https://ssrn.com/abstract=4100303 (accessed May 4, 2022).

Wang, M., Sun, D.-F., Wang, S., Qing, Y., Chen, S., Wu, D., et al. (2013). Polymorphic expression of UDP-glucuronosyltransferase UGTlA gene in human colorectal cancer. *PLoS One* 8:e57045. doi: 10.1371/journal.pone.0057045

Wang, S., Chen, H., Tang, X., Zhang, H., Hao, G., Chen, W., et al. (2020). The role of glyceraldehyde-3-phosphate dehydrogenases in NADPH supply in the oleaginous filamentous fungus *Mortierella alpina*. *Front. Microbiol.* 11:818. doi: 10.3389/fmicb.2020.00818

Wang, Z. B., Tian, F. J., Cai, L. J., Zhang, J., Liu, J. L., and Zeng, X. N. (2019). Identification of candidate ATP-binding cassette transporter gene family members in *Diaphorina citri* (Hemiptera: Psyllidae) via adult tissues transcriptome analysis. *Sci. Rep.* 9:15842. doi: 10.1038/s41598-019-52402-3

Wei, D. D., He, W., Miao, Z. Q., Tu, Y. Q., Wang, L., Dou, W., et al. (2020). Characterization of esterase genes involving malathion detoxification and establishment of an RNA interference method in *Liposcelis bostrychophila*. *Front. Physiol.* 11:274. doi: 10.3389/fphys.2020.00274

Wen, R. R., Wang, B. Y., Wang, B. W., and Ma, L. (2018). Characterization and expression profiles of juvenile hormone epoxide hydrolase from *Lymantria dispar* (Lepidoptera: Lymantridae) and RNA interference by ingestion. *J. Insect Sci.* 18, 1–7. doi: 10.1093/jisesa/iey002

Xing, X., Yan, M., Pang, H., Wu, F. A., Wang, J., and Sheng, S. (2021). Cytochrome P450s are essential for insecticide tolerance in the endoparasitoid wasp *Meteorus pulchricornis* (Hymenoptera: Braconidae). *Insects* 12:651. doi: 10.3390/insects12070651

Yoon, K. A., Kim, K., Kim, W. J., Bang, W. Y., Ahn, N. H., Bae, C. H., et al. (2020). Characterization of venom components and their phylogenetic properties in some aculeate bumblebees and wasps. *Toxins* 12:47. doi: 10.3390/toxins12010047

Zhang, Q.-H., Schlyter, F., and Birgersson, G. (2012). 2-methyl-3-buten-2-ol: A pheromone component of conifer bark beetles found in the bark of nonhost deciduous trees. *Psyche* 2012:414508.

Zhao, T., Ganji, S., Schiebe, C., Bohman, B., Weinstein, P., Krokene, P., et al. (2019). Convergent evolution of semiochemicals across Kingdoms: Bark beetles and their fungal symbionts. *ISME J.* 13, 1535–1545. doi: 10.1038/s41396-019-0370-7

frontiers | Frontiers in Forests and Global Change

TYPE Original Research
PUBLISHED 09 June 2023
DOI 10.3389/ffgc.2023.1167541

OPEN ACCESS

EDITED BY
Quan Lu,
Chinese Academy of Forestry, China

REVIEWED BY
San-an Wu,
Beijing Forestry University, China
Zhuhong Wang,
Fujian Agriculture and Forestry University, China

*CORRESPONDENCE
Olle Anderbrant
✉ olle.anderbrant@biol.lu.se

†PRESENT ADDRESS
Inis Winde,
Department of Aquatic Sciences and Assessment, Uppsala, Sweden

RECEIVED 16 February 2023
ACCEPTED 11 May 2023
PUBLISHED 09 June 2023

CITATION
Marques JF, Winde I, Jönsson AM and Anderbrant O (2023) Taxonomic relationship among four European *Physokermes* species (Hemiptera: Coccomorpha) based on nuclear and mitochondrial DNA.
Front. For. Glob. Change 6:1167541.
doi: 10.3389/ffgc.2023.1167541

Taxonomic relationship among four European *Physokermes* species (Hemiptera: Coccomorpha) based on nuclear and mitochondrial DNA

Joana F. Marques[1], Inis Winde[1†], Anna Maria Jönsson[2] and Olle Anderbrant[1*]

[1]Department of Biology, Lund University, Lund, Sweden, [2]Department of Physical Geography and Ecosystem Science, Lund University, Lund, Sweden

Introduction: Scale insects (Hemiptera: Coccomorpha) feed on a wide variety of agricultural crops and forest and ornamental trees worldwide. These pest insects damage plants not only by causing sap loss but also by reducing the plant's photosynthetic activity. This is because the honeydew they produce acts as a substrate for mold, which covers leaf surfaces. In the last decades, several outbreaks of *Physokermes spp.* (soft-scale insects) have occurred throughout Europe and have partly been attributed to unusual weather conditions or climate change, as some species seem to be expanding their distribution range. However, the small size of these insects and their large intraspecific morphological variation have hindered the identification of the species responsible for outbreaks.

Methods: In this study, mitochondrial DNA (cytochrome c oxidase subunit I, COI), ribosomal RNA (28S), and nuclear (elongation factor 1α, EF1α) DNA markers were used to reconstruct the phylogenetic relationships of four *Physokermes* species sampled throughout Europe in 2013–2015.

Results and discussion: The results allowed us to clearly distinguish *P. hellenicus* and *P. inopinatus* from each other, as these appeared in well-supported clades in the phylogenetic trees and from *P. piceae* and *P. hemicryphys*. However, *P. hemicryphus* appeared in a single clade in trees based on 28S and EF1α but among *P. piceae* in the COI tree. Further investigations are therefore required to determine the taxonomic status of *P. piceae* and *P. hemicryphys*, which seem to comprise a species complex.

KEYWORDS

Hungarian spruce scale, phylogeny, invasive species, forest pest, climate change

1. Introduction

Scale insects (Hemiptera: Coccomorpha) are important plant pests feeding on a wide range of agricultural crops as well as on forest and ornamental trees worldwide (Park et al., 2011). In addition to directly affecting host plants through sap loss, the honeydew produced by scale insects covers leaf surfaces, allowing mold development and thus reducing photosynthetic activity (Kozár et al., 2012). Because they are small and frequently found living within the plant, scale insects are often unseen. This contributes to their invasive potential and presents a huge challenge for plant quarantine (Andersen et al., 2010) and a major phytosanitary problem. The genus *Physokermes* comprises an important group of soft-scale insects infesting coniferous plants in the Holarctic region. In total, 13 species are currently recognized within *Physokermes* (Papanastasiou et al., 2021), but only four are

known to occur in Europe: the widespread *P. hemicryphus* (Dalman) and *P. piceae* (Schrank), the more easterly distributed *P. inopinatus (*Danzig & Kozár), and *P. hellenicus,* (Kozár & Gounari) described from *Abies cephalonica* (Pinaceae) in Greece (Kozár et al., 2012). Although commonly known as the Hungarian spruce scale, *P. inopinatus* caused a mass infestation in Sweden in 2010 (McCarthy and Skovsgaard, 2011), suggesting a considerable northward expansion of this species' distribution, possibly linked to climate change or the unrestricted transport of plants within Europe (Kozár et al., 2012). Indeed, the attack by *P. inopinatus* was triggered by a sequence of droughts that contributed to population expansions in the relatively dry summers of 2008–2009, leading to the severe mass infestation of 2010 (McCarthy and Skovsgaard, 2011; Olsson et al., 2012; Gertsson and Isacsson, 2014; Winde et al., 2018).

However, the identity of the species causing the 2010 outbreak in Sweden was not immediately determined. This was because morphological identification of scale insects requires a high level of expertise and is time consuming. It mostly relies on characters present only in adult females, which is difficult when the morphological variation observed between females of closely related species corresponds to natural intraspecific variation instead of interspecific variation (Malausa et al., 2011; Park et al., 2011). The limitations of this methodology have also raised concern about the possible non-identification of cryptic species complexes (Andersen et al., 2010), and thus, several DNA markers have been developed to distinguish between closely related species of scale insects, mainly mealybugs and armored scales (Kondo et al., 2008; Andersen et al., 2010; Gwiazdowski et al., 2010; Malausa et al., 2011 and references therein; Park et al., 2010; 2011; Abd-Rabou et al., 2012; Beltrà et al., 2012; Deng et al., 2012; Sethusa et al., 2014). Such markers include a set of gene regions providing reliable and rapid identification of scale insect species, even when only immature and male specimens are available. Although DNA barcoding based on *cytochrome c oxidase subunit I* (COI) sequence variation has become a popular tool for species delimitation in several insect groups (Hajibabaei et al., 2006), and therefore an ideal candidate for identifying scale insects (e.g., Kondo et al., 2008; Malausa et al., 2011; Park et al., 2011; Abd-Rabou et al., 2012; Beltrà et al., 2012; Deng et al., 2012; Sethusa et al., 2014), only 2,172 COI sequences of Coccidae are deposited in GenBank (http://www.ncbi.nlm.nih.gov; accessed November 8, 2022). Gene 28S has also been used to identify insect species (Campbell et al., 1994; Monaghan et al., 2006; Smith et al., 2008). Although lacking sufficient variation to delimitate some species (Park et al., 2011; Deng et al., 2012), gene 28S has been proposed as a complementary marker to COI in scale insects (Sethusa et al., 2014). This supports van Nieukerken et al. (2012) suggestion of including at least one nuclear marker in addition to COI in studies concerning cryptic lineages. Thus, in this study, three genes from three independent loci were amplified: COI (mitochondrial DNA), 28S (D2 and D3 regions, ribosomal RNA gene), and elongation factor 1alpha (EF1α, nuclear DNA). These genes represent a range of different rates of evolution: COI is a relatively fast-evolving mitochondrial gene (Simon et al., 1994), 28S is relatively conserved and represented in the nuclear genome as numerous tandem repeats (Hoy, 1994), and EF1α is a low-copy number nuclear protein-coding gene with conserved exons and variable introns (Hoy, 1994).

The DNA sequence analysis performed in this study for several *Physokermes* spp. populations across Europe aimed to (i) scan for cryptic species within taxonomically recognized *Physokermes* species; (ii) study the phylogenetic relationships between the identified taxa; and (iii) obtain a series of molecular markers suitable for the reliable identification of closely related *Physokermes* spp. in Europe, especially those with invasive pest status, thus contributing to more efficient pest management and quarantine procedures. Finding cryptic species will also provide the necessary background and molecular evidence to conduct thorough morphological studies on *Physokermes* specimens representative of several species. This will allow laying the foundations for a contemporary taxonomic revision and for the recognition of morphological characters important to species differentiation, similar to what has been done for *Chionaspis* spp. by Vea et al. (2012) following the work of Gwiazdowski et al. (2010). To date, only one molecular study of *Physokermes* spp. has been published, and it included COI sequence analysis of *P. hellenicus* from different Greek populations (Papanastasiou et al., 2018).

2. Materials and methods

2.1. Taxon sampling

In total, 203 *P. inopinatus*, *P. piceae, P. hemicryphus,* and *P. hellenicus* individuals were collected across their distribution ranges in Europe, i.e., from Turkey, in the southeast, to Sweden, in the northwest (Table 1). Sampling occurred in 2013–2015, and insects were immediately placed in 95% ethanol and kept at −20°C for DNA preservation. Taxonomic identity was determined by experienced scale insect specialists (see Acknowledgments) based on discriminating morphological characters published in reference studies (e.g., Kosztarab and Kozár, 1988; Kozár et al., 2012).

2.2. DNA extraction, amplification, and sequencing

Total genomic DNA was isolated from the 203 individuals using the QIAamp? DNA Mini Kit (QIAGEN, Hilden, Germany), following the manufacturer's protocol for the purification of total DNA from insects. The nucleotide sequences including the barcoding region of COI, 28S, and EF1α were amplified *via* PCR using the 5′-tailed primers and profiles described in Table 2. Amplification reaction mixtures (total volume = 20 μL) contained 10 μl DreamTaq™ PCR Master Mix (Fermentas™, Waltham, MA, USA), 1 μl each primer, 6 μl DNA-free water, and 2 μl template DNA. To check for contamination, negative controls (sterile water instead of template DNA) were included in each reaction array. The resulting PCR products were then visualized under UV light in 1% agarose gels stained with SYBR™ Safe DNA Gel Stain (ThermoFisher Scientific, Waltham, MA, USA). Those representing successful reactions were prepared for sequencing by digesting 5 μl of the PCR mixture with 0.5 μl Exonuclease I, and 1 μl FastAP™ Thermosensitive Alkaline Phosphatase (both from Fermentas™) during a thermal cycle consisting of 15 min at 37°C and 15 min at 85°C. PCR products were then sequenced in

TABLE 1 Collection sites and the number of *Physokermes* spp. individuals examined in the present study, and the number of cytochrome oxidase I (COI), 28S, and elongation factor 1 α (EF1α) sequences obtained.

Species	Location	Country	Coordinates	Host	N	Sample code in Phylogenetic trees	Sequences (number)		
							COI	28S	EF1α
P. inopinatus	Södra Sandby	Sweden		*Picea glauca* var. *conica*	20	Pino1.n; Pino2.n	12	13	17
P. piceae	Målilla	Sweden	57.337920, 15.754570	*Picea abies*	30	Ppic1Mn-Pic6Mn	82	60	72
	Tilburg	The Netherlands	51.540504, 5.016668	*Picea abies*	2	Ppic4.n			
	Ancara	Turkey	Not available	*Picea excelsa*	20	Ppic5.n-Ppic6.n			
	Szabadság Square, Budapest	Hungary	47.528272, 18.954156	*Picea abies*	4	Ppic2.n			
	Villány	Hungary	Not available	*Picea abies*	8	Ppic3.n			
	Kaszó	Hungary	46.320881, 17.223469	*Picea abies*	4	Ppic21.n			
	Nagykanizsa	Hungary	46.401989, 17.053061	*Picea abies*	6	Ppic24.n			
	Bosárkány	Hungary	47.689524, 17.251699	*Picea abies*	6	Ppic27.n			
	Mosonmagyaróvár	Hungary	47.884160, 17.25471	*Picea abies*	7	Ppic28.n			
	Vágáshuta	Hungary	48.423353, 21.5394	*Picea abies*	7	Ppic38.n			
	Mikóháza	Hungary	48.466467, 21.588708	*Picea abies*	6	Ppic40.n			
	Székelyvaja	Romania	46.440833, 24.64866	*Picea abies*	6	Ppic42.n			
	Lukailencfalva	Romania	46.463667, 24.531167	*Picea abies*	5	Ppic43.n			
	Farád	Hungary	47.604667, 17.204583	*Picea abies*	6	Ppic47.n			
	Berzence	Hungary	46.206400, 17.151934	*Picea abies*	6	Ppic48.n			
	Balavásár	Romania	46.409167, 24.704167	*Picea abies*	7	Ppic41.n			
P. hemicryphus	Lund	Sweden	55.714360, 13.196340	*Picea glauca* var. *conica*	24	Phem1.n, Phem2.n, Phem3.n, Phem4.n, Phem2L, Phem5L, Phem6L	14	16	4
	Målilla	Sweden	57.337920, 15.754570	*Picea abies*	2	Phem1M, Phem2M			
	Gellért Hill, Budapest	Hungary	Not available	Not available	15	Phem5.n, Phem6.n			
P. hellenicus	Mount Parnitha	Greece	38.172806, 23.731111	*Abies cephalonica*	10	Phel1.1n	9	5	7
				Total	**203**		**117**	**94**	**100**

10.3389/ffgc.2023.1167541

TABLE 2 Primers and PCR profiles used to amplify cytochrome oxidase I (COI), 28S, and elongation factor 1 α (EF1α) gene fragments in *Physokermes* spp.

Region	Primer	Sequence	Source	PCR
COI	C1-J-2753ywr	GTAAACCTAACATTTTTYCCWCARCA	Gwiazdowski et al., 2010	1′ @ 95°C; 30′′ @ 95°C, 1′ @ 40-50°C, 2′ @72°C; annealing T was decreased 2°C every 2 cycles from 50°C to the final T of 40°C; 10′ @72°C
COI	C2-N-3662	CCACAAATTTCTGAACATTGACC	Gwiazdowski et al., 2010	
COI barcode	PcoF1	CCTTCAACTAATCATAAAAATATYAG	Park et al., 2011	2′ @ 95°C; 5x (40′′ @ 94°C, 40′′ @ 45°C, 1′ @72°C); 40x (40′′ @ 94°C, 40′′ @ 51°C, 1′ @ 72°C); 5′ @72°C
COI barcode	LepR1	TAAACTTCTGGATGTCCAAAAAATCA	Park et al., 2011	
D2-D3 28S	s3660	GAGAGTTMAASAGTACGTGAAAC	Morse and Normark, 2006	@ 95°C; 30′′ @ 95°C, 1′ @58°C, 2′ @ 72°C; annealing T was lowered 2°C every 3 cycles until final annealing of 42°C, which was used for 18 Cycles; 10′ @ 72C
D2-D3 28S	28b	TCGGAAGGAACCAGCTACTA	Morse and Normark, 2006	
EF1α	EF1-a(a)	GATGCTCCGGGACAYAGA	Morse and Normark, 2006	
EF1α	EF2	ATGTGAGCGGTGTGGCAATCCAA	Morse and Normark, 2006	

both directions, to ensure high-quality reads, using PCR primers (Table 2) and the BigDye Terminator Cycle Reaction Kit (Applied Biosystems, Foster City, CA, USA).

2.3. Phylogenetic analyses

Contiguous sequences were assembled in Geneious® 8.1.15 (Biomatters, Auckland, New Zealand), aligned using the default parameters and cost matrix of the Geneious® alignment algorithm as included in Geneious® 8.1.15 and edited by eye to maximize blocks of sequence identity. Sequences were checked for homology by comparison with those deposited in GenBank, using the Basic Local Alignment Search Tool (BLAST) available on the NCBI website (NCBI, http://www.ncbi.nlm.nih.gov/Genbank). Translation into amino acids was also performed to confirm data correctness.

Using PartitionFinder 2 (Lanfear et al., 2012), the best partitioning scheme and model of nucleotide substitution were selected for each dataset based on the Bayesian information criterion. All possible combinations of codon positions were considered as candidate partitions (i.e., from a single partition for the entire sequence to each codon position treated as a partition), but only the nucleotide substitution models supported by MrBayes 3.2.6 (Ronquist and Huelsenbeck, 2003) were included in the candidate model pool. This procedure was repeated five times to ensure correct estimation. The resulting models and partition schemes were used in phylogenetic reconstructions based on maximum likelihood (ML) and Bayesian Inference (BI), performed in Garli 2.1 (Zwickl, 2006) and MrBayes 3.2.6, respectively. Because considerable statistical inconsistency can be found when using the maximum parsimony method of phylogenetic reconstruction on this type of data (different rates of evolution), it was not performed in this study.

In Garli, clade stability was evaluated by non-parametric bootstrapping (five independent search replicates of 10,000 generations each). In MrBayes, and starting from a random tree, alternative tree topologies were evaluated through the estimation of posterior probabilities by Markov chain Monte Carlo re-sampling. These were performed in two runs of four chains each (with the default settings implemented in MrBayes) for 10×10^6 generations with a sampling frequency of 100 (average standard deviation of split frequencies <0.01). These samples were then used to generate 50% majority-rule consensus trees. Commands "sumt" and "burnin = 5,000" were set to discard trees that did not reach the likelihood score detected with the "sump" command. Only bootstrap and posterior probabilities values >80% were considered to support clades.

The *species delimitation* plugin implemented in Geneious® was used to evaluate different scenarios of lineage divergence within *Physokermes* spp. based on a neighbor-joining (NJ) tree constructed for COI sequences. The distance-based species divergence criterion relies on the postulate that intraspecific genetic variation is small relative to interspecific variation. In this study, two clusters containing a pair of nearest neighbors with >2% distance from each other were considered different species, as this threshold has been proven efficient to discriminate other insect groups (Foottit et al., 2009; Zhu et al., 2017). Only monophyletic clades showing bootstrap support >80% were tested.

3. Results and discussion

The BLAST of all sequences against the NCBI database revealed that some (most of them corresponding to 28S sequences) matched those of internal parasites, parasitoids, or microorganisms infecting *Physokermes* spp.; hence, these sequences were excluded from further analysis. This higher-than-expected ratio of non-specific amplification might be due to the binding of one or both PCR primers to a sequence other than the target one, which is frequently a problem in the amplification of conserved sequences, such as ribosomal DNA. The 117 COI sequences (total length = 712 bp) and the 94 28S sequences (total

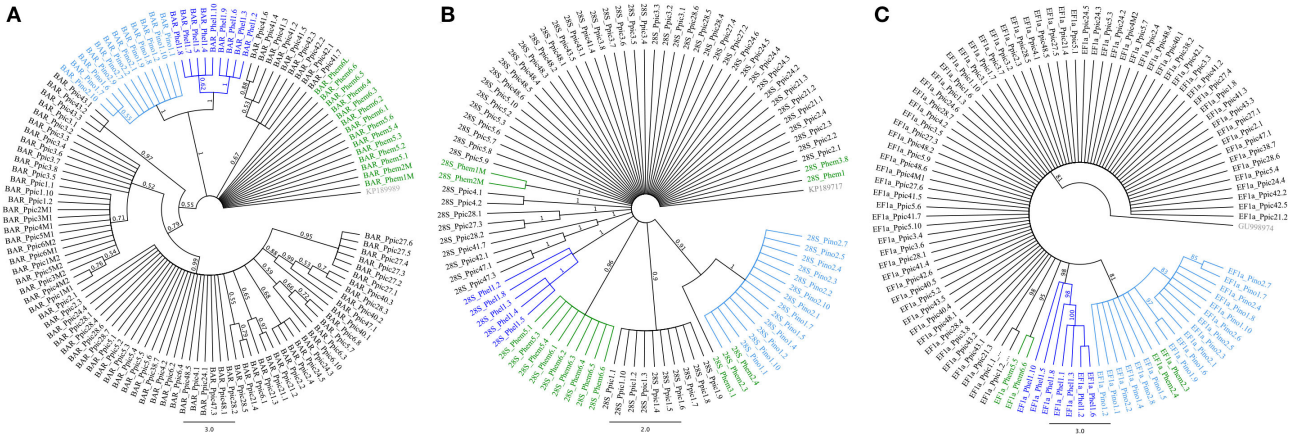

FIGURE 1
Bayesian inference phylogenetic trees constructed for *Physokermes inopinatus* (Pino), *P. hellenicus* (Phel), *P. piceae* (Ppic), and *P. hemicryphus* (Phem), based on cytochrome oxidase I [COI, **(A)**], 28S **(B)**, and elongation factor 1 α [EF1α, **(C)**] sequences, using the generalized time reversible (GTR) model with a gamma-distributed rate variation (G) among sites, the Hasegawa–Kishino–Yano (HKY) model with a proportion of invariable sites (I), and a partitioned model in which the first two positions evolved according to Felsenstein's 1981 model (F81) with G and the third according to HKY, respectively. Posterior probabilities (PP) are shown above branches; only clades with PP > 0.80 were considered well-supported. Numbers (and letters) next to species codes correspond to sample codes; numbers (and letters) before the dot to population codes; and the numbers (and letters) after the dot to individuals (see Table 1).

length = 842 bp) presented the highest sequence homology to *Physokermes jezoensis* Siraiwa isolate S2, whereas the 100 EF1α sequences (total length = 1,056 bp) presented the highest sequence homology to *Paralecanium* sp. (Coccomorpha) isolate D0764B. These BLAST hits are probably the result of the very low number of *Physokermes* species nucleotide sequences deposited in GenBank ($n = 22$, Available online at: http://www.ncbi.nlm.nih.gov; accessed November 8, 2022). In addition, the handling of specimens for morphological identification might have damaged the DNA quality leading to amplified fragments shorter than ideal for BLAST hits. Nevertheless, the most similar sequences were used as outgroups in the subsequent phylogenetic analyses. The sequences obtained and analyzed in the present study are deposited in GenBank under accession numbers OQ433782–898 (COI), OQ470427–526 (EF1α), and OQ657360–453 (28S).

According to PartitionFinder, the best nucleotide substitution model for *Physokermes* spp. COI evolution was a generalized time reversible (GTR) with a gamma-distributed rate variation (G) among sites, whereas 28S evolved according to the Hasegawa–Kishino–Yano (HKY) model with a proportion of invariable sites (I). A partitioned model of evolution was found for EF1α sequences, with the first two positions evolving according to Felsenstein's 1981 model (F81) with G and the third according to HKY. The ML and BI analyses performed for all datasets (Figure 1) revealed similar results, although BI usually presented higher support values, and therefore, these are the trees presented here. One clade comprising *P. hellenicus* and another comprising *P. inopinatus* were clearly evidenced and well-supported in all trees. However, only 28S and EF1α BI trees evidenced clades comprising *P. hemicryphus* alone (Figures 1B, C, respectively), with this species appearing mostly among *P. piceae* and *P. inopinatus*. In addition, *P. hemicryphus* samples from Hungary (Phem5.n and Phem6.n) appeared in a different clade from *P. hemicryphus* collected in Sweden (all other Phem codes). These populations do not seem to constitute host races, because they were both sampled from *Picea abies*, but might have been isolated by distance. Thus, the 28S nuclear gene is complementary to COI in *Physokermes* spp. identification, as proposed by Sethusa et al. (2014).

The NJ tree produced for the COI sequences (Figure 2) also evidenced well-supported clades containing *P. hellenicus* and *P. inopinatus*, and three other clades corresponding to *P. piceae* from Kaszó in Hungary (Ppic21.1 and Ppic21.2) and from Balavásár (Ppic41.2 and Ppic41.3) and Lukailencfalva (P.pic43.1, Ppic43.2, and Ppic43.3) in Romania. All these clades were monophyletic and their distance to the nearest neighbor varied from 3.5% (between *P. piceae* clades from Romania) to 6.3% (between *P. inopinatus* and *P. hellenicus*). These results support the distinction between *P. inopinatus* and *P. hellenicus*, as indicated in the ML and BI analyses. Moreover, the genetic distance found is similar to the congeneric 5.8% average mitochondrial DNA divergence (Pons et al., 2006) and within the 0.0–7.95% range (Hebert et al., 2004) reported for insects. The clade support and genetic distances found within *P. piceae* from Hungary and Romania (>2%) suggest the existence of cryptic species. Similar to other scale insects, *Physokermes* spp. females are flightless, males have a short lifespan, and both sexes have low dispersal capacity, all contributing to population differentiation in different areas and/or host species and promoting cryptic speciation, as observed in *Aspidiotus nerii* in Australia (Andersen et al., 2010) and in *Chionaspis heterophyllae* and *C. pinifoliae* in North America (Gwiazdowski et al., 2010). Because all the genetically differentiated *P. piceae* were sampled from *P. abies*, host species does not appear to be the factor contributing to such differentiation. Although explanations for the recent outbreaks remain elusive, particularly given the limited dispersal ability of *Physokermes* spp., changes in climate or weather conditions inducing rapid reproduction of endemic (and thus escaping detection) populations are more likely than sudden range expansions.

10.3389/ffgc.2023.1167541

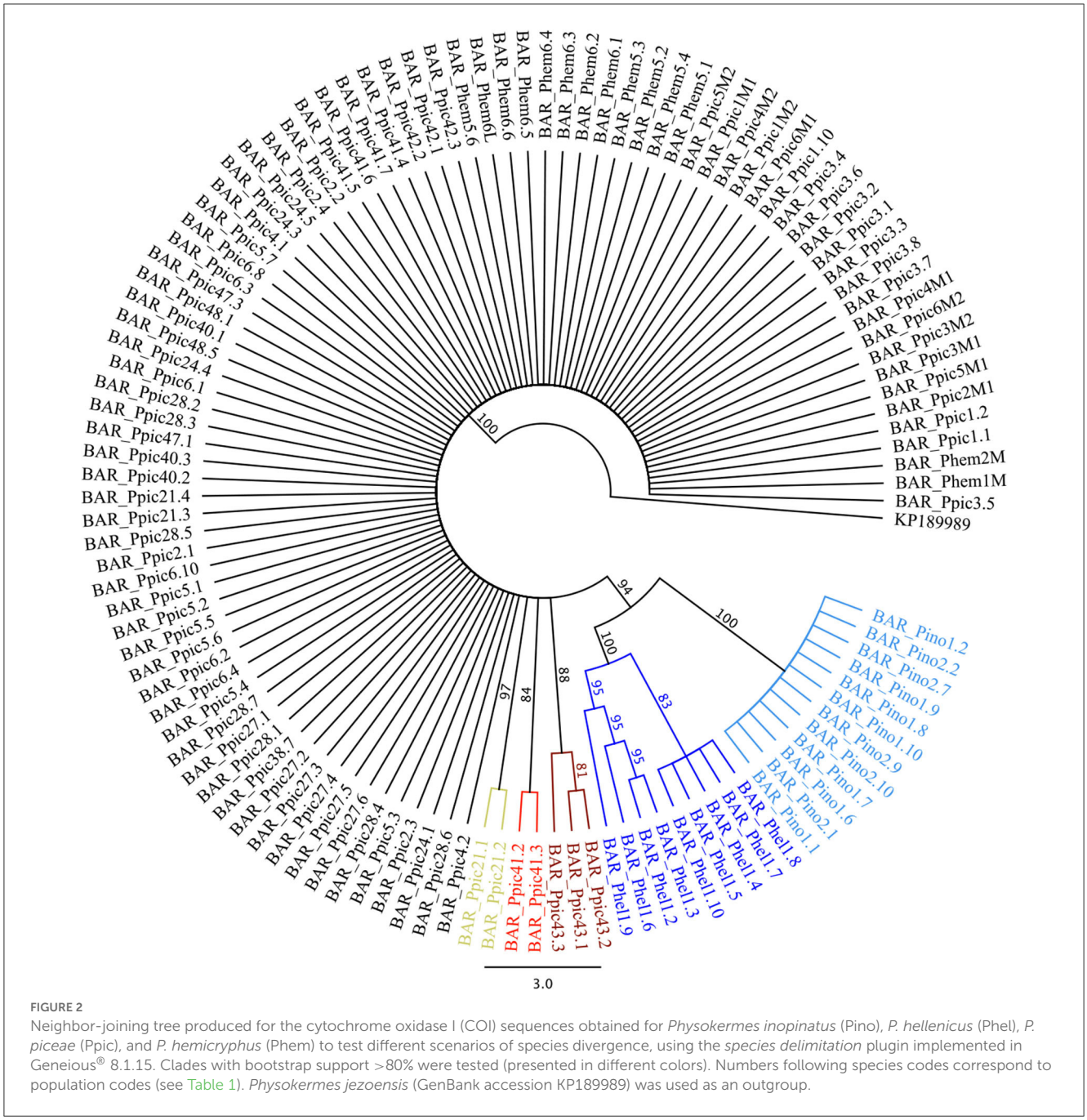

FIGURE 2
Neighbor-joining tree produced for the cytochrome oxidase I (COI) sequences obtained for *Physokermes inopinatus* (Pino), *P. hellenicus* (Phel), *P. piceae* (Ppic), and *P. hemicryphus* (Phem) to test different scenarios of species divergence, using the *species delimitation* plugin implemented in Geneious® 8.1.15. Clades with bootstrap support >80% were tested (presented in different colors). Numbers following species codes correspond to population codes (see Table 1). *Physokermes jezoensis* (GenBank accession KP189989) was used as an outgroup.

Overall, the results obtained here (i) clearly distinguished the closely related *P. hellenicus*, *P. inopinatus*, and (*P. piceae* + *P. hemicryphus*); (ii) revealed the existence of intraspecific variation and, possibly, of unknown complexes of species; and (iii) confirmed the value of using 28S in addition to COI for identifying scale insects. However, the differentiation of *P. hemicryphus* suggested in the nuclear data (particularly in 28S) analyses was not supported in the *species delimitation* analysis, as *P. hemicryphus* was not genetically distant from *P. piceae*. However, the sample size of *P. hemicryphus* and its geographic range was much smaller than that of *P. piceae,* and thus, further studies are needed to confirm the taxonomic status of *P. hemicryphus*.

Data availability statement

The gene sequences for this study can be found in GeneBank at https://www.ncbi.nlm.nih.gov/nuccore/?term=OQ433782:OQ433898[accn] for COI; https://www.ncbi.nlm.nih.gov/nuccore/?term=OQ4704273:OQ470526[accn] for EF1α; https://www.ncbi.nlm.nih.gov/nuccore/?term=OQ657360:OQ657453[accn] for 28S.

Author contributions

OA, AJ, and IW secured funding. IW ensured access to specimens. JM performed the genetic analyses and wrote

the first draft of the manuscript. All authors conceived the study, contributed to the manuscript, and approved the submitted version.

Funding

The study is a contribution to the Strategic Research Area Biodiversity and Ecosystem Services in a Changing Climate (BECC), and it was supported by the Carl Trygger Foundation for Scientific Research (CTS 14:17), the Tranemåla Foundation, and the Swedish Research Council Formas (Svenska Forskningsrådet Formas) (2010-822).

Acknowledgments

We would like to thank Éva Szita, Selma Ülgentük, Maurica Jansen, Gyuri Csóka, and Iosif Papanastasiou for generously supplying the insect samples, making our investigation possible and Carl-Axel Gertsson for additional species identity verification and general support to our work.

Conflict of interest

The authors declare that the research was conducted in the absence of any commercial or financial relationships that could be construed as a potential conflict of interest.

Publisher's note

References

Abd-Rabou, S., Shalaby, H., Germain, J. F., Ris, N., Kreiter, P., and Malausa, T. (2012). Identification of mealybug pest species (Hemiptera: Pseudococcidae) in Egypt and France, using a DNA barcoding approach. *Bull. Entomol. Res.* 102, 515–523. doi: 10.1017/S0007485312000041

Andersen, J. C., Normark, B. B., Morse, G. E., and Gruwell, M. E. (2010). Cryptic diversity in the *Aspidiotus nerii* complex in Australia. *Ann. Entomol. Soc. Am.* 103, 844–854. doi: 10.1603/AN10060

Beltrà, A., Soto, A., and Malausa, T. (2012). Molecular and morphological characterisation of Pseudococcidae surveyed on crops and ornamental plants in Spain. *Bull. Entomol. Res.* 102, 165–172. doi: 10.1017/S0007485311000514

Campbell, B. C., Steffen-Campbell, J. D., and Werren, J. H. (1994). Phylogeny of the *Nasonia* species complex (Hymenoptera: Pteromalidae) inferred from an internal transcribed spacer (ITS2) and 28S rDNA sequences. *Insect Mol. Biol.* 2, 225–237. doi: 10.1111/j.1365-2583.1994.tb00142.x

Deng, J., Yu, F., Zhang, T. X., Hu, H. Y., Zhu, CD, Wu, S.-A, et al. (2012). DNA barcoding of six *Ceroplastes* species (Hemiptera: Coccoidea: Coccidae) from China. *Mol. Ecol. Resour.* 12, 791–796. doi: 10.1111/j.1755-0998.2012.03152.x

Foottit, R. G., Maw, H. E. L., and Pike, K. S. (2009). DNA barcodes to explore diversity in aphids (Hemiptera: Aphididae and Adelgidae). *Redia* 92, 87–91.

Gertsson, C.-A., and Isacsson, G. (2014). The Hungarian spruce scale, *Physokermes inopinatus* Danzig and Kozár (Hemiptera: Coccoidea: Coccidae) in Sweden. *Acta Zool. Bulg. Suppl.* 6, 83–86.

Gwiazdowski, R. A., Vea, I. M., Andersen, J., and Normark, B. B. (2010). Discovery of cryptic species among North American pine-feeding *Chionaspis* scale insects (Hemiptera: Diaspididae). *Biol. J. Linn. Soc.* 104, 47–62. doi: 10.1111/j.1095-8312.2011.01716.x

Hajibabaei, M., Janzen, D. H., Burns, J. M., Hallwachs, W., and Hebert, P. D. N. (2006). DNA barcodes distinguish species of tropical Lepidoptera. *Proc. Natl. Acad. Sci. U.S.A.* 103, 968–971. doi: 10.1073/pnas.0510466103

Hebert, P. D., Stoeckle, M. Y., Zemlak, T. S., and Francis, C. M. (2004). Identification of birds through DNA barcodes. *PLoS Biol.* 2, e312. doi: 10.1371/journal.pbio.0020312

Hoy, M. A. (1994). "Insect molecular systematics and evolution," in *Insect Molecular Genetics: An Introduction to Principles and Applications,* ed M. A. Hoy (San Diego, CA: Academic Press) 337–387. doi: 10.1016/B978-0-12-357490-9.50016-X

Kondo, T., Gullan, P. J., and Williams, D. J. (2008). Coccidology. The study of scale insects (Hemiptera: Sternorrhyncha: Coccoidea). Revista Corpoica–Cienc. y Tecnol. *Agropecu.* 9, 55–61. doi: 10.21930/rcta.vol9_num2_art:118

Kosztarab, M., and Kozár, F. (1988). *Scale Insects of Central Europe.* Dr W. Junk, Budapest, Hungary. doi: 10.1007/978-94-009-4045-1

Kozár, F., Gounari, S., Hodgson, C. J., Fetyk, K., and Goras, G. (2012). A new species of *Physokermes* Targioni Tozzetti (Hemiptera: Coccoidea: Coccidae) from Greece. *Zootaxa* 3566, 23–38. doi: 10.11646/zootaxa.3566.1.3

Lanfear, R., Calcott, B., Ho, S. Y. W., and Guindon, S. (2012). Partitionfinder: combined selection of partitioning schemes and substitution models for phylogenetic analyses. *Mol. Biol. Evol.* 29, 1695–1701. doi: 10.1093/molbev/mss020

Malausa, T., Fenis, A., Warot, S., Germain, J. F., Ris, N., Prado, E., et al. (2011). DNA markers to disentangle complexes of cryptic taxa in mealybugs (Hemiptera: Pseudococcidae). *J. Appl. Entomol.* 135, 142–155. doi: 10.1111/j.1439-0418.2009.01495.x

McCarthy, R., and Skovsgaard, J. P. (2011). *Hungarian spruce scale on Norway spruce in southern Sweden: Correlation with climate, site and stand factors.* Southern Swedish Forest Research Centre, SLU.

Monaghan, M. T., Balke, M., Pons, J., and Vogler, A. P. (2006). Beyond barcodes: complex DNA taxonomy of a south pacific island radiation. *Proc. Royal Soc. B* 273, 887–893. doi: 10.1098/rspb.2005.3391

Morse, E. M., and Normark, B. B. (2006). A molecular phylogenetic study of armoured scale insects (Hemiptera: Diaspididae). *Syst. Entomol.* 31, 338–349. doi: 10.1111/j.1365-3113.2005.00316.x

Olsson, P.-O., Jönsson, A. M., and Eklundh, L. (2012). A new invasive insect in Sweden – *Physokermes inopinatus*: Tracing forest damage with satellite based remote sensing. *For. Ecol. Manage.* 285, 29–37. doi: 10.1016/j.foreco.2012.08.003

Papanastasiou, I., Evangelou, V., Papoutsis, L., Bouga, M., and Emmanouil, N. (2018). Molecular taxonomy of the genus *Physokermes* (Hemiptera: Coccidae) species in Greece, based on mtDNA sequencing data. *J. Apic. Res.* 57, 479–483. doi: 10.1080/00218839.2018.1494886

Papanastasiou, I., Kavallieratos, N. G., Papadoulis, G. T., Emmanouli, C., and Emmanouel, N. G. (2021). Geographical distribution and long-term monitoring of *Physokermes hellenicus* (Hemiptera: Coccomorpha: Coccidae) on *Abies* spp. (Pinales: Pinaceae) in Greece. *Insects* 12, 1001. doi: 10.3390/insects12111001

Park, D.-S., Suh, S.-J., Hebert, P. D. N., Oh, H.-W., and Hong, K.-J. (2011). DNA barcodes for two scale insect families, mealybugs (Hemiptera: Pseudococcidae) and armoured scales (Hemiptera: Diaspididae). *Bull. Entomol. Res.* 101, 429–434. doi: 10.1017/S0007485310000714

Park, D.-S., Suh, S.-J., Oh, H.-W., and Hebert, P. D. N. (2010). Recovery of the mitochondrial COI barcode region in diverse Hexapoda through tRNA-based primers. *BMC Genomics* 11, 423. doi: 10.1186/1471-2164-11-423

Pons, J., Barraclough, T. G., Gomez-Zurita, J., Cardoso, A., Duran, D. P., Hazell, S., et al. (2006). Sequence-based species delimitation for the DNA taxonomy of undescribed insects. *Syst. Biol.* 55, 595–609. doi: 10.1080/10635150600852011

Ronquist, F., and Huelsenbeck, J. P. (2003). Mrbayes 3: Bayesian phylogenetic inference under mixed models. *Bioinformatics* 19, 1572–1574. doi: 10.1093/bioinformatics/btg180

Sethusa, M. T., Yessoufou, K., Van der Bank, M., Millar, I. M., and Jacobs, A. (2014). DNA barcode efficacy for the identification of economically important scale insects (Hemiptera: Coccoidea) in South Africa. *Afr. Entomol.* 22, 257–266. doi: 10.4001/003.022.0218

Simon, C., Frati, F., Beckenbach, A., Crespi, B., Liu, H., and Flook, P. (1994). Evolution, weighting and phylogenetic utility of mitochondrial gene sequences and a compilation conserved polymerase chain reaction primers. *Ann. Entomol. Soc. Am.* 87, 651–701. doi: 10.1093/aesa/87.6.651

Smith, M. A., Rodriguez, J. J., Whitfield, J. B., Deans, A. R., Janzen, D. H., Hallwachs, W., et al. (2008). Extreme diversity of tropical parasitoid wasps exposed by iterative integration of natural history, DNA barcoding, morphology, and collections. *Proc. Natl. Acad. Sci. U.S.A.* 105, 12359–12364. doi: 10.1073/pnas.0805319105

van Nieukerken, E. J., Doorenweerd, C., Stokvis, F. R., and Groenenberg, D. S. J. (2012). DNA barcoding of the leaf-mining moth subgenus *Ectoedemia* s. str. (Lepidoptera: Nepticulidae) with COI and EF1-α: two are better than one in recognizing cryptic species. *Contrib. Zool.* 81, 1–24. doi: 10.1163/18759866-08101001

Vea, I. M., Gwiazdowski, R. A., and Normark, B. B. (2012). Corroborating molecular species discovery: Four new pine-feeding species of *Chionaspis* (Hemiptera, Diaspididae). *ZooKeys* 270, 37–58. doi: 10.3897/zookeys.270.2910

Winde, I., Anderbrant, O., and Jönsson, A. M. (2018). Tree recovery during the aftermath of an outbreak episode of the Hungarian spruce scale in southern Sweden. *Scand. J. For. Res.* 33, 313–319. doi: 10.1080/02827581.2018.1424932

Zhu, X.-C., Chen, J., Chen, R., Jiang, L.-Y., and Qiao, G.-X. (2017). DNA barcoding and species delimitation of Chaitophorinae (Hemiptera, Aphididae). *ZooKeys* 656, 25–50. doi: 10.3897/zookeys.656.11440

Zwickl, D. J. (2006). *Genetic Algorithm Approaches for the Phylogenetic Analysis of Large Biological Sequence Datasets Under the Maximum Likelihood Criterion*. Dissertation, Austin, TX: University of Texas.

frontiers | Frontiers in Forests and Global Change

TYPE Original Research
PUBLISHED 24 July 2023
DOI 10.3389/ffgc.2023.1166421

OPEN ACCESS

EDITED BY
Amit Roy,
Czech University of Life Sciences Prague, Czechia

REVIEWED BY
Jennifer Gene Klutsch,
University of Alberta, Canada
Jian J. Duan,
Agricultural Research Service (USDA), United States

*CORRESPONDENCE
Jeanne Romero-Severson
✉ jromeros@nd.edu

RECEIVED 15 February 2023
ACCEPTED 01 June 2023
PUBLISHED 24 July 2023

CITATION
Stanley RK, Carey DW, Mason ME, Doran A, Wolf J, Otoo KO, Poland TM, Koch JL, Jones AD and Romero-Severson J (2023) Emerald ash borer (*Agrilus planipennis*) infestation bioassays and metabolic profiles of green ash (*Fraxinus pennsylvanica*) provide evidence for an induced host defensive response to larval infestation. *Front. For. Glob. Change* 6:1166421. doi: 10.3389/ffgc.2023.1166421

Emerald ash borer (*Agrilus planipennis*) infestation bioassays and metabolic profiles of green ash (*Fraxinus pennsylvanica*) provide evidence for an induced host defensive response to larval infestation

Robert K. Stanley[1], David W. Carey[2], Mary E. Mason[2], Aletta Doran[3], Julia Wolf[3], Kingsley Owusu Otoo[1], Therese M. Poland[4], Jennifer L. Koch[2], A. Daniel Jones[5] and Jeanne Romero-Severson[1]*

[1]Department of Biological Sciences, University of Notre Dame, Notre Dame, IN, United States, [2]Northern Research Station, U.S. Department of Agriculture Forest Service, Delaware, OH, United States, [3]Holden Arboretum, Kirtland, OH, United States, [4]Northern Research Station, U.S. Department of Agriculture Forest Service, Lansing, MI, United States, [5]Department of Biochemistry and Molecular Biology, Michigan State University, East Lansing, MI, United States

Introduction: Larvae of the invasive emerald ash borer [EAB, *Agrilus planipennis* Fairmaire (Coleoptera: Buprestidae)], kill over 99% of green ash (*Fraxinus pennsylvanica* Marshall) trees they infest, yet a small percentage of green ash ("lingering ash") survive years of heavy EAB attack. In the face of an ongoing invasion that threatens multiple North American *Fraxinus* species with extinction, any evidence for reproducible defensive responses in the native species merits investigation.

Methods: We evaluated the capacity of three families of green ash F_1 progeny to kill EAB larvae when challenged in greenhouse studies by infestation with a uniform density of EAB eggs followed by dissection 8 weeks post-infestation and comparison of the host metabolomic profiles.

Results: The mean proportions of host-killed larvae in the two families of F_1 progeny from lingering ash parents were significantly higher than that of host-killed larvae in the family of F_1 progeny from susceptible ash parents ($p < 0.001$). Untargeted metabolomics comparing F_1 progeny in the quartile with the highest percent host-killed larvae (HHK) to F_1 progeny in the quartile with the lowest percent host-killed larvae (LHK) and to the uninfested F_1 progeny within each family revealed evidence for induced biochemical responses to EAB. Infested trees produced significantly higher levels of select secoiridoids than uninfested trees, and LHK progeny produced significantly higher levels of select secoiridoids than the HHK progeny. HHK progeny produced significantly higher abundances of three metabolites annotated as aromatic alkaloids than the LHK and uninfested individuals.

Discussion: Based on these results, we hypothesize that green ash responds to EAB infestation. However, only certain trees have the genetic capacity to tailor a response that kills enough EAB larvae to prevent lethal damage to the vascular

system. Rigorous tests of this hypothesis will require 15–20 years of additional crossing, phenotyping, and omics analyses. The results of this investigation will encourage the establishment and continuation of breeding programs that, in concert with biocontrol and management, could provide trees that slow, if not halt, the decimation of the *Fraxinus* gene pool. At the same time, ongoing work on host-insect interaction will contribute to our understanding of how forest trees recognize and defend themselves against phloem-feeding insects.

KEYWORDS

secoiridoid, emerald ash borer (*Agrilus planipennis* Fairmaire), green ash (*Fraxinus pennsylvanica*), liquid chromatography-mass spectrometry (LCMS), emerald ash borer infestation bioassay, induced host defensive response, *Fraxinus pennsylvanica* metabolic profiles, host-insect interaction

Introduction

Invasive pests and pathogens, now widely dispersed through globalization, threaten nearly two-thirds of North American forests (Potter et al., 2019). Exacerbated by climate instability, these increasingly severe infections and infestations threaten forested ecosystems and inflict billions of dollars in direct costs to individuals and local communities (Kovacs et al., 2010; Aukema et al., 2011; Hicke et al., 2012; Krist et al., 2014; Bradshaw et al., 2016; Lovett et al., 2016; Potter et al., 2019; Anderegg et al., 2020; Hoover and Riddle, 2020; Miniat et al., 2021). The emerald ash borer (EAB, *Agrilus planipennis* Fairmaire), a woodboring beetle native to Asia, was discovered in Michigan, United States, and Ontario, Canada, in 2002 (Poland and McCullough, 2006). EAB larvae feed on the vascular cambium, cork cambium, and phloem, inflicting severe vascular damage and consequently killing 95–99% of mature green ash [*Fraxinus pennsylvanica* Marshall (Lamilaes: Oleaceae) *Fraxinus* sect. *Meliodes*] trees within 3–5 years of peak infestation (Knight et al., 2013). EAB is the most damaging invasive forest insect pest ever to have invaded North America, threatening nearly all native species of *Fraxinus* with functional extinction (Poland and McCullough, 2006; Herms and McCullough, 2014; Aubin et al., 2015).

Green ash, the most widely distributed *Fraxinus* species in North America, is a diecious, diploid, and deciduous tree species native to the eastern and central United States and eastern Canada (Walters and Yawney, 2004). EAB infestation has resulted in the rapid loss of hundreds of millions of green ash, not only in forests and rural areas but also in cities, where green ash was once one of the most widely planted street and park trees in the United States (Knight et al., 2013; Hanberry, 2014). The ash mortality in EAB-infested stands can approach 100% within 6 years of local EAB detection (Knight et al., 2013).

Long-term forest plot monitoring initiated in 2005, 3 years after the initial detection of EAB in North America, revealed a small number of green ash (0.1–1%) that survive for years after all other surrounding green ash have died (Knight et al., 2012). Although the susceptibility of almost all healthy green ash suggests an absence of defensive capacity against EAB, the persistence of these few "lingering ash" in heavily infested stands suggests that innate defensive responses may be rare rather than absent. Lingering ash have been and continue to be propagated as potential sources of genetic resistance for a United States Forest Service (USFS) breeding research program (Koch et al., 2012, 2015). The USFS program identified green ash trees based on standard criteria for distinguishing *Fraxinus* species and selected lingering ash in natural forests based on two additional criteria: (1) a healthy canopy at least 2 years after the mortality rate of the stand exceeded 95 percent, and (2) a minimum diameter at breast height (DBH, 1.37 m above ground) of 26 cm, indicating that the tree was over the minimum size preferred by EAB when the infestation was at peak levels (Koch et al., 2015). These lingering ash trees show evidence of a less severe emerald ash borer infestation than susceptible phenotypes in the forest and maintain a healthy crown for years after local conspecifics have died (Steiner et al., 2019). Individuals meeting these criteria have been clonally propagated through grafting and subjected to EAB infestation bioassays (described below) that provided evidence of the ability of some selected lingering ash trees to mount defensive responses against EAB.

Infestation bioassay tests, conducted by placing controlled densities of EAB eggs on propagated clonal replicates of lingering green ash and then determining the fate of larvae when dissected 8 weeks post-infestation, revealed reproducible capabilities of hosts to kill EAB larvae (referred to as host-killed larvae) in most of the clonal lingering green ash selections tested (Koch et al., 2015). The reproducibility of this "proportion of host killed larvae" phenotype, detected in healthy grafted clones from lingering ash identified in forest plots, provided the first indication that the capacity to kill EAB larvae in a select group of host trees has a genetic basis (Mason et al., 2023).

Genetic variation in the profiles of plant-specialized metabolites occurs within species and even between local populations of the same species (Mithöfer and Boland, 2012; Chen et al., 2015; Gloss et al., 2022). Investigations on the role of specialized metabolites as defenses against EAB have focused on comparing cultivars and a limited number of open-pollinated seedlings from *Fraxinus spp.* to the naturally resistant but not immune Asian *F. mandshurica* cultivar *'Mancana' Fraxinus* sect. *Fraxinus* (Whitehill et al., 2012). Application of methyl jasmonate in the white ash (*F. americana* L. *Fraxinus* sect. *Melioides*) cultivar "Autumn purple" increased the concentration of the phenylethanoid glycoside verbascoside by over 170% and suppressed EAB larval development (Whitehill et al., 2014). These studies collectively proposed a positive association between lignan glycosides and host resistance, particularly

pinoresinol and verbascoside, and suggested a role for secoiridoid glycosides (Villari et al., 2016).

Many specialized metabolites, including secoiridoids, are also implicated in the response of European Ash (*F. excelsior* L. *Fraxinus* sect. *Fraxinus*) to ash dieback disease (ADB), causal agent *Hymenoscyphus fraxineus* (Baral et al., 2014). High abundances of specific secoiridoids were associated with tolerant genotypes in one study (Nemesio-Gorriz et al., 2020) and with highly susceptible genotypes in another (Sollars et al., 2017). Both groups of investigators proposed that the different levels of secoiridoids result from differential transcriptional regulation among individual trees. Similarly, investigations of resistance mechanisms in conifers have shown that some trees utilize specialized metabolite-based constitutive and induced defensive responses against wood-boring insects (Volf et al., 2015; López-Goldar et al., 2018, 2019). The abundance and profiles of specific plant specialized metabolites strongly predict resistance to the pine weevil (*Hylobius abietis* L.) in maritime pine *(Pinus pinaster* Aiton) after accounting for genetic relatedness among the host trees (López-Goldar et al., 2018). Other investigations in pine have shown that the response consists of altered synthesis rates for existing metabolites rather than the synthesis of unique compounds (Raffa and Smalley, 1995; López-Goldar et al., 2018).

The phenotypes observed in the first clonal replicates of lingering ash and susceptible ash trees under controlled larval infestations and uniform growing conditions showed that while many susceptible trees kill a few EAB larvae, lingering ash trees consistently kill more EAB larvae (Koch et al., 2015; Kelly et al., 2020). In this investigation, we combined untargeted metabolomics and intensive phenotyping on three F_1 families, using an experimental design that minimizes the confounding effect of age, environment, and genetic background to investigate the response of full-sibling progeny from crosses using parents verified as lingering ash and infestation bioassays. Our design included untargeted metabolomics to investigate the chemotypes of uninfested compared to infested individuals and trees that killed the most larvae compared to those that killed the fewest, all within the same family. This investigation provides the first evidence for an induced response to EAB infestation and the first evidence for chemotypic differences associated with host response to EAB in a controlled genetic background.

Materials and methods

Study system

Green ash is one of the most wide-ranging species in the *Melioides* section of the genus *Fraxinus*, the group of species native only to the Americas. Green ash is strictly diecious, each tree bearing only pistillate (female) or staminate (male) flowers. As trees in the *Melioides* section of *the Fraxinus* genus are sexually incompatible with the Asian *Fraxinus* section *Fraxinus*, the strong defenses of the Asian ash against EAB cannot be transferred into green ash using traditional hybrid breeding strategies. The lingering green ash parents used in this investigation were initially selected in the forest based on two criteria: (1) a healthy canopy at least 2 years after the mortality rate of the stand exceeded 95 percent, and (2) a minimum diameter at breast height (DBH, 1.37 m above ground) of 26 cm, indicating that the tree was over the minimum size preferred by EAB when the infestation was at peak levels (Koch et al., 2015). These "lingering ash" trees show evidence of less severe emerald ash borer infestation compared to susceptible phenotypes in the forest, often accompanied by evidence of vigorous wound healing, and maintaining a healthy crown for years after local conspecifics have died (Knight et al., 2012; Steiner et al., 2019). Over the last 14 years, individuals meeting these criteria have been clonally propagated through grafting and subjected to greenhouse bioassays that provided evidence of the ability of some selected lingering ash trees to mount defensive responses against EAB (Koch et al., 2015). Although there is evidence of multiple types of host defenses in *Fraxinus* (e.g., non-preference), this work focuses on assessing host defenses that result in larval mortality. Clonal replicates of lingering green ash genotypes, some used as parents in this study, consistently kill more larvae than the susceptible green ash controls (Koch et al., 2015).

All individuals in this investigation were generated by controlled pollination to produce full-sibling families of known parentage. Cross-pollination in green ash is only possible between trees of different sexes, and even then, not all crosses are successful. The tactical result was a limited selection of full-sibling progeny from parents known to be susceptible or lingering. A male 'Summit' tree was the susceptible parent for the control Family C. 'Summit' is a cultivar first marketed in 1957 by Summit Nursery in Stillwater, Minnesota, and was widely used as a street and park tree before the introduction of EAB. 'Summit' is susceptible to EAB in these environments. It was also susceptible in infestation bioassays and resulted in a proportion of host-killed larvae value of 0.08 (n = 30 ramets) (Mason et al., 2023). The female parent in Family C, Pe-97, was a field selection from a forest where EAB had yet to reach peak infestation. The lingering ash parents (Pe-53, Pe-56, and Pe-59) used in this investigation survived the initial EAB invasion, the buildup of EAB populations, and the peak infestation. The raw mean proportions of host-killed larvae for the lingering ash parents were 0.28 for Pe-53, 0.06 for Pe-56, and 0.10 for Pe-59 (Mason et al., 2023). Infestation bioassays were conducted on the parent trees in different years while calibrating EAB egg density, but 'Summit' was used as a susceptible control in most experiments allowing relative comparison (Mason et al., 2023). Although the proportion of host-killed larvae for Pe-56 was low, surviving larvae were typically smaller than larvae from susceptible parents. Crosses between lingering ash parents were made as part of a planned crossing design to estimate heritability. The two largest lingering ash families, Pe-Y from the cross Pe-53 x Pe-56 (Family Y) and Pe-Z from the cross Pe-53 x Pe-59 (Family Z), were selected for metabolomics experiments to take advantage of the largest pool of segregating individuals. The female parent is written first. The progeny individuals produced by these three crosses were reared in an outdoor growing area until 2 years of age, then transferred into an environmentally controlled greenhouse in the treatment year to allow acclimatization prior to the EAB infestation bioassay. At the time of the infestation bioassay, the trees were 1.5 to 2 meters tall, a height typical for green ash of this age in our growing conditions. A total of 83 trees were subjected to the infestation bioassay. We assayed 30 of the 42 trees in family Y, and set aside the remaining 12 trees as uninfested controls. We assayed 30 of 35 trees in family Z and set aside 5 trees as uninfested controls. We included 17 of the 23 assayed trees from family C and four uninfested controls in this

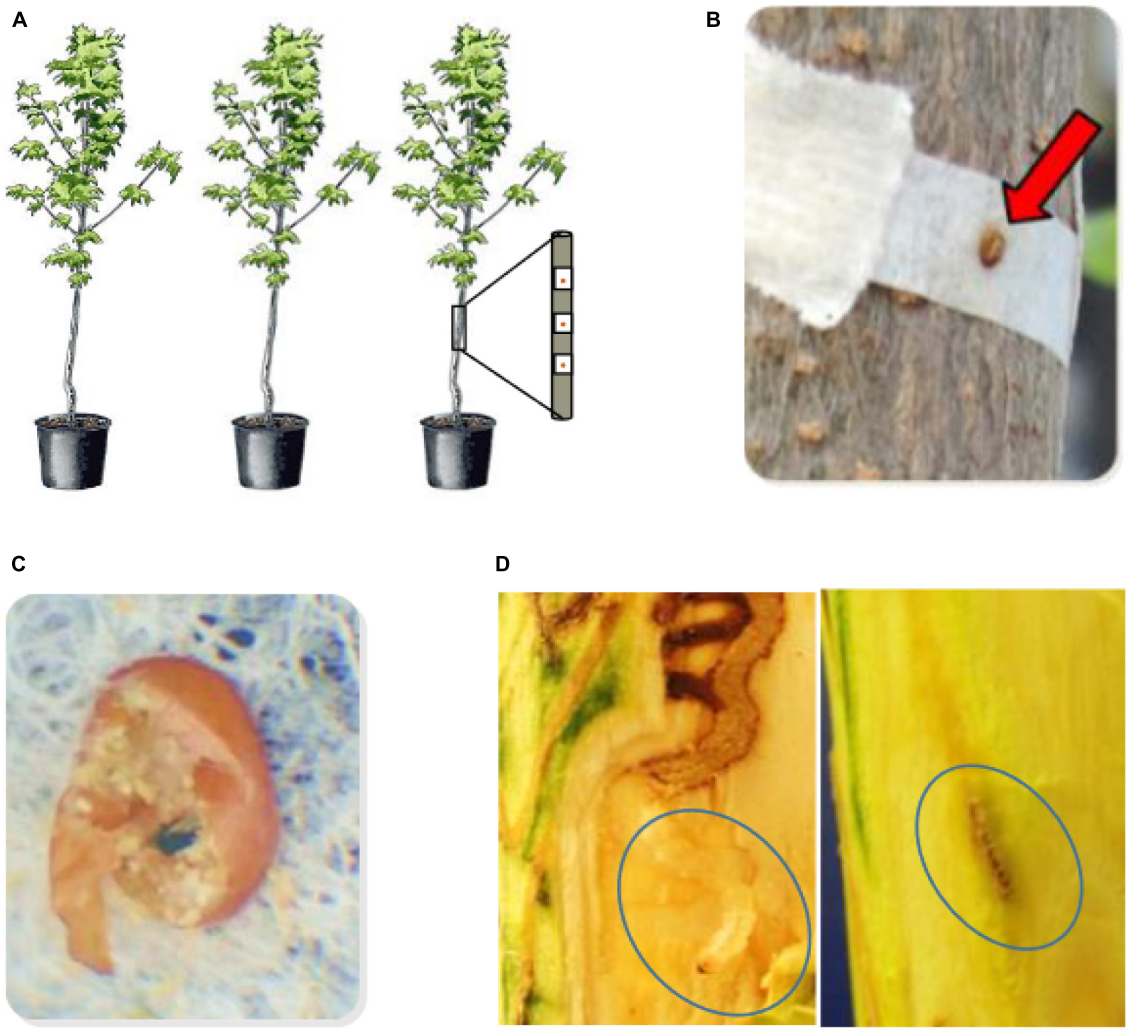

FIGURE 1
Infestation bioassay sequence. **(A)** Eggs were applied individually at a standardized density when the progeny trees were 2 years old, **(B)** close up of egg adhering to the coffee filter, **(C)** close up of the chorion of a "good egg" that had hatched and larva had entered the tree taken 3 weeks after application to the tree. The chlorion is broken to reveal frass and an exit hole in the coffee filter below the egg. The entry hole to the tree would be marked on the bark immediately below for reference when dissection begins 8 weeks after egg application. **(D)** Larval disection 8 weeks after egg application. Galleries are dissected and followed until the larva is located alive (left panel), or the gallery terminates with host defense reactions present (right panel) such as gallery termination with browning and callous (not all outcomes shown, see text).

investigation. We performed untargeted metabolomics on these 77 infested trees and 21 uninfested trees (98 trees total).

Emerald ash borer infestation bioassays

Emerald ash borer eggs were prepared as previously described (Koch et al., 2015), and twelve eggs were applied to each tree at a density of 400 eggs per square meter (Kelly et al., 2020) during June-August 2019. Individual eggs on filters were affixed to the stem beginning at the bottom and spaced at 400 per m^2 until the stem diameter reached the minimum (1.0 cm) or a total of 12 eggs, whichever came first (**Figure 1**). The minimum number of eggs applied was nine on four trees of smaller stem diameter due to variability in the size of trees at 2 years of age. Egg hatch and EAB entry holes were marked at 3 weeks, and larval galleries were dissected 8 weeks after eggs were applied, starting at the entry hole and following the gallery path to determine the status of each larva. The 8-week interval was chosen based on the time it typically takes for newly hatched larvae to reach the final instar before pupation in susceptible trees. Recovered larvae were designated as alive, host-killed (killed by a host defense response), or killed by parasitism, cannibalism, or disease as characterized and described in detail in other studies (Duan et al., 2015, 2017; Kelly et al., 2020; Mason et al., 2023). Galleries of host-killed larvae end in callous or browning, and larvae are not parasitized, cannibalized, or diseased (Duan et al., 2015, 2017; Koch et al., 2015). Parasitoid insects are visible on or in parasitized EAB larvae. Cannibalized larvae are characterized by intersecting larval galleries with only one gallery continuing and uneaten larval parts (e.g., only the head or posterior of one larva) in the terminated gallery. Larvae with undetermined deterioration (black, shriveled insect body) are rarely found and are coded as diseased. The proportions of host-killed larvae, first or second instar (L1 + L2) larvae, and third or fourth instar (L3 + L4) larvae

were calculated based on the number of larvae in each category divided by the total number of larvae that hatched and entered the tree (coded as GoodEgg). Larval instar stage was determined based on head capsule width and total body length (Chamorro et al., 2012). Average larval weight was determined based on the weights of the live larvae recovered intact (occasionally, live larvae were damaged and not weighed).

We tested differences in family means for the response variable proportion host-killed larvae by a fitting generalized linear model with family as a fixed effect (logit link function) and compared differences in least squared means with a Tukey adjustment for multiplicity (SAS 9.4, PROC GLIMMIX) (**Supplementary Figure 1**). We used the same approach for the response variable average larval weight (with a lognormal link function). Based on the distribution of phenotypes within families for the response variable proportion of host-killed larvae (total number of host-killed larvae/GoodEgg) (**Figure 2**), we designated the phenotypic class of individual progeny in the lowest quartile of percent host-killed larvae as low host-killed (LHK), and individual progeny in the highest quartile of percent host-killed larvae as high host killed (HHK). As a comparison, the resistant Asian ash (*F. mandshurica* sect. Fraxinus Oleaceae) typically kills 80–90% of EAB larvae when tested with the infestation bioassay (Koch et al., 2015).

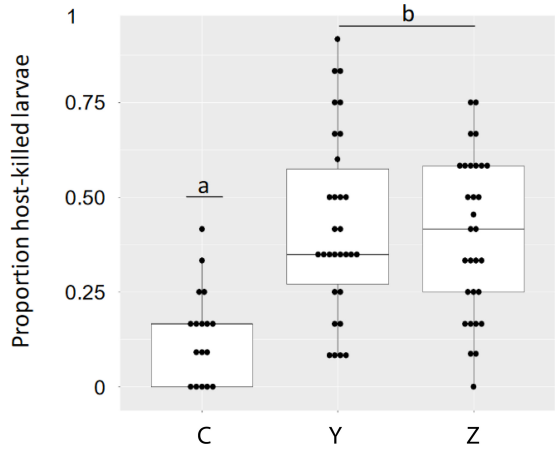

FIGURE 2
Proportion of EAB larvae killed by host defenses in Family C (one unselected and one susceptible parent) and Families Y and Z (lingering ash parents) when sampled 8 weeks post infestation. Means for Families Y and Z were both highly significantly different from the mean for Family C ($p < 0.001$) and means for Families Y and Z were not different from each other ($p = 0.488$) as assessed using GLMM (see text for model and LS means). The statistical analysis was performed on 93 infested trees, 30 trees each from families Y and Z and 33 from family C. The data shown are for the 77 infested trees used for untargeted metabolomics.

Profiling *F. pennsylvanica* woody tissue metabolites

All infested and uninfested trees were destructively sampled 8 weeks after infestation with EAB eggs to assess host defense phenotype and collect tissue for metabolite analyses. A 1.5 cm section of each stem, beginning 2.5 cm above the highest EAB larval galleries, was collected and stored immediately on dry ice before being transferred to −80°C storage. This ensured the collection of the vascular cambium, the cork cambium, the phloem, and the ray parenchyma. All samples were ground under liquid nitrogen in a Spex® SamplePrep freezer mill (Metuchen, NJ, USA) and stored at −80°C before extraction.

For each sample, 1 g of frozen powdered plant tissue was extracted in 10 ml of acetonitrile/isopropanol/water (3:3:2) containing 1.00 μM telmisartan (internal standard, Sigma-Aldrich) and 0.01% formic acid in 15-mL polypropylene Falcon tubes and incubated in the dark at 4°C for 24 h. Samples were then centrifuged at 4°C and 10,000*g* for 10 min, supernatants were transferred to fresh tubes, and 50:1 diluted aliquots were prepared by adding deionized water. An additional aliquot of undiluted extracted sample was archived at −80°C.

Ultra-high-performance liquid chromatography-high resolution mass spectrometry (UHPLC-MS) analyses were performed using a Shimadzu LC-20AD ternary pump coupled to a SIL-5000 autosampler, column oven, and Waters Xevo G2-XS QTof mass spectrometer equipped with an electrospray ionization source. The mass spectrometer operating parameters for the positive-ion mode analyses are as previously described (Lybrand et al., 2020). A 10 μL volume of each diluted extract was analyzed using a 20-min gradient method on an Ascentis Express C18 UHPLC column (2.1 × 100 mm, 2.7 μm) with mobile phases consisting of 10 mM ammonium formate in water, adjusted to pH 2.8 with formic acid (solvent A) and acetonitrile (solvent B). The 20-min method gradient was as follows: 1% B at 0.00 to 1.00 min, then step to 5% B at 1.01 min, linear gradient to 25% B at 8.00 min, then a linear gradient to 75% B at 12.50 min, another linear gradient to 98% B at 15.00 min, and a hold at 98% B until 18.00 min, a step to 1% B at 18.01 min, and a hold at 1% B until 20.00 min.

Analyte extracts were injected in a randomized order while process blank and quality control samples were injected at regular intervals beginning with a process blank and then alternating between quality control standards and blanks following each group of 10 samples, then finishing with a quality control sample and a blank at the end of the run. All calculated peak areas were normalized to the peak area for the internal standard telmisartan utilizing Progenesis QI v2.4 software (Non-linear Dynamics Ltd., Newcastle, UK). Oleuropein, apigenin, and salidroside standards were purchased from MilliporeSigma (St. Louis, United States), dissolved in the extraction solvent, and analyzed at 5 μg/mL to provide analytic confirmation and validation.

Untargeted metabolomics data processing

We produced untargeted metabolite profiles from acetonitrile:isopropanol:water extractions of ash tissues using UHPLC-MS. The levels of metabolites were normalized to a constant internal standard, with a constant mass of tissue extracted. For untargeted metabolomic analysis, data were initially processed using Progenesis Ql software. Leucine enkephalin lockmass correction (*m/z* 556.2766) was applied during data importation, and all analyses were aligned to retention times of a

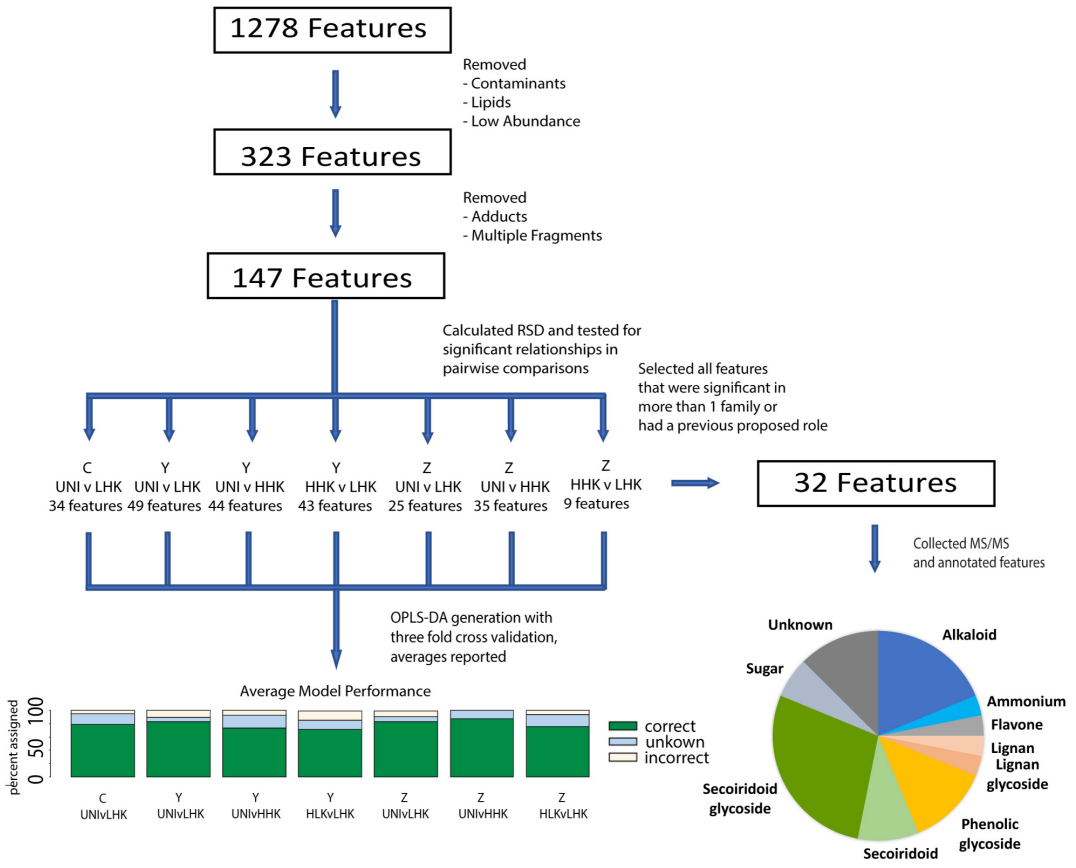

FIGURE 3
Data processing schematic. Flowthrough of the untargeted metabolomics workflow beginning with data generation, and highlighting the number of metabolite features at each stage of the analysis.

pooled QC sample run automatically selected by the software from a selection of QC samples. Peak selection and deconvolution were conducted as previously described (Sadre et al., 2016). Abundances of each metabolite feature were normalized to signals of the internal telmisartan standard (*m*/z 515.2448). After deconvolution, 1,278 compound ions remained (**Figure 3**). To remove metabolite features from the dataset introduced by solvents, glassware, or instrumentation and to remove lipids, several filters were applied to the 1,278 compound ions remaining after deconvolution. This was achieved by removing compounds with the highest mean abundance in process blank samples, maximum abundance less than 0.01% of the most abundant compound in the dataset, or retention times greater than 16 min. These selection criteria reduced the total number of metabolic features to 323. This number was reduced to 147 features through manual resolution of multiple adducts and fragments from individual features (**Supplementary Table 1**). Further analysis and statistical comparisons of compound signals extracted by Progenesis QI software were executed using EZinfo v3.0.2 software (Umetrics®, Umeå, Sweden).

To test for differences in the quantity of each metabolite feature, we applied one-way analyses of variance (ANOVA) tests for each family separately, and with infestation status plus phenotypic class (Uninfested (UNI), Low Host-killed larvae (LHK), and High Host-killed larvae (HHK)] as the main effect (**Figure 3**). *Post hoc* contrasts were used to assess the significance between infestation and phenotypic classes within families using the seven following contrasts: Family C: UNI vs. LHK; Family Y: UNI vs. LHK, UNI vs. HHK, LHK vs. HHK; Family Z: UNI vs. LHK, UNI vs. HHK, LHK vs HHK. ANOVA fit was assessed by examining residuals plots. Significant features ($p < 0.05$) were included in pairwise orthogonal partial least squares discriminant analysis (OPLS-DA) (**Figure 3**, **Supplementary Figure 2**, and **Supplementary Table 2**). OPLS-DA analyses, as implemented in EZinfo, were performed using Pareto scaling. To prevent overfitting of our model, we performed a threefold cross-validation on our data and took the averages in classification outcomes as metrics of the performance of our model. For all metabolic features extracted with Progenesis QI and used in downstream statistical analyses, spectra were processed using MassLynx v4.2 software (Waters Corporation, Milford, MA, United States) as previously described (Sadre et al., 2016).

We generated electrospray ionization tandem mass spectra (ESI-MS/MS) for these metabolite features detected in our analyses and annotated them based on theoretical molecular formulae that match the measured mass and isotopic distribution of the compounds detected ("elemental composition method" in Progenesis Q), comparison of MS/MS databases available using progenesis QI (ChemSpider and Metlin), and comparisons with other MS/MS databases including the Massbank of North America, along with published literature and purchased standards (Sidda et al., 2020). The annotation confidence is labeled according to the

recommendations of the Metabolomics Standards Initiative (MSI) (Sumner et al., 2007). Of the metabolites considered, the 31 that had significance ($p < 0.05$) in more than one family were annotated, as well as salidroside, which was higher in HHK than LHK progeny in Family Y (32 metabolites total) (**Figure 3** and **Supplementary Table 3**).

Results

Emerald ash borer infestation bioassays

A total of 952 eggs were applied in this experiment, only thirteen of which (1.4%) produced larvae that were killed by means other than the host response (**Table 1** and **Supplementary Table 4**). Least square family means and mean standard error for the proportion of host-killed larvae were 0.152 ± 0.022 (Family C), 0.442 ± 0.026 (Family Y), and 0.441 ± 0.027 (Family Z) (**Supplementary Figure 1**). Differences in family least squares means were highly significant for the comparison of Family Y vs. Family C (adjusted $p < 0.001$) and the comparison Family Z vs. Family C (adjusted $p < 0.001$). Least square family means for Family Y and Family Z were not significantly different from each other (adjusted $p = 0.488$). Models were well fitted as assessed by plots of studentized residuals (**Supplementary Figure 1**). Progeny in all three families were distributed over a range of values for the response variable proportion of host-killed larva (**Figure 2**). The differences among family least squares means for the response variable larval weight (Lwt) were not significant for any comparison: Family Y vs. Family C (adjusted $p = 0.99$), Family Z vs. Family C (adjusted $p = 0.403$), Family Y and Family Z (adjusted $p = 0.439$).

Metabolomics analysis

Untargeted metabolite profiling using UHPLC-MS revealed complex chemotypes with low deviation. The levels of metabolites were normalized to a constant internal standard, with a constant mass of tissue extracted. After deconvolution, 1,278 metabolite features were observed, which was reduced to 147 metabolite features for downstream analysis, as detailed above (**Figure 3**). The median relative standard deviation (RSD) of these metabolite features was 29.8% in pooled controls (**Supplementary Figure 3**).

The relationship of metabolites to infestation status [uninfested (Uni)] and phenotypic class [low host-killed larvae (LHK), high host-killed larvae (HHK)] within each family was assessed by ANOVA followed by *post hoc* contrasts for 147 metabolite features (**Figure 3** and **Supplementary Table 1**). All 147 metabolite features were significant ($p < 0.05$) in at least one contrast, with 9 to 49 metabolite features significant for different contrasts (**Figure 3** and **Supplementary Table 1**). The greatest number of significant metabolite features were identified in Family Y, and more metabolite features were identified in infested compared to uninfested progeny. There were fewer significant differences in the number of metabolite features between infested progeny with low host-killed larvae vs. high host-killed larvae within each family.

Following the identification of significant metabolite features, we used orthogonal partial least squares-discriminant analyses (OPLS-DAs) (Lee et al., 2018) to examine the metabolite features' ability to accurately classify the host-killed larvae phenotype (high or low proportion of host-killed larvae) in each pairwise comparison (**Figure 4** and **Supplementary Table 1**). To prevent overfitting, we performed a three-fold cross-validation on our data and reported the average prediction accuracies as the performance of our classification model. More than 70% of individuals were assigned correctly to the host-killed larvae phenotype class, with the majority of other individuals being unclassified but not incorrectly assigned (**Figure 4A** and **Supplementary Table 1**). The OPLS-DAs for the entire data set showed R2Y and Q2 values above 50% and within 20% of each other, indicating good classification performance (Bevilacqua and Bro, 2020). A specific example is the OPLS-DA for Family Y for the classes HHK and LHK, showing R2Y and Q2 values of 70 and 59%, respectively (**Figure 4B**).

We annotated 32 metabolite features, including the 31 that had a significant p-value in more than one family's comparisons and an additional metabolite feature (the phenylethanoid glycoside

TABLE 1 Results of the emerald ash borer (EAB) infestation bioassay consisting of a uniform egg density on each individual in family C, family Y, and family Z, and evaluated 3 and 8 weeks after egg application.

Phenotype	Statistic	Family C	Family Y	Family Z
	N	23	30	30
GoodEgg[2]	Mean[1]	11.435	11.4	11.1
	Median	12	12	12
	Min	9	9	8
	Max	12	12	12
HK[3]	Mean	1.739	5.033	4.9
	Median	1	4	5
	Min	0	1	0
	Max	7	11	9
L1 + L2[4]	Mean	0.261	0.2	0.1
	Median	0	0	0
	Min	0	0	0
	Max	4	2	1
L3 + L4[5]	Mean	7.348	4.933	4.367
	Median	8	4	4
	Min	3	1	1
	Max	11	11	9
Lwt (mg)[6]	Mean	66.26	64.91	75.06
	Median	74.45	67.4	74.74
	Min	11.56	19.83	19.65
	Max	113.84	110.4	130.2

[1]Summary statistics per family.
[2]Number of eggs producing larvae that successfully entered the tree, evaluated at 3 weeks after egg application, per tree.
[3]Number of host-killed larvae (larvae dying of other causes **Supplementary Table 4**) per tree, evaluated 8 weeks after egg application.
[4]The sum of first (L1) and second (L2) instar larvae per tree.
[5]The sum of third (L3) and fourth (L4) instar larvae per tree.
[6]Average weight of living larvae recovered per tree.

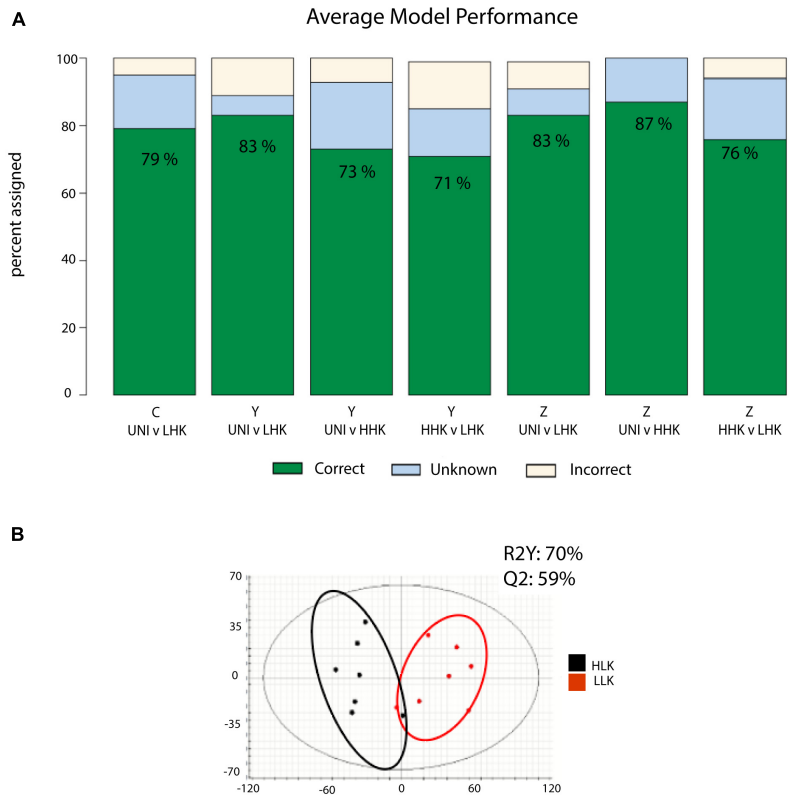

FIGURE 4
Summary of model results classifying individual host trees by infestation status (UNI) and phenotypic class (high host-killed larvae HHK, or low-host killed larvae LLK). **(A)** Orthogonal partial least squares projection to latent square discriminate analysis (OPLS-DA) model performance, averaged across triplicate prediction models. The graph indicates the percentage of individuals classified correctly, incorrectly, or unable to be classified by each model. **(B)** OPLS-DA model utilizing all test samples in a comparison of high vs. low host-killed larvae. R2Y is the explained variation. Q2 is the model predictive ability. Approximate groupings are visualized by color circles.

salidroside) previously identified as important for EAB defense (Chakraborty et al., 2014). Our annotations included compounds from a wide variety of chemical families, including the first detection of specialized alkaloid metabolites in green ash tissue: secoiridoid glycosides, secoiridoids, and phenolic glycosides (**Figures 5**, **6**, **Supplementary Figure 6**, and **Supplementary Table 2**).

The alkaloids noted appeared to belong to three main subgroups. Alkaloids 1 ($C_{12}H_{17}NO_4$) and 2 and 3 (both $C_{14}H_{19}NO_5$) shared key MS/MS product ions of *m/z* 196.09, 146.06, and 118.07 (**Supplementary Figures 4, 6** and **Supplementary Table 3**), which had even masses typical of an odd (non-zero) number of nitrogen atoms, and were elevated in HHK compared to LHK individuals. Based on inspection of extracted ion chromatograms, we cannot rule out the possibility that alkaloids 2 and 3 are a single compound exhibiting split chromatographic peaks. The low hydrogen/carbon ratios for these suggest they may be aromatic, perhaps indole-derived alkaloids, but searches of MS/MS databases available yielded no matches to known substances. These nitrogen-containing metabolites had low relative abundances and were not purified for NMR characterization during this experiment. Putative Alkaloid 4 ($C_{25}H_{30}N_6O_{11}$) had a significant fragment at *m/z* 232.07, did not share similar peaks with other alkaloids, and was at lowest abundance in HHK individuals. Putative alkaloids 5 ($C_{25}H_{34}N_4O_8$) and 6 ($C_{25}H_{32}N_4O_7$) also appear to share a similar base structure, both yielding MS/MS product ions at *m/z* 114.10 and 97.07 (**Supplementary Figure 6**) and were at higher abundances in UNI individuals compared to HHK individuals.

Among the 31 multi-family features, we annotated 16 secoiridoids and secoiridoid glycosides with structures similar to previously observed compounds (**Supplementary Figures 7, 8** and **Supplementary Table 2**), as compared to the 28 seen in leaves of *Fraxinus excelsior* (Sidda et al., 2020). We found that among these 16 annotated compounds, six were elevated in both LHK and HHK individuals compared to UNI individuals, an additional five were elevated in LHK compared to UNI individuals, and five of the 16 were elevated in LHK compared to HHK individuals (**Figure 5B** and **Supplementary Figures 3, 6, 7**). An additional three secoiridoid glycosides were noted in our study without any multi-family patterns (**Supplementary Figure 7**).

Secoiridoid 20 (*m/z 569.23*) was elevated in all infested comparisons (LHK v UNI, HHK v UNI) across all families. Another two secoiridoid glycosides, Nueznehide isomer 2 (*m/z* 704.2781) and GL5 (*m/z* 928.3429), previously found in higher abundances in trees that are highly susceptible to ash dieback in previous investigations (Sollars et al., 2017; Sidda et al., 2020), were significantly higher in LHK compared to UNI individuals across

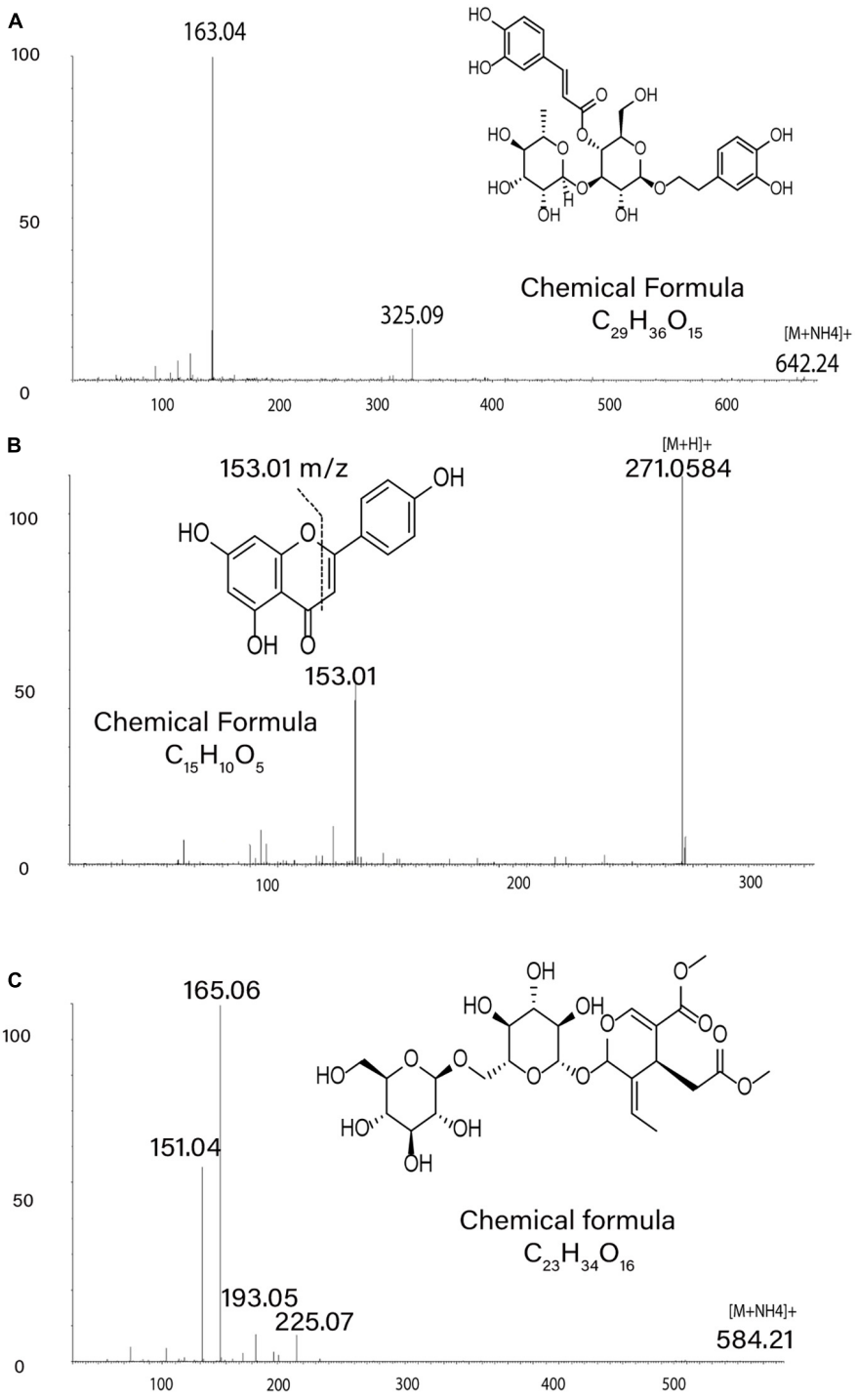

FIGURE 5
Metabolite Annotations. MS/MS spectra in positive ion mode support annotations of metabolite structures: **(A)** product ions of m/z 642.24 ($[M + NH_4]^+$) for verbascoside, **(B)** product ions of m/z 271.06 ($[M + H]^+$) for apigenin, **(C)** product ions of m/z 584.21 ($[M + NH_4]^+$) for Excelside A.

families (Supplementary Figure 4). Specific isomers had different patterns and were present at different abundances. For example, Nuzhenide isomer 2 was a more reliable predictor of infestation than Nuzhenide isomers 1 & 3. The phenylethanoid glycosides verbascoside and salidroside were not consistently associated with phenotype class. Verbascoside was highest in LHK individuals while having no detectable increase in HHK individuals compared to UNI individuals. Conversely, Salidroside was observed at a higher abundance in HHK compared to LHK individuals in family Y. The only compounds that were higher in HHK individuals compared to LHK individuals were three compounds annotated as aromatic alkaloids 1-3 and the phenylethanoid glycoside salidroside [Figure 6B (numbers 1–3 and 24), Supplementary Figure 4, and Supplementary Table 2].

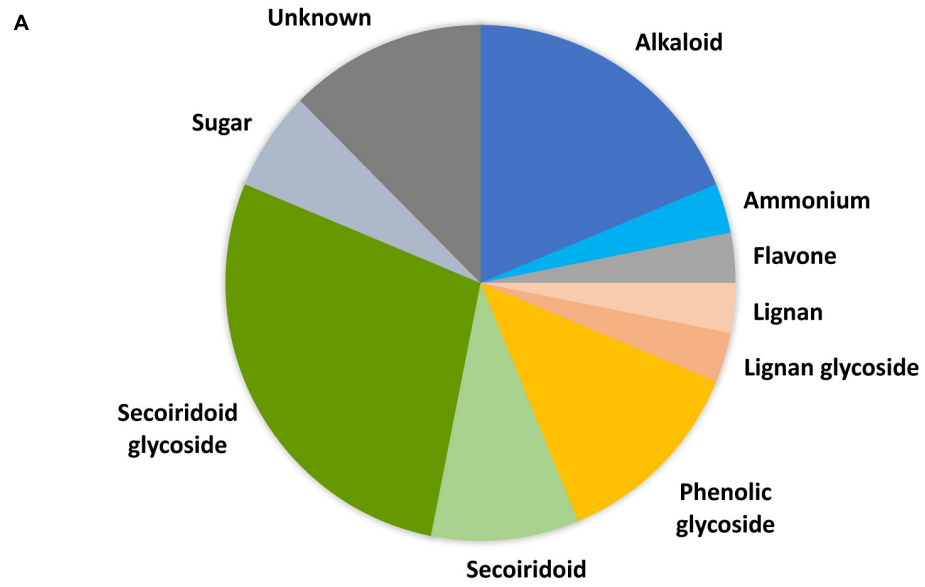

B

Number	LHK v UNI C	LHK v UNI Y	LHK v UNI Z	HHK v UNI Y	HHK v UNI Z	HHK v LHK Y	HHK v LHK Z	Compound Class
1		L					H	Alkaloid
2				H		H		Alkaloid
3				H		H	H	Alkaloid
4	L			U		L		Alkaloid
5				U	U			Alkaloid
6				U	U			Alkaloid
9		L	L	H	H			Secoirdoid glycoside
10		L	L		H			Secoirdoid glycoside
11	L	L				L		Secoirdoid glycoside
12	L				U	L	L	Secoirdoid glycoside
13	L	L				L		Secoirdoid glycoside
14	L	L		H				Secoirdoid glycoside
15	L	L		H				Secoirdoid glycoside
16		L	L		H			Secoirdoid glycoside
17	L	L						Secoirdoid glycoside
18				U		L		Secoirdoid
19	L	L				L		Secoirdoid
20	L	L	L	H	H			Secoirdoid
24						H		Phenylethanoid glycoside
25	L		L					Phenylethanoid glycoside

FIGURE 6
Chemical families of annotated compounds. **(A)** Proportions of the chemical families in the annotated metabolites. **(B)** Summary of pairwise comparisons for specific compounds. "Number" is metabolite number (Supplementary Table 2). LHK v UNI, HHK v UNI, HHK v LHK indicates pairwise comparisons between high (HHK) or low host-killed larvae (LHK) phenotypes or uninfested (UNI) individuals. C, Y, Z refer to full-sibling families Family C (susceptible parents), Families Y and Z (lingering ash parents) (Figure 1). Box with letter indicates the phenotypic category that had significantly higher concentration of the indicated metabolite ($p < 0.05$, L in red LHK, H in gray HHK, U in blue UNI). Annotated metabolites 1–6 are alkaloids, 9–17 are secoiridoid glycosides, 18–20 are secoiridoids, 24 and 25 are the phenylethanoid glycosides salidroside and verbascoside, respectively.

Discussion

We investigated the response of select green ash individuals to EAB infestation using segregating F_1 families, a reproducible phenotyping method, and an untargeted metabolomics approach. We minimized the environmental variance by growing the F_1 families from seed at the same time and testing them at the same age, in the same greenhouse, and in the same growing season. The results of the infestation bioassays show that the progeny of the lingering ash parent crosses killed significantly more larvae on average, but the average larval weight of the survivors was not different between the two lingering ash progeny families (Family Y and Family Z) and the susceptible Pe-97 x 'Summit' family (Family C). The ability of the host to kill a high proportion of early instar larvae may contribute to the survival of the trees, even though some surviving larvae reach the last instar. In similar EAB infestation bioassays conducted on different ash species, Kelly et al. (2020) found that some species had no L4 larvae; however, none of the species had 100% host-killed larvae, indicating that none of the hosts were immune to EAB. The results presented here are also consistent with observations in China, where Asian *Fraxinus* species are not entirely immune to EAB but can survive attack and are rarely killed by EAB unless stressed or weakened (Liu et al., 2003; Wei et al., 2004). We focused on the response variables host-killed larvae and larval weights because the former was the sole criterion used for the phenotypic contrast HLK vs. LLK and the latter, essentially the combined weights of large larvae, showed that the response we investigated was not immunity in the sense of the capacity to prevent biological attack. The other connotation of immunity, the capacity to withstand a biological attack, usually implies a set of operational responses that result in categorial phenotypes, which we certainly did not observe in this investigation (Miller et al., 2017).

In both green ash and Manchurian ash, healthy trees marshal sufficient defensive responses to survive the presence of native stem borers. Green ash are infested by the native stem borers *Podosesia syringae* Harris and *P. aureocincta* Möschler (Lepidoptera: Sesiidae), damaging the value of the wood but rarely killing the tree (Solomon, 1993). While these clearwing moths belong to a different order of insects than EAB (Coleoptera: Buprestidae), the larvae of all three attack phloem tissues. Manchurian ash are infested by EAB, with only a few insects managing to mature and reproduce (Dang et al., 2022). Only when a Manchurian ash tree is severely damaged or drought-stressed can EAB infestation kill the tree, similar to the mortality seen from native borers on green ash in North America. The shared common ancestry of the Asian ash *Fraxinus* section *Fraxinus* which includes the North American black ash and the North American *Fraxinus* section *Meliodies* may have resulted in similar regulatory networks and structural compounds useful for generalized defense against phloem feeders. Genetic diversity for defensive responses against native insects and pathogens could translate to genetic diversity for a measure of defensive responses against non-native insects and pathogens. The existence of native individuals with effective defensive responses to a pathogen with which the host has not recently evolved is well illustrated in the literature. Breeding programs based on native resistance to non-native invaders have produced American beech (*Fagus grandifolia* Ehrh.) resistant to beech bark disease (disease agent *Neonectria* spp. transmitted by the scale insect *Cryptococcus fagisuga* Lindinger, 1936 (Koch and Heyd, 2013). In the gymnosperms, recent examples include eastern white pine *(Pinus strobus* L.) resistant to white pine blister rust (disease agent *Cronartium ribicola* J.C. Fisch.*)* (Pike et al., 2018; Sniezko and Liu, 2022) and Port Orford cedar [*Chamaecyparis lawsoniana* (A.Murray bis) Parl.] resistant to a root rot oomycete pathogen [disease agent *Phytophthora lateralis* Tucker & Milbrath, (1942)] (Sniezko et al., 2012). The success of these and other programs demonstrate that heritable resistance to invasive pests and pathogens can exist in native populations.

The distribution of the response variable proportion of host-killed larvae is expected when the parents are heterozygous for multiple loci with additive effects (Hill and Mackay, 2004). Although the results of our investigation are consistent with a multigenic model, a rigorous test of this hypothesis will require additional families and multiple generations. The action of multiple genes is also suggested by the 53 candidate genes identified in comparative genomics studies of *Fraxinus* species with differing responses to EAB (Villari et al., 2016; Kelly et al., 2020).

The chemotypes of infested HHK and LHK individuals were distinguishable based on the relative abundances of select metabolites (**Figure 6** and **Supplementary Tables 1–3**), not their presence or absence. We provide an initial annotation of metabolites for further study, including secoiridoids and three putative aromatic alkaloids. This first detection of these alkaloids in green ash suggests a potential role for specific alkaloids in defense against herbivory in the Meliodes. Comparisons of the chemotypes of infested vs. uninfested individuals across families revealed that secoiridoids are associated with a response to infestation that does not predict effective defensive responses. Our data suggest that these specific secoiridoids and verbascoside may indicate a general defensive response. A review of constitutive metabolic differences among *Fraxinus* species suggested that secoiridoid compounds have a role in response to EAB, but these studies did not compare infested and uninfested individuals within the same species (Villari et al., 2016). This association of secoiridoids with a response to infestation is consistent with previous studies that suggested that infested trees or trees artificially stressed with methyl jasmonate produced higher amounts of these metabolites than uninfested trees (Whitehill et al., 2014). While high abundances of specific secoiridoids in *F. excelsior* are proposed to be indicative of tolerance (Nemesio-Gorriz et al., 2020) or susceptibility to ash dieback (Sollars et al., 2017) and were predicted to provide a future robust reservoir of anti-feeding deterrents to EAB (Sidda et al., 2020), our data does not support the hypothesis that secoiridoids play a significant role in defense against EAB larval infestation in green ash, but their broad scale induction under infestation may be effective against other threats.

The four metabolites, annotated as three aromatic alkaloids and salidroside that were significantly elevated in HHK individuals compared to LHK or uninfested individuals, require evaluation in other studies to confirm whether these metabolites are part of an effective induced response to EAB in lingering ash.

Conclusion

Identification of secoiridoids and alkaloids at different quantities in different phenotypic classes within family provides

the first evidence that the lingering ash phenotype may result from a rare but partially effective shift in the regulation of a number of genes. These compounds are potential candidates for biomarkers of infestation or effective responses to EAB, in addition to those identified using comparative genomics (Kelly et al., 2020) and transcriptomics approaches (Chiu et al., 2023). The results of this investigation support the continuance of breeding programs that, in concert with biocontrol and management, could provide trees that are resilient to EAB and help conserve the *Fraxinus* gene pool while ongoing work on host-insect interactions will contribute to our understanding of how forest trees recognize and defend themselves against stem-boring insects.

Data availability statement

The original contributions presented in this study are publicly available. The data can be found in the MetaboLites data repository, accession number MTBLS7999.

Author contributions

JR-S, JK, and RS conceived and designed the work. AJ made the substantial contributions to the conception and the design of the work. JK, TP, DC, MM, and RS coordinated the activities between Delaware facility, the AJ lab, the TP lab, and the JR-S lab. JK, DC, and MM selected the lingering ash and designed and carried out the breeding plan. MM performed the statistical GLMM statistical analyses. The TP lab provided the EAB eggs for the bioassay. TP with JK, DC, and MM developed and refined the EAB infestation bioassay protocols. DC, AD, JW, and MM provided the plant care and executed the infestation bioassay. DC, MM, and RS performed the stem dissections. RS performed the metabolomic analyses and analyzed the data with support from AJ. RS and JR-S wrote the manuscript. AJ, TP, MM, KO, and JK assisted with the manuscript revision and final editing. All authors have seen and approved the final submission.

Funding

JR-S acknowledges support from USDA-USFS APHIS grants 18-IA-11242316-105 and 20-JV-11242303-050 and the Tree Fund Foundation, Tree Fund grant 18-JD-01. RS acknowledges support from NIH training grant T32GM075762. JK acknowledges support from USDA APHIS 18-IA-11242316-105, Michigan Invasive Species Grant Program grant IS18-119, the Commonwealth of Pennsylvania Department of Conservation and Natural Resources Bureau of Forestry 18-CO-11242316-014, and the U.S. Forest Service Special Technology Development Program grant NA-2017-01. AJ acknowledges also support from Michigan AgBioResearch through the USDA National Institute of Food and Agriculture, Hatch project number MICL02474, and USDA-USFS grant 20-JV-11242303-050.

Acknowledgments

We thank Warren Chatwin, Benjamin Gombash, and Christina Murray for their helpful comments on the manuscript and Gavin Nupp, Miranda McKibben, and Jarod Sanchez for their work propagating and maintaining the study trees and assistance in conducting the ash resistance EAB infestation bioassays. We also thank Patrick Cunniff, Brandon Chou, Declan Thanner, and Julie Huston for assistance in collecting and organizing tissue samples and managing logistics.

Conflict of interest

The authors declare that the research was conducted in the absence of any commercial or financial relationships that could be construed as a potential conflict of interest.

Publisher's note

All claims expressed in this article are solely those of the authors and do not necessarily represent those of their affiliated organizations, or those of the publisher, the editors and the reviewers. Any product that may be evaluated in this article, or claim that may be made by its manufacturer, is not guaranteed or endorsed by the publisher.

Supplementary material

The Supplementary Material for this article can be found online at: https://www.frontiersin.org/articles/10.3389/ffgc.2023.1166421/full#supplementary-material

References

Anderegg, W. R. L., Trugman, A. T., Badgley, G., Anderson, C. M., Bartuska, A., Ciais, P., et al. (2020). Climate-driven risks to the climate mitigation potential of forests. *Science* 368:eaaz7005. doi: 10.1126/science.aaz7005

Aubin, I., Cardou, F., Ryall, K., Kreutzweiser, D., and Scarr, T. (2015). Ash regeneration capacity after emerald ash borer (Eab) outbreaks: Some early results. *For. Chronicle* 91, 291–298. doi: 10.5558/tfc2015-050

Aukema, J. E., Leung, B., Kovacs, K., Chivers, C., Britton, K. O., Englin, J., et al. (2011). Economic impacts of non-native forest insects in the continental United States. *PLoS One* 6:e24587. doi: 10.1371/journal.pone.0024587

Baral, H.-O., Queloz, V., and Hosoya, T. (2014). *Hymenoscyphus fraxineus*, the correct scientific name for the fungus causing ash dieback in Europe. *IMA Fungus* 5, 79–80. doi: 10.5598/imafungus.2014.05.01.09

Bevilacqua, M., and Bro, R. (2020). Can We Trust Score Plots? *Metabolites* 10:278. doi: 10.3390/metabo10070278

Bradshaw, C. J. A., Leroy, B., Bellard, C., Roiz, D., Albert, C., Fournier, A., et al. (2016). Massive yet grossly underestimated global costs of invasive insects. *Nat. Commun.* 7:12986. doi: 10.1038/ncomms12986

Chakraborty, S., Whitehill, J. G., Hill, A. L., Opiyo, S. O., Cipollini, D., Herms, D. A., et al. (2014). Effects of water availability on emerald ash borer larval performance and phloem phenolics of Manchurian and black ash. *Plant Cell Environ.* 37, 1009–1021.

Chamorro, M. L., Volkovitsh, M. G., Poland, T. M., Haack, R. A., and Lingafelter, S. W. (2012). Preimaginal stages of the emerald ash borer, *Agrilus planipennis* fairmaire (Coleoptera: Buprestidae): An invasive pest on ash trees (*Fraxinus*). *PLoS One* 7:e33185. doi: 10.1371/journal.pone.0033185

Chen, J., Xu, Y., Wei, G., Liao, S., Zhang, Y., Huang, W., et al. (2015). Chemotypic and genetic diversity in *Epimedium sagittatum* from different geographical regions of China. *Phytochemistry* 116, 180–187. doi: 10.1016/j.phytochem.2015.04.005

Chiu, C. C., Pelletier, G., Stival Sena, J., Roux-Dalvai, F., Prunier, J., Droit, A., et al. (2023). Integrative analysis of green ash phloem transcripts and proteins during an emerald ash borer infestation. *BMC Plant Biol.* 23:123. doi: 10.1186/s12870-023-04108-y

Dang, Y., Wei, K., Wang, X., Duan, J. J., Jennings, D. E., and Poland, T. M. (2022). Introduced plants induce outbreaks of a native pest and facilitate invasion in the plants' native range: Evidence from the emerald ash borer. *J. Ecol.* 110, 593–604. doi: 10.1111/1365-2745.13822

Duan, J. J., Bauer, L. S., Abell, K. J., Ulyshen, M. D., and Van Driesche, R. G. (2015). Population dynamics of an invasive forest insect and associated natural enemies in the aftermath of invasion: Implications for biological control. *J. Appl. Ecol.* 52, 1246–1254. doi: 10.1111/1365-2664.12485

Duan, J. J., Bauer, L. S., and Van Driesche, R. G. (2017). Emerald ash borer biocontrol in ash saplings: The potential for early stage recovery of North American ash trees. *For. Ecol. Manage.* 394, 64–72. doi: 10.1016/j.foreco.2017.03.024

Gloss, A. D., Vergnol, A., Morton, T. C., Laurin, P. J., Roux, F., and Bergelson, J. (2022). Genome-wide association mapping within a local *Arabidopsis thaliana* population more fully reveals the genetic architecture for defensive metabolite diversity. *Philos. Trans. R. Soc. B Biol. Sci.* 377:20200512. doi: 10.1098/rstb.2020.0512

Hanberry, B. B. (2014). Rise of *Fraxinus* in the United States between 1968 and 2013. *J. Torrey Bot. Soc.* 141, 242–249. doi: 10.3159/TORREY-D-13-00072.1

Herms, D. A., and McCullough, D. G. (2014). Emerald ash borer invasion of North America: History, biology, ecology, impacts, and management. *Annu. Rev. Entomol.* 59, 13–30. doi: 10.1146/annurev-ento-011613-162051

Hicke, J. A., Allen, C. D., Desai, A. R., Dietze, M. C., Hall, R. J., Ted Hogg, E. H., et al. (2012). Effects of biotic disturbances on forest carbon cycling in the United States and Canada. *Glob. Change Biol.* 18, 7–34. doi: 10.1111/j.1365-2486.2011.02543.x

Hill, W. G., and Mackay, T. F. C. (2004). D. S. Falconer and Introduction to Quantitative Genetics. *Genetics* 167, 1529–1536. doi: 10.1093/genetics/167.4.1529

Hoover, K., and Riddle, A. A. (2020). *Forest carbon primer*. Washington, DC: Congressional Research Service.

Kelly, L. J., Plumb, W. J., Carey, D. W., Mason, M. E., Cooper, E. D., Crowther, W., et al. (2020). Convergent molecular evolution among ash species resistant to the emerald ash borer. *Nat. Ecol. Evol.* 4, 1116–1128. doi: 10.1038/s41559-020-1209-3

Knight, K. S., Brown, J. P., and Long, R. P. (2013). Factors affecting the survival of ash (*Fraxinus* spp.) trees infested by emerald ash borer (*Agrilus planipennis*). *Biol. Invasions* 15, 371–383. doi: 10.1007/s10530-012-0292-z

Knight, K. S., Herms, D., Plumb, R., Sawyer, E., Spalink, D., Pisarczyk, E., et al. (2012). "Dynamics of surviving ash (*Fraxinus* spp.) populations in areas long infested by emerald ash borer (*Agrilus planipennis*)," in *Proceedings of the fourth international workshop on the genetics of host-parasite interactions in forestry: Disease and insect resistance in forest trees. Gen. Tech. Rep. PSW-GTR-240*, eds R. Sniezko, A. Yanchuk, J. Kliejunas, K. Palmieri, J. Alexander, and S. Frankel (Albany, CA: Pacific Southwest Research Station, Forest Service, US Department of Agriculture), 143–152.

Koch, J., Carey, D., Mason, M., Poland, T., and Knight, K. (2015). Intraspecific variation in *Fraxinus pennsylvanica* responses to emerald ash borer (*Agrilus planipennis*). *New For.* 46, 995–1011. doi: 10.1007/s11056-015-9494-4

Koch, J. L., Carey, D. W., Knight, K. S., Poland, T., Herms, D. A., and Mason, M. E. (2012). "Breeding strategies for the development of emerald ash borer-resistant North American ash," in *Proceedings of the fourth international workshop on the genetics of host-parasite interactions in forestry: Disease and insect resistance in forest trees. Gen. Tech. Rep. PSW-GTR-240*, eds R. Sniezko, A. Yanchuk, J. Kliejunas, K. Palmieri, J. Alexander, and S. Frankel (Albany, CA: Pacific Southwest Research Station, Forest Service, US Department of Agriculture), 235–239.

Koch, J. L., and Heyd, R. L. (2013). Battling beech bark disease: Establishment of beech seed orchards in Michigan. *Newslett. Michigan Entomol. Soc.* 58, 11–14.

Kovacs, K. F., Haight, R. G., Mccullough, D. G., Mercader, R. J., Siegert, N. W., and Liebhold, A. M. (2010). Cost of potential emerald ash borer damage in U.S. communities, 2009–2019. *Ecol. Econ.* 69, 569–578. doi: 10.1016/j.ecolecon.2009.09.004

Krist, F. Jr., Ellenwood, J., Woods, M., Mcmahan, A., Cowardin, J., Ryerson, D., et al. (2014). *National insect and disease forest risk assessment: 2013-2027*. Washington, DC: US Department of Agriculture.

Lee, L. C., Liong, C.-Y., and Jemain, A. A. (2018). Partial least squares-discriminant analysis (PLS-DA) for classification of high-dimensional (HD) data: A review of contemporary practice strategies and knowledge gaps. *Analyst* 143, 3526–3539. doi: 10.1039/C8AN00599K

Liu, H., Bauer, L. S., Gao, R., Zhao, T., Petrice, T. R., and Haack, R. A. (2003). Exploratory survey for the emerald ash borer, *Agrilus planipennis* (Coleoptera: Buprestidae), and its natural enemies in China. *Great Lakes Entomol.* 36:11.

López-Goldar, X., Villari, C., Bonello, P., Borg-Karlson, A. K., Grivet, D., Zas, R., et al. (2018). Inducibility of plant secondary metabolites in the stem predicts genetic variation in resistance against a key insect herbivore in maritime pine. *Front. Plant Sci.* 9:1651. doi: 10.3389/fpls.2018.01651

López-Goldar, X., Villari, C., Bonello, P., Borg-Karlson, A. K., Grivet, D., Sampedro, L., et al. (2019). Genetic variation in the constitutive defensive metabolome and its inducibility are geographically structured and largely determined by demographic processes in maritime pine. *J. Ecol.* 107, 2464–2477. doi: 10.1111/1365-2745.13159

Lovett, G. M., Weiss, M., Liebhold, A. M., Holmes, T. P., Leung, B., Lambert, K. F., et al. (2016). Nonnative forest insects and pathogens in the United States: Impacts and policy options. *Ecol. Appl.* 26, 1437–1455. doi: 10.1890/15-1176

Lybrand, D. B., Anthony, T. M., Jones, A. D., and Last, R. L. (2020). An integrated analytical approach reveals trichome acylsugar metabolite diversity in the wild tomato *Solanum pennellii*. *Metabolites* 10:401. doi: 10.3390/metabo10100401

Mason, M., Carey, D., Romero-Severson, J., Knight, K., Poland, T., and Koch, J. (2023). Select genotypes of white and green ash exhibit elevated resistance to emerald ash borer and estimates of genetic heritability. *New For.* (Under review).

Miller, R. N., Costa Alves, G. S., and Van Sluys, M. A. (2017). Plant immunity: Unravelling the complexity of plant responses to biotic stresses. *Ann. Bot.* 119, 681–687. doi: 10.1093/aob/mcw284

Miniat, C. F., Fraterrigo, J. M., Brantley, S. T., Callaham, M. A., Cordell, S., Dukes, J. S., et al. (2021). "Impacts of invasive species on forest and grassland ecosystem processes in the United States," in *Invasive species in forests and rangelands of the United States*, eds T. M. Poland, T. Patel-Weynand, D. M. Finch, C. F. Miniat, D. C. Hayes, and V. M. Lopez (Cham: Springer International Publishing). doi: 10.1007/978-3-030-45367-1_3

Mithöfer, A., and Boland, W. (2012). Plant defense against herbivores: Chemical aspects. *Annu. Rev. Plant Biol.* 63, 431–450. doi: 10.1146/annurev-arplant-042110-103854

Nemesio-Gorriz, M., Menezes, R. C., Paetz, C., Hammerbacher, A., Steenackers, M., Schamp, K., et al. (2020). Canditate metabolites for ash dieback tolerance in Fraxinus excelsior. *J. Exp. Bot.* 71, 6074–6083. doi: 10.1093/jxb/eraa306

Pike, C. C., Berrang, P., Rogers, S., David, A., Sweeney, C., and Hendrickson, J. (2018). Improving the resistance of eastern white pine to white pine blister rust disease. *For. Ecol. Manag.* 423, 114–119. doi: 10.1016/j.foreco.2018.03.001

Poland, T. M., and McCullough, D. G. (2006). Emerald ash borer: Invasion of the urban forest and the threat to North America's ash resource. *J. For.* 104, 118–124.

Potter, K., Escanferla, M., Jetton, R., and Man, G. (2019). Important insect and disease threats to United States tree species and geographic patterns of their potential impacts. *Forests* 10:304. doi: 10.3390/f10040304

Raffa, K. F., and Smalley, E. B. (1995). Interaction of pre-attack and induced monoterpene concentrations in host conifer defense against bark beetle-fungal complexes. *Oecologia* 102, 285–295. doi: 10.1007/BF00329795

Sadre, R., Magallanes-Lundback, M., Pradhan, S., Salim, V., Mesberg, A., Jones, A. D., et al. (2016). Metabolite diversity in alkaloid biosynthesis: A multilane (diastereomer) highway for camptothecin synthesis in Camptotheca acuminata. *Plant Cell* 28, 1926–1944. doi: 10.1105/tpc.16.00193

Sidda, J. D., Song, L., Parker, J. L., Studholme, D. J., Sambles, C., and Grant, M. (2020). Diversity of secoiridoid glycosides in leaves of UK and Danish ash provide new insight for ash dieback management. *Sci. Rep.* 10:19566. doi: 10.1038/s41598-020-76140-z

Sniezko, R., Yanchuk, A., Kliejunas, J., Palmieri, K., Alexander, J., and Frankel, S. (2012). *Fourth international workshop on the genetics of host-parasite interactions in forestry: Disease and insect resistance in forest trees, Eugene, Oregon, USA, 31 July-5 August 2011*. Eugene, OR: Pacific Southwest Research Station, USDA Forest Service. doi: 10.2737/PSW-GTR-240

Sniezko, R. A., and Liu, J.-J. (2022). Genetic resistance to white pine blister rust, restoration options, and potential use of biotechnology. *For. Ecol. Manage.* 520:120168. doi: 10.1016/j.foreco.2022.120168

Sollars, E. S., Harper, A. L., Kelly, L. J., Sambles, C. M., Ramirez-Gonzalez, R. H., Swarbreck, D., et al. (2017). Genome sequence and genetic diversity of European ash trees. *Nature* 541:212. doi: 10.1038/nature20786

Solomon, J. D. (1993). *Ash pests: A guide to major insects, diseases, air pollution injury, and chemical injury*. New Orleans, LA: US Department of Agriculture, Forest Service, Southern Forest Experiment Station. doi: 10.2737/SO-GTR-96

Steiner, K. C., Graboski, L. E., Knight, K. S., Koch, J. L., and Mason, M. E. (2019). Genetic, spatial, and temporal aspects of decline and mortality in a Fraxinus provenance test following invasion by the emerald ash borer. *Biol. Invasions* 21, 3439–3450. doi: 10.1007/s10530-019-02059-w

Sumner, L. W., Amberg, A., Barrett, D., Beale, M. H., Beger, R., Daykin, C. A., et al. (2007). Proposed minimum reporting standards for chemical analysis. *Metabolomics* 3, 211–221. doi: 10.1007/s11306-007-0082-2

Villari, C., Herms, D. A., Whitehill, J. G., Cipollini, D., and Bonello, P. (2016). Progress and gaps in understanding mechanisms of ash tree resistance to emerald ash borer, a model for wood-boring insects that kill angiosperms. *New Phytol.* 209, 63–79.

Volf, M., Hrcek, J., Julkunen-Tiitto, R., and Novotny, V. (2015). To each its own: Differential response of specialist and generalist herbivores to plant defence in willows. *J. Anim. Ecol.* 84, 1123–1132. doi: 10.1111/1365-2656.12349

Walters, R., and Yawney, H. (2004). *Silvics manual: Volume 2: Hardwoods. Agricultural Handbook 654.* Washington, DC: United States Department of Agriculture, Forest Service.

Wei, X., Reardon, D., Wu, Y., and Sun, J.-H. (2004). Emerald ash borer, *Agrilus planipennis* Fairmaire (Coleoptera: Buprestidae), in China: A review and distribution survey. *Acta Entomol. Sin.* 47, 679–685.

Whitehill, J. G., Opiyo, S. O., Koch, J. L., Herms, D. A., Cipollini, D. F., and Bonello, P. (2012). Interspecific comparison of constitutive ash phloem phenolic chemistry reveals compounds unique to Manchurian ash, a species resistant to emerald ash borer. *J. Chem. Ecol.* 38, 499–511. doi: 10.1007/s10886-012-0125-7

Whitehill, J. G., Rigsby, C., Cipollini, D., Herms, D. A., and Bonello, P. (2014). Decreased emergence of emerald ash borer from ash treated with methyl jasmonate is associated with induction of general defense traits and the toxic phenolic compound verbascoside. *Oecologia* 176, 1047–1059. doi: 10.1007/s00442-014-3082-8

frontiers | Frontiers in Forests and Global Change

TYPE Original Research
PUBLISHED 27 October 2023
DOI 10.3389/ffgc.2023.1240804

OPEN ACCESS

EDITED BY
Bernard Slippers,
University of Pretoria, South Africa

REVIEWED BY
Gaku Tokuda,
University of the Ryukyus, Japan
Braham Dhillon,
University of Florida, United States

*CORRESPONDENCE
Shulin He
✉ shulinhe@hotmail.com
Bin Jiang
✉ bin.jiang@ahnu.edu.cn

RECEIVED 15 June 2023
ACCEPTED 13 October 2023
PUBLISHED 27 October 2023

CITATION
He S, Chakraborty A, Li F, Zhou C, Zhang B, Chen B and Jiang B (2023) Genome-wide identification reveals conserved carbohydrate-active enzyme repertoire in termites. *Front. For. Glob. Change* 6:1240804. doi: 10.3389/ffgc.2023.1240804

Genome-wide identification reveals conserved carbohydrate-active enzyme repertoire in termites

Shulin He[1]*, Amrita Chakraborty[2], Fei Li[1], Cao Zhou[1], Binchuan Zhang[1], Bin Chen[1] and Bin Jiang[3]*

[1]College of Life Sciences, Chongqing Normal University, Chongqing, China, [2]Forest Microbiome Team, Faculty of Forestry and Wood Sciences, Czech University of Life Sciences Prague, Prague, Czechia, [3]College of Life Science, Anhui Normal University, Wuhu, China

Termites play an important role as decomposers of organic matter in forests by utilizing their gut symbionts and associated carbohydrate-active enzymes (CAZymes) to digest wood materials. However, there is a limited understanding of the entire repertoire of CAZymes and their evolution in termite genomes. Here we identified the gene families of CAZymes in publicly available termite genomes and analyzed the evolution of abundant gene families. We found that 79 CAZyme gene families from the carbohydrate-binding module and four CAZyme classes, including glycosyl transferase (GT), glycoside hydrolase (GH), auxiliary activity (AA) and carbohydrate esterase (CE), were present in termites with minor variations across termite species except for a few gene families. The gene trees of the large and conserved gene families have several groups of genes from all species, and each group encodes enzymes with complete corresponding domains. Three gene families, namely GT1, GH1 and AA3, exhibited significant variations in gene numbers and experienced several losses and a few duplications, which might be related to their rich gut symbionts and newly gained functions. Furthermore, the overall expression of CAZymes appears to have a caste- and tissue-specific pattern, reflecting a division of labor in termite colonies. Overall, these results reveal a likely stable CAZyme repertoire in termites and pave the way for further research on the functional contribution of termites to wood digestion.

KEYWORDS

wood digestion, glycosyl transferase, glycoside hydrolase, gene duplications, gene losses

Introduction

Termites are important decomposers of organic matter. They can digest recalcitrant plant materials predominantly composed of lignocellulose, contributing to the decomposition of more than half of the dead wood in tropical and subtropical forests (Griffiths et al., 2019; Wu et al., 2021). In addition to their essential role in nutritional cycling, they also can influence soil moisture in tropical forests via their mounds (Ashton et al., 2019). However, due to their wood digestion ability, termites cause damage to wooden constructions and crops, with an estimated 40 billion United States dollars of global annual economic losses (Rust and Su, 2012; Kalleshwaraswamy et al., 2022).

Originating from a wood-feeding ancestor, they can efficiently digest recalcitrant lignocellulose, which relies on a large number of carbohydrate digestion enzymes produced by their associated symbionts. Because of their diversified feeding habits, termites harbor diverse gut microbiota, producing abundant CAZymes to adapt to their feeding preferences (Arora et al., 2022). In lower termites the digestion ability mainly relies on the protists and associated bacteria in their guts. While in higher termites their digestion ability depends on their symbiotic bacteria (Brune, 2014; Brune and Dietrich, 2015; Arora et al., 2022) because of the loss of the protists during their evolution (Bucek et al., 2019). These symbiotic microbes can possess a diverse repertoire of carbohydrate-active enzymes (CAZymes), including plant cell wall digestion enzymes. CAZymes are generally classified into five classes: glycoside hydrolases (GHs), glycosyl transferases (GTs), polysaccharide lyases (PLs), carbohydrate esterases (CEs) and auxiliary activities (AAs). The termite symbionts possess a wide array of gene sets encoding active functional enzymes from these classes (Tartar et al., 2009; Marynowska et al., 2017; Hervé et al., 2020; Arora et al., 2022). Although the cellulolytic symbionts have been extensively investigated in termite digestion, the CAZyme genes originating from termites have gained traction since the discovery of the first cellulase in termites (Watanabe et al., 1998).

In addition to their symbionts, termites have specific CAZyme genes contributing to lignocellulose digestion. The combined efforts of both termite enzymes and those of their symbionts allow efficient digestion of wooden materials (Poulsen et al., 2014; Arora et al., 2022). Among them, endo-β-1,4-glucanases and β-glucosidases have been widely studied in cellulose hydrolysis. Both genes have multiple copies in each available termite genome (Tokuda, 2019) and were expressed mainly in salivary glands and gut with different expression patterns in different species (Tokuda et al., 2004; Fujita et al., 2008). For example, an endo-β-1,4-glucanase was specifically expressed in the salivary glands of lower termites, while it was mainly expressed in the midguts of higher termites (Tokuda et al., 2004). Similarly, a digestive β-glucosidase was explicitly expressed in the salivary glands of a lower termite *Neotermes koshunensis* (Shiraki) and the salivary glands and midguts of a higher termite *Nasutitermes takasagoensis* (Tokuda et al., 2002, 2009). Furthermore, due to the division of labor within the reproductive caste system, different termite castes showed different enzymatic activity. For instance, in a lower termite, *Hodotermopsis sjostesti*, the expression of endo-β-1,4-glucanase was higher in workers than soldiers (Fujita et al., 2008). In addition, other CAZyme genes were also characterized in termite species, such as chitin metabolism-related lytic polysaccharide monooxygenases (LPMOs) and auxiliary activity (AA) 15 in *Coptotermes gestroi* (Cairo et al., 2020).

Both well-studied gene families, endo-β-1,4-glucanases and β-glucosidases, have ancient origins (Davison and Blaxter, 2005; Shelomi et al., 2020; He et al., 2022). However, some of these genes have also gained functions other than digestion during termite evolution. A fascinating example is a GH1 β-glucosidase gene that is specifically expressed in the accessory glands of female ovaries (Shigenobu et al., 2022) and suppresses the production of new female reproductives in the colony (Korb et al., 2009; Zhang et al., 2012). In addition, another GH1 gene has been implicated in the recognition of termite eggs (Matsuura et al., 2009), although the gene is still not characterized.

With the advent of omics technologies, including genomics and transcriptomics, the CAZyme genes have been comprehensively investigated in several termite species (Yuki et al., 2008; Tartar et al., 2009; Zhang et al., 2012; Poulsen et al., 2014; Korb et al., 2015; Geng et al., 2018; Shigenobu et al., 2022). However, a systematic analysis of the evolution of the CAZyme gene families is still lacking. Currently genomes of 5 termite species belonging to four of the seven termite families are publicly available, including *Zootermopsis nevadensis* in Archotermopsidae, *Cryptotermes secundus* in Kalotermitidae, *Reticulitermes speratus* and *Coptotermes formosanus* in Rhinotermitidae, *Macrotermes natalensis* in termitidae. The former four termite species are wood-feeding lower termites, whereas *M. natalensis* is a fungus cultivating higher termites. In this study, we take advantage of these publicly available genomes to compare the digestion enzyme repertoire in five termite species to reveal the duplications and losses of CAZymes of termite origin during termite evolution.

Materials and methods

Data collection

The genomes, corresponding proteomes and GFF annotations were obtained from publicly available resources. Specifically, the data of *Zootermopsis nevadensis* and *Cryptotermes secundus* were retrieved from the NCBI RefSeq database; the data of *Coptotermes formosanus* was obtained from the NCBI genome assembly database (Itakura et al., 2020); the data of *Macrotermes natalensis* and *Reticulitermes speratus* were sourced from previously published datasets (Poulsen et al., 2014; Shigenobu et al., 2022).

CAZyme prediction and domain identification

To predict and annotate the CAZyme genes in the termite genomes, the longest isoform of each gene in *Z. nevadensis* and *C. secundus* were extracted by the function "retrieve_longest_isoforms" in the R package orthologr (Drost et al., 2015). The other three genomes have one protein for each gene in their proteomes. The completeness of proteomes was assessed by BUSCO with insecta_odb10 dataset before CAZyme gene prediction (Manni et al., 2021). Subsequently, the CAZyme genes in the termite genomes were annotated by the standalone tool run_dbCAN (Zhang et al., 2018), which uses three programs, including HMMER, diamond and eCAMI. The genes were considered to be confidently annotated if the protein had consistent annotations from at least two prediction programs. Subsequently, the proteins were mapped to the genomes for predicting unannotated CAZyme genes in all genomes by miniprot (Li, 2023), and the newly annotated genes were manually curated, and their corresponding proteins were subjected to CAZyme prediction as well. The confidently predicted CAZyme proteins of the genes were queried against the non-redundant protein database in NCBI to identify the origin of the predicted genes by following a method we described previously, and last common ancestor (LCA) of up to the top 10 best targets for each query was inferred using the ete3 toolkit (Huerta-Cepas et al., 2016). Additionally, the domains of the annotated proteins were identified by searching the InterPro database with InterProScan (Jones et al., 2014).

Gene phylogeny inference

For each gene family, the corresponding proteins of the studied species were retrieved and aligned by using MAFFT with L-INS-I (Katoh and Standley, 2013) and muscle (Edgar, 2004). After further refining with RASCAL (Thompson et al., 2003) and scoring by normd (Thompson et al., 2001), the alignment with the highest normd score was subjected to phylogeny construction. IQ-TREE (Minh et al., 2020) was employed to construct phylogenetic trees with model selection and 1,000 ultrafast bootstrap replicates.

Duplications and losses

We used Notung, which takes a non-dated species tree and the constructed gene trees as input to infer gene duplication and loss for large gene families. The phylogenetic relationships of the five termite species were inferred from a previously published study (Bucek et al., 2019). The duplication and losses were inferred with the rearrange model for reconciliation at a 90% threshold to reduce the penalty of low supported branches (Durand et al., 2005).

Duplication mode inference and collinearity analysis

For gene families with large duplications, specifically GT1, GH1 and AA3, we further inferred their duplication mode by using duplicate_gene_classifier in MCScanx (Wang et al., 2012) for each species. The duplicate genes of each species were classified into four modes: whole genome/segmental duplications (match genes in syntenic blocks), tandem duplications (continuous repeats), proximal duplications (not adjacent but in nearby chromosomal/scaffold regions at a maximum distance of 10 genes), and dispersed duplications (other modes than segmental, tandem, and proximal). The similarity of the duplications was determined by TBtools (Chen C. et al., 2020). The chromosomal location of these genes and their corresponding collinear blocks were also inferred in MCScanx. The results were visualized using circos (Krzywinski et al., 2009).

Expression analysis

To gain preliminary insights into the expression patterns of the identified gene families, we analyzed the expression of identified CAZyme genes in *R. speratus* using publicly available expression data (Shigenobu et al., 2022). The data contain two body parts, head and body (throax+abdomen), from three castes: workers, soldiers and reproductives. Raw data were filtered with a minimum of 1 count-per-million in at least three samples, then log-transformed for visualization using ggplot2 (Wickham, 2016).

Results

The identification of CAZymes

Four of the five CAZyme classes, including GT, GH, AA, and CE, are presented in all termite species with varying numbers. To sum up all the identified CAZyme genes, we found that *R. speratus* has the highest total CAZyme gene number (287), followed by *C. secundus* (277), *Z. nevadensis* (269) and *C. formosanus* (266), whereas *M. natalensis* has the lowest gene number (235) (Figure 1). Among them, 17 genes were newly annotated by homology-based mapping to the genomes (Supplementary Table S1) except RsGH9a, which was reported in the previous genome but without annotation. The most abundant class is GT, which accounts for approximately half of the identified genes. GH is the second largest class followed by AA, CBM (Carbohydrate-Binding Module) and CE.

Among the identified 43 GT gene families, 36 are present in all species, while seven families are absent in one or two species (Figure 1). Notably, GT1 (13–23 copies), GT27 (9–10 copies) and GT31 (8–12 copies) are the largest GT families in termites followed by GT2, GT13, GT49, GT4, GT22, GT7, GT8 and GT105 with 4–6 copies; the remaining families have 1–3 copies. In the GH class, 26 gene families exist in all species except GH152 lacking in *Z. nevadensis*. Among these GH families, the abundant families are GH1 (7–16 copies), GH18 (10–13 copies), GH13 (6–11 copies) and GH20 (8–9 copies) followed by GH16, GH31, GH47 and GH9 with 3–9 copies (Figure 1). In addition, we found a considerable variation of gene numbers in GH22 among termites ranging from three copies in *Z. nevadensis*, *C. secundus*, and *C. formosanus* to 14 copies in *R. speratus*. Within the AA class, three families are present in all species, with AA3 being the most abundant (18–32 copies) followed by AA1 (6–10 copies) and AA15 (3–4 copies) (Figure 1). In the CE class, only one family, CE9, is present in termites with one copy in each species. Apart from these four classes, we observed seven groups of CBM in termites, with CBM14, which is also present in GH18, being the most abundant, ranging from 10 to 14 copies.

Phylogenetic tree of gene families

Most gene families in CAZyme classes have a few but relatively stable gene numbers across the five termite species. We selected the abundant or highly variable gene families in each class for further phylogenetic analysis. Therefore, we constructed the gene trees for the following gene families: GT1, GT27, GT31, GH1, GH9, GH13, GH18, GH20, GH22, AA1, AA3 and CBM14.

As the largest family in GT, GT1 genes were classified into 12 groups (Figure 2A). Group 12 has the highest gene numbers, representing approximately a quarter of the identified GT1 genes in termites; while the remaining groups contain 1–3 gene copies from each species. However, no identified GT1 genes of *M. natalensis* was included in Group 1, 10, 11, and 12. GT27 and GT31 could be categorized into 9 and 11 groups, respectively, (Supplementary Figure S1); most groups contain one copy from each species except a few GT31 groups that either lack genes from less than two species or have no more than two copies from certain species.

In the GH class, GH1, GH9, and GH22 gene trees have clades with varying gene copies (up to 7) (Figure 2B; Supplementary Figure S2). In the gene trees of GH1 and GH22, most groups contain multiple genes from each species, while one group contains one gene from each species. The gene trees of GH13, GH18, and GH20 consist primarily of clades with one gene copy from each species, except a few groups that either lack genes from less than two species or have 2–3 copies (Supplementary Figure S3).

10.3389/ffgc.2023.1240804

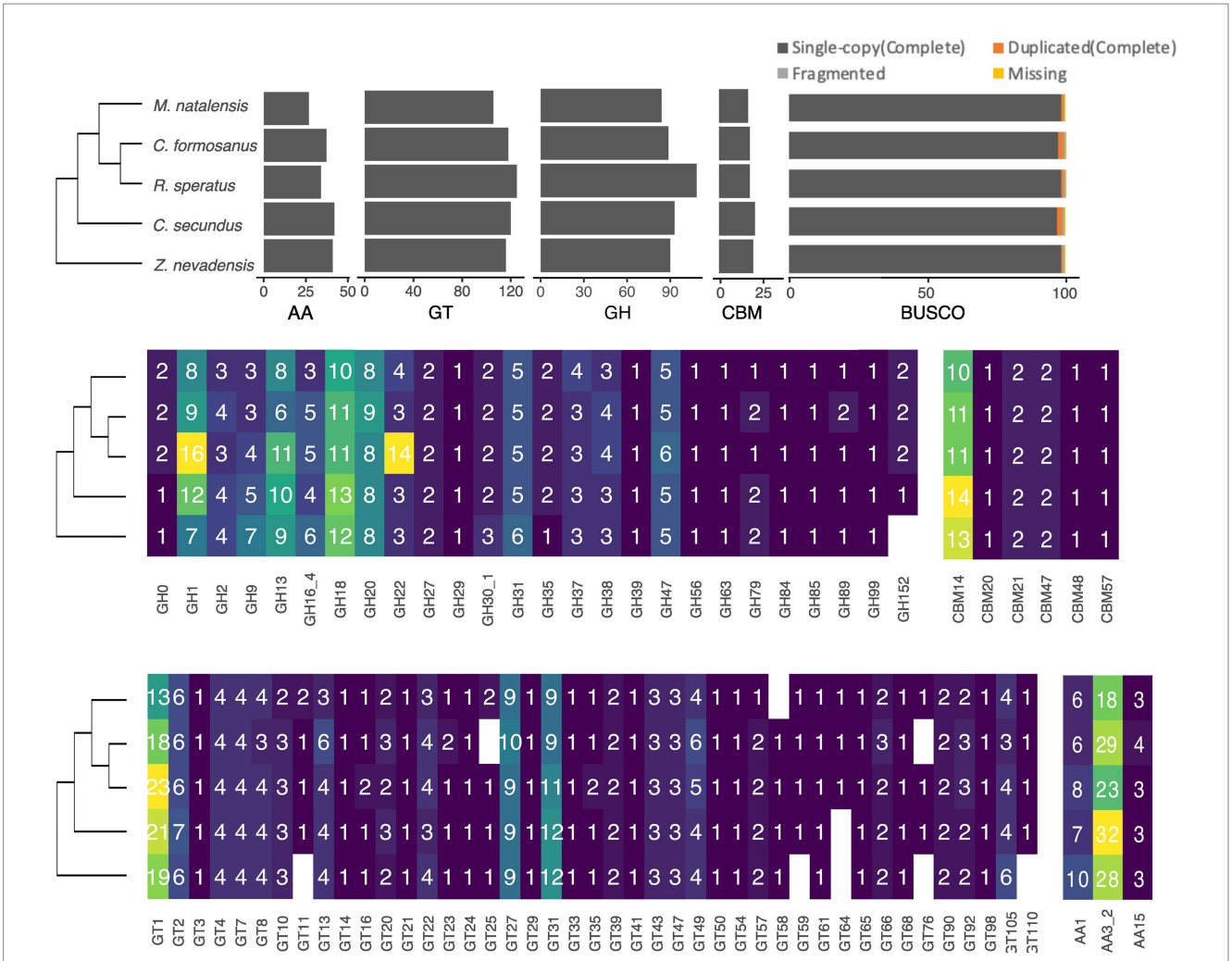

FIGURE 1
The identified gene numbers of CAZyme classes in different termite species based on a phylogeny inferred from published research (Bucek et al., 2019). At the top panel, the bar plots present the total gene numbers of four main CAZyme classes, including Auxiliary Activity (AA), Glycosyl Transferase (GT), Glycoside Hydrolase (GH), and Carbohydrate-Binding Module (CBM), as well as the BUSCO completeness of the genomes used in this study. The different gene numbers of GH gene families (middle-left panel), CBM (middle-right panel), GT (bottom-left panel), AA (bottom-right panel) are present along with the phylogeny of the top panel.

Similarly, in the AA class, the AA1 gene tree contains nine groups, of which eight groups have one gene from most species and one group contains only two gene copies of *Z. nevadensis* (Supplementary Figure S4). The gene tree of AA3 is more complex, where most groups and subgroups contain one gene copy from each species with some groups that lack genes from one or two species (Figure 2C). In contrast, several groups of AA3 have multiple copies (up to nine) from *C. formosanus*, *C. secundus* and *Z. nevadensis*.

In the CBM modules, most groups in the CBM14 gene tree contain only one copy from each species, although a few groups lack 1–2 species or have two copies from the same species (Supplementary Figure S4).

Domains in protein families

In the AA class, most AA1 proteins contain three domains: Multicopper oxidase C-terminal, Multicopper oxidase N-terminal, and Multicopper oxidase second cupredoxin domain. Five AA1 proteins in five gene groups and three species lack one or two of these domains (Supplementary Figure S5). Most AA3 proteins have both C-terminal and N-terminal domains of Glucose-methanol-choline oxidoreductase, except for two proteins that have Glucose-methanol-choline oxidoreductase N-terminal domain and a few proteins that have truncated domains (Supplementary Figure S6). However, two proteins from *Z. nevadensis* and *C. secundus* clustered together in a subgroup in the gene tree have dual C-terminal and N-terminal domains.

In the GH class, most GH1 proteins have a complete Glycoside hydrolase family 1 domain. However, six GH1s from *Z. nevadensis*, *C. secundus*, and *C. formosanus* spreading in groups 1, 2, 3, and 4 have two GH1 domains (Figure 3A). Additionally, five GH1s from *C. formosanus*, *M. natalensis*, and *R. speratus* in group 2 and 5 have truncated GH1 domain. For GH9 most proteins contain a single GH9 domain except for one gene from *M. natalensis*, which contains two domains with one being incomplete; a few proteins of *Z. nevadensis* in

10.3389/ffgc.2023.1240804

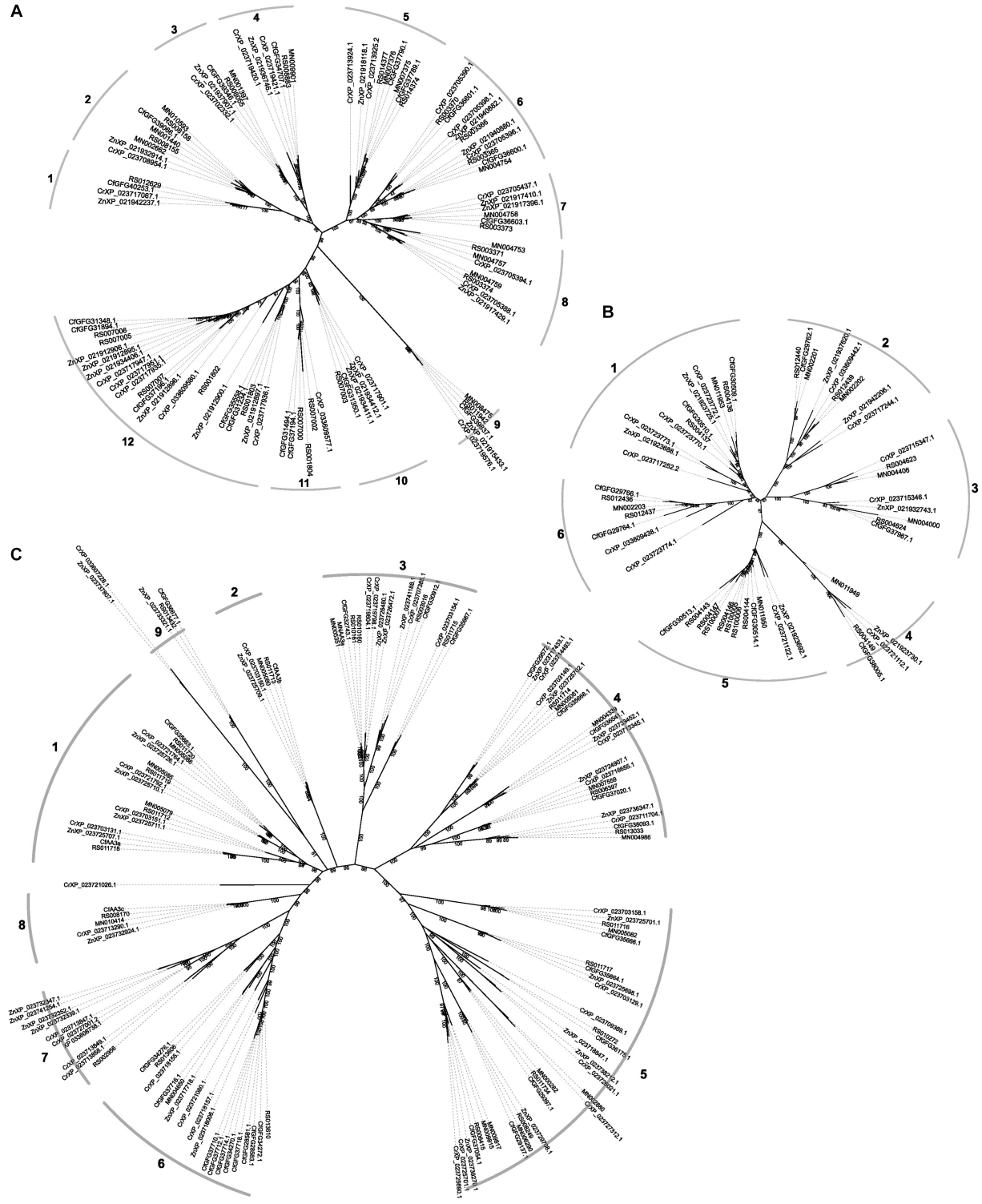

FIGURE 2
The gene trees of GT1 **(A)**, GH1 **(B)**, and AA3 **(C)** inferred from corresponding identified proteins with IQ-TREE. The ids in the phylogenies are the ids of identified genes for *R. speratus* (starting with RS) and *Macrotermes natalensis* (starting with MN), and labeled as species abbreviations (*Z. nevadensis*, Zn; *C. secundus*, Cr; *C. formosanus, Cf*) and related protein ids for the rest three species. The numbers in the gene trees represent bootstrap values for branch support; the numbers along the grey curves around the gene trees indicate the group numbers of each gene family.

group 3 and a protein of *R. speratus* have incomplete GH9 domains (Supplementary Figure S7). In GH13 proteins from group 25 and group 8 have conserved domains (glycoside hydrolase, family 13, N-terminal, Alpha-amylase/branching enzyme, C-terminal all beta, glycosyl hydrolase, family 13, catalytic domain; glycogen debranching enzyme, N-terminal domain, glucanotransferase domain, central

10.3389/ffgc.2023.1240804

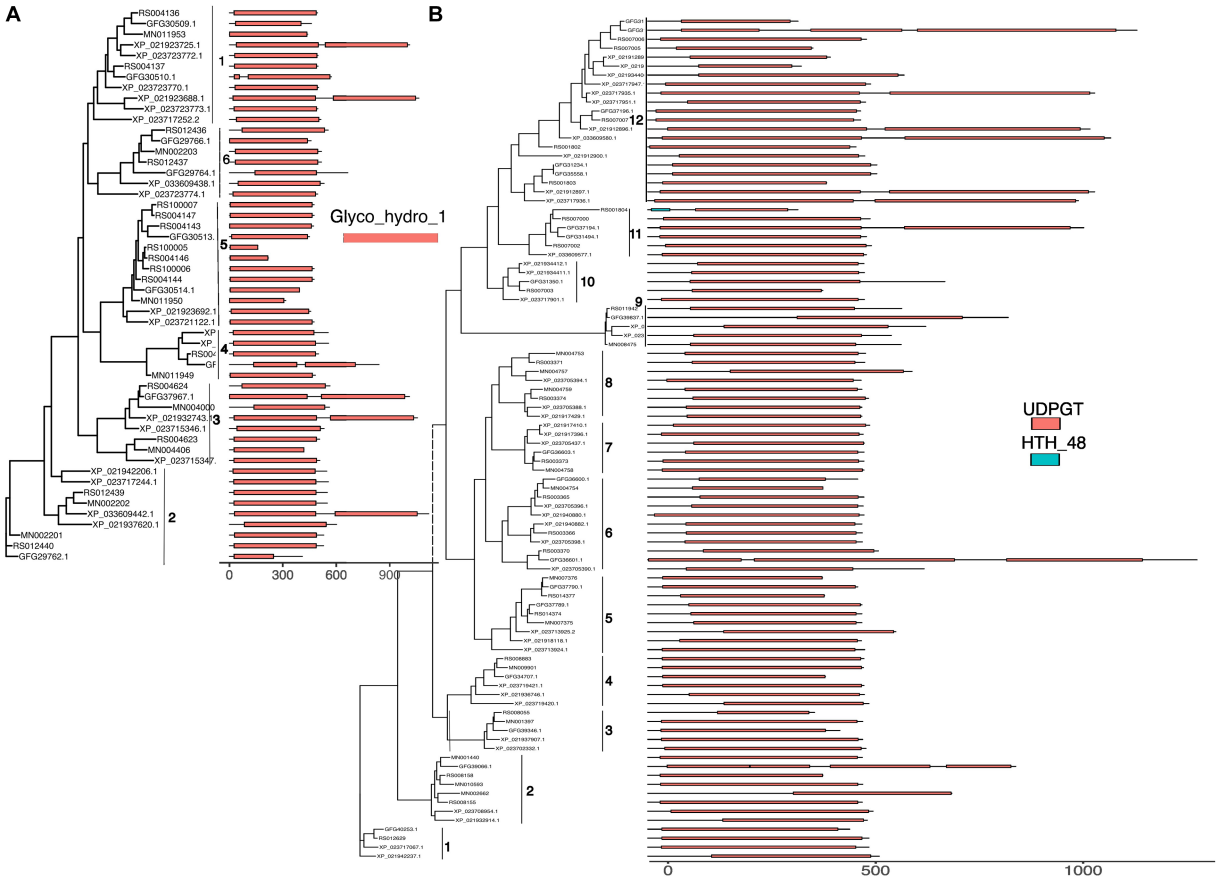

FIGURE 3
The domain structure (identified by searching the InterPro database with InterProScan, colored boxes) of GH1 **(A)** and GT1 **(B)** aligned to related gene trees from Figure 2. The x axis represents the length of the predicted proteins. Different numbers along the grey lines next to the gene phylogenies indicate the group numbers from Figure 2.

domain, C-terminal) in each gene from each species; whereas in GH13_15 most proteins have two domains (Alpha-amylase/branching enzyme, C-terminal all beta and Glycosyl hydrolase, family 13, catalytic domain) except for one protein that lacks one domain in each of *C. secundus*, *R. speratus*, and *C. formosanus* (Supplementary Figure S7). In GH13_17 most proteins in three groups have two domains (glycosyl hydrolase, family 13, catalytic domain; Solute carrier family 3 member 2, N-terminal domain), and proteins in one group have one domain (glycosyl hydrolase, family 13, catalytic domain). In GH20 all proteins contain a Glycoside hydrolase family 20, catalytic domain, and most proteins in groups 5–8 have an additional domain Beta-hexosaminidase, eukaryotic type, N-terminal (Supplementary Figure S8). In GH22 most proteins have a C-type lysozyme/alpha-lactalbumin family domain except for one gene from *R. speratus* and *C. formosanus* having a Destabilase domain (Supplementary Figure S8).

Similarly, most GT1 proteins have UDP-glucoronosyl and UDP-glucosyl transferase domains (Figure 3B). Five proteins in group 12 from *Z. nevadensis* and *C. secundus* and one protein in group 11 from *C. formosanus* have two domains, while each protein of *C. formosanus* in group 12, 6, and 2 have three domains; a few proteins in groups 3, 12, 11 have shorter domains than other members in the groups. All GT27 proteins have two domains, namely glycosyl transferase family 2 and Ricin-type beta-trefoil lectin domain, except for two proteins from *C. formosanus* and *R. speratus* in group 4, which lack the Ricin-type beta-trefoil lectin domain, and one protein from *R. speratus* in group 2 having N-terminal domain of galactosyltransferase instead of the GT2 domain (Supplementary Figure S9). In GT31 the proteins in groups 1–4 have one or two fringe-like domains, while the proteins in group 2 have a single chondroitin N-acetylgalactosaminyltransferase domain (Supplementary Figure S9). Additionally, the proteins in other groups of GT31 have one galactosyltransferase, except proteins in group 9, which have two galactosyltransferase domains. However, a protein of *M. natalensis*, MN006382-PA, has two domains, Bcl2−/adenovirus E1B nineteen kDa-interacting protein 2 and Divergent CRAL/TRIO domain.

Duplications and losses in different gene families

We analyzed the duplications and losses of relatively large gene families to explore the evolution of identified gene families. Overall, the large gene families had large gene numbers in the common ancestor of the selected species with numerous losses and only a few

duplications at most branches (Figure 4). Most duplications were found in the AA3 and GT1 gene families in *Z. nevadensis*, *C. formosanus*, and the ancestor of *R. speratus* and *M. natalensis*. In addition, five duplications of GH1 and AA3 were found in *R. speratus* and *C. secundus*, respectively. Moreover, most selected gene families had one duplication in the ancestor of *R. speratus, M. natalensis,* and *C. formosanus*.

Collinearity and duplication modes

As most of the examined CAZyme gene families had limited gene duplications in termites, we analyzed the collinearity and duplication modes of the gene families that experienced several duplications, namely GT1, GH1, and AA3.

In the GT1 gene family, more than half of the genes were tandem duplications and a few were proximal duplications, located in three collinear blocks among all species (Figure 5A). Additionally, approximately five GT1s in each species were dispersed duplications. Most GH1 genes were tandemly duplicated and are located in a few collinear blocks among all species, especially in a few blocks on one contig of *R. speratus* and a collinear block between *C. secundus*, *C. formosanus* and *R. speratus* (Figure 5B). Interestingly, nearly half of AA3 in all species were tandemly duplicated (Figure 5C). These tandem duplications in *M. natalensis*, *R. speratus*, and *Z. nevadensis* are located in a collinear block, whereas the duplications in *C. secundus* and *C. formosanus* are dispersed in multiple contigs.

The overall sequence similarity of the genes in the GT1, GH1, and AA3 gene families is 52.5%. The average sequence similarities for the dispersed, proximal, and tandem duplications of these three gene families are 46.89%, 55.27%, and 55.52%, respectively. Though the average similarities of different duplication types differ among these three gene families, the dispersed duplications have the lowest sequence similarity (AA3, 50.51%; GT1, 47.20%; GH1, 37.09%). In addition, the proximal duplications of GT1 and GH1 have slightly higher sequence similarities (GT1, 55.68%; GH1, 55.27%) than the corresponding tandem duplications (GT1, 51.85%; GH1, 55.52%). However, the tandem duplications of AA3 have a higher sequence similarity (62.15%) than its proximal duplications (54.50%).

Expression of genes in different castes and tissues of *Reticulitermes speratus*

Regarding the expression patterns of the identified CAZyme genes, we found an overall tissue- and caste-specific expression pattern but no noticeable sex difference except between the body parts of female and male reproductive (Supplementary Figure S6). Approximately half of the genes have generally low expression in the body parts of all castes. Among the expressed genes, 15 genes showed higher expression in the head than the body of different castes (Figure 6). Among them, a GH30_1 (RS014869) showed a specific expression in the head of workers and reproductives. Additionally, GH9 (RS012687), GH1 (RS004136), and GH16_4 (RS100018) had higher expression in the body of workers than the reproductives and soldiers. Another GH1 (RS004624) had a specific high expression in the body parts of female reproductives. In addition, we observed increased expression levels of three GH22 genes (RS014698, RS100022, and RS100023) in the body parts of soldiers.

We examined the expression levels for each gene family to gain further insights into the expression patterns of the gene families whose gene trees were constructed. High gene expression were found across all samples for three AA3s (RS011715 and RS010161, and RS013033), one GH18 (RS007511), one GH20 (RS015064), one GH22 (RS006054),

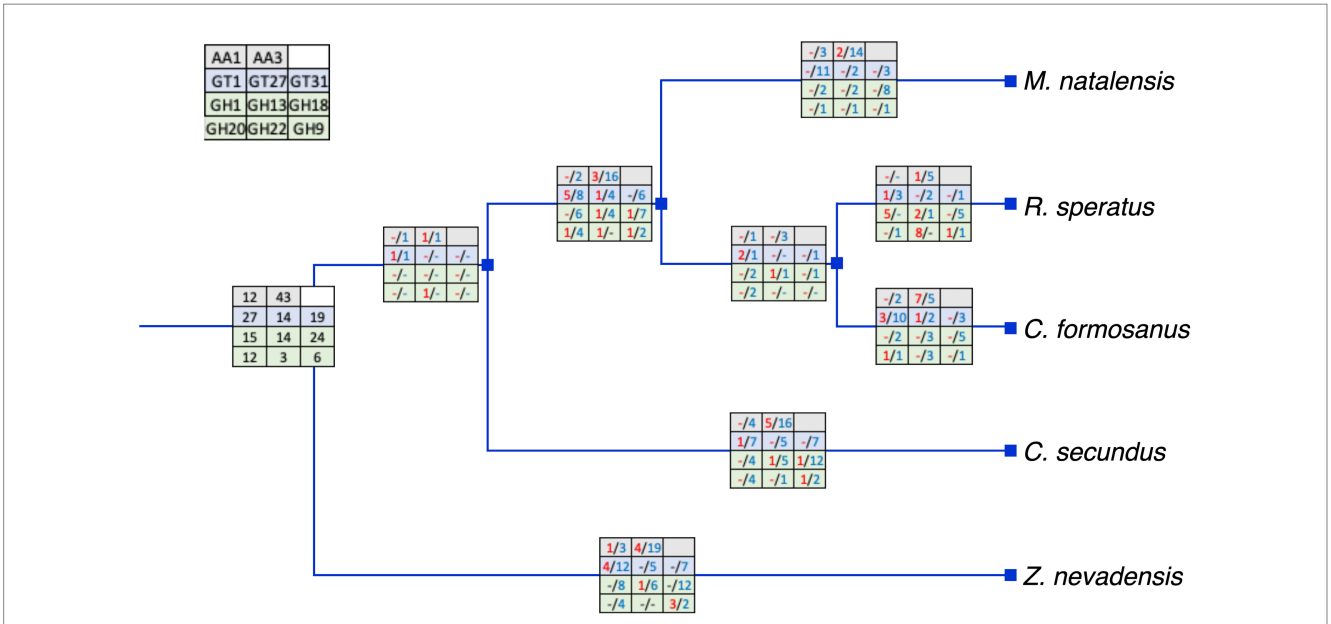

FIGURE 4
The inferred duplications and losses of selected gene families (left-up panel). Numbers in red represent duplications and numbers in blue represent losses. The duplications and losses were inferred by Notung with the species tree in Figure 1 and related gene trees in Figure 2. Represents no duplication or loss.

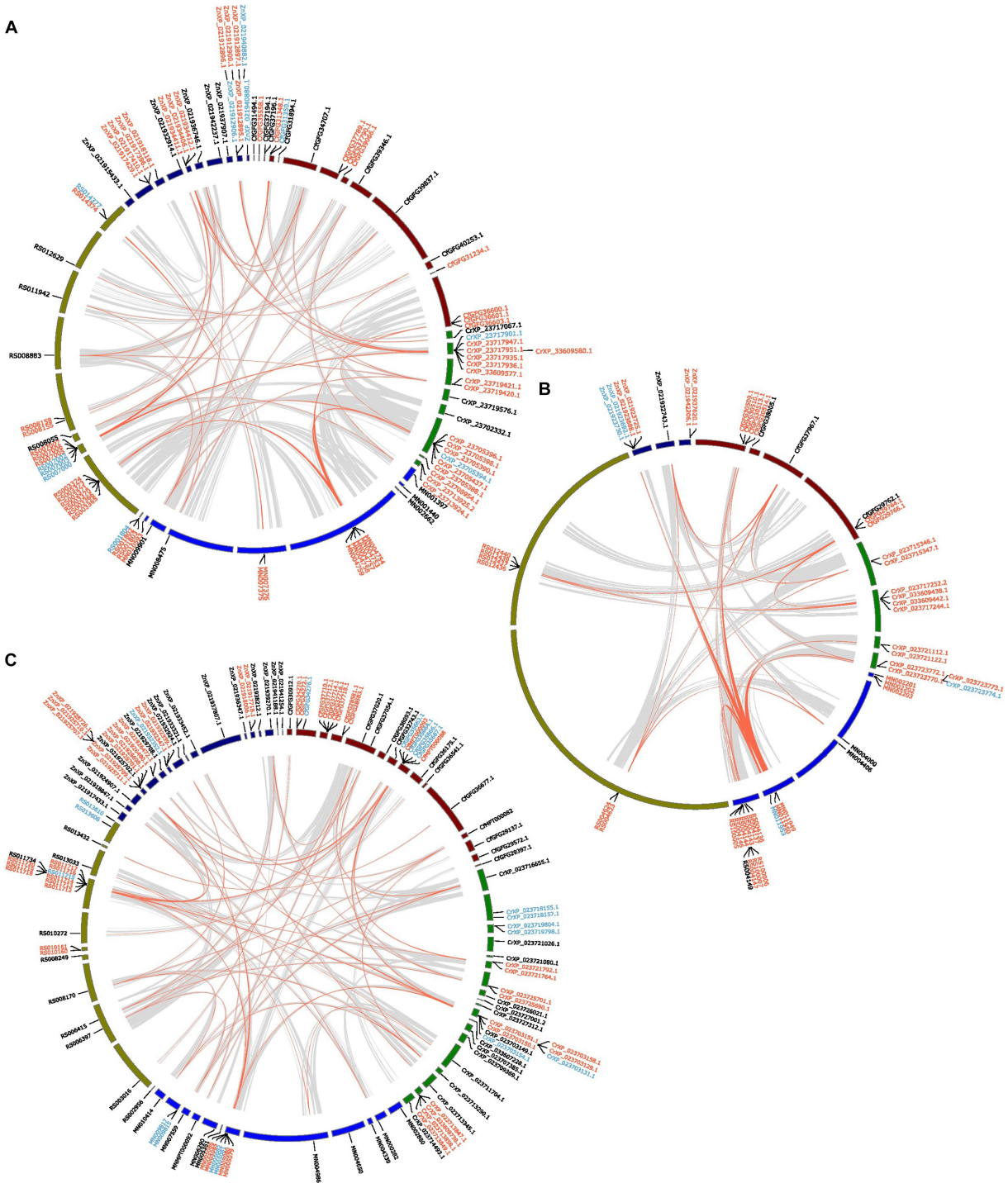

FIGURE 5
The inferred collinearity and duplication modes of GT1 **(A)**, GH1 **(B)**, AA3 **(C)** of five termite species. Gene ids in red represent tandem duplications, Gene ids in blue indicate proximal duplications, Gene ids in black represent dispersed duplications. The grey links show the collinear blocks between the scaffolds/contigs from different species that containing identified genes; the red links show the collinear blocks containing identified genes in the referred gene families. The collinearity analysis was performed at protein level.

three GT1s (RS008155, RS007006, RS007007), three GT27s (RS006342, RS004127, RS011165), and three GT31s (RS007129, RS009017, RS001752) (Supplementary Figure S6). Furthermore, we observed an increased expression of one AA1 (RS002049), two AA3 (RS003016 and RS010272), three GH13s (RS006197, RS006136, RS006137), two GH18s (RS009184 and RS015051), one GT1 (RS001802) in the bodies of all castes. A slightly overall higher expression of one AA1 (RS004166) was also found in both bodies and heads of soldiers than in the other two castes. In the GH1 gene family, we found a high expression of RS004136 in the bodies of workers and

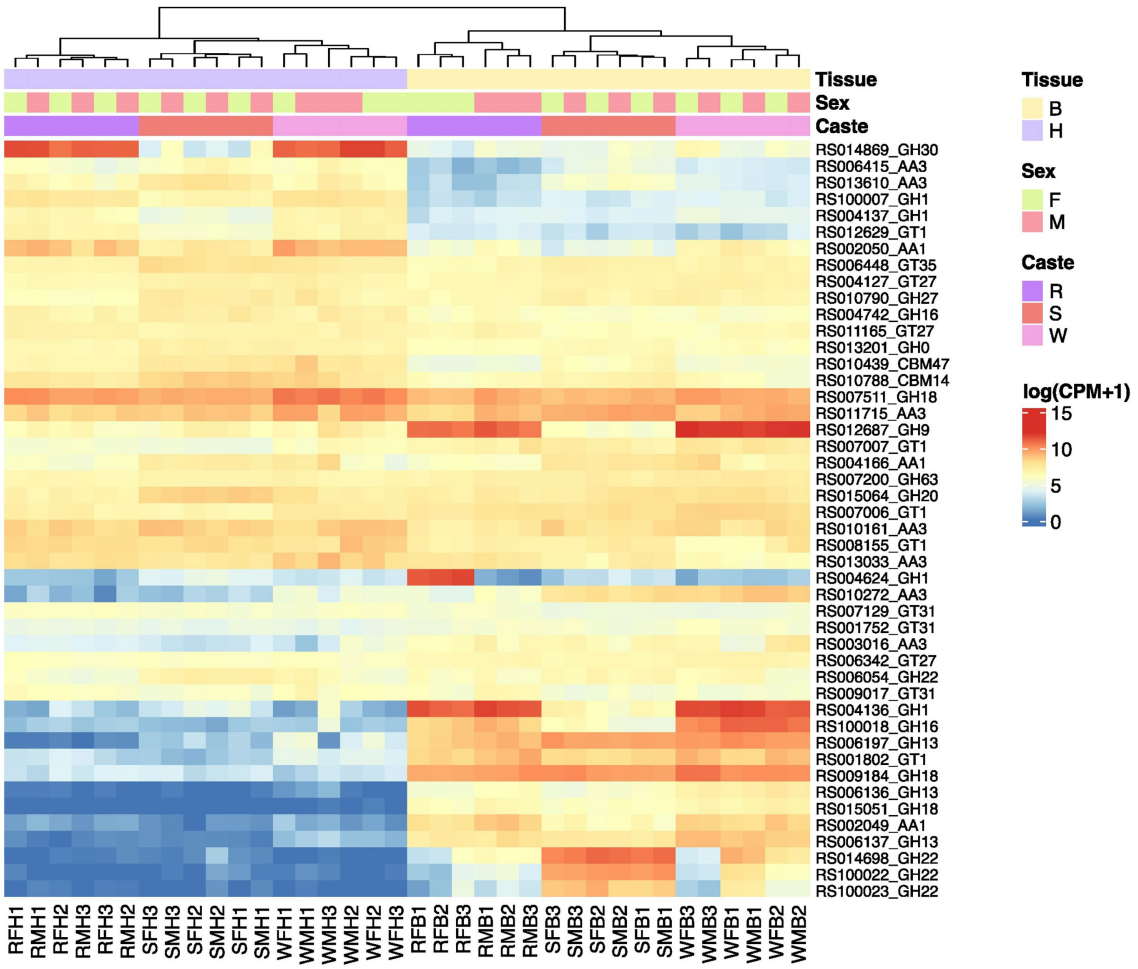

FIGURE 6
The expression of a number of identified CAZymes in *R. speratus* mentioned in the manuscript. R, reproductives, S, soldiers, W, workers, M, males, F, females, H, heads, B, body (throax+abdomen). The original data is from a previously published study (Shigenobu et al., 2022) and the expression data are presented as $\log_{10}(\text{cpm} + 1)$.

reproductives. Moreover, we found increased expression levels of one GH1 (RS012436) in the heads of workers, two GH1s (RS004137 and RS100007) and one AA1 (RS002050) in the heads of all castes.

Discussion

Termites have a diverse array of CAZyme genes belonging to four major classes, with a notable abundance of genes from the GH and GT classes, as previously reported in *C. formosanus* (Zhang et al., 2012). Most gene families are conserved with minor changes during termite evolution, suggesting their conserved roles in termite biology. The GT is the most diverse and abundant CAZyme class among the identified gene families. GT enzymes catalyze the formation of glycoside bonds by using activated nucleotide sugar and are involved in multiple physiological activities in insects, such as the detoxification of plant compounds, participation in various developmental processes, chemosensation, and stress response (Nagare et al., 2021). GT1, the largest family in the GT class due to their excellent glycosylation capacities (Zhang et al., 2020) and playing a pivotal role in insect detoxification of xenobiotics (Nagare et al., 2021). It is the most abundant family within GT gene families in all termites. The GT1 gene family is also commonly known as UDP-glycosyltransferase (UGT) in insects with various numbers in different species. A previous study on the nine insect genomes showed that the UGT numbers range from 12 in *Apis mellifera* to 58 in *Acyrthosiphone pisum* (Ahn et al., 2012); moreover, a recent report showed different numbers of UGTs ranging from 29 to 50 in various *Drosophila* species (Ahn and Marygold, 2021). As termites primarily feed on wood and consume a wide range of plant metabolites, high GT1 gene numbers would provide sufficient repertoire genes for detoxification. The GT1 gene family could also use a wide range of natural products, including glycolipids, flavonoids and macrolides (Zhang et al., 2020), which might be related to the various gene groups of the gene family in termites.

Interestingly, we found several losses but a few duplications in different termites, while a large gene number in the termite ancestor. Along with the collinearity blocks, these losses might be the consequence of the functional redundancy of gene duplicates during termite evolution. The retained GT1 genes during termite evolution might gain additional functions other than detoxification, such as olfaction in *Bombyx mori* (Huang et al., 2008), which could be supported by higher expression of certain GT1 genes observed in

the head than the body of *R. speratus*. Intriguingly, we found that groups 10, 11 and 12 of GT1 gene tree contain no *M. natalensis* GT1 gene; however, why the higher termite lost these genes is yet to be investigated.

Another two GT gene families with large gene numbers in termites, GT27 and GT31, are related to insect development (Ji et al., 2018; Nagare et al., 2021). These genes have a stable number in termites, but the domain analysis revealed that a few genes encoded additional or truncated domains. This suggests that the genes had undergone evolutionary changes during termite evolution, supported by the inferred duplications and losses. Both gene families had likely been through duplications and strong selection due to the physiological significance of maintaining their functions. This might be corroborated by the constitutive expression of the corresponding genes in the different body parts of different castes of *R. speratus*. However, as some of these genes are related to embryo development (Brückner et al., 2000), it would be necessary to investigate their expression patterns through different developmental stages to provide insights into their roles in termite development.

The second most abundant gene class in termites is GH, which breaks down glycol bounds in carbohydrates, suggesting their significant contribution to termite wood feeding. Among them, GH1 is the most variable in termites, which might be related to their diversified functions in insects (He et al., 2022). The primary function of GH1 in termites is wood digestion (Tokuda et al., 2002, 2009), reflecting the ancestral function of GH1 in insects (He et al., 2022). As the ancestors of termites were wood feeders, it is not surprising that many GH1 genes were inferred from their ancestor. However, we found a large number of gene losses during termite evolution, indicating that the presence of termite gut symbionts might have compensated for some of the functions related to wood digestion. Furthermore, a GH1 gene specifically expressed in the accessory glands of the ovary (Shigenobu et al., 2022) was associated with termite caste formation (Korb et al., 2009; Matsuura et al., 2009). This is likely an ancestral function of GH1 in termites (He et al., 2022; Shigenobu et al., 2022).

The most abundant gene family of GH in termites is GH18, which is widely spread in all groups of organisms (Karlsson and Stenlid, 2009) and contains hydrolytic chitinases and β-N-acetylglucosaminidases as well as non-hydrolytic proteins such as lectins or xylanase inhibitors (Chen C. et al., 2020). In insects the GH18s were classed into 11 groups and contribute to diverse functions, including molting, nutrition, cell proliferation, and immune defense (Chen W. et al., 2020); the functional GH18s, including groups 1, 2, 3, and 4, previously found in other insects are present in termites. The presence of nine groups in termites, including five groups having a single copy and three groups having duplicates, suggests conserved functions of GH18 genes. However, the continual loss of GH18s in termites indicates the reshaping of the gene families during evolution, as also supported by the presence of fragmented domains in GH18 proteins. In addition, we found one group of termite GH18s does not cluster together with any classified groups, which might be due to the misplacement of the group in the gene phylogeny as shown with a low support value.

Another GH family, GH13, is the largest family of glycoside hydrolases and encodes several enzymes acting on several substrates (Kuriki and Imanaka, 1999; da Costa-Latge et al., 2021). In termites most GH13 genes belong to GH13_17 subfamilies, which encode α-glucosidase, with a few copies of GH13_15, encoding α-Amylase (Stam et al., 2006). The GH20 gene family, involved in insect cuticle formation or degradation (Intra et al., 2008; Yang and Chen, 2019), is another conserved large gene family in termites, suggesting their conserved role in termites. The other two gene families, GH22 and GH9, contain lysozymes and cellulases and are involved in digestion (Davison and Blaxter, 2005; Moraes et al., 2014). A large gene number of GH22 with high expression in the body of *R. speratus* soldiers suggest their roles other than digestion, possibly related to the division of labor or defense in *R. speratus* (Shigenobu et al., 2022). However, GH9, a well-studied cellulase in termites (Xu et al., 2010; Bujang et al., 2014), shows a large gene number in *Z. nevadensis*. The GH9 genes had an ancient origin but experienced diversification in termite species (Davison and Blaxter, 2005; Xu et al., 2010), which might explain the large number of cellulase in termites. A previous study on the evolution of GH9 in higher termites showed duplications of GH9 in the highly diversified feeding group (Bujang et al., 2014). Therefore, a comprehensive understanding of its evolution would require further analysis with a larger size of termite genomes.

Among the other CAZyme gene classes, AA is related to lignocellulose digestion. A large number of AA3, which are closely related FAD-dependent enzymes required for class II peroxidases to oxidize lignin (Levasseur et al., 2013), suggest their involvement in wood-feeding in termites. The observed losses during termite evolution suggest potential compensation by the termite symbionts in lignin degradation. However, we found relatively constant gene numbers of AA1, which contains laccase, ferroxidase and laccase-like multicopper oxidase in all termites, suggesting their conserved role in termite digestion.

The CAZyme class with the least number of members is CE, with only one CE9 in each species, which is the second largest group in CAZyme families and catalyzes the de-*O* or de-*N*-acylation by removing the ester decorations from carbohydrates (Nakamura et al., 2017). In addition, we found no PL in termites, which cleaves uronic acid-containing polysaccharides using an elimination instead of a hydrolytic mechanism (Lombard et al., 2010). In the CAZyme database, the CE and PL classes currently have 20 and 42 classified families, respectively; the studies on the function or characterization of both classes are rather limited in insects. Among these families, CE4, the largest family of CE, chitin deacetylases (CDA) in insects, plays roles in molting, pupation, and chitin modification (Li et al., 2021). However, the limited presence of both classes suggests that termites may not rely heavily on them for digestion or other physiological activities, which might be compensated by other mechanisms or gene families. For instance, the role of PL gene families in termites is likely to be compensated by their gut microbiota, which possesses a suite of PL gene families (Arora et al., 2022). This kind of complementary relationship has been proposed in *M. natalensis* (Poulsen et al., 2014), and we assume it should be common in most termite species because of their close relation to gut symbionts (Bourguignon et al., 2018). This has been also observed in tortoise leaf beetles and their pectinolytic *Stammera* symbionts that encode rhamnogalacturonan lyase, a PL4, for the adaptation of beetles to herbivory (Salem et al., 2020).

In addition to enzyme classes, CAZymes include carbohydrate-binding modules that lack catalytic activities but play an essential role in carbohydrate digestion. Among the CBM families, CBM14 is the largest in termites and is present in all domains of life. CBM14 is

known to bind to chitin (Chang and Stergiopoulos, 2015a,b), suggesting its involvement in termite chitin metabolism. In insects, CBM14, also known as the peritrophin-A domain, contributes to the formation of insect peritrophic matrix (Shen and Jacobs-Lorena, 1999; Tellam et al., 1999). Half of them contain multiple repeats within a single protein, indicating their potential interactions with other catalytic ligninolytic enzymes. In termites the different CBM14 gene groups might have different functions as the CBM14s in *Tribolium castaneum*, which were classified into three subfamilies with different functions, including PM and cuticle formation (Jasrapuria et al., 2010).

Overall, this study compared the CAZymes in different termite species, providing preliminary insights into their evolution. The prevalence of GH and GT enzyme classes in termite hosts and their gut symbionts (Arora et al., 2022) indicates their importance in termite wood digestion. A large number of losses, along with the relatively stable number of genes across species, might be attributed to the abundance of these gene families in their ancestors and the subsequent redundancy during termite evolution. However, it is worth noting that this study analyzed the genomes of only five termite species from two of five feeding termite groups, including Group I (all wood-feeding lower termites), Group II (wood-feeding higher termites), Group IIF (fungus-cultivating higher termites), Group III (soil feeders with a large amount of plant materials), and Group IV (true soil feeders) (Inward et al., 2007). Among the relatively stable CAZyme repertoire, we found fewer gene numbers of GT1 and AA3 in fungus-cultivating higher termites (*M. natalensis*) than wood-feeding lower termites (the other four termite species). The effect of feeding preferences on the CAZyme repertoire would require multiple genomes of termite species with other feeding preferences. In addition, these genomes were constructed by different projects and pipelines, which may affect the prediction accuracy of gene numbers, domain structures and duplication modes investigated in this study. To gain a more comprehensive understanding of their evolution, further investigations involving a larger number of high-quality termite genomes and the genomes of closely related species would be necessary. Nevertheless, the present study will aid in formulating some testable hypotheses, such as GT1 duplicates functioning in termite olfaction, evolution of CAZyme gene expression being related to the division of labor, and higher termites largely relying on symbionts for lignin degradation, that can be functionally validated in the future and facilitate identifying suitable targets for future species-specific targets for RNAi-mediated termite management practices (Mogilicherla et al., 2022).

Data availability statement

The NCBI datasets presented in this study can be found in online repositories. The names of the repository/repositories and accession number(s) can be found at: https://www.ncbi.nlm.nih.gov/-, GCF_000696155.1, GCF_002891405.2 and GCA_013340265.1.

Author contributions

SH conceived this study and analyzed the data. All authors contributed to the writing and revision of the manuscript.

Funding

SH is supported by the Foundation of Chongqing Normal University (no. 22XLB028) and Natural Science Foundation of Chongqing (no. 2022NSCQ-MSX2875). AC is financed by "EVA 4.0" (no. CZ.02.1.01/0.0/0.0/16 019/0000803) by the OP RDE and "Excellent Team Grants" (2023–2024) from the Faculty of Forestry and Wood Sciences, Czech University of Life Sciences, Prague, Czechia. BJ is supported by Anhui Provincial Key Laboratory of Molecular Enzymology and Mechanism of Major Diseases in Anhui Normal University (no. fzmx202007) and Special Funds for Supporting Innovation and Entrepreneurship for Returned Overseas-students in Anhui Province (no. 2020LCX035).

Acknowledgments

We acknowledge Amit Roy, Forest Molecular Entomology Lab, Faculty of Forestry and Wood Sciences, Czech University of Life Sciences for his constructive comments in the earlier version of the manuscript. We appreciate the helpful feedback provided by the reviewers and especially the handling editor.

Conflict of interest

The authors declare that the research was conducted in the absence of any commercial or financial relationships that could be construed as a potential conflict of interest.

Publisher's note

Supplementary material

The supplementary material for this article can be found online at: https://www.frontiersin.org/articles/10.3389/ffgc.2023.1240804/full#supplementary-material

References

Ahn, S. J., and Marygold, S. J. (2021). The Udp-glycosyltransferase family in *Drosophila melanogaster*: nomenclature update, gene expression and phylogenetic analysis. *Front. Physiol.* 12:648481. doi: 10.3389/fphys.2021.648481

Ahn, S. J., Vogel, H., and Heckel, D. G. (2012). Comparative analysis of the Udp-glycosyltransferase multigene family in insects. *Insect Biochem. Mol. Biol.* 42, 133–147. doi: 10.1016/j.ibmb.2011.11.006

Arora, J., Kinjo, Y., Šobotník, J., Buček, A., Clitheroe, C., Stiblik, P., et al. (2022). The functional evolution of termite gut microbiota. *Microbiome* 10:78. doi: 10.1186/s40168-022-01258-3

Ashton, L. A., Griffiths, H. M., Parr, C. L., Evans, T. A., Didham, R. K., Hasan, F., et al. (2019). Termites mitigate the effects of drought in tropical rainforest. *Science* 363, 174–177. doi: 10.1126/science.aau9565

Bourguignon, T., Lo, N., Dietrich, C., Šobotník, J., Sidek, S., Roisin, Y., et al. (2018). Rampant host switching shaped the termite gut microbiome. *Curr. Biol.* 28, 649–654.e2. doi: 10.1016/j.cub.2018.01.035

Brückner, K., Perez, L., Clausen, H., and Cohen, S. (2000). Glycosyltransferase activity of fringe modulates Notch-Delta interactions. *Nature* 406, 411–415. doi: 10.1038/35019075

Brune, A. (2014). Symbiotic digestion of lignocellulose in termite guts. *Nat. Rev. Microbiol.* 12, 168–180. doi: 10.1038/nrmicro3182

Brune, A., and Dietrich, C. (2015). The gut microbiota of termites: digesting the diversity in the light of ecology and evolution. *Annu. Rev. Microbiol.* 69, 145–166. doi: 10.1146/annurev-micro-092412-155715

Bucek, A., Šobotník, J., He, S., Shi, M., Mcmahon, D. P., Holmes, E. C., et al. (2019). Evolution of termite symbiosis informed by transcriptome-based phylogenies. *Curr. Biol.* 29, 3728–3734.e4. doi: 10.1016/j.cub.2019.08.076

Bujang, N. S., Harrison, N. A., and Su, N.-Y. (2014). A phylogenetic study of endo-beta-1,4-glucanase in higher termites. *Insect. Soc.* 61, 29–40. doi: 10.1007/s00040-013-0321-7

Cairo, J. P. L., Cannella, D., Oliveira, L. C., Gonçalves, T. A., Rubio, M. V., Terrasan, C. R. F., et al. (2020). On the roles of Aa15 lytic polysaccharide monooxygenases derived from the termite *Coptotermes gestroi*. *J. Inorg. Biochem.* 216:111316. doi: 10.1016/j.jinorgbio.2020.111316

Chang, T.-C., and Stergiopoulos, I. (2015a). Evolutionary analysis of the global landscape of protein domain types and domain architectures associated with family 14 carbohydrate-binding modules. *FEBS Lett.* 589, 1813–1818. doi: 10.1016/j.febslet.2015.05.048

Chang, T.-C., and Stergiopoulos, I. (2015b). Inter- and intra-domain horizontal gene transfer, gain–loss asymmetry and positive selection mark the evolutionary history of the Cbm14 family. *FEBS J.* 282, 2014–2028. doi: 10.1111/febs.13256

Chen, C., Chen, H., Zhang, Y., Thomas, H. R., Frank, M. H., He, Y., et al. (2020). Tbtools: an integrative toolkit developed for interactive analyses of big biological data. *Mol. Plant* 13, 1194–1202. doi: 10.1016/j.molp.2020.06.009

Chen, W., Jiang, X., and Yang, Q. (2020). Glycoside hydrolase family 18 chitinases: the known and the unknown. *Biotechnol. Adv.* 43:107553. doi: 10.1016/j.biotechadv.2020.107553

Da Costa-Latge, S. G., Bates, P., Dillon, R., and Genta, F. A. (2021). Characterization of glycoside hydrolase families 13 and 31 reveals expansion and diversification of α-amylase genes in the phlebotomine Lutzomyia longipalpis and modulation of sandfly glycosidase activities by leishmania infection. *Front. Physiol.* 12:635633. doi: 10.3389/fphys.2021.635633

Davison, A., and Blaxter, M. (2005). Ancient origin of Glycosyl hydrolase family 9 Cellulase genes. *Mol. Biol. Evol.* 22, 1273–1284. doi: 10.1093/molbev/msi107

Drost, H.-G., Gabel, A., Grosse, I., and Quint, M. (2015). Evidence for active maintenance of Phylotranscriptomic hourglass patterns in animal and plant embryogenesis. *Mol. Biol. Evol.* 32, 1221–1231. doi: 10.1093/molbev/msv012

Durand, D., Halldórsson, B. V., and Vernot, B. (2005). A Hybrid Micro-Macroevolutionary Approach to Gene Tree Reconstruction. Research in Computational Molecular Biology: 9th Annual International Conference, Recomb 2005, Cambridge, MA, USA, May 14–18, 2005. Springer, 250–264.

Edgar, R. C. (2004). Muscle: multiple sequence alignment with high accuracy and high throughput. *Nucleic Acids Res.* 32, 1792–1797. doi: 10.1093/nar/gkh340

Fujita, A., Miura, T., and Matsumoto, T. (2008). Differences in cellulose digestive systems among castes in two termite lineages. *Physiol. Entomol.* 33, 73–82. doi: 10.1111/j.1365-3032.2007.00606.x

Geng, A., Cheng, Y., Wang, Y., Zhu, D., Le, Y., Wu, J., et al. (2018). Transcriptome analysis of the digestive system of a wood-feeding termite (*Coptotermes formosanus*) revealed a unique mechanism for effective biomass degradation. *Biotechnol. Biofuels* 11:24. doi: 10.1186/s13068-018-1015-1

Griffiths, H. M., Ashton, L. A., Evans, T. A., Parr, C. L., and Eggleton, P. (2019). Termites can decompose more than half of deadwood in tropical rainforest. *Curr. Biol.* 29, 105–119. doi: 10.1016/j.cub.2019.01.012

He, S., Jiang, B., Chakraborty, A., and Yu, G. (2022). The evolution of glycoside hydrolase family 1 in insects related to their adaptation to plant utilization. *Insects* 13:786. doi: 10.3390/insects13090786

Hervé, V., Liu, P., Dietrich, C., Sillam-Dussès, D., Stiblik, P., Šobotník, J., et al. (2020). Phylogenomic analysis of 589 metagenome-assembled genomes encompassing all major prokaryotic lineages from the gut of higher termites. *PeerJ* 8:e8614. doi: 10.7717/peerj.8614

Huang, F.-F., Chai, C.-L., Zhang, Z., Liu, Z.-H., Dai, F.-Y., Lu, C., et al. (2008). The Udp-glucosyltransferase multigene family in *Bombyx mori*. *BMC Genomics* 9:563. doi: 10.1186/1471-2164-9-563

Huerta-Cepas, J., Serra, F., and Bork, P. (2016). Ete 3: reconstruction, analysis, and visualization of Phylogenomic data. *Mol. Biol. Evol.* 33, 1635–1638. doi: 10.1093/molbev/msw046

Intra, J., Pavesi, G., and Horner, D. S. (2008). Phylogenetic analyses suggest multiple changes of substrate specificity within the Glycosyl hydrolase 20 family. *BMC Evol. Biol.* 8:214. doi: 10.1186/1471-2148-8-214

Inward, D. J., Vogler, A. P., and Eggleton, P. (2007). A comprehensive phylogenetic analysis of termites (Isoptera) illuminates key aspects of their evolutionary biology. *Mol. Phylogenet. Evol.* 44, 953–967. doi: 10.1016/j.ympev.2007.05.014

Itakura, S., Yoshikawa, Y., Togami, Y., and Umezawa, K. (2020). Draft genome sequence of the termite, *Coptotermes formosanus*: genetic insights into the pyruvate dehydrogenase complex of the termite. *J. Asia Pac. Entomol.* 23, 666–674. doi: 10.1016/j.aspen.2020.05.004

Jasrapuria, S., Arakane, Y., Osman, G., Kramer, K. J., Beeman, R. W., and Muthukrishnan, S. (2010). Genes encoding proteins with peritrophin A-type chitin-binding domains in *Tribolium castaneum* are grouped into three distinct families based on phylogeny, expression and function. *Insect Biochem. Mol. Biol.* 40, 214–227. doi: 10.1016/j.ibmb.2010.01.011

Ji, S., Samara, N. L., Revoredo, L., Zhang, L., Tran, D. T., Muirhead, K., et al. (2018). A molecular switch orchestrates enzyme specificity and secretory granule morphology. *Nat. Commun.* 9:3508. doi: 10.1038/s41467-018-05978-9

Jones, P., Binns, D., Chang, H. Y., Fraser, M., Li, W., Mcanulla, C., et al. (2014). InterProScan 5: genome-scale protein function classification. *Bioinform* 30, 1236–1240. doi: 10.1093/bioinformatics/btu031

Kalleshwaraswamy, C. M., Shanbhag, R. R., and Sundararaj, R. (2022). "Wood degradation by termites: ecology, economics and protection" in *Science of Wood Degradation and Its Protection*. ed. R. Sundararaj (Springer Singapore: Singapore)

Karlsson, M., and Stenlid, J. (2009). Evolution of family 18 glycoside hydrolases: diversity, domain structures and phylogenetic relationships. *J. Mol. Microbiol. Biotechnol.* 16, 208–223. doi: 10.1159/000151220

Katoh, K., and Standley, D. M. (2013). Mafft multiple sequence alignment software version 7: improvements in performance and usability. *Mol. Biol. Evol.* 30, 772–780. doi: 10.1093/molbev/mst010

Korb, J., Poulsen, M., Hu, H., Li, C., Boomsma, J. J., Zhang, G., et al. (2015). A genomic comparison of two termites with different social complexity. *Front. Genet.* 6:9. doi: 10.3389/fgene.2015.00009

Korb, J., Weil, T., Hoffmann, K., Foster, K. R., and Rehli, M. (2009). A gene necessary for reproductive suppression in termites. *Science* 324:758. doi: 10.1126/science.1170660

Krzywinski, M., Schein, J., Birol, I., Connors, J., Gascoyne, R., Horsman, D., et al. (2009). Circos: an information aesthetic for comparative genomics. *Genome Res.* 19, 1639–1645. doi: 10.1101/gr.092759.109

Kuriki, T., and Imanaka, T. (1999). The concept of the α-amylase family: structural similarity and common catalytic mechanism. *J. Biosci.* 87, 557–565. doi: 10.1016/S1389-1723(99)80114-5

Levasseur, A., Drula, E., Lombard, V., Coutinho, P. M., and Henrissat, B. (2013). Expansion of the enzymatic repertoire of the Cazy database to integrate auxiliary redox enzymes. *Biotechnol. Biofuels* 6:41. doi: 10.1186/1754-6834-6-41

Li, H. (2023). Protein-to-genome alignment with miniprot. *Bioinform* 39:btad014. doi: 10.1093/bioinformatics/btad014

Li, Y., Liu, L., Yang, J., and Yang, Q. (2021). An overall look at insect chitin deacetylases: promising molecular targets for developing green pesticides. *J. Pestic. Sci.* 46, 43–52. doi: 10.1584/jpestics.D20-085

Lombard, V., Bernard, T., Rancurel, C., Brumer, H., Coutinho, P. M., and Henrissat, B. (2010). A hierarchical classification of polysaccharide lyases for glycogenomics. *Biochemist* 432, 437–444. doi: 10.1042/BJ20101185

Manni, M., Berkeley, M. R., Seppey, M., Simão, F. A., and Zdobnov, E. M. (2021). Busco update: novel and streamlined workflows along with broader and deeper phylogenetic coverage for scoring of eukaryotic, prokaryotic, and viral genomes. *Mol. Biol. Evol.* 38, 4647–4654. doi: 10.1093/molbev/msab199

Marynowska, M., Goux, X., Sillam-Dussès, D., Rouland-Lefèvre, C., Roisin, Y., Delfosse, P., et al. (2017). Optimization of a metatranscriptomic approach to study the lignocellulolytic potential of the higher termite gut microbiome. *BMC Genomics* 18:681. doi: 10.1186/s12864-017-4076-9

Matsuura, K., Yashiro, T., Shimizu, K., Tatsumi, S., and Tamura, T. (2009). Cuckoo fungus mimics termite eggs by producing the cellulose-digesting enzyme β-glucosidase. *Curr. Biol.* 19, 30–36. doi: 10.1016/j.cub.2008.11.030

Minh, B. Q., Schmidt, H. A., Chernomor, O., Schrempf, D., Woodhams, M. D., Von Haeseler, A., et al. (2020). Iq-tree 2: new models and efficient methods for phylogenetic inference in the genomic era. *Mol. Biol. Evol.* 37, 1530–1534. doi: 10.1093/molbev/msaa015

Mogilicherla, K., Chakraborty, A., Taning, C., Smagghe, G., and Roy, A. (2022). Rnai in termites (Isoptera): current status and prospects for pest management. *Entomol Gen* 43, 55–68. doi: 10.1127/entomologia/2022/1636

Moraes, C. D. S., Diaz-Albiter, H. M., Faria, M. D. V., Sant'anna, M. R. V., Dillon, R. J., and Genta, F. A. (2014). Expression pattern of glycoside hydrolase genes in Lutzomyia longipalpis reveals key enzymes involved in larval digestion. *Front. Physiol.* 5:276. doi: 10.3389/fphys.2014.00276

Nagare, M., Ayachit, M., Agnihotri, A., Schwab, W., and Joshi, R. (2021). Glycosyltransferases: the multifaceted enzymatic regulator in insects. *Insect Mol. Biol.* 30, 123–137. doi: 10.1111/imb.12686

Nakamura, A. M., Nascimento, A. S., and Polikarpov, I. (2017). Structural diversity of carbohydrate esterases. *Biotechnol Res Innov* 1, 35–51. doi: 10.1016/j.biori.2017.02.001

Poulsen, M., Hu, H., Li, C., Chen, Z., Xu, L., Otani, S., et al. (2014). Complementary symbiont contributions to plant decomposition in a fungus-farming termite. *Proc. Natl. Acad. Sci. U. S. A.* 111, 14500–14505. doi: 10.1073/pnas.1319718111

Rust, M. K., and Su, N. Y. (2012). Managing social insects of urban importance. *Annu. Rev. Entomol.* 57, 355–375. doi: 10.1146/annurev-ento-120710-100634

Salem, H., Kirsch, R., Pauchet, Y., Berasategui, A., Fukumori, K., Moriyama, M., et al. (2020). Symbiont digestive range reflects host plant breadth in herbivorous beetles. *Curr. Biol.* 30, 2875–2886.e4. doi: 10.1016/j.cub.2020.05.043

Shelomi, M., Wipfler, B., Zhou, X., and Pauchet, Y. (2020). Multifunctional cellulase enzymes are ancestral in Polyneoptera. *Insect Mol. Biol.* 29, 124–135. doi: 10.1111/imb.12614

Shen, Z., and Jacobs-Lorena, M. (1999). Evolution of chitin-binding proteins in invertebrates. *J. Mol. Evol.* 48, 341–347. doi: 10.1007/PL00006478

Shigenobu, S., Hayashi, Y., Watanabe, D., Tokuda, G., Hojo, M. Y., Toga, K., et al. (2022). Genomic and transcriptomic analyses of the subterranean termite Reticulitermes speratus: gene duplication facilitates social evolution. *Proc. Natl. Acad. Sci. U. S. A.* 119:e2110361119. doi: 10.1073/pnas.2110361119

Stam, M. R., Danchin, E. G., Rancurel, C., Coutinho, P. M., and Henrissat, B. (2006). Dividing the large glycoside hydrolase family 13 into subfamilies: towards improved functional annotations of alpha-amylase-related proteins. *Protein Eng. Des. Sel.* 19, 555–562. doi: 10.1093/protein/gzl044

Tartar, A., Wheeler, M. M., Zhou, X., Coy, M. R., Boucias, D. G., and Scharf, M. E. (2009). Parallel metatranscriptome analyses of host and symbiont gene expression in the gut of the termite *Reticulitermes flavipes*. *Biotechnol. Biofuels* 2:25. doi: 10.1186/1754-6834-2-25

Tellam, R. L., Wijffels, G., and Willadsen, P. (1999). Peritrophic matrix proteins. *Insect Biochem. Mol. Biol.* 29, 87–101. doi: 10.1016/S0965-1748(98)00123-4

Thompson, J. D., Plewniak, F., Ripp, R., Thierry, J. C., and Poch, O. (2001). Towards a reliable objective function for multiple sequence alignments. *J. Mol. Biol.* 314, 937–951. doi: 10.1006/jmbi.2001.5187

Thompson, J. D., Thierry, J. C., and Poch, O. (2003). Rascal: rapid scanning and correction of multiple sequence alignments. *Bioinform* 19, 1155–1161. doi: 10.1093/bioinformatics/btg133

Tokuda, G. (2019). Plant cell wall degradation in insects: recent progress on endogenous enzymes revealed by multi-omics technologies. *Adv in Insect Phys* 57, 97–136. doi: 10.1016/bs.aiip.2019.08.001

Tokuda, G., Lo, N., Watanabe, H., Arakawa, G., Matsumoto, T., and Noda, H. (2004). Major alteration of the expression site of endogenous cellulases in members of an apical termite lineage. *Mol. Ecol.* 13, 3219–3228. doi: 10.1111/j.1365-294X.2004.02276.x

Tokuda, G., Miyagi, M., Makiya, H., Watanabe, H., and Arakawa, G. (2009). Digestive β-glucosidases from the wood-feeding higher termite, Nasutitermes takasagoensis: intestinal distribution, molecular characterization, and alteration in sites of expression. *Insect Biochem. Mol. Biol.* 39, 931–937. doi: 10.1016/j.ibmb.2009.11.003

Tokuda, G., Saito, H., and Watanabe, H. (2002). A digestive β-glucosidase from the salivary glands of the termite, Neotermes koshunensis (Shiraki): distribution, characterization and isolation of its precursor cdna by 5′- and 3′-race amplifications with degenerate primers. *Insect Biochem. Mol. Biol.* 32, 1681–1689. doi: 10.1016/S0965-1748(02)00108-X

Wang, Y., Tang, H., Debarry, J. D., Tan, X., Li, J., Wang, X., et al. (2012). McscanX: a toolkit for detection and evolutionary analysis of gene synteny and collinearity. *Nucleic Acids Res.* 40:e49. doi: 10.1093/nar/gkr1293

Watanabe, H., Noda, H., Tokuda, G., and Lo, N. (1998). A cellulase gene of termite origin. *Nature* 394, 330–331. doi: 10.1038/28527

Wickham, H. (2016). *Ggplot2: Elegant Graphics for Data Analysis*, Cham, Switzerland, Springer International Publishing.

Wu, C., Ulyshen, M. D., Shu, C., Zhang, Z., Zhang, Y., Liu, Y., et al. (2021). Stronger effects of termites than microbes on wood decomposition in a subtropical forest. *For. Ecol. Manag.* 493:119263. doi: 10.1016/j.foreco.2021.119263

Xu, Q., Zhou, Y., Li, J., Chen, H., Lu, J., Chen, K.-P., et al. (2010). Diversifying evolution of endo-beta-1,4-glucanase in termites (Isoptera). *Sociobiology* 56, 623–636.

Yang, Q., and Chen, W. (2019). Structural and biochemical analysis completes the puzzle of chitin hydrolysis in insects. *FASEB J.* 33:798.10. doi: 10.1096/fasebj.2019.33.1

Yuki, M., Moriya, S., Inoue, T., and Kudo, T. (2008). Transcriptome analysis of the digestive organs of Hodotermopsis sjostedti, a lower termite that hosts mutualistic microorganisms in its hindgut. *Zool. Sci.* 25, 401–406. doi: 10.2108/zsj.25.401

Zhang, D., Lax, A. R., Henrissat, B., Coutinho, P. M., Katiya, N., Nierman, W. C., et al. (2012). Carbohydrate-active enzymes revealed in *Coptotermes formosanus* (Isoptera: Rhinotermitidae) transcriptome. *Insect Mol. Biol.* 21, 235–245. doi: 10.1111/j.1365-2583.2011.01130.x

Zhang, H., Yohe, T., Huang, L., Entwistle, S., Wu, P., Yang, Z., et al. (2018). dbcan2: a meta server for automated carbohydrate-active enzyme annotation. *Nucleic Acids Res.* 46, 95–101. doi: 10.1093/nar/gky418

Zhang, P., Zhang, Z., Zhang, L., Wang, J., and Wu, C. (2020). Glycosyltransferase Gt1 family: phylogenetic distribution, substrates coverage, and representative structural features. *Comput. Struct. Biotechnol. J.* 18, 1383–1390. doi: 10.1016/j.csbj.2020.06.003

frontiers | Frontiers in Forests and Global Change

TYPE Original Research
PUBLISHED 11 January 2024
DOI 10.3389/ffgc.2023.1215813

OPEN ACCESS

EDITED BY
Frank Chidawanyika,
International Centre of Insect Physiology and Ecology (ICIPE), Kenya

REVIEWED BY
Inusa Jacob Ajene,
International Centre of Insect Physiology and Ecology (ICIPE), Kenya
Casper Nyamukondiwa,
Botswana International University of Science and Technology, Botswana

*CORRESPONDENCE
Anna Jirošová
jirosovaa@fld.czu.cz

†These authors have contributed equally to this work

RECEIVED 02 May 2023
ACCEPTED 19 December 2023
PUBLISHED 11 January 2024

CITATION
Ramakrishnan R, Roy A, Hradecký J, Kai M, Harant K, Svatoš A and Jirošová A (2024) Juvenile hormone III induction reveals key genes in general metabolism, pheromone biosynthesis, and detoxification in Eurasian spruce bark beetle.
Front. For. Glob. Change 6:1215813.
doi: 10.3389/ffgc.2023.1215813

Juvenile hormone III induction reveals key genes in general metabolism, pheromone biosynthesis, and detoxification in Eurasian spruce bark beetle

Rajarajan Ramakrishnan[1†], Amit Roy[1], Jaromír Hradecký[1], Marco Kai[2], Karel Harant[3], Aleš Svatoš[2,4] and Anna Jirošová[1*†]

[1]Faculty of Forestry and Wood Sciences, Czech University of Life Sciences Prague, Prague, Czechia, [2]Max Planck Institute for Chemical Ecology, Jena, Germany, [3]Laboratory of Mass Spectrometry, BIOCEV, Faculty of Science Charles University in Prague, Prague, Czechia, [4]Institute of Organic Chemistry and Biochemistry, Czech Academy of Sciences, Prague, Czechia

Introduction: In recent years, bark beetle *Ips typographus*, has caused extensive damage to European Norway spruce forests through widespread outbreaks. This pest employs pheromone-assisted aggregation to overcome tree defense, resulting in mass attacks on host spruce. Many morphological and behavioral processes in *I. typographus* are under the regulation of juvenile hormone III (JH III), including the biosynthesis of aggregation pheromones and associated detoxification monoterpene conjugates.

Objectives and Methods: In this study, we topically applied juvenile hormone III (JH III) and performed metabolomics, transcriptomics, and proteomics in *I. typographus* both sexes, with focused aims; 1. Highlight the JH III-regulated metabolic processes; 2. Identify pheromone biosynthesis-linked genes; and 3. Investigate JH III's impact on detoxification conjugates linked to pheromonal components.

Results: Numerous gene families were enriched after JH III treatment, including genes associated with catalytic and oxidoreductase activity, esterases, phosphatases, and membrane transporters. Sex-specific enrichments for reproduction-related and detoxification genes in females and metabolic regulation genes in males were observed. On the protein level were enriched metal ion binding and transferase enzymes in male beetles. After JHIII treatment, mevalonate pathway genes, including terminal isoprenyl diphosphate synthase (IPDS), were exclusively 35- folds upregulated in males, providing evidence of *de novo* biosynthesis of pheromone components 2-methyl-3-buten-2-ol and ipsdienol. In addition, cytochrome P450 genes likely involved in the biosynthesis of *cis/trans*-verbenol, detoxification, and formation of ipsdienol, were 3-fold upregulated in the male gut. The increase in gene expression correlated with the heightened production of the respective metabolites. Detoxification conjugates, verbenyl oleate in the beetle fat body and verbenyl diglycosides in the gut, were induced by JHIII application, which confirms the hormone regulation of their formation. The JH III induction also increased the gene contigs esterase and glycosyl hydrolase up to proteins from male gut tissue. The esterase was proposed to release pheromone *cis*-verbenol in adult males by breaking down verbenyl oleate. The correlating analyses confirmed a reduction in the abundance of verbenyl oleate in the induced male beetle.

Conclusion: The data provide evidence of JH III's regulatory role in the expression of genes and enzymes related to fundamental beetle metabolism, pheromone biosynthesis, and detoxification in *Ips typographus*.

KEYWORDS

***Ips typographus*, juvenile hormone III, hormonal regulation, mevalonate pathway, CyP450, esterase, monoterpenyl diglycosides, isoprenyl di phosphate synthase**

1 Introduction

The Eurasian Spruce Bark Beetle (*Ips typographus*, Coleoptera: Curculionidae) is a pest that severely affects Norway spruce (*Picea abies*) survival across Eurasia (Ward et al., 2022). In recent years, changing climate patterns resulting in extended periods of drought, along with human-induced factors such as establishing monoculture spruce tree plantations, have played a role in exacerbating its outbreaks (Hlasny et al., 2021). In the Czech Republic, from 2018 till 2022, over 50 million m^3 of spruce forest have been recorded with bark beetle-infested wood (Knizek et al., 2023). In Europe as a whole, *I. typographus* has killed twice as many trees in the past decade, approximately 70.1 million m^3 of timber, nearly all of it Norway spruce (Patacca et al., 2023).

In the class Insecta, many morphological and behavioral changes, such as body development, reproduction, parental care, mating behavior, molt and growth, diapause, and many other functions are hormonally regulated (Jindra et al., 2013; Smykal et al., 2014). The two most important classes of insect hormones are ecdysteroids and juvenile hormones (Pandey and Bloch, 2015). In Coleoptera pheromone biosynthesis concepts, juvenile hormone III (JH III) is the most studied (Keeling et al., 2016). The primary function of these hormones is to maintain juvenile characteristics and prevent premature metamorphosis (Goodman and Cusson, 2012). JH III is synthesized in the exocrine gland corpus allatum and transported through the hemolymph by binding proteins to its target receptors (Jindra and Bittova, 2020). JH III has been extensively used to study many gene families involved in insect growth and metamorphosis, along with social behavior (Riddiford et al., 2010; Trumbo, 2018).

First instar insect larvae initially contain a high titer of JH III, which is subsequently reduced as, the larvae undergo metamorphosis into pupae (Treiblmayr et al., 2006). In the pre-metamorphic stages, JH III has been studied for its influence on the development of larval muscles and the prothoracic glands producing ecdysteroids, as well as its role in restructuring gut development, fat body, and epidermis in various insect species (Riddiford et al., 2001; Riddiford, 2012; Jindra et al., 2013). In the adult insects, JH III influences various aspects, including pheromone production (Tillman et al., 2004) and social behavior (Trumbo, 2018), caste determination (Cristino et al., 2006); aggression and display (Emlen et al., 2006), migration (Zhu et al., 2009), and neuronal remodeling (Leinwand and Scott, 2021).

In bark beetles, JH III effects have primarily been studied in relation to pheromone biosynthesis induction. When the beetles bore into the host tree, JH III is released from the endocrine gland, initiating a series of hormonal signaling processes that lead to the production of aggregation pheromone components in male beetles (Bakke et al., 1977; Schlyter et al., 1987). In nature, this potent blend attracts conspecifics, both males and females, to mass attack to help overcome tree defense. In controlled laboratory conditions, pheromone biosynthesis induction can be achieved by topically applying JH III on the beetle abdomen (Byers and Birgersson, 1990; Ivarsson et al., 1993; Seybold et al., 1995; Tillman et al., 1998). This method triggers the *de novo* synthesis of pheromone compounds while avoiding potential interference with the metabolic pathways involved in the digestion of ingested phloem tissues. Pheromone induction using JH III has been demonstrated in bark beetles such as *Ips pini*, *Dendroctonus ponderosae*, and *Ips typographus* (Nardi et al., 2002; Tillman et al., 2004; Zhang et al., 2017; Fang et al., 2021a,b; Ramakrishnan et al., 2022a). However, certain *Ips* species such as *I. confusus* and *Ips grandicollis*, have been reported to be unresponsive to JH III-induced pheromone induction (Tillman et al., 2004; Bearfield et al., 2009).

The molecular-level effects of JH III on pheromone biosynthesis have been subsequently investigated in various species, including *Ips paraconfusus* (Ivarsson and Birgersson, 1995), *Ips pini* (Tillman et al., 1998; Blomquist et al., 2010), and *Dendroctonus ponderosae* (Keeling et al., 2016). JH III induction has been found to activate multiple gene families responsible for pheromone biosynthesis, especially in the mevalonate pathway (Sarabia et al., 2019).

In *I. typographus*, male pioneer beetles produce aggregation pheromone blends made up of several terpenoid compounds 2-methyl-3-buten-2-ol, *cis*-verbenol and minor amount of ipsdienol, after successfully boring into the tree bark. Both 2-methyl-3-buten-2-ol and ipsdienol are synthesized in beetle guts through the mevalonate pathway (Figure 1; Ramakrishnan et al., 2022a). In the context of bark beetle pheromone biosynthesis, previous studies have identified key enzymes in the pathway (Tillman et al., 1998). The pathway involves the condensation of acetoacetyl-CoA with acetyl-CoA catalyzed by *3-hydroxy-3-methyl glutaryl coenzyme-A synthase* (HMG-S), followed by a reduction of hydroxymethyl glutaryl-CoA to mevalonate, catalyzed by *3-hydroxy-3-methyl glutaryl coenzyme-A reductase* (HMG-R). Later, the mevalonate is phosphorylated by *phosphomevalonate kinase* (PMK), followed by several steps of modification to form the isoprenoid biosynthetic units, isopentenyl diphosphate and dimethyl allyl diphosphate (Buhaescu and Izzedine, 2007). Condensation of two isoprenoid units catalyzed by *geranyl diphosphate synthase* (GPPS) synthesizes geranyl diphosphate, the precursor of bark beetle monoterpenoid pheromones, such as myrcene and ipsdienol (Gilg et al., 2005; Keeling et al., 2006; Bearfield et al., 2009; Ramakrishnan et al., 2022a). In *I. typographus*, a gene was recently reported that likely encodes an *isoprenyl-diphosphate synthase* (IPDS) responsible for converting dimethylallyl diphosphate into 2-methyl-3-buten-2-ol, a transformation unique in insects (Ramakrishnan et al., 2022a). Ipsdienol biosynthesis also involves the oxidation of myrcene catalyzed by the cytochrome P450 enzyme CyP450T1/T2 (Sandstrom et al., 2006).

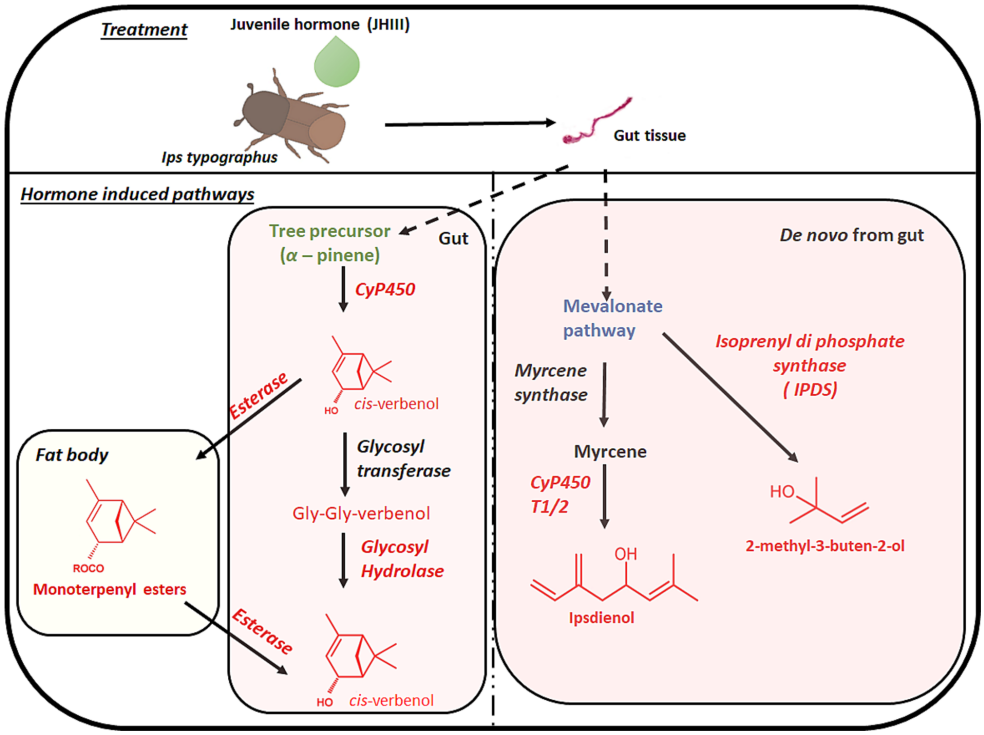

FIGURE 1
Proposed pheromone biosynthesis pathway with relative gene families from gut tissue and fat body of *Ips typographus* after topical application of JHIII. Red colour font highlights the pheromone compounds and relative gene families that are explained in this research article.

The third pheromonal component in *I. typographus*, *cis*-verbenol, is not synthesized *de novo* but is instead produced through the CyP450 catalyzed oxidation of (−)-α-pinene that adult beetles sequester from the tree (Renwick et al., 1976; Chiu et al., 2019). Additionally, a substantial amount of *cis*-verbenol has been detected in the gut of immature beetles that develop inside the bark, which is believed to be a result of detoxification of toxic α-pinene by these juvenile beetles (Ramakrishnan et al., 2022a). As part of this detoxification process, *cis*-verbenol (along with myrtenol as another detox product) is deposited in the form of monoterpenyl fatty acid esters in the fat body (Chiu et al., 2018; Ramakrishnan et al., 2022a). These conjugates can be hydrolyzed to provide free *cis*-verbenol in adult males when a supply of this pheromonal component is needed. In *I. typographus*, a candidate gene encoding a carboxylesterase (fatty acyl transferase) for the formation of verbenyl oleate (a fatty acid ester) in juvenile beetles was proposed and another carboxylesterase with ester bond cleaving function was suggested to be present in adult males (Ramakrishnan et al., 2022a,b). Another *cis*-verbenol conjugates, created through diglycosylation, has recently been discovered in the gut tissues of *I. typographus* (Ramakrishnan et al., 2022a). Detoxification via glycosylation is a common feature in insects (Hilliou et al., 2021), with UDP-*glycosyltransferases* being commonly studied as detoxification enzymes (Dai et al., 2021; Powell et al., 2021). In *I. typographus*, *cis*-verbenyl diglycosylate has been proposed as a potential parallel reservoir for the pheromone *cis*-verbenol released by adult males, a hypothesis that aligns with early hypotheses in *D. ponderosae* (Hughes, 1974; White et al., 1980). The effect of JH III on the formation of these detoxification conjugates or cleavage into pheromone-precursors has not been studied yet.

To learn more about the effect of JH III on bark beetle metabolism, we topically applied JH III to *I. typographus* and analyzed changes at the levels of gene transcripts, proteins, and metabolites in both sexes. The primary tissue studied was the gut, the site of pheromone biosynthesis and detoxification.

We hypothesize that JH III will induce correlated changes in genes, proteins and metabolites that reflect the requirements of adult beetles to aggregate and overcome the defense of their host trees by feeding on the phloem and reproduce. These changes are expected to occur in a sex-specific fashion. We also hypothesize that JH III will induce pheromone biosynthesis and the detoxification of spruce defense metabolites, especially those involved in the formation of aggregation pheromones.

By checking the above-mentioned hypothesis, genetic-level research of the bark beetle, *I. typographus* can lead to practical implications using RNA *interference* silencing of targeted genes and influence the pheromone metabolism. The RNAi technique for Coleopteran (wood-boring) insects has proven for highly susceptible and demonstrated recently on insects such as Emerald ash borer, Asian longhorn beetles, Chinese White pine beetle and Mountain pine beetle (Rodrigues et al., 2017; Dhandapani et al., 2020; Kyre et al., 2020).

2 Materials and methods

2.1 Beetle rearing

Spruce logs (*Picea abies*) naturally infested with *I. typographus* were collected from the Czech University of Life Sciences, Forest

Enterprise in Kostelec and Černými lesy, Czech Republic. The infested logs were stored in a cold chamber (4°C) until further use. The fresh spruce logs (approximately 50 cm) were infested with F0 generation beetles (150 beetles per log) and maintained under laboratory conditions (70% humidity, 24°C, 16:8 h day/night period, and ventilated plastic containers of 56 × 39 × 28 cm/45 L volume) for incubation to establish the F1 generation. After 4 weeks of incubation, F1-generation beetles were collected and sorted for male and female beetles. Subsequently, the beetles were treated with 0.5 µL of acetone (control) or 0.5 µL of a solution of 20 µg/µl JH III in acetone (10 µg of JH III) topically on the abdomen of the beetles. After application, the beetles were kept under laboratory conditions for 8 h. Beetles were frozen in liquid nitrogen and stored at −80°C until further use. Before analysis, the guts were dissected from stored frozen beetles for further downstream analysis. In this study, the beetle body refers to the tissue with fat remaining after removing the gut, elytra, and wings (Ramakrishnan et al., 2022a,b).

2.2 Metabolome

2.2.1 Gas chromatographic-mass spectrometry analysis

The frozen beetles were dissected to extract their guts, which were then placed in 2 mL analytical vials containing 100 µL of cold pentane (10 guts per vial). The beetle bodies were placed in separate vials containing 1 mL of chloroform (10 beetle bodies per vial). The extracts are obtained after overnight incubation at 4°C and tissue free solvents were separated using a short centrifuge (4,000 rpm,30s) and used for injection.

A Pegasus 4D GC × GC–MS system (LECO, St. Joseph, MI, USA) employing an Agilent 7,890 B and a consumable-free modulator was used to analyze the samples. One microliter of the extract was injected into a cold PTV injector (20C) in split mode at a ratio of 1:3. After injection, the inlet was heated to 275°C at a rate of 8°C/s. Separation was conducted on an HP-5MS UI capillary column (30 m, 0.25 mm i.d., 0.25 µm film thickness, Agilent) coupled to BPX-50 (1.2 m, 0.1 mm i.d., 0.1 µm film thickness, SGE). The GC oven temperature program was as follows: 40°C for 2 min; then ramped at a rate of 10°C min^{-1} to 200°C; then at 5°C min^{-1} to 320°C and held for 15 min. The second-dimension oven modulator had offsets of 5°C and 15°C, respectively. The modulation period was 5 s. The total GC runtime was 57 min. Ions (ionization energy of 70 eV) were collected in the mass range of 35–500 Da at a frequency of 100 Hz.

Automated spectral deconvolution and peak-finding algorithms were applied using ChromaTOF software (LECO, St. Joseph, MI, USA). For identification of the compounds, the mass spectra and retention indexes from the National Institute of Standards and Technology (NIST, 2017) mass spectral customized library were used. In the case of fatty acid ester (oleate) was identified using a targeted search using mass spectra and retention indexes obtained from synthetic standards (Chiu et al., 2018) measured under same conditions as in our previous studies (Ramakrishnan et al., 2022a). Relative abundances were defined as the percentage of the peak area of the targeted metabolite in relation to the sum of peak areas of all peaks in the chromatogram.

2.2.2 Ultra-high-performance liquid chromatography-electrospray ionization -high-resolution tandem mass spectrometry analysis

The polar fraction of guts was extracted by adding methanol, water, and acetic acid in a ratio of 70/30/0.5 (v/v) at a volume of 7 mL per gut. The mixture contained ^{13}C2-myristic acid (1 µg/mL) as an internal standard. The gut tissue was sonicated on ice for 5 min and disrupted using a pre-chilled Eppendorf tip. The samples were then centrifuged at 4000 RPM for 3 min, and the supernatant collected in a new vial with a 100 µL glass insert. The polar fractions of gut extracts were subjected to UHPLC-HRMS/MS analysis.

UHPLC-ESI-HRMS/MS was performed using an Ultimate 3,000 series RSLC system (Dionex) coupled to a Q-Exactive HF-X mass spectrometer (Thermo Fisher Scientific). Solvents A-water and B-acetonitrile (LiChrosolv hyper grade for LC–MS; Merck, Darmstadt, Germany), both with 0.1% v/v formic acid (eluent for LC–MS, Sigma Aldrich, Steinheim, Germany), were used for the binary solvent system. 10 µL of the extract was injected, and chromatographic separation was performed with a constant flow rate of 300 µL/min using an Acclaim C18 column (150 × 2.1 mm, 2.2 µm; Dionex, Borgenteich, Germany). Solvent gradients (B 0.5–100% v/v for 15 min; 100% B for 5 min; 100–0.5% v/v for 0.1 min; 0.5% for 5 min) were used. Ionization in the HESI ion source was achieved by 4.2 kV cone voltage, 35 V capillary voltage, and 300°C capillary temperature in the transfer tube in positive ion mode and 3.3 kV cone voltage, 35 V capillary voltage, and 320°C capillary temperature in negative mode. Mass spectra were recorded in both modes at a mass range of m/z 80–800 in duplicate. The obtained fragments with retention time values were interpreted using XCALIBUR software (Thermo Fisher Scientific, Waltham, United States; Ramakrishnan et al., 2022a,b). Metabolite samples were compared and statistically evaluated using MetaboAnalyst 4.0, and the determined masses were compared with the database (Chong et al., 2018). The amounts of three diglycosides of oxygenated monoterpenes (verbenol) were determined with mass spectra obtained from our previous work (Ramakrishnan et al., 2022b).

2.3 Transcriptome

2.3.1 Sample preparation

The beetle guts were dissected in RNAlater. Four biological replicate included three technical replicates each containing 10 pooled guts was used. Total RNA was extracted from male gut tissue samples using a pre-optimized protocol (Sellamuthu et al., 2022) and sent for sequencing with a NOVAseq6000 (PE150, 30 million raw reads) after quality determination using an agarose gel and a bioanalyzer. RNA (1 µg) was used for cDNA synthesis using the M-MLV reverse transcriptase kit following the manufacturer's protocol and stored at −80°C for downstream analysis.

2.3.2 Differential gene expression analysis

RNA-seq. Data were analyzed using CLC workbench 21.0.5 (QIAGEN Aarhus, Denmark) with a pre-optimized setting for mapping exon regions with genome reference (Naseer et al., 2023). Furthermore, sequence datasets and relative transcript expression levels were obtained using TPM values. Finally, an empirical DGE analysis was performed using the optimum parameters

(Ramakrishnan et al., 2022a). Genes with a false discovery rate (FDR)-corrected value of p cut-off of <0.05 and a fold change cut-off of ± four-fold as a threshold value for being significant. Differentially expressed genes were functionally searched in a cloud BLAST using the CLC Genomic Workbench. Gene Ontology term identification was performed using three categories (biological processes, molecular functions, and cellular components), and similar names were identified from the Kyoto Encyclopedia of Genes and Genomes pathway database (Kanehisa, 2002; Kanehisa et al., 2017).

2.3.3 Quantitative-real time PCR analysis

To validate the RNA seq. Data, genes were selected for qRT-PCR based on their varied expression levels. Primers were designed using IDT primer design software (Supplementary Table 4). A synthesized cDNA template was used for qRT-PCR validation using SYBR™ Green PCR master mix (Applied Biosystems, United States) under the following parameters: 95°C for 3 min, 40 cycles of 95°C for 3 s, and 60°C for 34 s. A melting curve was generated to ensure single-product amplification and eliminate the possibility of primer dimers and nonspecific amplicons. The relative expression levels of the target genes were calculated using the $2^{-\Delta\Delta Ct}$ method with two housekeeping genes (Sellamuthu et al., 2022) as a reference for normalization with four biological replications.

2.4 Proteome

2.4.1 Sample preparation

Frozen beetles were dissected under on dry ice, and four biological replicates of each treatment were used for protein extraction and analysis. Each biological replicate contained tissue of three individual guts. Protein extraction was lysed in cold buffer containing 50 mm Tris–HCl, pH 7.5, 1 mM EDTA, 150 mM NaCl, 1% N-octylglycoside, and 0.1% sodium deoxycholate. Gut tissue in the buffer with protease inhibitor mixture (Roche) was incubated for 15 min on ice. Lysates were cleared by centrifugation, and after precipitation with chloroform/methanol, proteins were resuspended in 6 m urea, 2 m thiourea, 10 mm HEPES, pH 8.0 and proceeded for digestion (Cox et al., 2014).

2.4.2 Protein digestion

The samples were homogenized and lysed by boiling at 95°C for 10 min in 100 mM TEAB (triethylammonium bicarbonate) containing 2% SDC (sodium deoxycholate), 40 mM chloroacetamide, and 10 mM Tris (2-carboxyethyl) phosphine, and further sonicated (Bandelin Sonoplus Mini 20, MS 1.5). The protein concentration was determined using a standard protein assay kit (Thermo Fisher Scientific). About 30 µg of protein per sample was used for MS sample preparation.

SP3 beads were used for sample processing. Five µl of SP3 beads were mixed with 30 µg protein in a lysis buffer and made up to 50 µL with TEAB (100 mM). Protein binding was induced by adding ethanol to a final concentration of 60% (vol/vol). The samples were thoroughly mixed and incubated at 24°C for 5 min. After SP3 was bound to the proteins, the tubes were placed on a magnetic rack, and the remaining unbound supernatant was discarded. Using 180 µL of 80% ethanol, beads were washed twice. After washing, samples were digested with trypsin (trypsin/protein ratio 1/30) and reconstituted in 100 mM TEAB at 37°C overnight. Digested samples were acidified with trifluoro acetic acid (TFA) to a final concentration of 1%. Finally, peptides were desalted using in-house stage tips packed with C18 disks (Empore; Rappsilber et al., 2007).

2.4.3 Nanoliquid chromatography-MS/MS analysis

nLC–MS/MS analysis was performed with nano-reversed-phase columns (EASY-Spray column, 50 cm × 75 µm ID, PepMap C18, 2 µm particles, 100 µm pore size). In this analysis, mobile phase buffer A (0.1% formic acid in water) and mobile phase buffer B (acetonitrile and 0.1% formic acid) were used. Samples were loaded in a trap column of C18 PepMap100, 5 µm particle size, 300 µm x 5 mm from Thermo Scientific. About 4 min at 18 µL/min loading buffer with water, 2% acetonitrile, and 0.1% trifluoroacetic acid were used for loading. Peptides were eluted with a mobile phase B gradient of 4–35% over 120 min. The eluted peptide cations were converted into gas-phase ions by electrospray ionization. A Thermo Orbitrap Fusion (Q-OT-qIT, Thermo Scientific) was used for the analysis. Survey scans of peptide precursors from 350 to 1,400 m/z were performed using an Orbitrap at 120 K resolution (200 m/z) with a 5×10^5 ion count target. Tandem MS was isolated at 1,5 Th using a quadrupole, HCD fragmentation with a normalized collision energy of 30, and rapid scan analysis in the ion trap. The second mass spectral ion count target was set to 10^4, and the maximum injection time was 35 ms. Precursors with charge state 2–6 were strictly sampled. The dynamic exclusion duration was set to 30 s with a 10 ppm tolerance around the selected precursor and its isotopes. Monoisotopic precursor selection was then performed. The instrument was run in top-speed mode with 2 s cycles (Hebert et al., 2014).

All data were analyzed and quantified using MaxQuant software (version 2.0.2.0; Cox and Mann, 2008). The FDR was limited to 1% for both full proteins and small peptides. The peptide lengths of the seven amino acids are specified. An MS/MS spectral search was performed using the Andromeda search engine against the *I. typographus* genome database. The C-termini of Arg and Lys were set for enzyme specificity, allowing the cleavage of proline bonds with a maximum of two missed cleavages. Cysteine dithiomethylation was selected as the fixed modification. Various modifications were considered with N-N-terminal protein acetylation and methionine oxidation. Matches between the run features from MaxQuant were used to transfer the identified peaks to other LC–MS/MS systems. Runs based on masses and retention times (with a maximum deviation of 0.7 min) were also considered for quantification. A label-free MaxQuant algorithm was used for quantification (Cox et al., 2014). Data analysis was performed using Perseus 1.6.15.0 (Tyanova et al., 2016).

2.5 Statistics

LC–MS data analysis was performed using MetaboAnalyst 4.0. GCxGC-TOF-MS data were cleaned for residua of analysis, normalized (constant raw sum), and evaluated using principal component analysis (PCA) in the SIMCA 17 software (Sartorius Stedim Data Analytics AB, Malmô, Sweden). T-test with 95% confidence interval was used to compare the abundance of control and treatment groups in TIBCO Statistics (United States, 2021). The data from transcriptome and proteome was normalized using CLC workbench 21.0.5 (QIAGEN Aarhus, Denmark) and MaxQuant software (version 2.0.2.0) respectively, and significant data ($p < 0.05$) were extracted for further

analysis. qRT-data was analyzed with one-way ANOVA, Fisher LSD test in TIBCO Statistics (United States, 2021).

3 Results

3.1 Total gene enrichment analysis from guts of males and females after JH III topical treatment

The functional aspects of JH III influenced gene families from adult males and females were gained by a gene enrichment analysis. The data gained from differential gene expression (DGE) with significance (FDR-corrected value of p <0.05).

In males, the analysis revealed that a significant number of enriched genes were involved in metabolic processes. Additionally, functions such as catalytic activity, ester hydrolase, phosphatase activity, transporter and glycosyltransferase activities were also determined to be over-represented after JH III treatment by enrichment analysis. Gene functions related to lyase activity, small-molecule metabolic processes, carbohydrate metabolic processes, and lipid biosynthesis were also over-represented. Most importantly, we found that gene groups involved in pheromone biosynthesis functions, including isoprenoid biosynthesis, metabolic processes, and dephosphorylation were enriched. Gene functions related to oxidoreductase and alkaline phosphatase activity had the least coverage in terms of gene sequences (Figure 2A).

In female gut tissue, the GEA showed enrichment of membrane-related and membrane transporter activity-related genes rather than metabolic synthesis genes as in males. Several gene groups with functions related to detoxification, such as carboxylic acid transmembrane transporter, organic acid membrane transporter, amino acid transporter, alkaline phosphate activity, phosphatase activity, and protein dephosphorylation were identified as enriched. Genes responsible for oxidoreductase and catalytic activities, phosphoric ester hydrolase activity, phosphatase, and lipid metabolism process had higher sequence coverage in females than males. Furthermore, metal ion binding genes such as zinc ion binding and, carbohydrate metabolic process gene families were identified exclusively in female gut tissue. The gene groups for lyase activity and hydrolase activity were enriched in females as in males and many unknown genes were clustered under the "others" category "(Figure 2B). Taken together,

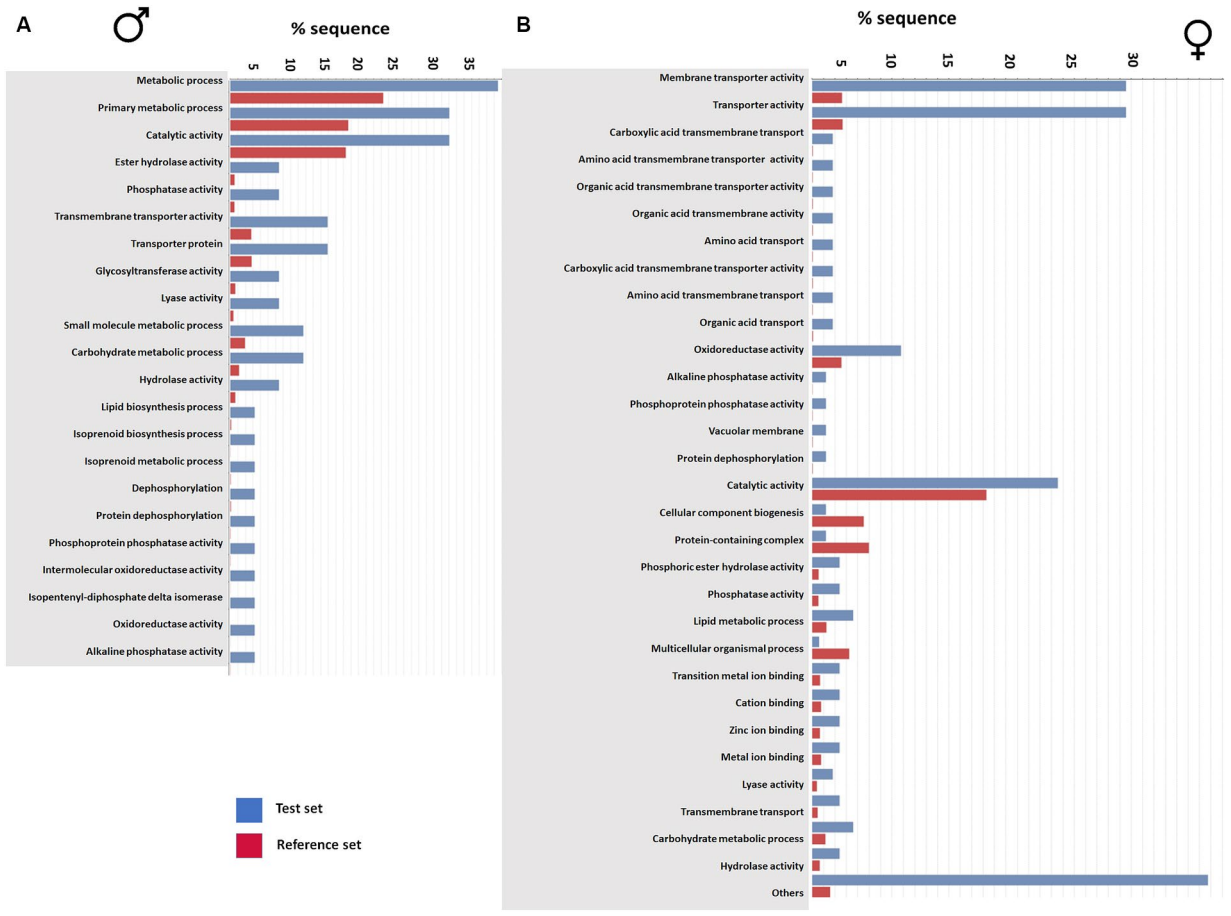

FIGURE 2
Gene enrichment analysis of transcripts from male gut tissue **(A)** and female gut tissue **(B)** after JHIII treatment. The data set were given as a test set (blue) to reference set (red) gene families known from reference websites as Gene Ontology. The possible functions of the genes were listed against the percentage of sequence coverage.

the gene enrichment analysis provided valuable insights into the over-representation of genes in males and females after JH III treatment.

3.2 Total protein enrichment analysis from guts of males and females after JH III topical treatment

The list of detected proteins was organized based on functional relevance. In the male gut tissue after JH III treatment, the identified proteins clustered into 456 known functions, while in the treated female gut formed 489 functional groups. Of these, 347 groups were common to both male-treated and female-treated gut samples. Similar to gene enrichment analysis, both sexes exhibited the highest numbers of plasma membrane-associated proteins (Supplementary Table 5).

The functional groups identified in male and female guts after JH III treatment were largely similar. Proteins related to the nucleus and nucleolus, ATP and RNA binding proteins were enriched in both sexes. However, in males, the number of proteins with functions related to metal ion binding and transferase activity was higher compared to females (Figure 3A). Whereas, in the female gut, the reproduction-related embryo development proteins were higher protein numbers (Figure 3B; Supplementary Table 5). Nevertheless, the differences between male and female guts after JH III treatment were minor in terms of gene transcripts and protein enrichments.

3.3 Metabolome

3.3.1 GC–MS analysis of extracts from guts and bodies of males and females after JH III topical treatment

Extracts of the guts and bodies of male and female *I. typographus* beetles subjected to JHIII treatment, were compared to their respective control groups, using comprehensive two-dimensional gas chromatography.

The initial Principal Component Analysis (PCA) revealed a distinct separation of JH III treated male gut samples from control samples treated with acetone. The first two components of the PCA plot accounted for 46.5% of the variance in the data (see Figure 4A). The primary compound responsible for this separation was identified as the main *I. typographus* aggregation pheromone component, 2-methyl-3-buten-2-ol. Additionally, compounds such as *cis*-verbenol and phenylethanol (male-specific compound) also contributed to this separation. In contrast, control male guts contained only phenylethanol and trace amounts of *cis*-verbenol, along with traces of other compounds such as verbenone, ipsdienol, and myrtenol (refer to Supplementary Figure 1).

The relative abundance of the pheromone precursor verbenyl oleate was determined in extracts from both the guts and the bodies (including the fat body) of beetles following JH III treatment and compared to a control (see Figure 4B). In both male and female beetle body extracts, JH III topical treatment led to a significant increase (1.5x in males, 15x in females) in the levels of verbenyl oleate compared to the control group.

This trend was also observed in extracts from female guts (15x increase). However, in the gut extracts of male beetles, JH III treatment resulted in a significant decrease (1.8x decrease) in the relative abundance of verbenyl oleate compared to the control group. This decrease is likely attributable cleavage of these monoterpene conjugates to give the free pheromone *cis*-verbenol (refer to Figure 4B). The absolute amount of verbenyl oleate in different beetle life stadia was 250 ng/mg of beetle body weight, as previously quantified (Ramakrishnan et al., 2022a) The content of free *cis*-verbenol in the guts of freshly emerged beetle was 5 ng/gut, which can be compared with control beetles in this study.

3.3.2 UHPLC-ESI-HRMS/MS analysis of guts extracts of males and females JH III topical treatment

Metabolic profiling of non-volatile and polar compounds in the gut tissues of JH III-treated males and females was conducted using a

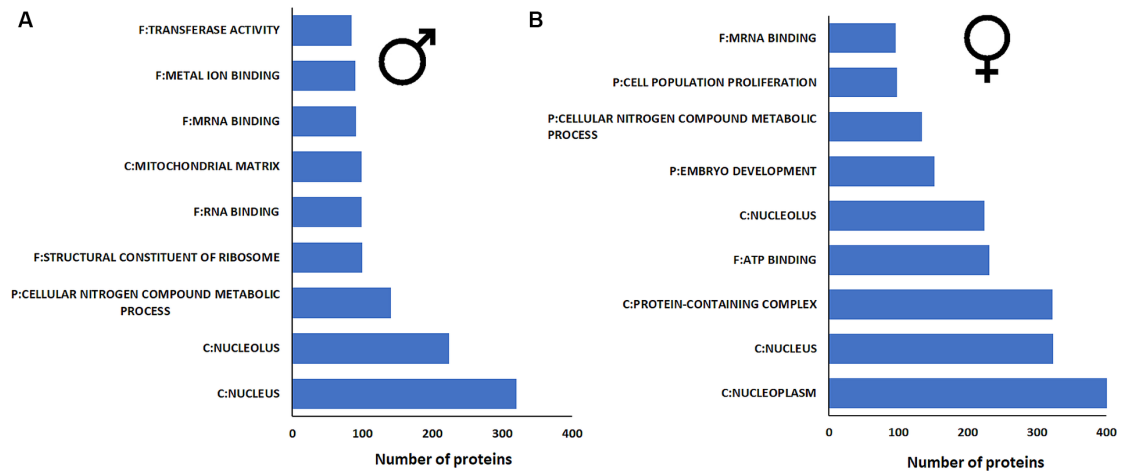

FIGURE 3
Protein enrichment analysis of proteins from **(A)** male gut tissue and **(B)** female gut tissue after JHIII treatment. The possible protein functions with significance $p < 0.05$ and functions containing more than 100 protein numbers are listed in this figure. A list of remaining functions with lower protein numbers are given in supplementary table 5.

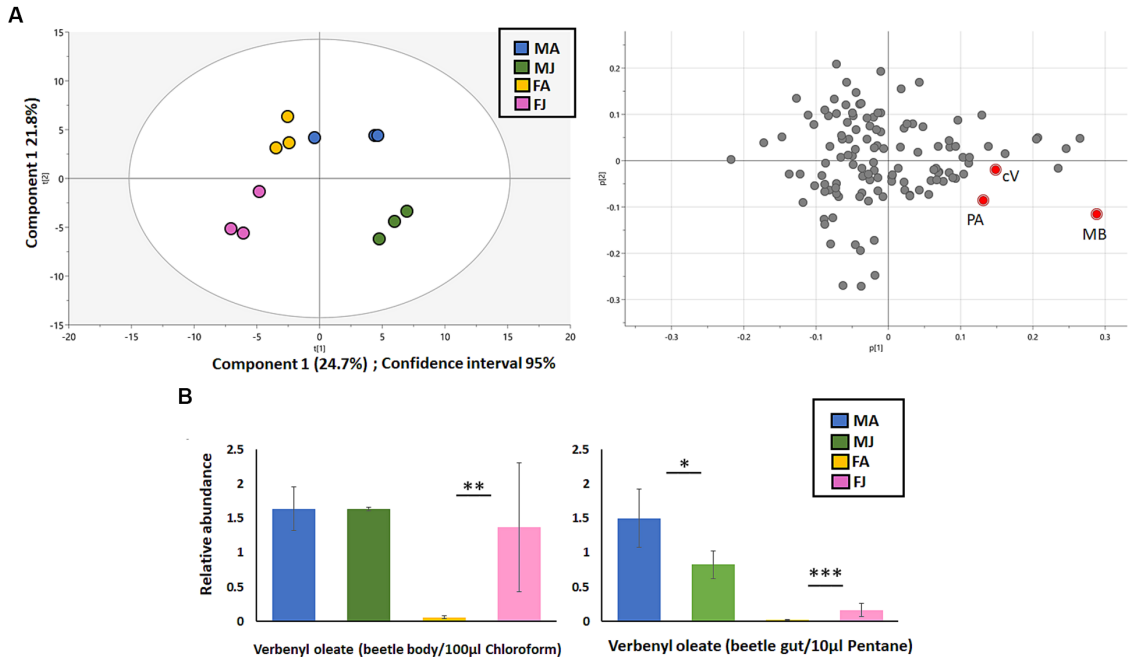

FIGURE 4
(A) Principal component analysis (PCA)of compounds identified by GCxGC-MS from *I. typographus* gut samples after JHIII induction in both sexes. The key component responsible for separation are highlighted in red color- PA- Phenylethyl alcohol, MB- 2-methyl-3-buten-2-ol, cV-*cis*-verbenol. **(B)** Relative abundance of Verbenyl ester in *I. typographus* beetle body (left) and gut tissue (right) after JHIII induction compared to the control. MA, Males topically treated with acetone – control; MJ, Males topically treated with JHIII – treatment, FA, Females topically treated with acetone – control, FJ, Females topically treated with JHIII – treatment. Statistics: T test with paired independent parameters. *** represents $p < 0.001$, ** represents $p < 0.01$, * represents $p < 0.05$. $N = 3$.

non-targeted analysis via UHPLC/HRMS in both positive and negative ion modes. An unsupervised multivariate PCA was employed to assess differences among the sample groups.

In both ion modes measurements, JH III-treated males and females clustered distinct from the control group. In the negative ion mode, the PC analysis explained 55 and 61.2% of the total variance in males and females, respectively, (see Figure 5A, left). In the positive ion mode, the PC explained 60 and 50% of the total variance in males and females, respectively, (see Figure 5A, right). The determination of the total abundance of verbenyl diglycosides was calculated as the sum of the peak areas from the three individual verbenyl diglycoside peaks. After treatment with JH III in beetles, the total abundance of diglycosides content significantly increased in the guts of both sexes compared to the acetone-treated controls. There was no significant difference in the induction of these compounds by JH III between males and females (see Figure 5B). The actual amount of these compounds per beetle gut could not be determined due to the lack of standards.

3.4 Regulation of genes and proteins after JH III treatment in transcriptome and proteome of adult males and female beetles

3.4.1 Transcriptome-differential gene expression analysis

Overall, DGE analysis using the CLC workbench from the RNA sequence data obtained from beetle guts provided a clear distinction between gene sets in JH III-treated versus control beetles and males versus females, with samples from each group clustered together in principal component analysis (Supplementary Figure 2A). After JH III treatment, approximately 710 transcripts were upregulated, and 545 were downregulated in male gut tissue only, as depicted in a Venn diagram (Figure 6A). On the other hand, in female gut tissue only a total of 518 transcripts were upregulated, and 456 transcripts were downregulated. However, approximately 5,155 transcripts were upregulated, and 4,595 transcripts were downregulated in both male and female gut tissues. Notably, the total number of genes upregulated after treatment in the male beetle gut was higher (10,385 transcripts) than that in the female beetles (9,682 transcripts; Figure 6A; Supplementary Table 1).

3.4.2 Proteome-differential protein expression analysis

The results of the DPE analysis of JH III-treated beetle gut tissue yielded a comprehensive list of identified proteins exhibiting a significant fold change in their expression following treatment. Samples from each treatment (JH III vs. control) were clustered in principal component analysis (Supplementary Figure 2B). It is noteworthy that although JH III treatment is conventionally associated with pheromone production in adult male beetles, the female beetle gut tissue exhibited a higher number of identified proteins after treatment, 449 versus 229 in males. Among the total number of upregulated proteins, 79 were male-specific, 302 were female specific and 145 were detected in both male and female guts. Among the total number of downregulated proteins, 68 proteins male specific, 69 were

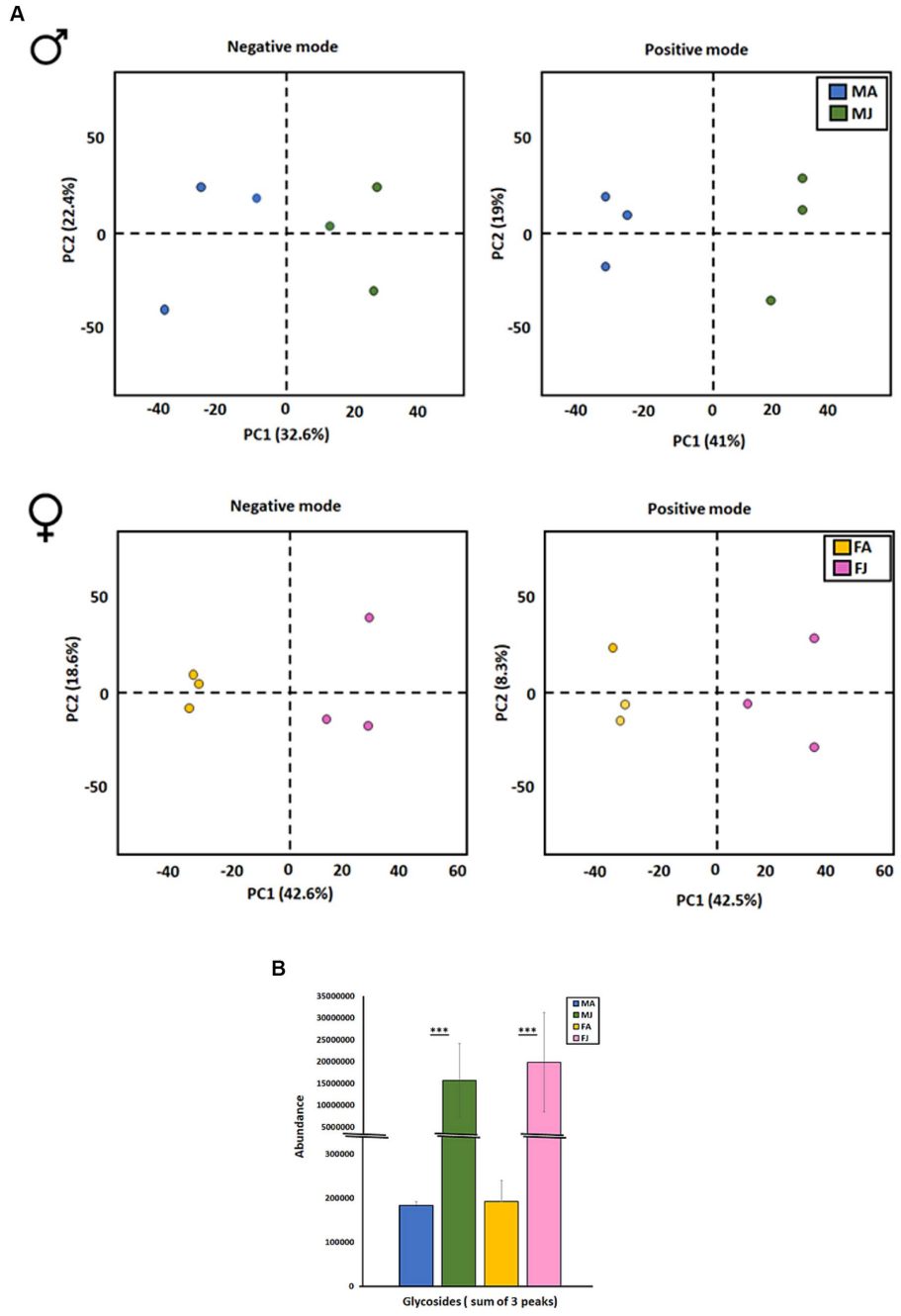

FIGURE 5
(A) Principal component analysis (PCA) of compounds identified by UHPLC-ESI-HRMS/MS analysis measured in negative (left) and positive mode (right). The data shows the overall separation of *I. typographus* gut samples after JHIII treatment in male (up) and female (down). **(B)** Abundance of Verbenyl di glycosides in *I. typographus* gut tissue after JHIII induction. MA, Males topically treated with acetone – control; MJ, Males topically treated with JHIII – treatment, FA, Females topically treated with acetone – control, FJ, Females topically treated with JHIII – treatment. T test with paired independent parameters. *** represents $p < 0.001$.

female specific and 27 were detected in both male and female guts (Figure 6B; Supplementary Table 2).

3.4.3 Comparison of transcriptome and proteome

To narrow down the upregulated genes from male gut tissue with possible functional significance, we compared the contig lists from the DGE and DPE analyses (Figure 6C). Although the number of identified proteins was 100-fold lower than the number of transcripts from the DGE analysis, the results of the comparison helped identify a unique set of gene contigs for further evaluation. The male gut tissue had 129 contigs from transcript and protein analysis, names are provided in Supplementary Table 3A. The key mevalonate pathway gene Ityp09271, isoprenyl-diphosphate synthase (IPDS) gene (functionally proposed for 2-methyl-3-buten-2-ol synthesis), was among the highly upregulated gene contigs. Other mevalonate pathway genes such as Ityp06045 phosphomevalonate kinase (PMK), Ityp09137,

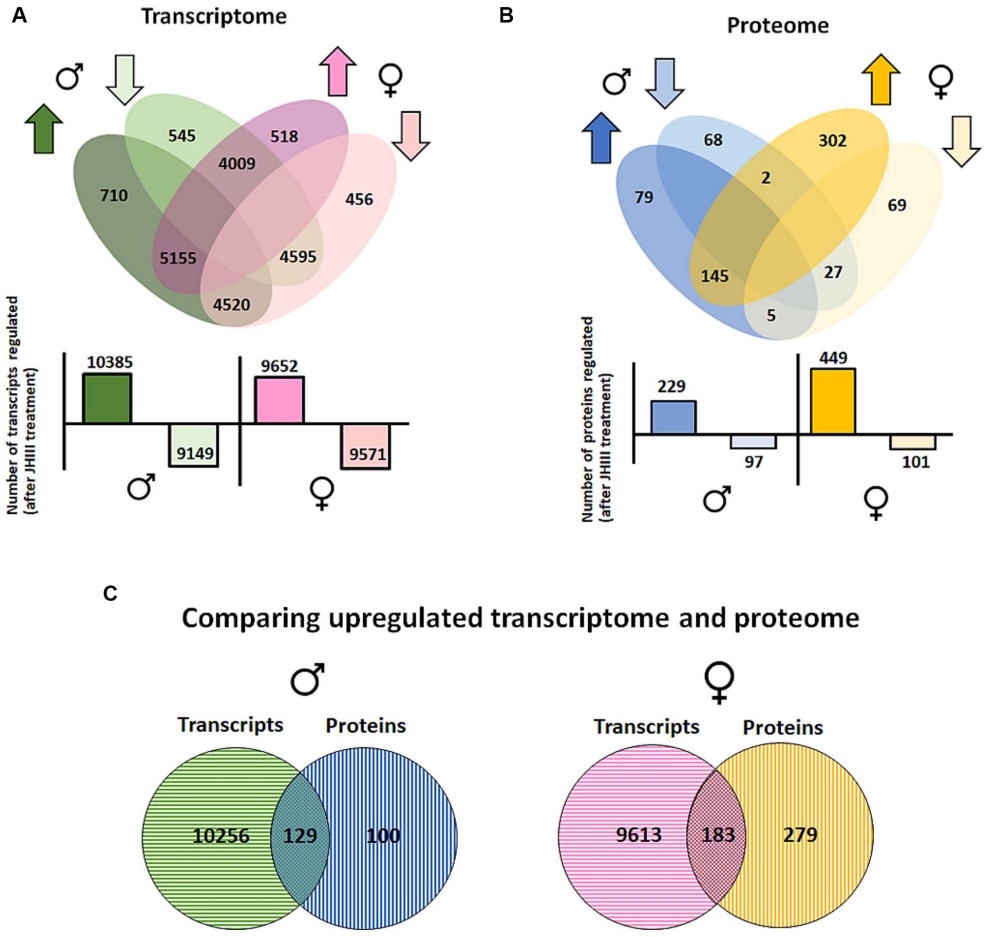

FIGURE 6
(A) Transcriptome and **(B)** proteome. Regulated in *I. typographus* male and female gut tissue after JHIII treatment. Up arrow - upregulation and down arrow - down-regulation. Green and blue represents male gut tissue. Pink and yellow color represents female gut tissue. The graph below Venn diagram represents the total number of gene transcripts and proteins regulated in both sexes after treatment. **(C)** comparison of upregulated gene transcripts and proteins from males (left) and females (right) after treatment. Jvenn platform was used for the comparison analysis.

3-hydroxy-3methyl glutaryl Co-A synthase (HMG-S), and Ityp04875, isopentenyl-di-phosphate isomerase (IPPI) were also upregulated at the gene transcript level. A similar pattern was seen for the contigs involved in hydrolase function (listed in the table as myrosinase), which are known to have a functional role for glycosyl hydrolase activity, acting on glycosyl bonds (GO:0016798), and transferase contigs, such as acetyltransferase and UDP-glucuronosyltransferase (highlighted in Supplementary Table 3A). Many ribosomal and membrane transporter contigs, such as V-type ATPases, were also upregulated, while several genes that have an unknown function were identified among the male-specific upregulated gene contigs (Supplementary Table 3A).

The female gut tissue had approximately 183 contigs from transcripts and protein analysis (Figure 6C; Supplementary Table 3B). Although the number identified in females was higher than that in males, mevalonate pathway genes were not predominant in the list of identified contigs in females. However, another geranyl-diphosphate synthase (Ityp17861) was upregulated. Furthermore, gene families, such as glycine dehydrogenase, ubiquitin carboxyl-terminal hydrolase, and vitellogenin-like, with functions likely in detoxification and oocyte formation, were found to be upregulated (Supplementary Table 3B). Similar to males, many genes related to mitochondria-related ribosomal proteins, elongation factors, binding proteins, and many functionally unknown genes and proteins were also found to be upregulated (Supplementary Table 3B).

3.4.4 Regulation of the mevalonate pathway after JH III treatment (involved in *de novo* pheromone biosynthesis)

Combining gene and protein expression with qRT-PCR allowed a more comprehensive overview of the effect of JHIII treatment and sex on the steps of the mevalonate pathway, which makes the *I. typographus* aggregation pheromones and pheromone precursors *de novo*. Information was obtained for the upregulation of the following genes by RNA-Seq and qRT-PCR: PMK (Ityp06045), HMG-S (Ityp09137), HMG-R (Ityp17150), IPPI (Ityp04875), and IPDS (Ityp09271; Figure 7A). Not all of these steps were identified at the protein level, but analysis revealed the upregulation of HMG-S, IPPI, and IPDS. Notably, we found that the IPDS gene was upregulated by up to 35-fold in male gut tissue compared with that in female gut tissue after JH III treatment (Figure 7B). Besides the IPDS gene,

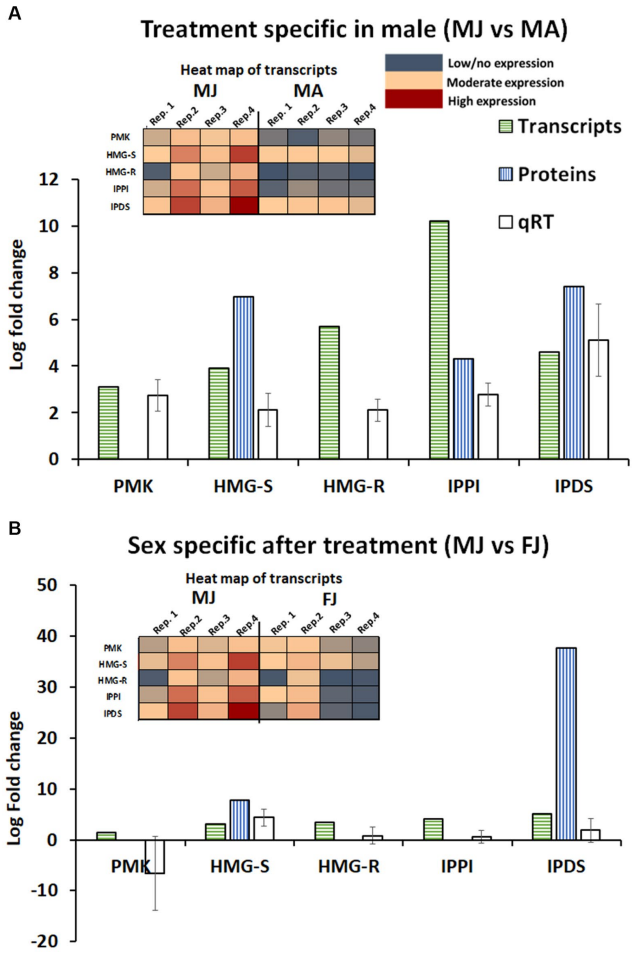

FIGURE 7
Mevalonate pathway key gene contigs expression pattern in transcriptome and proteome and qRT-PCR analysis of male gut tissue. **(A)** Treatment specific in male (JHIII vs. acetone). **(B)** Sex-specific after treatment (male vs. female). Phosphomevalonate kinase (PMK), 3-hydroxy-3-methyl glutaryl coenzyme-A synthase (HMG-S), 3-hydroxy-3-methyl glutaryl coenzyme-A reductase (HMG-R), isopentyl-di-phosphate isomerase (IPPI), and isoprenyl-di-phospate synthase (IPDS). MA, Males topically treated with acetone – control; MJ, Males topically treated with JHIII – treatment, FA, Females topically treated with acetone – control, FJ, Females topically treated with JHIII – treatment. $N = 4$. The error bar indicates standard error. The expression patterns of the gene transcripts are given in a heat map along with log fold change graph.

HMG-S was also significantly upregulated in JH III treated male gut tissue compared with that in treated females (Figure 7B). Additionally, we also found that IPPI was exclusively abundant in proteins from female gut tissue after treatment (Supplementary Figure 3).

3.4.5 Regulation of the cytochromeP450 (CyP450) gene family after JH III treatment (involved in pheromone biosynthesis and pheromone formation from host tree precursors)

A similar combined approach was taken to explore the regulation of CyP450 genes that are involved in pheromone biosynthesis by RNA-Seq and qRT-PCR; no proteins of this family were detected in our proteomic investigation. CyP450 contigs showing expression patterns above a 2-fold change with a significant value of p ($p < 0.05$) were confirmed by qRT-PCR analysis. Among the contigs previously proposed to be involved in pheromone biosynthesis (Ramakrishnan et al., 2022a), contigs Ityp3903 and Ityp0496 (proposed for verbenol synthesis), contigs Ityp3140 (proposed for detoxification), and Ityp3153 (proposed for ipsdienol) were all found to be upregulated genes in the JH III-treated male gut and are among the most highly upregulated genes measured in this study (Figure 8).

3.4.6 Regulation of esterase gene family after JH III treatment (involved in formation and cleavage of verbenyl fatty acid ester conjugates-possible pheromone precursors)

Among the esterase genes proposed for converting the stored verbenyl ester to *cis*-verbenol, Ityp11977 (which occurred in the early life stage) was not significantly influenced by JH III treatment in males according to transcriptome and proteome analysis. However, another esterase contig, Ityp09460, was found to be upregulated in the protein analysis and qRT-PCR but downregulated in the RNA-Seq. transcriptome (Figure 9A). In female gut tissue, none of these contigs were detected, except for Ityp11977 in qRT-PCR (Figure 9B).

3.4.7 Regulation of Glycosyl hydrolase gene family after JH III treatment (involved in formation and cleavage of verbenyl diglycoside conjugates possible pheromone precursor)

When comparing DGE and DPE analyses in male gut tissue, a set of gene families known for glycosyl-hydrolase function (GO:0016798) was significantly upregulated after JHIII treatment at both the transcript and protein levels with male specificity. This gene family nearly as abundant as the genes of the mevalonate pathway, may cleave stored verbenyl glucoside conjugates to give the free pheromone. Twelve gene contigs were detected from the family, four of which were also detected and significantly upregulated at the protein level, Ityp11770, Ityp00535, Ityp00943, and Ityp04256. These were also upregulated by qRT-PCR except for contig Ityp11770 (Figure 10A). All three contigs were more upregulated in males than in females (Figure 10B); for females, DGE, DPE, and qRT-PCR did not show consistent upregulation after JHIII treatment (Figure 10B; Supplementary Figure 4).

4 Discussion

4.1 Changes in gene expression, proteins, and metabolites after JHIII application to *I. Typographus*, highlighting overall metabolic regulation

The topical application of JH III to adult beetles has been studied in many bark beetle species (Keeling et al., 2016; Tian et al., 2020). In *I. typographus*, we have identified numerous metabolic pathways affected by this hormone by changes in their genes, proteins, and metabolites. JH III treatment has been demonstrated to induce pheromone biosynthesis in male *I. typographus* exclusively and the formation of monoterpene detoxification conjugates in both sexes. These findings correlate with the earlier reported impact of JH III on other bark beetles such as *D. ponderosa* (Chiu et al., 2018).

JH III treatment led to the notable upregulation of metabolic processes and relevant membrane transporters, consistent with observations on other Ips species (Keeling et al., 2006). In addition, there were strong differences in gene expression patterns between males and females of *I. typographus* encompassing functions such as catalytic activity, oxidoreductase activity, esterases, and phosphatases.

In male beetles, the treatment primarily influenced metabolic regulation, whereas, in females, it led to the induction of numerous reproduction-related genes such as vitellogenins (involved in oocyte biosynthesis). This observation can fit the well-documented influence of JH III on parenting behaviors in social insects (Trumbo, 2018). In addition to many membrane transporter activity genes in female guts, genes regulating detoxification processes, such as carboxylases and ubiquitin-carboxyl hydrolases were upregulated (Supplementary Table 3B).

A complementary protein enrichment analysis in this study also found sex-specific differences after JH III treatment. The male gut was enriched with proteins involved in metabolic processes and transferase activity-related proteins. These steps are key in the pheromone biosynthesis of *I. typographus* pioneer males. In the female gut after treatment, the embryo development-related proteins were among those upregulated (over 100 protein candidates), which correlated with the finding of vitellogenin upregulation at the gene level. Both sexes demonstrated upregulation of proteins involved in nuclear and detoxification processes. Unexpectedly, detoxification products of the host tree monoterpene-pinene, verbenyl fatty acid esters, were induced in the guts of both sexes by JHIII. This finding supports the recently proposed hypothesis that detoxification conjugates are produced in both sexes of bark beetles and later diverted to pheromone biosynthesis to the greatest extent in the pioneer sex in host finding-the males in *I. typographus* (Chiu et al., 2018; Ramakrishnan et al., 2022a). Nevertheless, the pathways involved in detoxification and pheromone biosynthesis need more study to understand the linkages between them.

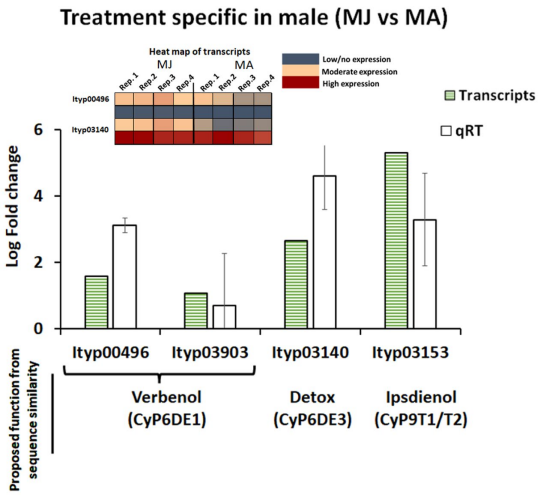

FIGURE 8
Cytochrome P450 gene contigs expression pattern in transcriptome and qRT-PCR expression analysis from *I. typographus* male gut tissue after JHIII treatment. The error bar indicates standard error. MA, Males topically treated with acetone – control; MJ, Males topically treated with JHIII – treatment. *N* = 4. The expression pattern of the transcripts is given in a heat map along with log fold change graph.

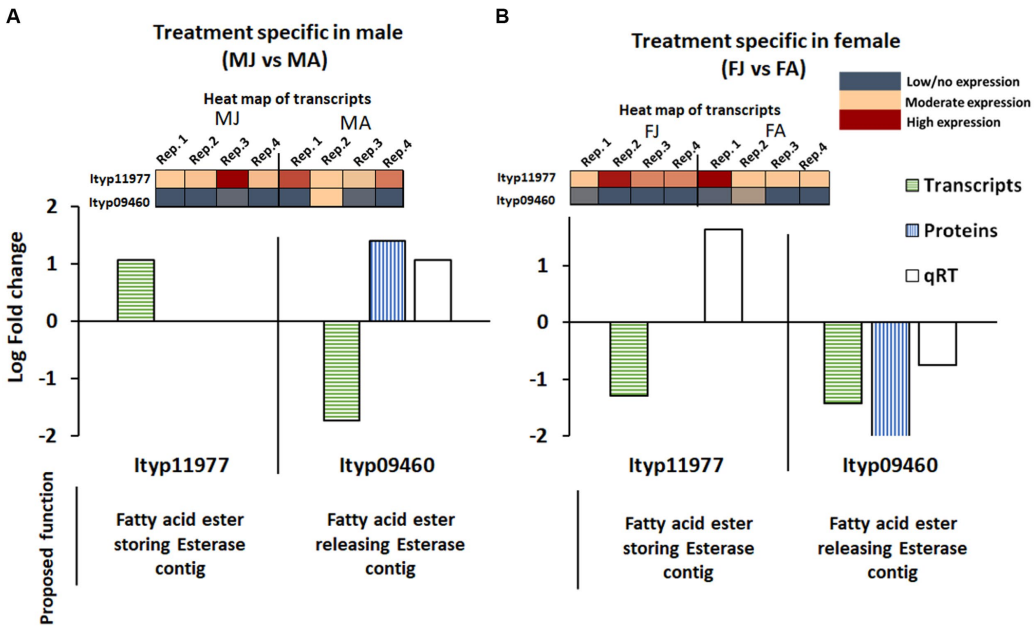

FIGURE 9
Esterase gene contigs expression pattern in the transcriptome, proteome, and qRT-PCR analysis from *I. typographus* male **(A)** and female **(B)** gut tissue after JHIII treatment. MA, Males topically treated with acetone – control; MJ, Males topically treated with JHIII – treatment, FA, Females topically treated with acetone – control, FJ, Females topically treated with JHIII – treatment. *N* = 4. The expression patterns of the gene transcripts are given in a heat map along with fold change graph.

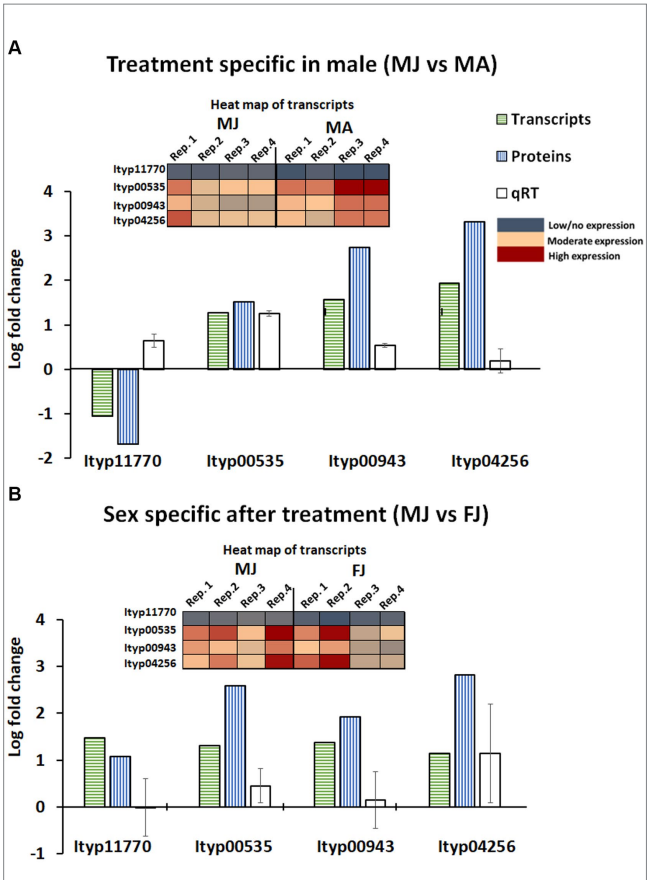

FIGURE 10
Glycosyl hydrolase gene contigs expression pattern in transcripts, proteins, and qRT-PCR analysis. MA, Males topically treated with acetone – control; MJ, Males topically treated with JHIII – treatment, FA, Females topically treated with acetone – control, FJ, Females topically treated with JHIII – treatment. *N* = 4. The error bar indicates standard error. The expression patterns of the gene transcripts are given in a heat map along with log fold change graph.

4.2 Identification of key genes responsible for pheromone biosynthesis

Two of the major male aggregation pheromone components of *I. typographus* are isoprenoids produced *de novo* by the mevalonate pathway were identified (Figure 7). The genes for this pathway have been annotated in the *I. typographus* genome (Powell et al., 2021; Naseer et al., 2023), and many of them are shown here to be upregulated exclusively in males. After JH III treatment, these genes have also been implicated in pheromone formation in other *Ips* species (Keeling et al., 2004).

In male *I. typographus*, topical treatment with JH III led to the overexpression of certain, upstream genes of the mevalonate pathway, including PMK (Ityp06045), HMG-S (Ityp09137), HMG-R (Ityp17150), and IPPI (Ityp04875). were relatively overexpressed in the gut. In addition, the upregulation of IPDS (Ityp09271) was observed at both the transcript and protein levels. This gene is a candidate for encoding the biosynthesis of the hemiterpene 2-methyl-3-buten-2-ol, which has not yet been functionally demonstrated. The upregulation of Ityp09271 aligns with the significant increase in 2-methyl-3-buten-2-ol content observed in the male gut after the treatment and corresponds with the biosynthetic pathway proposed in our previous study (Ramakrishnan et al., 2022a). In females, there was also reported upregulation of another IPDS, an ortholog of geranyl diphosphate synthase (Ityp17861; Ivarsson et al., 1993).

In addition to the observed increase in the levels of 2-methyl-3-buten-2-ol induced by JH III, two other pheromone components were also upregulated: ipsdienol (presumably produced *de novo*) and *cis*-verbenol (likely synthesized from α-pinene) and sequestered as a fatty acid ester (Ramakrishnan et al., 2022a). GC–MS measurements of gut tissue following the induction further revealed a significant increase in *I. typographus* male-specific compounds, such as myrtenol and phenyl ethanol (Supplementary Figure 1). Although behavioral activity for these compounds has not been reported in *I. typographus*, they also produced by the pheromone-producing sex of related bark species, *D. ponderosae* and *I. pini*, where their upregulation after the treatment has also been documented (Keeling et al., 2006, 2016). This suggests that the effect of JH III on pheromone biosynthesis is not limited solely to known behaviorally active compounds.

The effect of JH III- treatment on CyP450 enzymes was also studied, but this was only feasible at the gene transcript level as CyP450 proteins could not be identified in our proteomics work. In the transcriptome analysis, we searched for gene candidates with sequence similarities to functionally known genes from other bark beetle studies, including those involved in *cis*-verbenol biosynthesis (Chiu et al., 2019; Ramakrishnan et al., 2022a), detoxification mechanisms (CyP6DE3), and ipsdienol biosynthesis (CyP9T1/T2; Song et al., 2013; Nadeau et al., 2017).

Interestingly, CyP450s genes in all three functional classes were upregulated after JH III treatment with CyP6DE1, known in another bark beetle species for its role in *trans*-verbenol biosynthesis (Chiu et al., 2019). The contigs from *I. typographus* male gut exhibited lower expression levels compared to the gene contigs suggested for detoxification (CyP6DE3) and ipsdienol biosynthesis (CyP9T1/T2; Sandstrom et al., 2006). The effect of topically applied JH III on pheromone biosynthesis appears to be broader than just the induction of *de novo* synthesized compounds. In addition to regulating isoprenoid biosynthesis, this hormone affects the production of pheromonal components by influencing a variety of other biosynthetic mechanisms such as the hydroxylation of host tree monoterpenes.

4.3 Effects of JH III on the formation and cleavage of detoxification conjugates related to pheromonal components

In this study, topically applied JH III also influenced the production of verbenyl-fatty acid ester and verbenyl-diglycosides, which are conjugates of the pheromone *cis*-verbenol. Since *cis*-verbenol may also be regarded as a detoxification product of α-pinene, its esters, and glycosides may help to alleviate toxicity by stabilizing the initial detoxification product. However, our main objective was to test the hypothesis that these esters and glycosides are precursors of *cis*-verbenol in adult males when they need to release large quantities of these pheromones during the attack on the host tree.

Furthermore, the compound, verbenyl-oleate production after JH III treatment has significantly induced in the fat bodies of both sexes of adult beetles. The induction rate was 10 times higher in females than in males. We previously established from the production curve of this compound at different life stages (Ramakrishnan et al., 2022a) that verbenyl oleate

abundance is male-specific during adult beetle stages. However, in this study, we report that treatment can also induce its production in female adult beetles. This finding suggests a strong regulatory role for JH III in the formation of these compounds in the beetle.

The content of verbenyl oleate in the gut is 100 times lower than in the fat body of *I. typographus* (Ramakrishnan et al., 2022a). Despite the gut being the site for biosynthesis of this compound during the juvenile stages and later in adult males free *cis*-verbenol release occurs. Also, JH III induced an increase in verbenyl oleate abundance in female guts similar to that in the fat body and reduced its content in male guts. These findings support the existing hypothesis that the cleavage of verbenyl fatty acyl esters is specific to adult males and that verbenyl esters serve as precursors for the active pheromonal *cis*-verbenol in pioneer male *I. typographus* (Ramakrishnan et al., 2022a). Both the formation and cleavage steps of verbenyl fatty acid esters are regulated by JH III, indicating that the responsible enzymes (esterase, also known as carboxylesterases or fatty acid transferases) are likely regulated at the gene or protein level.

The esterase contig Ityp11977, which was previously reported in earlier life stages of *I. typographus* for verbenyl fatty acyl ester formation (Ramakrishnan et al., 2022a), was also identified in the guts of beetles after treatment. This observation aligns with the finding that the candidate Ityp11977 was exclusively expressed (as shown in qRT-PCR analysis) in the female gut after treatment (see Figure 9). We also identified another contig from esterase - Ityp09460, expressed in the male gut following the treatment, coinciding with a reduction in verbenyl ester levels. This observation leads us to propose the involvement of this esterase candidate in the release of *cis*-verbenol through the cleavage of ester bonds in the male gut, a novel finding in *I. typographus*. It is worth noting that this esterase is known for several detoxification functions in other insects (Blomquist et al., 2021).

In our previous study, other *cis*-verbenyl conjugates in the guts of beetles were identified as three verbenyl-diglycosides differing structurally by glycosidic parts (Ramakrishnan et al., 2022a,b). Glycosylated alcohols are known to serve as detoxification products, and they may have relevance to bark beetle pheromone biosynthesis in other species (Blomquist et al., 2021). In this study, we observed a significant 100-fold increase in the content of these compounds in the guts following the treatment, and this induction showed similar rates in both sexes of adult beetles. This demonstrates the JH III regulation over the formation of these compounds.

Furthermore, to test the hypothesis that these compounds could serve as alternative pheromonal *cis*-verbenol precursors, we searched and identified for possible genes within specific glycosyl hydrolase gene families. Later, the gene for potential male-specific release to free *cis*-verbenol. Notably, we identified four contigs from the glycosyl hydrolase gene family that were overexpressed exclusively in the male gut after treatment. However, the uncertainty in the abundance of male-specific verbenyl diglycosides (not similar to verbenyl ester), together with low quantity in the gut and absence in the fat body (unpublished data) we presume that these compounds are more likely a detoxification product rather than a pheromone precursor. Thus, we have observed a strong induction of JH III on the formation of both verbenyl conjugates discussed. Originally, these compounds serve as binding agents for the detoxification product of α-pinene, specifically *cis*-verbenol in our case, but additionally, our findings proved that verbenyl fatty acyl esters are possessed by adult males as an alternative pheromone precursor (Chiu et al., 2018; Ramakrishnan et al., 2022a).

Hence, obtaining the specific gene candidates directs us to practical application by targeting the genes of pheromone biosynthesis for silencing in *I. typographus*. Targeting the species-specific non-lethal genes of the beetle along with characterizing them aims to address the pest's aggregation behavior with minimum ecological damage. A similar approach was demonstrated in a moth, Helicoverpa armigera when reproduction was modified by silencing genes responsible for sex pheromones production (Dong et al., 2017).

The main objective of RNAi-based Forest pest management is to reduce the forest pest population level below the epidemic level (Hlasny et al., 2021). Similarly, genes involved in pheromone production in bark beetles can be targeted via RNAi to disrupt communication, such as aggregation of pheromone signal for a mass attack in *I. typographus*. However, selecting an appropriate delivery method for specific insect orders is challenging. In wood-feeding insects, the aspect of dsRNA delivery can be achieved by spraying over the tree trunk (Li et al., 2015) or by injecting it into the tree's sap stream (Hunter et al., 2012). The delivery of dsRNA by these methods will be used for effective silencing of the pheromone biosynthetic genes in the beetle upon phloem-feeding. However, appropriate method should be considered while choosing the for effective outcome (Joga et al., 2021). This approach is familiar with existing forest pest management practices (i.e., silvicultural, biological), and can aid a multi-faceted management approach that keeps the tree-killing forest pest populations in the endemic stage while conserving the beneficial species.

In conclusion, these findings establish a foundation for understanding the genetic mechanisms underlying pheromone biosynthesis in *I. typographus* following JH III treatment. However, a logical next step would be to conduct functional validation of the identified gene candidates involved in pheromone biosynthesis. This approach could lead to effective pest management strategies, such as RNA interference, aimed at manipulating the mass attack behavior of this aggressive pest (Joga et al., 2021).

Data availability statement

All the data and resources generated for this study are included in the article and the supplemental materials. The RNA sequences have been submitted in NIH under the accession PRJNA934749. The Proteome data have been submitted in Proteome Xchange under the identifier PXD039243. We are willing to share all the data and resources in this study with the public.

Ethics statement

Ethical approval was not required for the study involving animals in accordance with the local legislation and institutional requirements because We have performed all beetle experiments that comply with the ARRIVE guidelines and were carried out in accordance with (Scientific Procedures) Act, 1986 and associated guidelines, EU Directive 2010/63/EU for animal experiments.

Author contributions

RR: conceptualization, methodology, formal analysis, resources, and writing – original draft. AR: RNA-seq, data curation, molecular

work support, and writing – review and editing. JH: GC-metabolomic data analysis and method writing. MK: UHPLC/HRMS-MS data analysis. KH: proteomics data analysis and method writing. AS: UHPLC/HRMS-MS data analysis and reviewing. AJ: conceptualization, methodology, formal analysis, writing – review and editing, and supervision. All authors contributed to the article and approved the submitted version.

Funding

RR, AR, JH, AS, and AJ are supported by Czech Science Foundation "GACR," no. 23-07916S; RR was supported by IGA A_20_22 RAJARAJAN RAMAKRISHNAN at the Faculty of Forestry and Wood Sciences, Czech University of Life sciences, Prague, CR; AR is supported by Excellent team grant 202 3–24, Faculty of Forestry and Wood Sciences, Czech University of Life Sciences, Prague, CR; AR, JH, and AJ were supported by Ministry of Education, Youth and Sport, Operational Program Research, Development and Education "EXTEMIT-K," no. CZ.02.1.01/0.0/0.0/15_003/0000433.

Acknowledgments

We acknowledge the editing and valuable comments of Jonathan Gershenzon on the final manuscript version and the constructive comments of Fredrik Schlyter, Hynek Burda and Ewald Grosse-Wilde on the earlier version of the manuscript.

Conflict of interest

The authors declare that the research was conducted in the absence of any commercial or financial relationships that could be construed as a potential conflict of interest.

Publisher's note

All claims expressed in this article are solely those of the authors and do not necessarily represent those of their affiliated organizations, or those of the publisher, the editors and the reviewers. Any product that may be evaluated in this article, or claim that may be made by its manufacturer, is not guaranteed or endorsed by the publisher.

Supplementary material

The Supplementary material for this article can be found online at: https://www.frontiersin.org/articles/10.3389/ffgc.2023.1215813/full#supplementary-material

References

Bakke, A., Froyen, P., and Skattebol, L. (1977). Field response to a new pheromonal compound isolated from *Ips-typographus*. *Naturwissenschaften* 64, 98–99. doi: 10.1007/bf00437364

Bearfield, J. C., Henry, A. G., Tittiger, C., Blomquist, G. J., and Ginzel, M. D. (2009). Two regulatory mechanisms of Monoterpenoid pheromone production in *Ips* spp. of bark beetles. *J. Chem. Ecol.* 35, 689–697. doi: 10.1007/s10886-009-9652-2

Blomquist, G. J., Figueroa-Teran, R., Aw, M., Song, M. M., Gorzalski, A., Abbott, N. L., et al. (2010). Pheromone production in bark beetles. *Insect Biochem. Mol. Biol.* 40, 699–712. doi: 10.1016/j.ibmb.2010.07.013

Blomquist, G. J., Tittiger, C., MacLean, M., and Keeling, C. I. (2021). Cytochromes P450: terpene detoxification and pheromone production in bark beetles. *Current Opinion in Insect Sci.* 43, 97–102. doi: 10.1016/j.cois.2020.11.010

Buhaescu, I., and Izzedine, H. (2007). Mevalonate pathway: a review of clinical and therapeutical implications. *Clin. Biochem.* 40, 575–584. doi: 10.1016/j.clinbiochem.2007.03.016

Byers, J. A., and Birgersson, G. (1990). Pheromone production in a bark beetle independent of myrcene precursor in host pine species. *Naturwissenschaften* 77, 385–387. doi: 10.1007/bf01135739

Chiu, C. C., Keeling, C. I., and Bohlmann, J. (2018). Monoterpenyl esters in juvenile mountain pine beetle and sex-specific release of the aggregation pheromone *trans*-verbenol. *Proc. Natl. Acad. Sci. U. S. A.* 115, 3652–3657. doi: 10.1073/pnas.1722380115

Chiu, C. C., Keeling, C. I., and Bohlmann, J. (2019). The cytochrome P450 CYP6DE1 catalyzes the conversion of α-pinene into the mountain pine beetle aggregation pheromone *trans*-verbenol. *Sci. Rep.* 9:1477. doi: 10.1038/s41598-018-38047-8

Chong, J., Soufan, O., Li, C., Caraus, I., Li, S. Z., Bourque, G., et al. (2018). MetaboAnalyst 4.0: towards more transparent and integrative metabolomics analysis. *Nucleic Acids Res.* 46, W486–W494. doi: 10.1093/nar/gky310

Cox, J., Hein, M. Y., Luber, C. A., Paron, I., Nagaraj, N., and Mann, M. (2014). Accurate proteome-wide label-free quantification by delayed normalization and maximal peptide ratio extraction. *Termed MaxLFQ. Molecular & Cellular Proteomics* 13, 2513–2526. doi: 10.1074/mcp.M113.031591

Cox, J., and Mann, M. (2008). MaxQuant enables high peptide identification rates, individualized p.p.b.-range mass accuracies and proteome-wide protein quantification. *Nat. Biotechnol.* 26, 1367–1372. doi: 10.1038/nbt.1511

Cristino, A. S., Nunes, F. M., Lobo, C. H., Bitondi, M. M., Simões, Z. L., da Fontoura Costa, L., et al. (2006). Caste development and reproduction: a genome-wide analysis of hallmarks of insect eusociality. *Insect Mol. Biol.* 15, 703–714. doi: 10.1111/j.1365-2583.2006.00696.x

Dai, L. L., Gao, H. M., and Chen, H. (2021). Expression levels of detoxification enzyme genes from *Dendroctonus armandi* (Coleoptera: Curculionidae) fed on a solid diet containing pine phloem and Terpenoids. *Insects* 12:15. doi: 10.3390/insects12100926

Dhandapani, R. K., Gurusamy, D., Duan, J. J., and Palli, S. R. (2020). RNAi for management of Asian long-horned beetle, Anoplophora glabripennis: identification of target genes. *J Pest Sci* 93, 823–832. doi: 10.1007/s10340-020-01197-8

Dong, K., Sun, L., Liu, J. T., Gu, S. H., Zhou, J-J., Yang, R-N., et al. (2017). RNAi-Induced Electrophysiological and Behavioral Changes Reveal Two Pheromone Binding Proteins of Helicoverpa armigera Involved in the Perception of the Main Sex Pheromone Component Z11-16:Ald. *J. Chem. Ecol.* 43, 207–214. doi: 10.1007/s10886-016-0816-6

Emlen, D., Szafran, Q., Corley, L., and Dworkin, I. (2006). Insulin signaling and limb-patterning: candidate pathways for the origin and evolutionary diversification of beetle 'horns'. *Heredity* 97, 179–191. doi: 10.1038/sj.hdy.6800868

Fang, J. X., Zhang, S. F., Liu, F., Cheng, B., Zhang, Z., Zhang, Q. H., et al. (2021a). Functional investigation of monoterpenes for improved undestanding of the relationship between hosts and bark beetles. *J. Appl. Entomol.* 145, 303–311. doi: 10.1111/jen.12850

Fang, J. X., Du, H. C., Shi, X., Zhang, S. F., Liu, F., Zhang, Z., et al. (2021b). Monoterpenoid signals and their transcriptional responses to feeding and juvenile hormone regulation in bark beetle *Ips hauseri*. *J. Exp. Biol.* 224:9. doi: 10.1242/jeb.238030

Gilg, A. B., Bearfield, J. C., Tittiger, C., Welch, W. H., and Blomquist, G. J. (2005). Isolation and functional expression of an animal geranyl diphosphate synthase and its role in bark beetle pheromone biosynthesis. *Proc. Natl. Acad. Sci. U. S. A.* 102, 9760–9765. doi: 10.1073/pnas.0503277102

Goodman, W. G., and Cusson, M. (2012). The juvenile hormones. *Insect Endocrinol.* 8, 310–365. doi: 10.1016/B978-0-12-384749-2.10008-1

Hebert, A. S., Richards, A. L., Bailey, D. J., Ulbrich, A., Coughlin, E. E., Westphall, M. S., et al. (2014). The one hour yeast proteome. *Mol. Cell. Proteomics* 13, 339–347. doi: 10.1074/mcp.M113.034769

Hilliou, F., Chertemps, T., Maibeche, M., and Le Goff, G. (2021). Resistance in the genus Spodoptera: key insect detoxification genes. *Insects* 12:27. doi: 10.3390/insects12060544

Hlasny, T., Konig, L., Krokene, P., Lindner, M., Montagne-Huck, C., Muller, J., et al. (2021). Bark beetle outbreaks in Europe: state of knowledge and ways forward for management. *Current Forestry Reports* 7, 138–165. doi: 10.1007/s40725-021-00142-x

Hughes, P. R. (1974). Myrcene - precursor of pheromones in *Ips* beetles. *J. Insect Physiol.* 20, 1271–1275. doi: 10.1016/0022-1910(74)90232-7

Hunter, W. B., Glick, E., Paldi, N., and Bextine, B. R. (2012). Advances in RNA interference: dsRNA Treatment in Trees and Grapevines for Insect Pest Suppression. *Southwest. Entomol.* 37, 85–87. doi: 10.3958/059.037.0110

Ivarsson, P., and Birgersson, G. (1995). Regulation and biosynthesis of pheromone components in the double spined bark beetle *ips duplicatus* (coleoptera, scolytidae). *J. Insect Physiol.* 41, 843–849. doi: 10.1016/0022-1910(95)00052-v

Ivarsson, P., Schlyter, F., and Birgersson, G. (1993). Demonstration of *de-novo* pheromone biosynthesis in *Ips-duplicatus* (coleoptera, scolytidae) - inhibition of ipsdienol and e-myrcenol production by compactin. *Insect Biochem. Mol. Biol.* 23, 655–662. doi: 10.1016/0965-1748(93)90039-u

Jindra, M., and Bittova, L. (2020). The juvenile hormone receptor as a target of juvenoid "insect growth regulators". *Arch. Insect Biochem. Physiol.* 103:e21615. doi: 10.1002/arch.21615

Jindra, M., Palli, S. R., and Riddiford, L. M. (2013). "The juvenile hormone signaling pathway in insect development" in *Annual review of entomology*. ed. M. R. Berenbaum, vol. 58, 181–204. doi: 10.1146/annurev-ento-120811-153700

Joga, M. R., Moglicherla, K., Smagghe, G., and Roy, A. (2021). RNA interference-based forest protection products (FPPs) against wood-boring coleopterans: Hope or hype? *Front. Plant Sci.* 12:733608. doi: 10.3389/fpls.2021.733608

Kanehisa, M. (2002). The KEGG database. *Silico Simulation of Biolog. Processes* 247, 91–103. doi: 10.1002/0470857897.ch8

Kanehisa, M., Furumichi, M., Tanabe, M., Sato, Y., and Morishima, K. (2017). KEGG: new perspectives on genomes, pathways, diseases and drugs. *Nucleic Acids Res.* 45, D353–D361. doi: 10.1093/nar/gkw1092

Keeling, C. I., Bearfield, J. C., Young, S., Blomquist, G. J., and Tittiger, C. (2006). Effects of juvenile hormone on gene expression in the pheromone-producing midgut of the pine engraver beetle, *Ips pini*. *Insect Mol. Biol.* 15, 207–216. doi: 10.1111/j.1365-2583.2006.00629.x

Keeling, C. I., Blomquist, G. J., and Tittiger, C. (2004). Coordinated gene expression for pheromone biosynthesis in the pine engraver beetle, *Ips pini* (Coleoptera: Scolytidae). *Naturwissenschaften* 91, 324–328. doi: 10.1007/s00114-004-0523-y

Keeling, C. I., Li, M., Sandhu, H. K., Henderson, H., Saint Yuen, M. M., and Bohlmann, J. (2016). Quantitative metabolome, proteome and transcriptome analysis of midgut and fat body tissues in the mountain pine beetle, *Dendroctonus ponderosae* Hopkins, and insights into pheromone biosynthesis. *Insect Biochem. Mol. Biol.* 70, 170–183. doi: 10.1016/j.ibmb.2016.01.002

Knizek, M., Zahradník, P., and Liška, J. (2023). Sborník referátů z celostátního semináře s mezinárodní účastí Přípravky na ochranu lesa – realita a budoucnost. *Zpravodaj ochrany lesa, Škodliví činitelé v lesích Česka. Svazek*. 26, 2022/23.

Kyre, B. R., Bentz, B. J., and Rieske, L. K. (2020). Susceptibility of mountain pine beetle (Dendroctonus ponderosae Hopkins) to gene silencing through RNAi provides potential as a novel management tool. *For. Ecol. Manag.* 73, 0378–1127. doi: 10.1016/j.foreco.2020.118322

Leinwand, S. G., and Scott, K. (2021). Juvenile hormone drives the maturation of spontaneous mushroom body neural activity and learned behavior. *Neuron* 109, 1836–1847.e5. doi: 10.1016/j.neuron.2021.04.006

Li, H., Guan, R., Guo, H., and Miao, X. (2015). New insights into an RNAi approach for plant defence against piercing-sucking and stem-borer insect pests. *Plant Cell Environ*, 38:2277–2285. doi: 10.1111/pce.12546

Nadeau, J. A., Petereit, J., Tillett, R. L., Jung, K., Fotoohi, M., MacLean, M., et al. (2017). Comparative transcriptomics of mountain pine beetle pheromone-biosynthetic tissues and functional analysis of CYP6DE3. *BMC Genomics* 18:311. doi: 10.1186/s12864-017-3696-4

Nardi, J. B., Young, A. G., Ujhelyi, E., Tittiger, C., Lehane, M. J., and Blomquist, G. J. (2002). Specialization of midgut cells for synthesis of male isoprenoid pheromone components in two scolytid beetles, *Dendroctonus jeffreyi* and *Ips pini*. *Tissue Cell* 34, 221–231. doi: 10.1016/s0040-8166(02)00004-6

Naseer, A., Mogilicherla, K., Sellamuthu, G., and Roy, A. (2023). Age matters life-stage, tissue, and sex-specific gene expression dynamics in *Ips typographus* (Coleoptera: Curculionidae: Scolytinae). *Front. for. glob.* 6:1124754. doi: 10.3389/ffgc.2023.1124754

NIST (2017).Inorganic Crystal Structure Database. *NIST Standard Reference Database Number 3*, Gaithersburg MD: National Institute of Standards and Technology. 20899. doi: 10.18434/M32147

Pandey, A., and Bloch, G. (2015). Juvenile hormone and ecdysteroids as major regulators of brain and behavior in bees. *Current Opinion in Insect Sci.* 12, 26–37. doi: 10.1016/j.cois.2015.09.006

Patacca, M., Lindner, M., Lucas-Borja, M. E., Cordonnier, T., Fidej, G., Gardiner, B., et al. (2023). ISignificant increase in natural disturbance impacts on European forests since 1950. *Glob. Change Biol.* 29, 1359–1376. doi: 10.1111/gcb.16531

Powell, D., Grosse-Wilde, E., Krokene, P., Roy, A., Chakraborty, A., Lofstedt, C., et al. (2021). A highly-contiguous genome assembly of the Eurasian spruce bark beetle, *Ips typographus*, provides insight into a major forest pest. *Commun. Biol.* 4:1059. doi: 10.1038/s42003-021-02602-3

Ramakrishnan, R., Hradecky, J., Roy, A., Kalinova, B., Mendezes, R. C., Synek, J., et al. (2022a). Metabolomics and transcriptomics of pheromone biosynthesis in an aggressive forest pest *Ips typographus*. *Insect Biochem. Mol. Biol.* 140:103680. doi: 10.1016/j.ibmb.2021.103680

Ramakrishnan, R., Roy, A., Kai, M. R., Svatos, A., and Jirosova, A. (2022b). Metabolome and transcriptome related dataset for pheromone biosynthesis in an aggressive forest pest *Ips typographus*. *Data Brief* 41:107912. doi: 10.1016/j.dib.2022.107912

Rappsilber, J., Mann, M., and Ishihama, Y. (2007). Protocol for micro-purification, enrichment, pre-fractionation and storage of peptides for proteomics using StageTips. *Nat. Protoc.* 2, 1896–1906. doi: 10.1038/nprot.2007.261

Renwick, J. A. A., Hughes, P. R., and Krull, I. S. (1976). Selective production of *cis*-verbenol and *trans*-verbenol from (−)- and (+)-α-pinene by a bark beetle. *Science* 191, 199–201. doi: 10.1126/science.1246609

Riddiford, L. M. (2012). How does juvenile hormone control insect metamorphosis and reproduction? *Gen. Comp. Endocrinol.* 179, 477–484. doi: 10.1016/j.ygcen.2012.06.001

Riddiford, L. M., Cherbas, P., and Truman, J. W. (2001). Ecdysone receptors and their biological actions. *Vitamins and Hormones - Advan. Res. App.* 60, 1–73. doi: 10.1016/s0083-6729(00)60016-x

Riddiford, L. M., Truman, J. W., Mirth, C. K., and Shen, Y. C. (2010). A role for juvenile hormone in the prepupal development of *Drosophila melanogaster*. *Development* 137, 1117–1126. doi: 10.1242/dev.037218

Rodrigues, T. B., Dhandapani, R., Duan, J., and Palli, S. R. (2017). RNA interference in the Asian Longhorned Beetle: Identification of Key RNAi Genes and Reference Genes for RT-qPCR. *Scientific Reports*. 7:8913. doi: 10.1038/s41598-017-08813-1

Sandstrom, P., Welch, W. H., Blomquist, G. J., and Tittiger, C. (2006). Functional expression of a bark beetle cytochrome P450 that hydroxylates myrcene to ipsdienol. *Insect Biochem. Mol. Biol.* 36, 835–845. doi: 10.1016/j.ibmb.2006.08.004

Sarabia, L. E., Lopez, M. F., Obregon-Molina, G., Cano-Ramirez, C., Sanchez-Martinez, G., and Zuniga, G. (2019). The differential expression of mevalonate pathway genes in the gut of the bark beetle *Dendroctonus rhizophagus* (Curculionidae: Scolytinae) is unrelated to the de novo synthesis of terpenoid pheromones. *Int. J. Mol. Sci.* 20:20. doi: 10.3390/ijms20164011

Schlyter, F., Birgersson, G., Byers, J. A., Lofqvist, J., and Bergstrom, G. (1987). Field response of spruce bark beetle, Ips typographus to aggregation pheromone candidates. *J. Chem. Ecol.* 13, 701–716. doi: 10.1007/BF01020153

Sellamuthu, G., Bily, J., Joga, M. R., Synek, J., and Roy, A. (2022). Identifying optimal reference genes for gene expression studies in Eurasian spruce bark beetle, *Ips typographus* (Coleoptera: Curculionidae: Scolytinae). *Sci. Rep.* 12:4671. doi: 10.1038/s41598-022-08434-3

Seybold, S. J., Quilici, D. R., Tillman, J. A., Vanderwel, D., Wood, D. L., and Blomquist, G. J. (1995). De-novo biosynthesis of the aggregation pheromone components ipsenol and ipsdienol by the pine bark beetles *Ips paraconfusus* lanier and *Ips pini* (say) (coleoptera-scolytidae). *Proc. Natl. Acad. Sci. U. S. A.* 92, 8393–8397. doi: 10.1073/pnas.92.18.8393

Smykal, V., Daimon, T., Kayukawa, T., Takaki, K., Shinoda, T., and Jindra, M. (2014). Importance of juvenile hormone signaling arises with competence of insect larvae to metamorphose. *Dev. Biol.* 390, 221–230. doi: 10.1016/j.ydbio.2014.03.006

Song, M. M., Kim, A. C., Gorzalski, A. J., MacLean, M., Young, S., Ginzel, M. D., et al. (2013). Functional characterization of myrcene hydroxylases from two geographically distinct *Ips pini* populations. *Insect Biochem. Mol. Biol.* 43, 336–343. doi: 10.1016/j.ibmb.2013.01.003

Tian, C. B., Li, Y. Y., Huang, J., Chu, W. Q., Wang, Z. Y., and Liu, H. (2020). Comparative transcriptome and proteome analysis of heat acclimation in predatory mite *Neoseiulus barkeri*. *Front. Physiol.* 11:16. doi: 10.3389/fphys.2020.00426

Tillman, J. A., Holbrook, G. L., Dallara, P. L., Schal, C., Wood, D. L., Blomquist, G. J., et al. (1998). Endocrine regulation of de novo aggregation pheromone biosynthesis in the pine engraver, *Ips pini* (say) (Coleoptera: Scolytidae). *Insect Biochem. Mol. Biol.* 28, 705–715. doi: 10.1016/s0965-1748(97)00117-3

Tillman, J. A., Lu, F., Goddard, L. M., Donaldson, Z. R., Dwinell, S. C., Tittiger, C., et al. (2004). Juvenile hormone regulates *de novo* isoprenoid aggregation pheromone biosynthesis in pine bark beetles, *Ips* spp., through transcriptional control of HMG-CoA reductase. *J. Chem. Ecol.* 30, 2459–2494. doi: 10.1007/s10886-004-7945-z

Treiblmayr, K., Pascual, N., Piulachs, M.-D., Keller, T., and Belles, X. (2006). Juvenile hormone titer versus juvenile hormone synthesis in female nymphs and adults of the German cockroach, *Blattella germanica*. *J. Insect Sci.* 6, 1–7. doi: 10.1673/031.006.4301

Trumbo, S. T. (2018). Juvenile hormone and parental care in subsocial insects: implications for the role of juvenile hormone in the evolution of sociality. *Current Opinion in Insect Sci.* 28, 13–18. doi: 10.1016/j.cois.2018.04.001

Tyanova, S., Temu, T., Sinitcyn, P., Carlson, A., Hein, M. Y., Geiger, T., et al. (2016). The Perseus computational platform for comprehensive analysis of (prote)omics data. *Nat. Methods* 13, 731–740. doi: 10.1038/nmeth.3901

Ward, S. F., Brockerhoff, E. G., Turner, R. M., Yamanaka, T., Marini, L., Fei, S. L., et al. (2022). Prevalence and drivers of a tree-killing bark beetle, *Ips typographus* (Coleoptera, Scolytinae), in international invasion pathways into the USA. *J. Pest. Sci.* 96, 845–856. doi: 10.1007/s10340-022-01559-4

White, R. A., Agosin, M., Franklin, R. T., and Webb, J. W. (1980). Bark beetle pheromones - evidence for physiological synthesis mechanisms and their ecological implications. *Zeitschrift Fur Angewandte Entomologie-J. Applied Entomol.* 90, 255–274. doi: 10.1111/j.1439-0418.1980.tb03526.x

Zhang, W. N., Ma, L., Xiao, H. J., Liu, C., Chen, L., Wu, S. L., et al. (2017). Identification and characterization of genes involving the early step of juvenile hormone pathway in *Helicoverpa armigera*. *Sci. Rep.* 7:16542. doi: 10.1038/s41598-017-16319-z

Zhu, H., Gegear, R. J., Casselman, A., Kanginakudru, S., and Reppert, S. M. (2009). Defining behavioral and molecular differences between summer and migratory monarch butterflies. *BMC Biol.* 7:14. doi: 10.1186/1741-7007-7-14

frontiers | Frontiers in Forests and Global Change

TYPE Original Research
PUBLISHED 21 February 2024
DOI 10.3389/ffgc.2024.1325897

OPEN ACCESS

EDITED BY
Quan Lu,
Chinese Academy of Forestry, China

REVIEWED BY
Diana Marčiulynienė,
Lithuanian Research Centre for Agriculture and Forestry, Lithuania
Yong Li,
Chinese Academy of Forestry, China

*CORRESPONDENCE
Nargues Falahi Charkhabi
✉ falahicharkhabi@ut.ac.ir

†These authors have contributed equally to this work

RECEIVED 22 October 2023
ACCEPTED 23 January 2024
PUBLISHED 21 February 2024

CITATION
Araeinejhad M-H, Charkhabi NF, Brady C and Rahimian H (2024) Reliable and specific detection and identification of *Brenneria goodwinii*, the causal agent of oak and oriental beech decline.
Front. For. Glob. Change 7:1325897.
doi: 10.3389/ffgc.2024.1325897

Reliable and specific detection and identification of *Brenneria goodwinii*, the causal agent of oak and oriental beech decline

Mohammad-Hossein Araeinejhad[1†], Nargues Falahi Charkhabi[1*†], Carrie Brady[2] and Heshmat Rahimian[3]

[1]Department of Entomology and Plant Pathology, College of Agricultural Technology, University College of Agriculture and Natural Resources, University of Tehran, Tehran, Iran, [2]Centre for Research in Bioscience, Faculty of Health and Life Sciences, University of the West of England, Bristol, United Kingdom, [3]Department of Plant Protection, Sari Agricultural Science and Natural Resources University, Sari, Iran

Chestnut-leaved oak (*Quercus castaneifolia*) and oriental beech (*Fagus orientalis*) are among the major tree species in the Hyrcanian forests. *Brenneria goodwinii* was identified as the causal agent of necrotic lesions and stem bleeding on affected oak trees in different countries. Oak and oriental beech trees with bleeding symptoms were observed in a few forest sites in northern Iran. The objectives of the present study were to identify and characterize the causal agents of bark canker in oak and oriental beech trees and develop a primer set for specific detection, using polymerase chain reaction (PCR), of *Brenneria goodwinii* strains. A total of 31 and 20 samples from oak and oriental beech trees, respectively, with stem bleeding and bark canker symptoms were collected from Golestan and Mazandaran forests in northern Iran in 2020–2021. Bacterial strains displaying a green metallic sheen on EMB-agar medium were isolated from symptomatic oak (105 strains) and oriental beech samples (32 strains), while 31 and 20 strains were also isolated from healthy oak and oriental beech, respectively. Pathogenicity tests indicated that 51 and 25 strains isolated from oak and oriental beech, respectively were able to induce a necrotic area on oak acorns 15 days following inoculation. Moreover, four and two representative strains inoculated on oak and oriental beech twigs, respectively induced necrosis on all inoculated green twigs 1 month after inoculation. The sequences of the 16S rRNA and *gyrB* genes of representative strains isolated from and proved pathogenic on oak and oriental beech trees were 100% and over 99% similar to *B. goodwinii* LMG 26270^T, respectively, which revealed the strains belong to *B. goodwinii* species. The primer pair BgF3/R2, which was designed to target the *hrpN* gene, was proven to be specific in the detection of *B. goodwinii* strains. The primer pair amplified a 618-bp DNA fragment from strains of *B. goodwinii* only and not from strains belonging to *Rahnella*, *Gibbsiella*, *Lonsdalea,* and the other *Brenneria* species among several other pathogenic bacteria tested. No fragment was amplified from DNA extracted from healthy trees or seedlings in PCR using this primer pair.

KEYWORDS

emerging diseases, forest decline, *Fagus orientalis*, *Quercus castaneifolia*, Iran

Introduction

Chestnut-leaved oak (*Quercus castaneifolia*) and oriental beech (*Fagus orientalis*) are among the main tree species in the Hyrcanian or Caspian forests in northern Iran, with a history that dates back to 25–50 million years (Alavi et al., 2020).

Forest decline, described as loss in tree vigor and increased mortality due initially to climate change events (e.g., climate warming and drought) and accompanied by the contribution of pathogens and pests (Manion, 1991), is becoming widespread in some local stands (Sangüesa-Barreda et al., 2015). Several bacterial species including *Gibbsiella quercinecans* (Brady et al., 2010), *Brenneria goodwinii* (Denman et al., 2012), *Brenneria roseae* (Brady et al., 2014a), *Rahnella victoriana* (Brady et al., 2014b), *Bacillus pumilus* and *Stenotrophomonas maltophilia* (Ahmadi et al., 2019), and "*Brenneria izadpanahii*" (Bakhshi Ganje et al., 2021) have been identified as the causal agents of necrotic lesions and stem bleeding on oak trees with decline symptoms. Although several bacterial species were found to be associated with acute oak decline (AOD) (Denman et al., 2012), the most frequently encountered pathogens are *G. quercinecans* (Brady et al., 2010) and *B. goodwinii* (Denman et al., 2012). The latter is supposed to be the most damaging among AOD agents (Doonan et al., 2019). *B. goodwinii* was isolated from different *Quercus* species in the United Kingdom (UK) (Denman et al., 2012), Latvia (Zalkalns and Celma, 2021), Spain (González and Ciordia, 2020), Iran (Bakhshi Ganje et al., 2020), Switzerland (Ruffner et al., 2020), and Poland (Tkaczyk et al., 2021). Additionally, it was associated with acute decline symptoms on hornbeam (*Carpinus betulus*) trees in Iran (Moradi-Amirabad et al., 2019).

Diagnostic approaches commonly employed for the identification of *B. goodwinii* species consist of traditional (phenotypic biochemical and nutritional) and pathogenicity tests and sequencing of housekeeping genes including *gyrB*, *infB*, *rpoB*, and *atpD* (Denman et al., 2012; Bakhshi Ganje et al., 2020), which are both time- and labor-consuming procedures. Recently, a multiplex *Taq*Man polymerase chain reaction (PCR) assay was developed for simultaneous detection of four bacterial species involved in the AOD syndrome in the UK, including *B. goodwinii*, *G. quercinecans*, *R. victoriana*, and *Lonsdalea britannica* (Crampton et al., 2020). Nonetheless, a reliable molecular method for the rapid, accurate, and culture-independent detection and identification of *B. goodwinii* strains in infected plant samples is still lacking.

Stem bleeding and bark canker of oak and oriental beech trees, similar to those reported in bacterial canker, were observed in the Hyrcanian or Caspian forests in northern Iran during the summer months of 2020–2021 in the forests of Golestan and Mazandaran provinces. The objectives of the present study were to identify and characterize the causal agents of bark canker in oak and oriental beech trees by bacterial isolation and prove pathogenicity on oak and oriental beech seedlings and oak acorns, phenotypic characterization, and phylogenetic analyses based on 16S rRNA and *gyrB* genes. As no species-specific primers have thus far been designed for the detection of *B. goodwinii* strains, attempts were made to devise and prove the reliability of a primer set for specific detection, using PCR, of *B. goodwinii* strains from different hosts.

Materials and methods

Sampling and isolation

Samples of the outer bark, inner bark, and sapwood tissues from cankered sites on the trunk and main branches of oak (*Q. castaneifolia*) and oriental beech (*F. orientalis*) trees were collected from Gorgan, Golestan province and Sari, Mazandaran province, respectively, in the summer of 2020–2021. Five symptomless samples were collected from the healthy trees of each host. Moreover, three samples were collected from two- and three-year-old healthy oak seedlings in the greenhouse. Tissues were washed under tap water for 5 min, then surface sterilized in 70% ethanol for 30 s and rinsed three times in sterile distilled water (SDW). The symptomatic tissues were ground to small pieces in SDW using a mortar and pestle and a loopful of resulting suspensions streaked on plates of EMB medium (Merck, Darmstadt, Germany) containing 1% glycerol and 0.5% yeast extract and incubated at 28°C. Bacterial colonies were isolated after 48–72 h and purified by streaking on nutrient agar (NA) (Merck, Germany, Darmstadt) plates. The strains were stored in 15% glycerol stocks at −80°C. Bacterial strains included in this study are listed in Table 1.

Pathogenicity assay

Pathogenicity testing of all strains, including 105 and 32 strains isolated from oak and oriental beech symptomatic trees, was performed on chestnut-leaved oak acorns by injecting 10 µL of a bacterial suspension of each isolate prepared from an overnight culture on NA in SDW with an optical density of 0.1 at 600 nm using a disposable insulin syringe with needle (González and Ciordia, 2020). *B. goodwinii* FRB 141^T, *G. quercinecans* LMG 25500^T, and *R. victoriana* FRB 225^T were used as positive controls and SDW as the negative control, respectively. Symptom progression was observed for 15 days. Pathogenicity assays were performed in two replicates each containing three acorns per strain.

Moreover, pathogenicity of representative strains (UT-Bg 21, 44, 100, 115, 235, and 245) isolated from oak and oriental beech trees was tested by inoculating two- and three-year-old oak and oriental beech seedlings. Seedlings were kept in a greenhouse under conditions of 16 h light at 28°C and 8 h dark at 24°C with 75% relative humidity. The surface of the young green twigs was first disinfected using 95% ethanol for 1 min. The bacterial suspensions of the representative strains with $OD_{600} = 0.1$ were prepared in SDW and injected into twigs using sterile syringes. Inoculated twigs were covered with parafilm, and symptoms were monitored 2 months post-inoculation. To fulfill Koch's postulates, bacterial re-isolation from inoculated acorns, and twigs were performed 15 and 30 days post-inoculation on EMB-agar, respectively. Representative strains were inoculated on twigs in three replicates. Re-isolated bacteria were identified by colony morphology on EMB-agar and PCR using specific primers.

Phenotypic characterization

Ten strains isolated from each host were subjected to the following diagnostic tests: Gram reaction using 3% KOH (Suslow et al., 1982), levan formation from sucrose, oxidase reaction, starch hydrolysis, and

TABLE 1 Bacterial strains used in this study.

Species	Strain	References/Origin
Brenneria goodwinii	FRB 141^T	Denman et al. (2012)
	FRB 186, BAC 30–03-01, BAC 56e-01	Brady, C., University of the West of England
	BS1	Moradi-Amirabad et al. (2019)
	UT-Bg 17, 21*, 27, 28, 29, 30, 31, 32, 33, 35, 38, 39, 44*, 46, 47, 48, 49, 50*, 97, 98, 99, 100*, 101, 103, 105, 107, 108, 109, 111, 112, 115*, 116, 117, 118, 119, 121, 123, 125, 127, 128, 129, 130, 136, 137, 138, 139, 140, 147, 148, 153, 201†, 202, 203*, 205, 207, 210, 211, 213, 217, 220, 221, 222, 227, 228, 232, 233, 235*, 236, 237, 239*, 241, 242, 245, 249, 250.	This study
Brenneria roseae subsp. *roseae*	FRB 222^T	Brady et al. (2014a)
Brenneria roseae subsp. *americana*	FRB 223^T	Brady et al. (2014a)
Brenneria nigrifluens	DSM 30175^T	Wilson et al. (1957)
	M2	Falahi Charkhabi et al. (2010)
Brenneria salicis	DSM 30166^T	Day (1924)
Brenneria alni	DSM 11811^T	Surico et al. (1996)
Brenneria rubrifaciens	DSM 4483^T	Wilson et al. (1967)
Brenneria tiliae	TWs2*Brenneria*2ii	Kile et al. (2022)
Rahnella aquatilis	LMG 2794^T	Izard et al., 1979
Rahnella perminowiae	SL6^T	Brady et al. (2022)
Rahnella bonaserana	H11b^T	Brady et al. (2022)
Rahnella rivi	FC061912-K^T	Brady et al. (2022)
Rahnella ecdela	FRB 231^T	Brady et al. (2022)
Rahnella victoriana	FRB 225^T	Brady et al. (2014b)
Rahnella variigena	FOD 20.8	Brady et al. (2014b)
Rahnella inusitata	FOD 9.5a	Brady et al. (2014b)
Rahnella bruchi	FRB 226^T	Brady et al. (2014b)
Rahnella woolbedingensis	FRB 227^T	Brady et al. (2014b)
Gibbsiella quercinecans	FRB 97^T	Brady et al. (2010)
Gibbsiella greigii	FRB 224^T	Brady et al. (2014c)
Gibbsiella dentisursi	DSM 23818^T	Saito et al. (2012)
"*Gibbsiella acetica*"	C22	Hu (2012)
Lonsdalea quercina	LMG 2724^T	Brady et al. (2012)
Lonsdalea britannica	FRB 18^T	Brady et al. (2012)
Lonsdalea iberica	1915-14^T	Brady et al. (2012)

*Strains used in phylogenetic analyses.
†Underlined strains isolated from the oriental beam (Fagus orientalis).

several other phenotypic tests according to Schaad et al. (2001). Utilization of carbon sources was assayed using the basal medium of Ayers et al. (1919) supplemented with filter-sterilized carbohydrate sources at 0.25% final concentration. Cultures of *Brenneria nigrifluens* M2 (Falahi Charkhabi et al., 2010), *B. goodwinii* FRB 141^T, *G. quercinecans* LMG2 5500^T, and *R. victoriana* FRB 225^T were also used as reference strains in all tests.

Molecular characterization

Genomic DNA was extracted from overnight cultures on NA using the alkalic lysis procedure (Niemann et al., 1997). PCR was performed in a final volume of 20 µL containing 2x *Taq* DNA Polymerase Master Mix (Ampliqon A/S, Odense, Denmark), 10 pmol of each primer, and 2 µL of template DNA. The reaction was performed in a thermocycler (Mastercycler®, Eppendorf, Hamburg, Germany). PCR amplification of the 16S rRNA gene of the five strains (UT-Bg 21, 44, 100, 235, and 239) was performed using the primer pair 27F/1492R (Lane, 1991; Stackebrandt and Liesack, 1993; Table 2). The PCR program used consisted of an initial denaturation at 94°C for 4 min, followed by 30 cycles of denaturing at 94°C for 1 min, annealing at 59°C for 1 min, and extension at 72°C for 2.5 min. The final extension was performed at 72°C for 10 min.

A 1050 bp fragment of the housekeeping gene *gyrB* (DNA gyrase subunit β) of each of the eight strains including UT-Bg 21, 44, 50, 100,

TABLE 2 Name, sequence, target, product size, and reference of primers used in this study.

Name	Sequence (5′-3′)	Gene target	Product size (bp)	References
27F	AGAGTTTGATCCTGGCTCAG	16S rDNA	1,500	Lane (1991)
1492R	TACGGCTACCTTGTTACGACTT			Stackebrandt and Liesack (1993)
gyrB 01-F	TAARTTYGAYGAYAACTCYTAYAAAGT	gyrB-PCR	971	Brady et al. (2008)
gyrB 02-R	CMCCYTCCACCARGTAMAGTT			
gyrB 07-F	GTVCGTTTCTGGCCVAG	gyrB-Sequencing		
Bg-F1	GCTGAACGGGTATTTTTCGCCTCA	*impG*	427	This study
Bg-R1	GAAAGGAACATATTCCTGCTCTTTTA			
Bg-F3	ATGCTTAAAGATGTTATCGGCAA	*hrpN*	618	This study
Bg-R2	CCAGCGTATTGCCGAGCTGAGA			

115, 203, 235, and 239 was amplified and sequenced using the primers and conditions previously published (Brady et al., 2008; Table 2).

The amplified fragments were electrophoresed in 0.5X TBE buffer (tris-borate) and visualized by staining with ethidium bromide. The conserved genes were sequenced by Microsynth Co. (Balgach, Switzerland) using the Sanger method, and the obtained sequences were compared with those deposited in GenBank. Alignments were performed in ClustalW (Thompson et al., 1994), and phylogenetic trees were constructed using MEGA X (Kumar et al., 2018) with the maximum likelihood method based on the lowest value of the Bayesian information criterion (BIC). The robustness of the branches was determined by bootstrap analysis using 1000 replicates. *Xenorhabdus nematophila* ATCC 19061^T (DSM 3370^T) was used as an outgroup.

Primer designing

The genome sequence of *B. goodwinii* FRB 141^T (GenBank accession no. NZ_CP014137.1) was aligned against genomes of the other *B. goodwinii* strains including *B. goodwinii* FRB 171 (NZ_MJLY00000000.1) and *B. goodwinii* OBR1 (CGIG01000001.1). Genes with more than 95% similarity were selected and aligned with those of '*Affinibrenneria salicis*' strain L3-3HA, *Brenneria corticis* CFCC 11842, '*B. izadpanahii*' Iran 50, *B. nigrifluens* ATCC 13028, *B. nigrifluens* LMG 2694^T, *Brenneria populi* EniD312, *B. roseae* subsp. *roseae* LMG 27714^T, *B. roseae* subsp. *americana* LMG 27715^T, *Brenneria rubrifaciens* 6D370, *Brenneria salicis* ATCC 15712^T, and *Brenneria* sp. hezel4-2-4. Potential genes with less than 85% similarity were screened, and candidate genes were aligned with those of *Brenneria* (taxid:71655), *Gibbsiella* (taxid:929812), *Rahnella* (taxid:34037), *Lonsdalea* (taxid:1082702), *Dickeya* (taxid:204037), *Pantoea* (taxid:53335), *Serratia* (taxid:613), *Pectobacterium* (taxid:122277), Enterobacterales (taxid:91347), *Xanthomonas* (taxid:338), and *Pseudomonas* (taxid:286), as well as NCBI BioProject PRJNA342025. Finally, the gene encoding protein IpmG of the type VI secretion system and the gene encoding HrpN of the type III secretion system in *B. goodwinii* strains FRB 141^T, FRB 171, and OBR1 were selected for designing the primers. Two primer pairs were designed and evaluated for PCR detection of *B. goodwinii*: BgF1/R1, which amplified a 427 bp fragment of *impG* gene and BgF3/R2 that amplified a 618 bp fragment of *hrpN* as the target (Table 2). Primers were synthesized by the Metabion Company (Bavaria, Germany).

Primer specificity

The two primer pairs BgF1/R1 and BgF3/R2 were evaluated for their specificity in targeting the specific genes in *B. goodwinii*. PCR was performed in 20 µL-reaction mixtures containing 2x *Taq* DNA Polymerase Master Mix (Ampliqon A/S, Odense, Denmark), 10 pmol of each primer, and 2 µL of template DNA. The PCR program consisted of an initial denaturation step of 5 min at 94°C, followed by 28 cycles of 1 min at 94°C, 1 min at 56°C, and 45 s at 72°C, and a final extension step of 5 min at 72°C. *B. goodwinii* FRB 141^T and *B. goodwinii* BS1 (Moradi-Amirabad et al., 2019) were used as positive controls. SDW and strains of the other species and representative species of *Brenneria*, *Rahnella*, *Gibbsiella*, and *Lonsdalea* inciting decline on other forest trees (Table 1), plus strains of some distantly related or unrelated genera, including *Enterobacter ludwigii* A21, *Serratia marcescens* A80, *Pectobacterium carotovorum* ATCC 15713^T, *Xanthomonas translucens* pv. *undulosa* ICMP11055, *X. translucens* pv. *cerealis* ICMP 5752, *Pantoea agglomerans* NK16, *Agrobacterium radiobacter* PK, *Pseudomonas viridiflava* ATCC 13223^T, *P. viridiflava* FBF52, *Pseudomonas* sp. A44, *Pseudomonas tolaasii* T7, and *Pseudomonas amygdali* pv. *lachrymans* GSPB 82a, A77: *Klebsiella oxytoca* A77, *Enterobacter ludwigii* A21, *Bacillus* sp. A11, and *Lysinibacillus* sp. A31, were all used as negative controls. Bacterial strains isolated from symptomless oak trees and seedlings were also used in the specificity assay.

In planta detection of *Brenneria Goodwinii*

For direct detection of *B. goodwinii* in infected tissues, oak symptomatic samples collected from Golestan and Mazandaran forests as well as oriental beech artificially inoculated plants were used. Inoculation was performed as described above. Three weeks after inoculation, 0.5 g of artificially infected oriental beech twig tissues was cut and homogenized with a mortar pestle in 4-ml SDW and incubated at room temperature for 1 h. Moreover, oak symptomatic samples were homogenized with a mortar pestle in phosphate-buffered saline buffer and incubated at room temperature for 1 h. DNA was extracted from the suspension using the alkalic lysis procedure (Niemann et al., 1997), 2 µL of which was used in the species-specific PCR as described above. Twigs injected with SDW were used as a negative control.

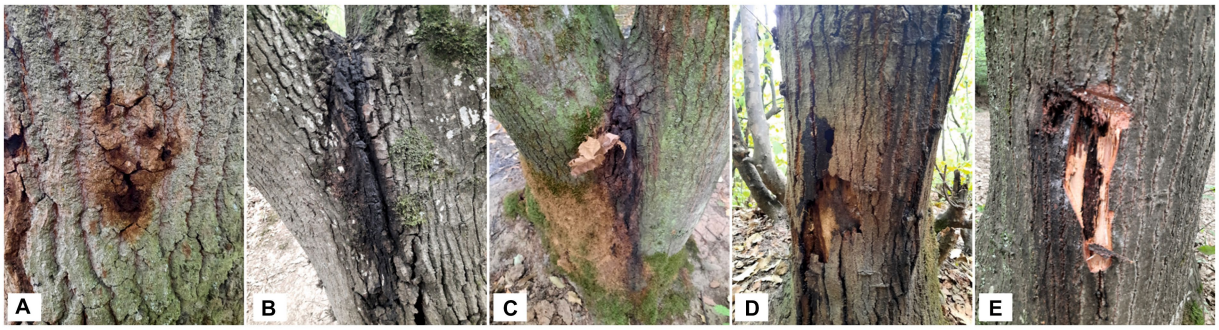

FIGURE 1
Symptoms of acute decline of chestnut-leaved oak (*Quercus castaneifolia*) in Iran, canker lesions, stem bleeding of a dark sticky fluid from vertical cracks **(A–C)**, and necrotic underlying tissue lesions in the inner bark **(D–E)**.

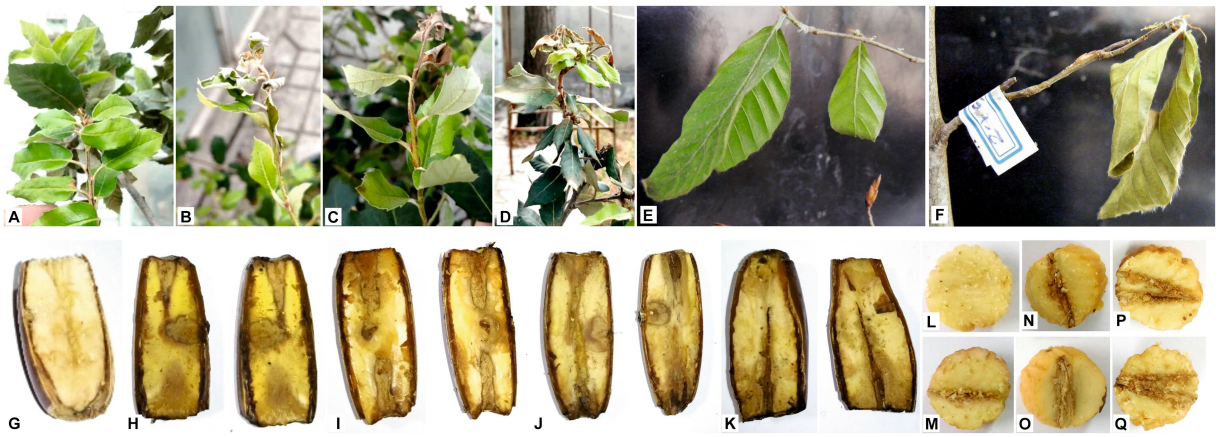

FIGURE 2
Pathogenicity assays of Brenneria goodwinii strains isolated from chestnut leaved oak (Quercus castaneifolia) and oriental beech (Fagus orientalis) on the oak and oriental beech seedlings and oak acorns, 30 and 15 days after inoculation, respectively. **(A,E,G,L)** Negative control infiltrated using sterile deionized water; oak seedlings inoculated using strains UT-Bg 21 **(B)**, UT-Bg 100 **(C)**, UT-Bg 115 **(D)**; oriental beech seedling inoculated using strain UT-Bg 245 **(F)**, acorn inoculated using strains UT-Bg 46 **(H)**, UT-Bg 98 **(I)**, UT-Bg 222 **(J)**, UT-Bg 235 **(K)**, UT-Bg 115 **(M)**, UT-Bg 21 **(N)**, UT-Bg 44 **(O)**, UT-Bg 239 **(P,Q)**.

Primer sensitivity

To determine the sensitivity and limit of detection of the designed primer pair, DNA was extracted from serial 10-fold dilutions of *B. goodwinii*, with suspensions starting with $OD_{600} = 0.1$, by the alkalic lysis procedure (Niemann et al., 1997), and 2 µL was used as templates in the PCR tests as described above.

Results

Symptoms, sampling, and isolation

In the summer of 2020–2021, 31 samples and 20 samples from decline-affected oak and oriental beech trees were collected in different areas of the Golestan and Mazandaran forests, respectively. The most characteristic symptoms were tissue necrosis, canker, and bleeding of a dark sticky fluid from vertical cracks in the bark of the trunk and scaffold branches of the infected trees (Figure 1). A total of 105 and 32 strains with a green metallic sheen on EMB-agar medium were isolated from the symptomatic oak and oriental beech samples, respectively. Thirty-one strains were also isolated from symptomless oak and oriental beech trees. Additionally, 15 strains were isolated from two- and three-year-old oak seedlings in the greenhouse and used in some tests.

Pathogenicity tests

All strains were inoculated on oak acorns, among which 51 strains isolated from oak and 25 strains isolated from oriental beech were able to induce a necrotic area 15 days following inoculation (Figures 2H–K,M–Q). Furthermore, *B. goodwinii* FRB 141^T, *G. quercinecans* LMG 25500^T, and *R. victoriana* FRB 225^T also induced necrotic areas on oak acorns. Four representative strains induced necrosis on all inoculated oak green twigs, 1 month after inoculation under greenhouse conditions (Figures 2B–D). Moreover, two strains inoculated on oriental beech caused necrosis on green twigs and die-back (Figure 2F). Re-isolation from the inoculated six acorn

samples, four oak, and three oriental beech twigs was performed on EMB and yielded a profuse number of colonies with a green metallic sheen similar to the inoculated ones. Moreover, the identification of re-isolated strains was confirmed by PCR using the developed specific primers. No symptoms were observed on test acorns and twigs injected with SDW (Figures 2A,E,G,L).

Phenotypic characteristics

Twenty strains isolated from the affected trees were Gram-negative. Colonies on nutrient agar were cream-colored, circular, convex, and smooth with entire margins and produced a green metallic sheen on EMB-Agar. Strains were negative in tests for oxidase, starch, Tween 20 hydrolysis, and the production of levan. Acid was produced from arabinose, fructose, D-lactose, trehalose, mannitol, and sorbitol. Strains utilized histidine, alanine, and serine but not arginine, lysine, ornithine, and tryptophan as sole carbon sources. The phenotypic characters of isolated strains were identical with *B. goodwinii* LMG 26270^T, which indicated the strains belong to *B. goodwinii* species.

Sequence analysis

Sequences of 976 bp and 718 bp fragments of the 16S rRNA and *gyrB* genes, respectively, of representative strains isolated from oak and oriental beech revealed similarity levels of 100% and over 99% to *B. goodwinii* LMG 26270^T, respectively, which revealed the strains belong to *B. goodwinii* species. The sequences were deposited in the NCBI GenBank database under accession numbers ON398765 to ON398769 for 16S rRNA (UT-Bg 21, 44, 100, 235, and 239), and ON412785 to ON412792 for *gyrB* (UT-Bg 21, 44, 50, 100, 115, 203, 235, and 239).

In the phylogenetic tree (Figure 3A) inferred from the 16S rRNA gene sequences of strains UT-Bg 21, 44, 100, 235, and 239, the strains clustered within the type strain of *B. goodwinii* supported with bootstrap values of 100%. In the phylogenetic tree constructed from the *gyrB* sequences of strains UT-Bg 21, 44, 50, 100, 115, 203, 235, and 239, all strains clustered with *B. goodwinii* LMG 26270^T and *B. goodwinii* FRB 171 with high bootstrap support (Figure 3B). Based on phenotypic characters and phylogenetic analysis, the strains belong to *B. goodwinii* species.

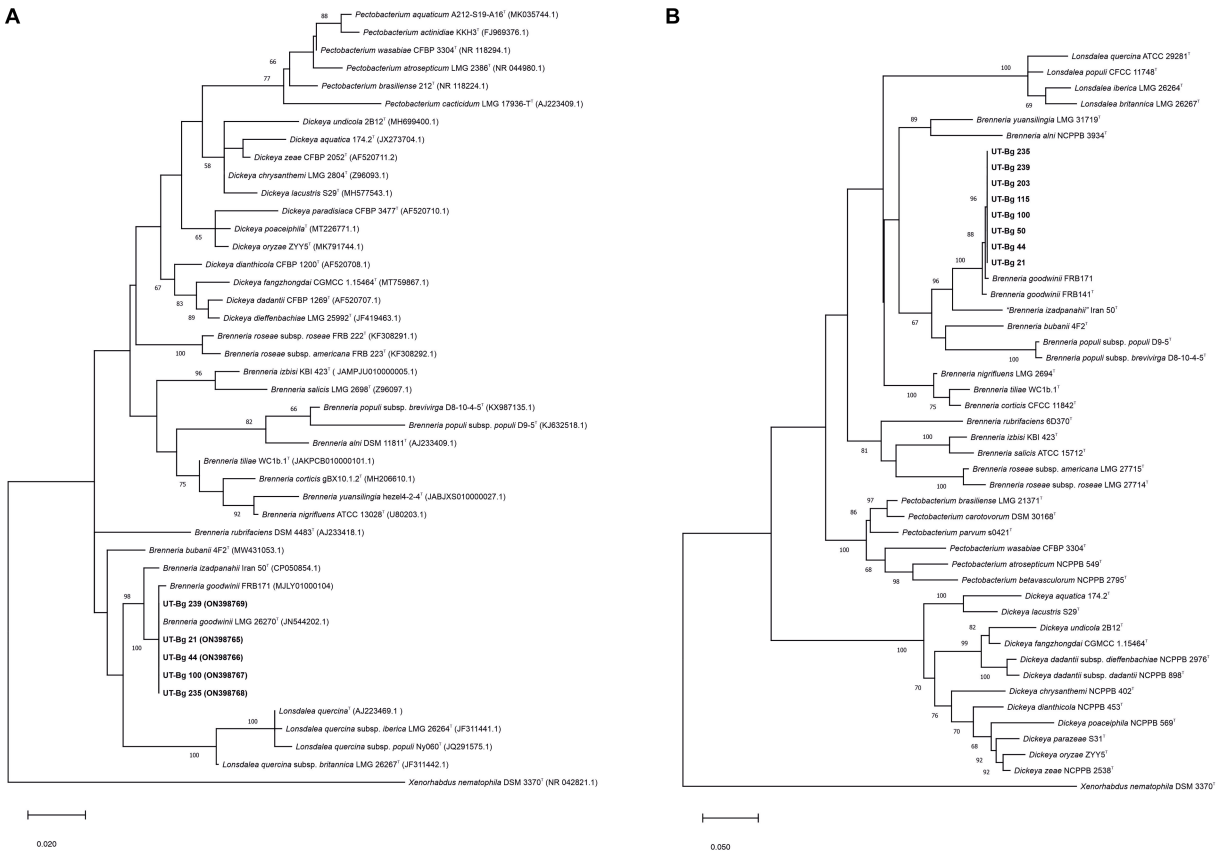

FIGURE 3
(A) Maximum likelihood phylogenetic tree based on partial sequence of 16S rRNA gene showing the taxonomic position of *Brenneria goodwinii* strains isolated from oak (UT-Bg 21, UT-Bg 44, UT-Bg 100) and oriental beech (UT-Bg 235 and UT-Bg 239). The tree was constructed using the Hasegawa-Kishino-Yano (HKY+ G+ I) based on the lowest Bayesian information criterion (BIC) score. Bootstrap values calculated for 1,000 replications are indicated. *Xenorhabdus nematophila* ATCC 19061^T (DSM 3370^T) was used as the outgroup. **(B)** Maximum likelihood phylogenetic tree based on partial sequence of *gyrB* gene showing the taxonomic position of *Brenneria goodwinii* strains isolated from oak (UT-Bg 21, UT-Bg 44, UT-Bg 50, UT-Bg 100, and UT-Bg 115) and oriental beech (UT-Bg 203, UT-Bg 235, and UT-Bg 239). The tree was constructed using the general time reversible (GTR) with a gamma distribution and invariant sites (GTR + G + I) based on the lowest BIC score. Bootstrap values calculated for 1,000 replications are indicated. *Xenorhabdus nematophila* ATCC 19061^T (DSM 3370^T) was used as the outgroup.

Primer specificity

The designed primer pair BgF1/R1 amplified a 427-bp fragment from *B. goodwinii* FRB 141^{T} and *B. goodwinii* BS1 strains. This primer pair amplified the desired fragment in two-thirds of *B. goodwinii* strains (data not shown). Contrarily, the primer pair BgF3/R2 amplified a 618 bp DNA fragment from 51 and 25 *B. goodwinii* strains isolated from affected oak and oriental beech, respectively, as well as FRB 141^{T} (Denman et al., 2012), BS1 (Moradi-Amirabad et al., 2019), and FRB 186, BAC 30–03-01, and BAC 56e-01. None of the bacterial strains belonging to the genera *Rahnella*, *Gibbsiella*, *Lonsdalea,* or other *Brenneria* species inciting decline on other forest trees, as well as strains representing a number of the other plant pathogenic bacteria, were amplified by these primer pairs (Figure 4). DNA samples and crude extracts of healthy trees or seedlings used did not yield any amplified product in PCR with these primer sets (Figure 5).

In planta detection of *Brenneria Goodwinii*

B. goodwinii was successfully re-isolated from artificially infected oriental beech inoculated with UT-Bg 235 and 239 strains. As expected, a specific amplicon of 618 bp was obtained from all seven artificially infected oriental beech twigs three weeks post-inoculation. Furthermore, the desired fragment was amplified in four oak symptomatic samples. Twigs injected with SDW resulted in no symptoms and negative PCR reactions.

Primer sensitivity

The sensitivity threshold of BgF3/R2 primer pair in the detection of *B. goodwinii*, as estimated by a 10-fold dilution in SDW of cell cultures of the strain UT-Bg 100 from the initial suspension having $OD_{600} = 0.1$ (containing 1×10^{11} CFU/mL) on NA (Merck, Germany, Darmstadt), was approximately 1×10^{6} CFU/mL (data not shown).

Discussion

Decline is described as decreasing health and vigor of forest trees incited by abiotic and biotic agents (Helms, 1998). Forest tree declines characterized by trunk bark necrosis and bleeding of a dark sticky fluid from the vertical cracks developed on the trunks have been increasing in prevalence and severity in the Alborz and Zagros forests of oak, walnut, and alder in Iran (Ahmadi et al., 2019; Bakhshi Ganje et al., 2020; Moradi-Amirabad and Khodakaramian, 2020; Allahverdipour et al., 2021; Bakhshi Ganje et al., 2021). In the present study, we characterized strains of *B. goodwinii* associated with oak and oriental beech trees; the latter was identified for the first time as a new host species impacted by *B. goodwinii*.

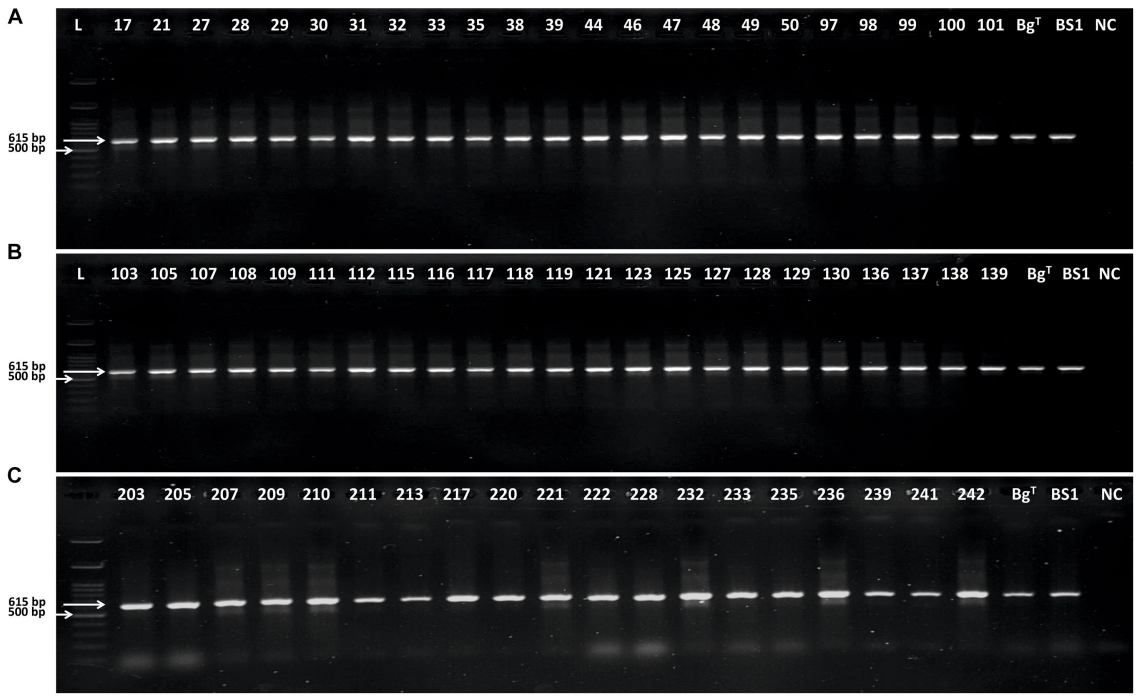

FIGURE 4
Gel electrophoresis analysis of polymerase chain reaction products amplified using BgF3/R2 primer pair. **(A)** L: 100 bp DNA Ladder Ready to Load (RT), Solis BioDyne, Tartu, Estonia;17–101: *Brenneria goodwinii* strains UT-Bg 17 to UT-Bg 101 isolated from oak; Bg^{T}: *B. goodwinii* FRB 141^{T}; BS1: *B. goodwinii* BS1; and NC: negative control. **(B)**: 103–129: B. *goodwinii* strains UT-Bg103 to UT-Bg 129 isolated from oak; Bg^{T}: *B. goodwinii* FRB 141^{T}; BS1: *B. goodwinii* BS1; and NC: negative control. **(C)**: 203–242: B. *goodwinii* strains UT-Bg203 to UT-Bg 242 isolated from oriental beech; Bg^{T}: *B. goodwinii* FRB 141^{T}; BS1: *B. goodwinii* BS1; NC: negative control.

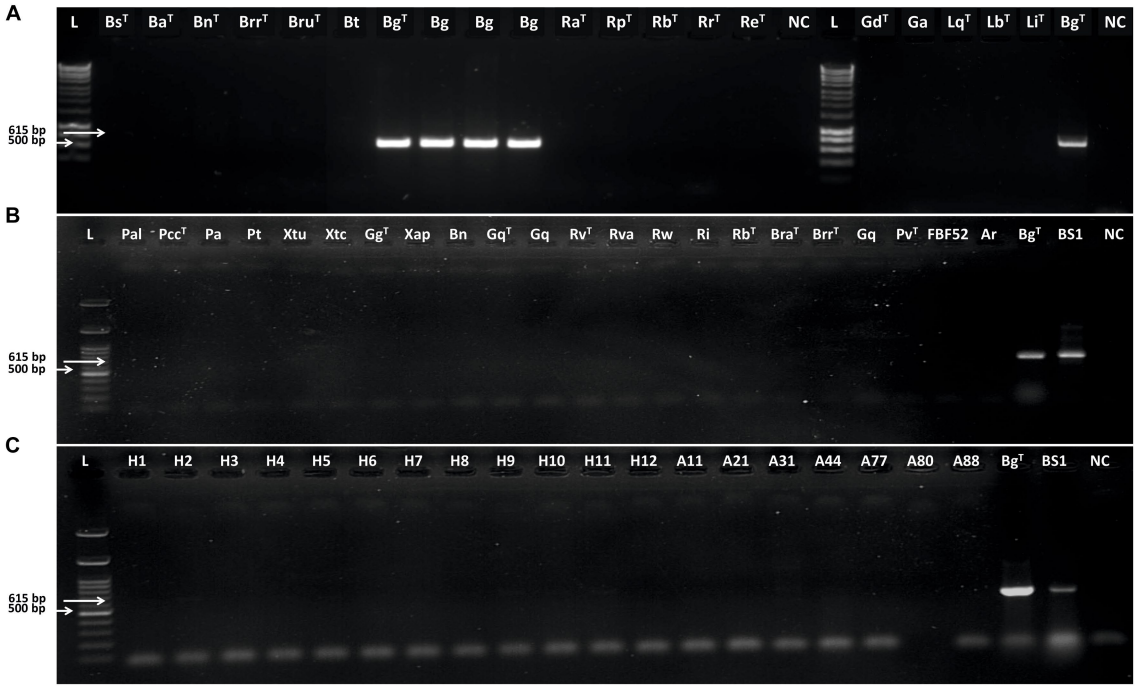

FIGURE 5
Gel electrophoresis analysis of polymerase chain reaction products amplified using BgF3/R2 primer pair. **(A)** L: Hyperladder 1 kb (Bioline); Bs^T: *Brenneria salicis* DSM 30166^T, Ba^T: *Brenneria alni* DSM 11811^T: Bn: *Brenneria nigrifluens* DSM 30175^T; Brr^T: *Brenneria roseae* ssp. *roseae* FRB 222^T; Br^T: *Brenneria rubrifaciens* DSM 4483^T; Bt: *Brenneria tiliae;* TWs2II: *Brenneria tiliae*; Bg^T; *Brenneria goodwinii* FRB 141^T; Bg1: *B. goodwinii* FRB 186; Bg2: *B. goodwinii* BAC 30–03-01;Bg3: *B. goodwinii* BAC 56e-01; Ra^T: *Rahnella aquatilis* LMG 2794^T; Rp^T: *Rahnella perminowiae* SL6^T; Rb^T: *Rahnella bonaserana* H11b^T; Rr^T: *Rahnella rivi* FC061912-K^T; Re^T: *Rahnella ecdela* FRB 231^T; NC: Negative Control; L: Hyperladder 1 kb (Bioline); Gd^T: *Gibbsiella dentisursi* DSM 23818^T; Ga: *"Gibbsiella acetica"* C22; Lq^T: *Lonsdalea quercina* LMG 2724^T; Lb^T: *Lonsdalea britannica* FRB 18^T; Li^T: *Lonsdalea iberica* 1915-14^T; Bg^T: *B. goodwinii* FRB 141^T; and NC: negative control. **(B)**: L: 100 bp DNA Ladder Ready to Load (RT), Solis BioDyne, Tartu, Estonia; Pal: *Pseudomonas amygdali* pv. *lachrymans*; Pcc^T: *Pectobacterium carotovorum* ATCC 15713; Pa: *Pantoea agglomerans* NK16; Pt: *Pseudomonas tolaasii* T7; Xtu: *Xanthomonas translucens* pv. *undulosa* ICMP 11055; Xtc: *X. translucens* pv. *cerealis* ICMP 5752; Gg^T: Gg: *Gibbsiella greigii* FRB 224^T; Xap: *X. arboricola* pv. *pruni*; Bn: *Brenneria nigrifluens* M2; Gq^T: Gq^T: *Gibbsiella quercinecans* FRB 97^T; Gq: *G. quercinecans* I2; Rv^T: *Rahnella victoriana* FRB 225^T; Rva: *Rahnella variigena* FOD 20.8; Rw^T: *Rahnella woolbedingensis* FRB 227^T; Ri: *Rahnella inusitata* FOD 9.5a; Rb: *Rahnella bruchi* FRB 226^T; Bra^T: *Brenneria roseae* subsp. *americana* FRB 223^T; Brr^T: *Brenneria roseae* subsp. *roseae* FRB 222^T; Gq: *G. quercinecans* KE1; *Pseudomonas viridiflava* ATCC 13223^T; FBF52: *P. viridiflava* FBF52; Ar: *Agrobacterium radiobacter* PK, Bg^T: *B. goodwinii* FRB 141^T; BS1: *B. goodwinii* BS1; and NC: negative control. **(C)**: L: 100 bp DNA Ladder Ready to Load (RT), Solis BioDyne, Tartu, Estonia; H1-H12: Strains isolated from healthy trees and seedlings; A11: *Bacillus* sp. A11; A21: *Enterobacter ludwigii* A21; A31: *Lysinibacillus* sp. A31; A44: *Pseudomonas putida* A44; A77: *Klebsiella* sp. A77; A80: *Serratia marcescens* A80; A88: *Stenotrophomonas maltophilia* A88; *B. goodwinii* FRB 141^T; BS1: *B. goodwinii* BS1; and NC: negative control.

Pathogenicity assay of isolated strains was performed on oak acorns according to González and Ciordia (2020), which was conducted for stains associated with forest tree decline symptoms. As the isolated pathogens and symptoms in oak and oriental beach trees were the same, pathogenicity assays of all strains were performed on oak acorns, and the results indicated that *B. goodwinii* strains, regardless of the host species, are pathogenic on oak acorns. Moreover, the pathogenicity of representative strains on the corresponding plant hosts showed that *B. goodwinii* strains cause necrosis and die-back on the host twigs.

In this study, bacterial colonies with a green metallic sheen on EMB-agar were consistently isolated from the oak and oriental beech trees displaying canker and stem bleeding symptoms in northern Iran. The strains were identified as *B. goodwinii* on the basis of their phenotypic characteristics, pathogenicity features, and sequences of 16S rRNA and *gyrB* genes. All strains plus the type strain and four other known strains of *B. goodwinii* were also detected by PCR, using the newly developed primer pair BgF3/R2, which targets the *hrpN* gene of *B. goodwinii*.

The decline and bleeding stem canker of beech in Europe and the United States are mostly caused by *Phytophthora* × *cambivora* (Jung et al., 2005, 2017). The disease is characterized by dark-colored bleeding areas, which usually appear near the collar, and occasionally, bleeding may be observed on the trunk. In this study, *B. goodwinii* was identified as associated with brown spots, tissue necrosis, and canker on the trunk of oriental beech. To the best of our knowledge, this is the first bacterial disease of oriental beech.

B. goodwinii, as a key species involved in characteristic weeping symptoms and live bark degradation, has a type 3 secretion system (T3SS) and associated harpins and effectors that could manipulate the host. The other two prevalent bacterial species, *G. quercinecans* and *R. victoriana* (Brady et al., 2017; Denman et al., 2018), mainly with enzyme-degrading plant cell walls, enhance or facilitate necrosis (Doonan et al., 2019).

Although identification of *B. goodwinii* by sequencing housekeeping genes is a robust and reliable method, it is also laborious and time-consuming. Here, we indicated that PCR using specific primers is a valuable, efficient, and less labor-intensive method for direct and culture-independent detection of *B. goodwinii* in forest trees, as well as its rapid and precise identification in samples or cultures. The designed PCR requires only a commercial DNA Polymerase Master Mix that is not expensive. Therefore, this protocol is easy to use in different laboratories, including those located in low-income countries. Moreover, the target gene was detected in PCR with DNA extracted directly and culture-independently using the alkalic procedure that is rapid and cheap. Regarding the increase in tree diseases in Iran, the development of specific primers could facilitate rapid identification of the pathogen.

Pathogenicity/virulence genes like *pth*, *hrp,* and *vir* of several other phytopathogenic genera and species were the most commonly used targets for designing primers specific for detection and identification of the phytopathogenic bacteria at the species or subspecies level by PCR (López et al., 2003). For instance, for designing specific primers *pel* (pectate lyase) genes are used for detecting *Pectobacterium* and *Dickeya* species (Darrasse et al., 1994; Louws et al., 1999). Designing primers from conserved regions of pathogenicity gene clusters could avoid non-specific amplicon production from non-pathogenic species or other pathogens. In this study, we used the *hrpN* gene in detecting *B. goodwinii* strains in oak and oriental beech bark samples. HrpN, encoded by *hrpN*, induces the hypersensitive response (HR) in resistant hosts and non-host plants, implying that the *hrp* genes may also be involved in host specificity (Yang et al., 2002; Holeva et al., 2004). These results indicated that the *hrpN* primer pair has both a high degree of sensitivity and specificity in detecting *B. goodwinii* from the bacterial strains belonging to the genera *Rahnella*, *Gibbsiella*, *Lonsdalea,* or other *Brenneria* species inciting decline on other forest trees. Moreover, this primer pair was able to detect *B. goodwinii* from symptomatic tissues. Thus, *hrpN* was determined to be useful as an appropriate target for the specific detection of *B. goodwinii* directly from infected or diseased tissues.

Data availability statement

The datasets presented in this study can be found in online repositories. The names of the repository/repositories and accession number(s) can be found in the article/supplementary material.

Ethics statement

This research does not contain any studies with human participants or animals performed by any of the authors.

Author contributions

M-HA: Investigation, Validation, Writing – review & editing, Funding acquisition. NC: Validation, Writing – review & editing, Conceptualization, Formal analysis, Investigation, Methodology, Project administration, Software, Supervision, Visualization, Writing – original draft. CB: Methodology, Validation, Writing – review & editing. HR: Conceptualization, Methodology, Writing – review & editing.

Funding

The author(s) declare financial support was received for the research, authorship, and/or publication of this article. This study was funded by University of Tehran (Grant numbers: 148605).

Acknowledgments

The authors thank Mohammad-Ali Mirhabibi and Mohammad Ashrafi for their help in performing the experiments.

Conflict of interest

The authors declare that they have no conflict of interest and the authors declare that the research was conducted in the absence of any commercial or financial relationships that could be construed as a potential conflict of interest.

Publisher's note

References

Ahmadi, E., Kowsari, M., Azadfar, D., and Salehi Jouzani, G. (2019). *Bacillus pumilus* and *Stenotrophomonas maltophilia* as two potentially causative agents involved in Persian oak decline in Zagros forests (Iran). *For. Pathol.* 49:12541. doi: 10.1111/efp.12541

Alavi, S. J., Ahmadi, K., Dormann, C. F., Serra-Diaz, J., and Nouri, Z. (2020). Assessing the dominant height of oriental beech (*Fagus orientalis* L.) in relation to edaphic and physiographic variables in the Hyrcanian forests of Iran. *Biotechnol. Agron. Soc. Environ.* 24, 262–273.

Allahverdipour, T., Shahryari, F., and Falahi Charkhabi, N. (2021). *Gibbsiella quercinecans* and *Brenneria roseae* subsp. *roseae* associated to the canker disease of walnut trees in northwestern Iran. *Eur. J. Plant Pathol.* 161, 783–797. doi: 10.1007/s10658-021-02359-9

Ayers, S. H., Rupp, P., and Johnson, W. T. (1919). A study of the alkali-forming bacteria in milk. *U. S. Dep. Agric. Bull.* 782, 1–39. doi: 10.5962/bhl.title.108233

Bakhshi Ganje, M., Mackay, J., Nicolaisen, M., and Shams-Bakhsh, M. (2021). Comparative genomics, pangenome and phylogenomic analyses of *Brenneria* spp., delineation of *Brenneria izadpanahii* sp. nov. *Phytopathology* 111, 78–95. doi: 10.1094/PHYTO-04-20-0129-FI

Bakhshi Ganje, M., Shams-Bakhsh, M., Mackay, J., and Rahimian, H. (2020). Identification and characterization of bacterial strains associated with diseased oak trees in northern Iran. *For. Pathol.* 50:12571. doi: 10.1111/efp.12571

Brady, C., Arnold, D., McDonald, J. E., and Denman, S. (2017). Taxonomy and identification of bacteria associated with acute oak decline. *World J. Microbiol. Biotechnol* 33:1. doi: 10.1007/s11274-017-2296-4

Brady, C., Asselin, J. A., Beer, S., Brurberg, M. B., Crampton, B., Venter, S., et al. (2022). Emended description of the genus Rahnella. *Int. J. Syst. Evol. Microbiol.* 72: p.005190. doi: 10.1099/ijsem.0.005190

Brady, C. L., Cleenwerck, I., Denman, S., Venter, S. N., Rodríguez-Palenzuela, P., Coutinho, T. A., et al. (2012). Proposal to reclassify *Brenneria quercina* (Hildebrand and Schroth 1967) Hauben et al. 1999 into a new genus, *Lonsdalea* gen. nov., as *Lonsdalea quercina* comb. nov., descriptions of *Lonsdalea quercina* subsp. *quercina* comb. nov., *Lonsdalea quercina* subsp. *iberica* subsp. nov. and *Lonsdalea quercina* subsp. *britannica* subsp. nov., emendation of the description of the genus *Brenneria*, reclassification of *Dickeya dieffenbachiae* as *Dickeya dadantii* subsp. *dieffenbachiae* comb. nov., and emendation of the comb. nov., and emendation of the description of *Dickeya dadantii*. *Int. J. Syst. Evol. Microbiol.* 62, 1592–1602. doi: 10.1099/ijs.0.035055-0

Brady, C., Cleenwerck, I., Venter, S., Vancanneyt, M., Swings, J., and Coutinho, T. (2008). Phylogeny and identification of *Pantoea* species associated with plants, humans and the natural environment based on multilocus sequence analysis (MLSA). *Syst. Appl. Microbiol.* 31, 447–460. doi: 10.1016/j.syapm.2008.09.004

Brady, C., Denman, S., Kirk, S., Venter, S., Rodríguez-Palenzuela, P., and Coutinho, T. (2010). Description of *Gibbsiella quercinecans* gen. Nov., sp. nov., associated with acute oak decline. *Syst. Appl. Microbiol.* 33, 444–450. doi: 10.1016/j.syapm.2010.08.006

Brady, C., Hunter, G., Kirk, S., Arnold, D., and Denman, S. (2014a). Description of *Brenneria roseae* sp. nov. and two subspecies, *Brenneria roseae* subspecies *roseae* ssp. nov and *Brenneria roseae* subspecies *Americana* ssp. nov. isolated from symptomatic oak. *Syst. Appl. Microbiol.* 37, 396–401. doi: 10.1016/j.syapm.2014.04.005

Brady, C., Hunter, G., Kirk, S., Arnold, D., and Denman, S. (2014b). *Rahnella victoriana* sp. nov., *Rahnella bruchi* sp. nov., *Rahnella woolbedingensis* sp. nov., classification of *Rahnella* genomospecies 2 and 3 as *Rahnella variigena* sp. nov. and *Rahnella inusitata* sp. nov., respectively and emended description of the genus. *Rahnella*. *Syst. Appl. Microbiol.* 37, 545–552. doi: 10.1016/j.syapm.2014.09.001

Brady, C., Hunter, G., Kirk, S., Arnold, D., and Denman, S. (2014c). Gibbsiella greigii sp. nov., a novel species associated with oak decline in the USA. *Syst. Appl. Microbiol.* 37, 417–422. doi: 10.1016/j.syapm.2014.07.002

Crampton, B. G., Plummer, S. J., Kaczmarek, M., McDonald, J. E., and Denman, S. (2020). A multiplex real-time PCR assay enables simultaneous rapid detection and quantification of bacteria associated with acute oak decline. *Plant Pathol.* 69, 1301–1310. doi: 10.1111/ppa.13203

Darrasse, A., Priou, S., Kotoujansky, A., and Bertheau, Y. (1994). PCR and restriction fragment length polymorphism of a *pel* gene as a tool to identify *Erwinia carotovora* in relation to potato diseases. *Appl. Environ. Microbiol.* 60, 1437–1443. doi: 10.1128/aem.60.5.1437-1443.1994

Day, W. R. (1924). *Watermark disease of the cricket-bat willow*. Oxford Forestry Memoirs. 3, 1–30.

Denman, S., Brady, C. L., Kirk, S., Cleenwerck, I., Venter, S. N., Coutinho, T. A., et al. (2012). *Brenneria goodwinii* sp. nov., associated with acute oak decline in the UK. *Int. J. Syst. Evol. Microbiol.* 62, 2451–2456. doi: 10.1099/ijs.0.037879-0

Denman, S., Doonan, J., Ransom-Jones, E., Broberg, M., Plummer, S., Kirk, S., et al. (2018). Microbiome and infectivity studies reveal complex polyspecies tree disease in acute oak decline. *ISME J.* 12, 386–399. doi: 10.1038/ismej.2017.170

Doonan, J., Denman, S., Pachebat, J. A., and McDonald, J. E. (2019). Genomic analysis of bacteria in the acute oak decline pathobiome. *Microb. Genom.* 5:e000240. doi: 10.1099/mgen.0.000240

Falahi Charkhabi, N., Shams-bakhsh, M., and Rahimian, H. (2010). Genetic diversity among *Brenneria nigrifluens* strains in Iran. *Eur. J. Plant Pathol.* 128, 303–310. doi: 10.1007/s10658-010-9667-0

González, A. J., and Ciordia, M. (2020). *Brenneria goodwinii* and *Gibbsiella quercinecans* isolated from weeping cankers on *Quercus robur* L. *Spain. Eur. J. Plant Pathol.* 156, 965–969. doi: 10.1007/s10658-019-01891-z

Helms, J. A. (1998). *The dictionary of forestry*. Bethesda, MD: The Society of American Foresters. 210.

Holeva, M. C., Bell, K. S., Hyman, L. J., Avrova, A. O., Whisson, S. C., Birch, P. R., et al. (2004). Use of a pooled transposon mutation grid to demonstrate roles in disease development for *Erwinia carotovora* subsp. *atroseptica* putative type III secreted effector (DspE/A) and helper (HrpN) proteins. *Mol. Plant Microbe Interact.* 17, 943–950. doi: 10.1094/MPMI.2004.17.9.943

Hu, B. (2012). *Origin of strain: C22 Exudate of pear tree*. China.

Izard, D., Gavini, F., Trinel, P. A., and Leclerc, H. (1979). *Rahnella aquatilis*, nouveau membre de la famille des Enterobacteriaceae. *Ann. Microbiol.* 130, 163–177.

Jung, T., Hudler, G. W., Jensen-Tracy, S. L., Griffiths, H. M., Fleischmann, F., and Osswald, W. (2005). Involvement of *Phytophthora* species in the decline of European beech in Europe and the USA. *Mycologist* 19, 159–166. doi: 10.1017/S0269-915X(05)00405-2

Jung, T., Jung, M. H., Cacciola, S. O., Cech, T., Bakonyi, J., Seress, D., et al. (2017). Multiple new cryptic pathogenic *Phytophthora* species from Fagaceae forests in Austria, Italy and Portugal. *IMA Fungus* 8, 219–244. doi: 10.5598/imafungus.2017.08.02.02

Kile, H., Arnold, D., Allainguilaume, J., Denman, S., and Brady, C. (2022). *Brenneria tiliae* sp. nov., isolated from symptomatic *Tilia*× *moltkei* and *Tilia*× *europaea* trees in the UK. *Int. J. Syst. Evol. Microbiol.* 72:5515. doi: 10.1099/ijsem.0.005515

Kumar, S., Stecher, G., Li, M., Knyaz, C., and Tamura, K. (2018). MEGA X: molecular evolutionary genetics analysis across computing platforms. *Mol. Biol. Evol.* 35, 1547–1549. doi: 10.1093/molbev/msy096

Lane, D. J. (1991). "16S/23S rRNA sequencing" in *Nucleic acid techniques in bacterial systematics*. ed. E. G. M. Stackebrandt (New York: John Wiley & Sons, Inc.), 115–176.

López, M. M., Bertolini, E., Olmos, A., Caruso, P., Gorris, M. T., Llop, P., et al. (2003). Innovative tools for detection of plant pathogenic viruses and bacteria. *Int. Microbiol.* 6, 233–243. doi: 10.1007/s10123-003-0143-y

Louws, F. J., Rademaker, J. L. K., and de Bruijn, F. J. (1999). The three ds of PCR-based genomic analysis of phytobacteria: diversity, detection, and diagnosis. *Annu. Rev. Phytopathol.* 37, 81–125. doi: 10.1146/annurev.phyto.37.1.81

Manion, P. D. (1991). *Tree disease concepts (no. 634.963 M278 1991)*. Hoboken: Prentice Hall.

Moradi-Amirabad, Y., and Khodakaramian, G. (2020). First report of bleeding canker caused by sp. on *Populus nigra* in Iran. *New Dis. Rep.* 41:37. doi: 10.5197/j.2044-0588.2020.041.037

Moradi-Amirabad, Y., Rahimian, H., Babaeizad, V., and Denman, S. (2019). *Brenneria* spp. and *Rahnella victoriana* associated with acute oak decline symptoms on oak and hornbeam in Iran. *For. Pathol.* 49:12535. doi: 10.1111/efp.12535

Niemann, S., Pühler, A., Tichy, H. V., Simon, R., and Selbitschka, W. (1997). Evaluation of the resolving power of three different DNA fingerprinting methods to discriminate among isolates of a natural *Rhizobium meliloti* population. *J. Appl. Microbiol.* 82, 477–484. doi: 10.1046/j.1365-2672.1997.00141.x

Ruffner, B., Schneider, S., Meyer, J., Queloz, V., and Rigling, D. (2020). First report of acute oak decline disease of native and non-native oaks in Switzerland. *New Dis. Rep.* 41, 18–5197. doi: 10.5197/j.2044-0588.2020.041.018

Saito, M., Shinozaki-Kuwahara, N., and Takada, K. (2012). *Gibbsiella dentisursi* sp. nov., isolated from the bear oral cavity. *Microbiol. Immunol.* 56, 506–512. doi: 10.1111/j.1348-0421.2012.00464.x

Sangüesa-Barreda, G., Camarero, J. J., Oliva, J., Montes, F., and Gazol, A. (2015). Past logging, drought and pathogens interact and contribute to forest dieback. *Agric. For. Meteorol.* 208, 85–94. doi: 10.1016/j.agrformet.2015.04.011

Schaad, N. W., Jones, J. B., and Chun, W. (2001). *Laboratory guide for the identification of plant pathogenic bacteria (No. Ed. 3)*. St. Paul, MN: American Phytopathological Society (APS Press).

Stackebrandt, E., and Liesack, W. (1993). "Nucleic acids and classification" in *Handbook of new bacterial systematics*. eds. M. Goodfellow and A. G. O'Donnell (London, England: Academic Press)

Surico, G., Mugnai, L., Pastorelli, R., Giovannetti, L., and Stead, D. E. (1996). *Erwinia alni*, a new species causing bark cankers of alder (*Alnus* miller) species. *Int. J. Syst. Evol. Microbiol.* 46, 720–726. doi: 10.1099/00207713-46-3-720

Suslow, T. V., Schroth, M. N., and Isaka, M. (1982). Application of a rapid method for gram differentiation of plant pathogenic and saprophytic bacteria without staining. *Phytopathology* 72:917. doi: 10.1094/Phyto-72-917

Thompson, J. D., Higgins, D. G., and Gibson, T. J. (1994). CLUSTAL W: improving the sensitivity of progressive multiple sequence alignment through sequence weighting, position-specific gap penalties and weight matrix choice. *Nucleic Acids Res.* 22, 4673–4680. doi: 10.1093/nar/22.22.4673

Tkaczyk, M., Celma, L., Ruņģis, D. E., and Bokuma, G. (2021). First report of *Brenneria goodwinii* and *Gibbsiella quercinecans* bacteria, detected on weaken oak trees in Poland. *Balt. For.* 27:563. doi: 10.46490/BF563

Wilson, E. E., Starr, M. P., and Berger, J. A. (1957). Bark canker, a bacterial disease of the Persian walnut tree. *Phytopathology* 47, 669–673.

Wilson, E. E., Zeitoun, F. M., and Fredrickson, D. L. (1967). Bacterial phloem canker, a new disease of Persian walnut trees. *Phytopathology* 57, 618–621.

Yang, C. H., Gavilanes-Ruiz, M., Okinaka, Y., Vedel, R., Berthuy, I., Boccara, M., et al. (2002). *Hrp* genes of *Erwinia chrysanthemi* 3937 are important virulence factors. *Mol. Plant-Microbe Interact.* 15, 472–480. doi: 10.1094/MPMI.2002.15.5.472

Zalkalns, O., and Celma, L. (2021). The distribution of bacteria *Gibbsiella quercinecans* and *Brenneria goodwinii* in oak (*Quercus robur* L.) stands in Latvia. In IOP Conference Series: Earth and Environmental Science.

frontiers | Frontiers in Forests and Global Change

TYPE Original Research
PUBLISHED 04 June 2024
DOI 10.3389/ffgc.2024.1376465

OPEN ACCESS

EDITED BY
Quan Lu,
Chinese Academy of Forestry, China

REVIEWED BY
Jana Albrechtova,
Charles University, Czechia
Zheng Wang,
Shandong Agricultural University, China

*CORRESPONDENCE
Ivana Tomášková
✉ tomaskova@fld.czu.cz

RECEIVED 25 January 2024
ACCEPTED 03 May 2024
PUBLISHED 04 June 2024

CITATION
Pastierovič F, Čepl J, Kalyniukova A, Mogilicherla K, Hradecký J, Bláha J and Tomášková I (2024) Time is of the essence: unveiling the rapid response of *Populus* to insect feeding.
Front. For. Glob. Change 7:1376465.
doi: 10.3389/ffgc.2024.1376465

Time is of the essence: unveiling the rapid response of *Populus* to insect feeding

Filip Pastierovič[1], Jaroslav Čepl[1], Alina Kalyniukova[1], Kanakachari Mogilicherla[1,2], Jaromír Hradecký[1], Jaromír Bláha[1] and Ivana Tomášková[1]*

[1]Faculty of Forestry and Wood Sciences, Czech University of Life Sciences, Prague, Czechia, [2]ICAR-Indian Institute of Rice Research (IIRR), Hyderabad, India

Plant metabolism response to insect herbivores is the central theme of this publication. Genetically uniform individuals of European aspen (*Populus tremula*) were exposed to recurrent feeding by spongy moths (*Lepidoptera*) at specific time intervals. Changes in physiology, contents of phenolics and saccharides were quantified over the first hour. The unconventional experiment design, integrating analytical methods, and timeline led to the revealing of unexpected dynamics in plant metabolism. The time interval between herbivory initiation and sample collection revealed a pivotal moment, with induced defense activating strongly after 5 min of chewing resulting in an increase in catechin and procyanidin B1. After 10 min, a shift to a tolerant strategy occurs and induced substance concentrations return to control levels. Delayed physiological response was recorded as the first significant difference in transpiration between affected and nonaffected plants and was found after 10 min. A different strategy in exploitation of saccharides after spongy moths infestation was applied because the pool of selected saccharides was rising in the leaves but decreasing in the roots. Placing our results in the context of existing knowledge highlights the uncertain conceptual basis behind the often rigid and definitive classifications in induced plant defense or tolerance strategy.

KEYWORDS

induced defense, net photosynthesis, phenolics, resource allocation, spongy moth, transpiration

Introduction

From a paleontological perspective, the origins of interactions between taxonomic kingdoms of plants (*Plantae*) and animals (*Animalia*), specifically within the phylum *Arthropoda*, extend back to the geological period of the early Devonian, as evidenced by findings in the studies of Labandeira (2007, 2013) and Fürstenberg-Hägg et al. (2013). The early Devonian period is defined by a temporal interval ranging from approximately 397 to 407 million years ago (Gerrienne et al., 2011). While phytophagous insect species, during the course of this coevolutionary relationship, adapted to exploit their host plants, plants simultaneously developed defense systems in response to herbivore attacks (Anderson and Mitchell-Olds, 2010; Johnson, 2011).

Insect herbivory triggers a cascade of processes occurring in plant tissues that can be qualified and quantified. When insects interact with plants, there is an induction of: defense proteins (Haruta et al., 2001; Fürstenberg-Hägg et al., 2013; War et al., 2021); volatile organic

compounds (Holopainen and Gershenzon, 2010; Rosenkranz and Schnitzler, 2016); secondary metabolites (Smith, 2007; Wink, 2018; Khare et al., 2020); changes in gene expression (Vogel et al., 2014; Birnbaum and Abbot, 2020); changes in the level of photosynthesis and gas exchange (Garcia and Eubanks, 2018); and substance transport and resource allocation (Gomez et al., 2012; Schultz et al., 2013).

The outcome of hundreds of millions of years of coevolution between insects and plants suggests that both participants have equipped themselves with the ability for rapid temporal response. Decisions made by insects in selecting a host plant occur on a time scale of tens to hundreds of milliseconds (Bruce and Pickett, 2011). Moreover, scent plumes with an uneven structure, encounter the chemical molecules of the plants only for fractions of a second (Webster et al., 2010). However, the range of descriptions of plant responses to herbivory over time is limited. Insect herbivory in plant tissues causes the accumulation of reactive oxygen species and changes in Ca^{2+} concentrations in the cytoplasm, thereby triggering a chain of defense reactions (Pandey et al., 2000; Medvedev, 2005). The earliest is a change in membrane potential at the plasma membrane, immediately followed by changes in intracellular Ca^{2+} concentration and H_2O_2 formation. Within minutes, the kinases and phytohormones jasmonic acid (JA) and salicylic acid (SA) are detectable and gene activation and subsequent metabolic changes are first noticeable after about 1 h (Maffei et al., 2007).

The focal point of any discussion on carbon allocation in response to herbivory is photosynthesis, which serves as the primary source of nearly all saccharides in green plants (Zhou et al., 2015). Although the impacts of herbivory on photosynthetic efficiency are generally perceived as negative (reducing efficiency), a relatively recent meta-analysis (Garcia and Eubanks, 2018) identified 67 plant species that exhibit a certain degree of overcompensation in response to insect herbivory. Additionally, arguments advocating the implementation of management strategies to enhance market yield using insect herbivores are documented (Poveda et al., 2013, 2017). Spongy moth (*Lymantria dispar*) caterpillars have a substantial impact on the net photosynthetic rate (Pn) of poplar (*Populus* sp.) leaves and these attacks lead to reduced photosynthetic activity due to extensive defoliation, ultimately resulting in a decrease in the leaf area available for photosynthesis (Zhang et al., 2022). Hindering of stomatal conductance (Gs) and transpiration (Tr) can potentially disrupt the equilibrium between water loss and carbon dioxide absorption, and this not only impacts the water-use efficiency of poplar trees but also affects their overall physiological performance (Pilipoviš et al., 2015). Nevertheless, the response in Pn to a chewing insect is a dynamic process depending on the scale of damage. Even moderate feeding with removing of 10% of the leaf area results in 12% Pn reduction in oak (*Quercus* sp.) (Copolovici et al., 2017). Intracellular CO_2 concentration (Ci) increases slightly in oak leaves in response to moth chewing even though Gs decreased about 50% similarly to Pn (Copolovici et al., 2017).

As Delaney (2008) points out, many studies have focused on whole plant processes and fewer studies have included analysis of changes at the physiological level – i.e. gas exchange, photosynthetic changes. According to the studies of Visakorpi et al. (2020) and Fyllas et al. (2022), a combination of several analytical approaches appears to be logically consistent for further revealing the metabolic responses of plants to the attacks of insect herbivores. Gomez et al. (2012) contribute valuable insights into the complex relationships within the primary metabolism of both aboveground and belowground plant components, emphasizing critical aspects of resource allocation essential for plant resistance and tolerance. Primary metabolism assumes a key role in plant resistance and tolerance, closely linked to the efficiency of the formation of defense substances (constitutive defense/induced defense). This link arises from the fact that products of primary metabolism, namely amino acids and saccharides, act as precursors and substrates for the biosynthesis of defense metabolites (Hanik et al., 2010a). An approach describing the dynamics of physiological and biochemical traits over time during herbivore feeding is still missing because, as it is well known, plant-insect interactions are both dynamic processes.

The research's uniqueness of the present study stems from exploring the interplay between biochemical and physiological responses, primary and secondary metabolism, specifically within the initial hour following an insect attack. By concentrating on the timing of these responses, we aim to offer a comprehensive understanding of the complex interactions between European aspen (*Populus tremula*) and polyphagous spongy moth (*Lymantria dispar*).

Materials and methods

Plant material

For the minimization of genotype influence and standardization of experimental conditions, genetically uniform individuals of *Populus tremula* produced through somatic embryogenesis were employed. *Populus tremula* seeds were selected as the starting plant material for the experiment. The seeds were obtained through controlled crossing of parent trees aged 40–50 years, located in the Czech Republic, specifically in Sušice (Svatobor) and Krušné hory (Fláje). The controlled crossing took place in early spring 2019. Within 5–7 days after seed collection, the seed material was utilized for *in vitro* propagation. A total of 218 seedlings sprouted and, out of them, individual number 22 was chosen due to its superior performance in *in vitro* culture.

Seeds of *P. tremula* were washed in 200 mL distilled water with 1–2 drops of Tween 20® for 10–15 min, then sterilized in 0.1% HgCl2 for 6 min. After rinsing, seeds were placed in jars with Murashige and Skoog (MS) medium solidified with Danish® agar and supplemented with myo-inositol and 6-benzylaminopurine (BAP). The pH-adjusted medium was autoclaved, and explants were cultivated under 16/8 h light/dark with a temperature of 22 ± 1 / 20 ± 1°C. Germination occurred within 1–3 weeks. Shoots were subcultured every 2–3 weeks until sufficient material was obtained. *In vitro* rooting was done on segments with at least three buds using half-strength MS medium supplemented with indole-3-butyric acid (IBA). Roots developed after about 4 weeks, and after 6–8 weeks, rooted shoots were transferred *ex vitro*. Rooted shoots were washed and transferred to sterile substrate in plastic pots, treated with Previcur Energy®, and cultivated under controlled conditions. Humidity was gradually decreased, and plants were fertilized bi-weekly during growth. Forty elite individuals were selected from the genetically uniform *in vitro* culture based on phenotypic characteristics. These plants were transplanted into round flowerpots with a diameter and height of 20 cm each during the transfer from *in vitro* to *ex vitro* conditions at the somatic

embryogenesis laboratory. The soil was prepared by sterilizing the substrate through steam treatment, and the plants were then placed into growth chambers. A specialized commercial mixture for sowing and growing plants was used as the soil substrate. The mixture is carefully formulated from a blend of selected light and dark peat, adjusted to achieve the desired pH level. Perlite is then added as an additional component. Furthermore, this substrate is enriched with a comprehensive range of essential and trace nutrients by adding fertilizers (Forestina, Czech Republic). The start of the experiment took place when the plants reached the age of 6 months, the leaves were fully mature and the individuals were approximately 1.2 m high. Throughout the duration of the experiment, all *Populus* individuals showed good health and growth was observable.

Insect breeding

The collection of spongy moths (*Lymantria dispar*) was delivered by Institute of Forest Entomology, Forest Pathology and Forest Protection at the University of Natural Resources and Life Sciences, Vienna from sterile laboratory cultures. Upon hatching, the larvae were provided with a nutritionally balanced agar diet (*Lymantria dispar* agar, Southland products Inc., United States) in sterile Petri dishes.

Lymantria dispar eggs were placed in sterile Petri dishes in a climatic chamber with a day and night regime (12 h dark/12 h light) with a temperature oscillation during the day of 24°C and a drop to 20°C at night. The moment the eggs started to hatch into caterpillars, they were given nutritionally balanced boiled agar. Once every 2–3 days, the caterpillars were transferred to new, clean Petri dishes in a sterile environment.

In the experiment, caterpillars were used after the fourth molting. To enhance feeding activity, they were incubated in darkness and deprived of food for 48 h, considering their nocturnal behavior (Hajek, 2001).

Experimental facility

For increased reproducibility and comparability of results, standardization of experimental conditions was implemented using growth chambers: Step-In FytoScope FS-SI (Photon Systems Instruments, Drasov, Czech Republic). The growth chambers were set to simulate optimal environmental conditions, including a humidity level of 75%, an average Photosynthetic Photon Flux Density of 250 $\mu mol.m^2.s^{-1}$, a CO_2 concentration of 420 ppm, and a light–dark cycle of 2 h of dawn, 10 h of light, 2 h of twilight, and 10 h of darkness.

An Agilent 1,290 Infinity II (Agilent, USA) liquid chromatography system coupled with an Agilent 6,546 LC/MS quadrupole time-of-flight (qTOF) system (Agilent, USA) was used for non-volatile compounds analysis.

For gasometrical measurement, an open portable photosynthesis system with an infrared gas analyzer LI-6400 XT (LICOR, Lincoln, NE, USA) was used. The light of 1,500 $\mu mol.m^{-2}\ s^{-1}$ overlapping the point of light saturation (usually round 450 $\mu mol.m^{-2}\ s^{-1}$) has been measured to obtain a net photosynthetic rate (Pn), transpiration (Tr), stomatal conductance (Gs), and internal-to-ambient CO_2 concentration ratio (Ci/Ca). The measurement referred to the ambient CO_2 concentration of 420 $\mu mol.m^{-2}\ s^{-1}$. A standard leaf chamber with a red/blue LED light source was used. The samples were taken from 11 am to 2 pm. Measurements were performed inside the chamber so as not to change microclimatic conditions.

Experimental design

Out of the initial pool of 40 individuals, which underwent a 6-month incubation period under optimal conditions in the growth chamber, the top 20 elite individuals were chosen for the experiment. For clarity in understanding the methodology, the experiment design (Figure 1) and procedures will be detailed for a single individual plant among the selected 20. The experimental framework drew on previous research such as the work of Boeckler et al. (2013) and Stevens and Lindroth (2005), which provided empirical support for the chosen approach.

The biochemical response of the *Populus* tree was investigated at four time moments in the first 60 min of moth caterpillar insects feeding on one individual poplar leaf. In the first phase, the selected individual was isolated for 10 days after selection (Figure 1), in order to stabilize the stress reactions to handling. Subsequently, measurements were conducted on a specific fully mature leaf located in the midsection of the trunk, using an open gasometric system. The spongy moths were put on the leaf using aseptic entomological tweezer from the Petri dishes and after chewing in individual time segments removed back from the leaf. The investigated leaves were always under the full sunlight with defined light in the growth chambers (LI-6400 XT). Immediately after the measurement, the leaf was aseptically cut with sterile scissors and placed in a sterile 50 mL test tube, which was pre-frozen in a liquid nitrogen bath. After closing the falcon tube in which the leaf was inserted, it was immediately placed in a bath of liquid nitrogen. This was followed by a 10-day rest period, allowing the metabolism to stabilize after leaf cutting.

In the second phase, another leaf of comparable quality and age was selected, and three spongy moths individuals were introduced. The precise moment of the first bite was recorded, and after 5 min of continual feeding, the caterpillars were removed. The leaf was promptly sealed in the LI-6400 XT measurement chamber. Gas exchange was assessed on intact leaves via a chamber measuring 2×3 cm, capturing CO_2 uptake from the entire area. The leaf completely filled the chamber area to ensure accurate gas exchange measurements. Following completion of measurements, the leaf was cut with sterile scissors and immediately placed in a 50 mL test tube, subsequently stored in liquid nitrogen. Another 10-day period was granted to restore metabolic homeostasis. In order to eliminate the influence of the circadian rhythm of the plants, the collection of samples was always carried out at the same time of a day (i.e., from 11 am to 2 pm) at an interval of 3 h.

Subsequent stages replicated the entire process, with the only variation being the measurement time, set at 5, 10, 30, and 60 min from the first bite.

In the final step, root samples were obtained from the designated individual, both as a control and after 60 min of feeding. Throughout, the methodology was strictly followed to ensure active caterpillar feeding and their presence on the selected leaf. This procedural approach was consistently applied to all selected individuals and in all time segments. Throughout the experiment, everything was done in a

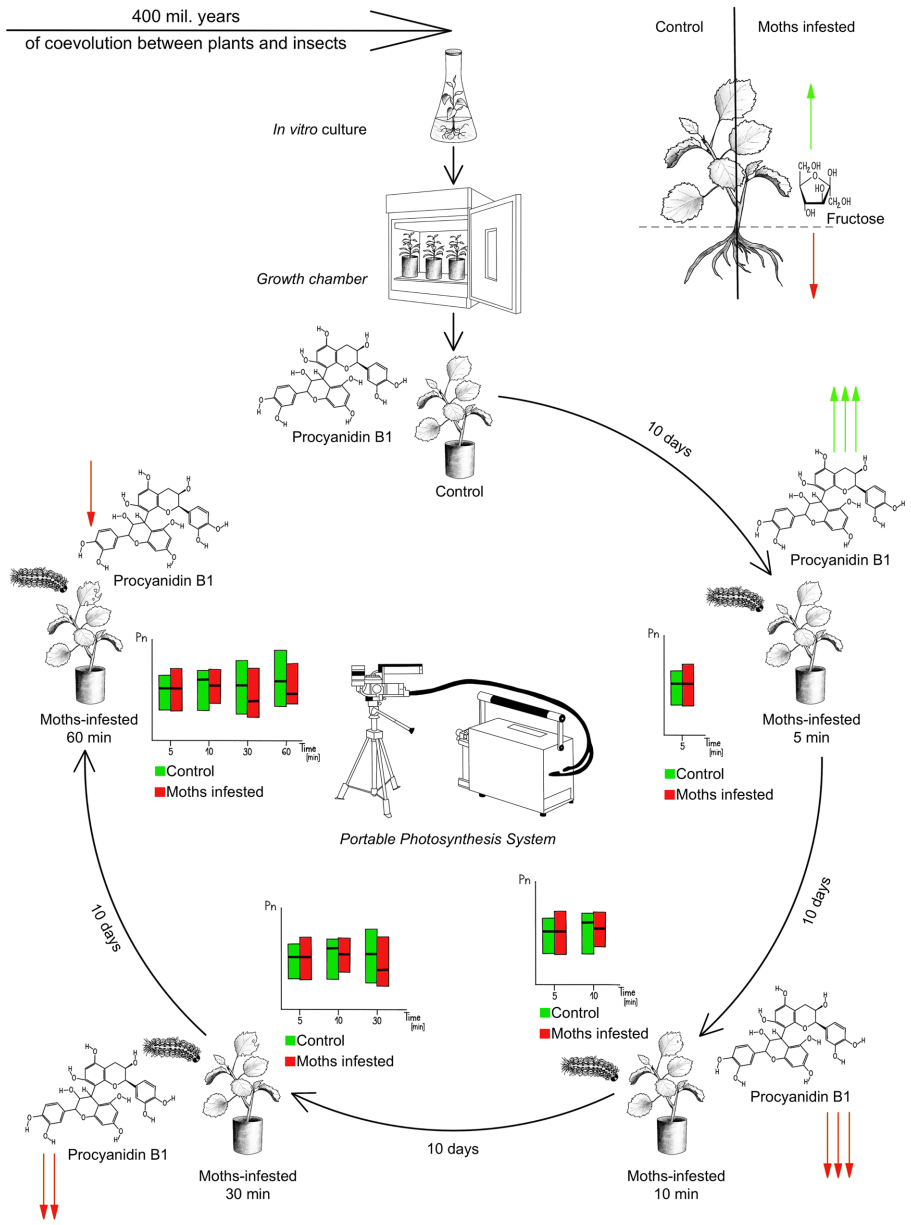

FIGURE 1
Experimental design. Genetically uniform poplar seedlings from *in vitro* culture were transplanted into pots and maintained under controlled conditions. The cycle of one plant within the experiment is shown. Early events in plant metabolism were investigated in time segments after 5, 10, 30, 60 min continuous feeding of *Lymantria dispar*. There were 10-day intervals between individual segments for plant recovery. Green arrows and their number graphically show the rate of increase in concentration, red arrows show the decrease in procyanidin B1 concentration over time.

growth chambers environment to eliminate the effect of handling the plant or the effect of different spectral composition of light on the plant. A total of 4 growth chambers were used, which were appropriately combined in order to eliminate the influence of intraspecific chemical communication between poplars. Before starting the laboratory work, the samples were stored in a −80°C cooling box.

For root saccharides analysis, roots were collected simultaneously with leaf control samples. Each plant was carefully removed from its pot, and approximately 50 mg of roots of various sizes were collected using sterile scissors. Following collection, the roots were promptly washed in demineralized water and stored in a microtube in liquid nitrogen for immediate preservation. The root samples were processed in the same way when the sample was harvested after 60 min of continuous feeding, when the leaf was harvested first and then the roots.

Chemical analysis

Extraction of phenolic compounds in leaves

A freeze-dried and homogenized sample (10 mg) was placed into a test tube, followed by the addition of 0.5 mL of 70% chilled methanol. After vortexing for 30 s, the test tube was then immersed in an

ultrasonic bath with ice for a duration of 10 min. The resultant solution was centrifugated at 13,000 rpm and 4°C for 10 min. Prior to LC–MS-qTOF analysis, the supernatant was filtered using a 0.22 µm PTFE filter. After 5 µL in concentration of 25 µg mL^{-1} of internal standard indole 3-acetic acid was added. All sample handling procedures were conducted on ice. The prepared samples were stored at a temperature of −80°C.

Extraction procedure for determination of saccharides in leaves and roots

Freeze-dried homogenized sample (30 mg) was introduced into a 2-mL test tube, and 1.5 mL of methanol:water (80:20 v/v) was added. The tube was vortexing and placed into a thermoshaker for 30 min at 50°C and 1,000 rpm. Then, the samples underwent centrifugation at 12,500 rpm for 10 min. The resulting supernatant was carefully collected and subsequently filtered through a PVDF syringe filter (0.22 µm) prior to LC-qTOF-MS/MS analysis (Šulc et al., 2021).

LC-qTOF-MS/MS saccharides analysis in leaves and roots

Saccharides analysis was performed on Agilent 1,290 Infinity II liquid chromatography system, coupled with an Agilent 6,546 LC/MS quadrupole time-of-flight (qTOF) detector (Agilent, USA). for LC-qTOF-MS/MS analysis. Chromatographic separation was executed on a Supel Co apHera NH^2 Polymer column (150×2 mm, 5 µm) maintained at 30°C. The mobile phase consisted of acetonitrile (A) and water (B). The gradient elution started at 80:20 (A:B) for the mobile phase, transitioning to 55:45 (A:B) from 0.5 to 13 min, and returning to 80:20 (A:B) from 14 to 15 min, at a flow rate of 0.2 mL min^{-1}. The injection volume was set to 1 µL. The system operated in negative ionization mode (Madsen et al., 2015).

Optimized QTOF parameters, established using glucose, sucrose, fructose, and mannitol standards, were as follows: scan range of 100–1,000 m/z, drying gas temperature of 280°C, sheath gas flow rate at 12.0 L/min, sheath gas temperature of 400°C, capillary voltage set to 2.0 kV, fragmentor at 120 V, and collision energy at 10, 20, and 40 eV. MS/MS data were acquired within a scan range of 50–800 m/z. Throughout the analysis, reference masses at 112.9855 m/z and 922.0098 m/z were continuously monitored for mass correction. Agilent Mass Hunter Acquisition software was employed for data collection, while Qualitative Analysis 10.0 and Q-TOF Quantitative analysis tools were utilized for data analysis (Madsen et al., 2015). External calibration curves using standards of target compounds (fructose, glucose, sucrose and mannitol) were used for quantification.

LC-qTOF-MS/MS analysis of polyphenolic compounds in leaves

The same instrument was used for phenolics analysis as in the case of saccharide analysis, but with Zorbax Eclipse Plus C18 column (2.1×50 mm, 1.8 µm) (Agilent, United States). Mobile phase A contained 0.05% formic acid, while mobile phase B consisted of acetonitrile. The gradient elution protocol was as follows: 0–0.1 min, 95% A; 0.1–8 min, 72% A; 8–9.1 min, 25% A; 9.1–11 min, 95% A. The mobile phase flowed at a rate of 1.1 mL min^{-1}, and the column temperature was maintained at 35°C. A 1 µL injection volume was used, and the system was operated in negative ionization mode.

Prior to analysis, qTOF parameters were optimized using standards. The qTOF parameters were set as follows: scan range of 100–1,000 m/z; drying gas temperature of 350°C; sheath gas flow rate at 12.0 L min-1; sheath gas temperature of 400°C; capillary voltage set to 5.0 kV; nozzle voltage at 0.9 kV; fragmentor set to 140 V; collision energy set at 10, 20, and 40 eV. MS/MS data were acquired within a scan range of 50–800 m/z, with a retention time window of 0.5 min, an isolation window of 1.3 amu, and an acquisition rate of 2 spectra per second. Throughout the analysis, reference masses of 112.9855 m/z and 966.0007 m/z were continuously monitored for mass correction.

Agilent Mass Hunter Acquisition software was used for data collection, while data analysis was performed using Mass Hunter Qualitative Analysis 10.0 and Q-TOF Quantitative analysis tools (Agilent, USA). External calibration curves using standards of target compounds (catechin. Epigallocatechin, ferulic acid, chlorogenic acid, procyanidin B1, gallic acid, rutin, kaempferol, quercetin, taxifolin) were used for quantification.

Statistical analysis

For the statistical analyses and data visualization, R statistical software (R Core Team, 2021) was used.

Since a single plant was measured multiple times, paired t-test and linear mixed models for repeated measures were employed.

Saccharides from roots were analyzed using paired t-test (as default by *t.test* function from R's stat package).

Linear mixed models were fitted using ASReml-R v4.1. For gasometry data, the fixed effects were specified as:

$$\sim \boldsymbol{Time} + Treatment + \boldsymbol{Time} : Treatment$$

where *Time* has 4 levels of 5 min, 10 min 30 min and 60 min of infestation and Treatment has two levels: infested and control.

Random factors were specified in a model as:

$$\sim IDplant + IDplant \boldsymbol{: Time}$$

Where ID_{plant} has 20 levels for each plant.

For each *Time:Treatment* combination, mean values, standard errors, and significance for pairwise comparison were extracted using predictPlus function form asremlPlus package. *p*-values were then adjusted using the false discovery rate method. The effect size of differences was calculated using Cohen's *d* approach (difference of means divided by pooled standard deviation; so $d = 1$ means that means are 1 standard deviation apart).

Residuals were checked for normality and constancy of variances.

For phenolic compounds the fixed effects were specified as:

$$\sim Time$$

where *Time* has five levels of 0 (pre-infestation control), 5 min, 10 min, 30 min, and 60 min of infestation.

Repeated measures were tackled specifying heterogenous correlation in residuals specifying:

$$residual = \sim id\left(IDplant\right) : corgh\left(\boldsymbol{Time}\right)$$

Where ID_{plant} has 20 levels for each plant.

Again, the significance for pairwise comparison was extracted using predictPlus function form asremlPlus package. p-values were then adjusted using FDR method. Effect size of differences was calculated using Cohen's d approach.

Results

In leaves, the concentration of fructose and glucose together with mannitol rose in moth-infested treatment in comparison to the control during the whole investigated period of 60 min. The concentration of sucrose – the most important saccharide - did not change in the investigated period and reached 253 ± 13 μg/g in moth-infested treatment and 238 ± 49 μg/g in the control group (Figure 2). Excluding sucrose, the differences between the control and moth-infested treatment were statistically significant from 10 min for glucose and mannitol. The concentrations of both monosaccharides were 5x higher after 60 min of chewing than in the control group. These shifts indicate possible saccharides transport between the roots and leaves.

Regarding the response of root sugar concentrations to hourly feeding by spongy moths, the results are shown in the graph (Figure 3). Sugars involved in the fructose and mannose metabolic pathway (namely glucose, fructose, and mannitol) showed a consistent pattern. Specifically, root fructose concentration significantly decreased from the control level of 66 ± 35 μg/g after feeding to 33 ± 23 μg/g, reflecting a reduction to 49% of the control value. Glucose showed an 85% decrease from the original concentration in the moth-infested treatment, while mannitol decreased to 87.5% of its concentration. In

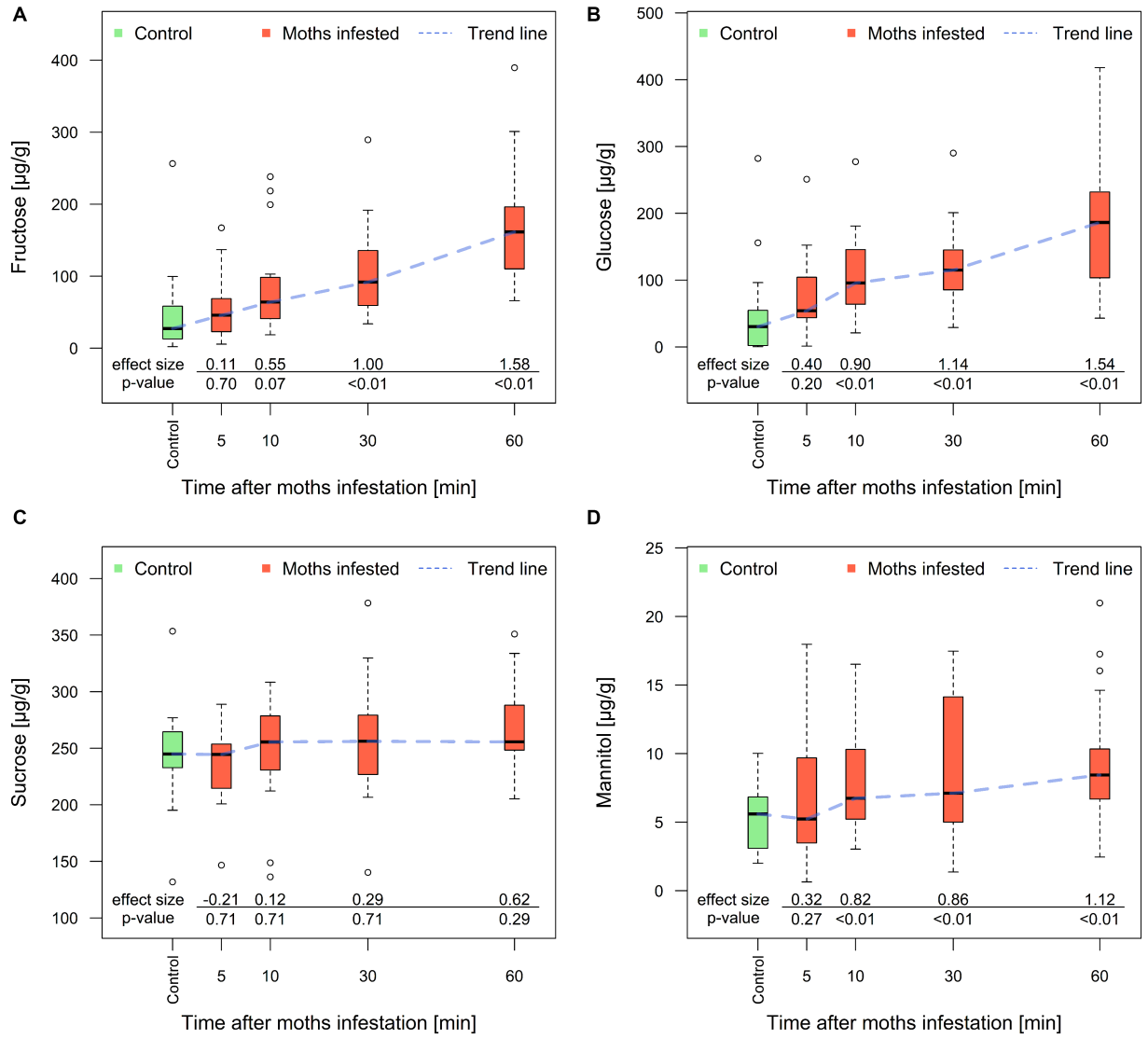

FIGURE 2
Concentration of fructose **(A)**, glucose **(B)**, sucrose **(C)**, and mannitol **(D)** in poplar leaves obtained after 5, 10, 30, and 60 min of spongy moth chewing. The Y-axis represents the relative shift from the control group on a natural logarithmic (ln) scale. Thick line in the box represents median values, the box range represents lower and upper quartile value, whiskers minimum and maximum values, and circles extreme values. The effect size is a quantitative measure of the magnitude of the experimental effect (Cohen's *d*).

10.3389/ffgc.2024.1376465

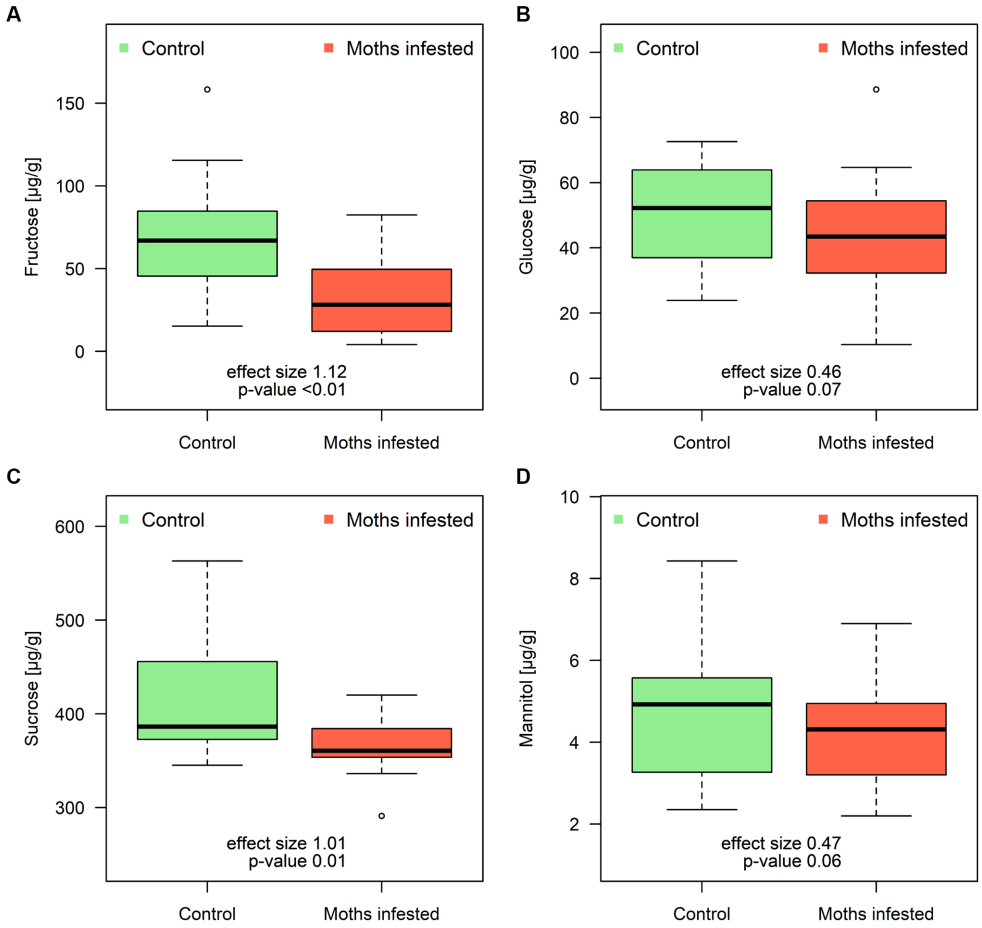

FIGURE 3
Concentration of fructose **(A)**, glucose **(B)**, sucrose **(C)**, and mannitol **(D)** in poplar roots obtained after 60 min of spongy moth chewing. Thick line in the box represents median values, the box range represents lower and upper quartile value, whiskers minimum and maximum values, and circles extreme values. The effect size is a quantitative measure of the magnitude of the experimental effect (Cohen's *d*).

the context of the galactose metabolic pathway, there was a significant decrease in sucrose, which dropped from control values of 418 ± 66 µg/g to 368 ± 29 µg/g (12% difference between treatment and control group) after 60 min of individual leaf feeding by spongy moth.

Physiological response of *Populus* to the moths

The physiological response of poplar to chewing insects was very fast and maintained even after the investigated time. The Pn in damaged plants was comparable to the control group at 5 and 10 min of feeding. Nonetheless, compared to the control, a substantial reduction ($p < 0.01$) in Pn was noted following 30 min of insect chewing (Figure 4A). The control group maintained Pn at 11 ± 4 µmol. m^{-2} s^{-1} but the group with spongy moth damage only reached 9.9 ± 3.7 µmol.m^{-2} s^{-1}. Similar trends were observed for Gs (Figure 4B) with a significant drop off at 30 min (0.50 ± 0.23 mol.m^{-2} s^{-1} in control group and 0.46 ± 0.23 mol.m^{-2} s^{-1} in moth-infested group, respectively). The significant decrease in Tr (Figure 4C) started even after 10 min of chewing (2.66 ± 0.89 mmol.m^{-2} s^{-1} and 2.58 ± 0.71 mmol. m^{-2} s^{-1}, respectively). The reduction in Pn, Gs, and Tr remained similar at 30 and 60 min, ranging between 8 and 12% when compared to the control group. Interestingly, no significant changes were observed in the intercellular CO_2 concentration (Ci) (Figure 4D), which implies that the ratio of Ci to ambient CO_2 concentration (Ca) remained constant throughout the entire investigation period (0.85 ± 0.05 µmol CO_2 mol^{-1}). The stable Ci/Ca ratio indicates that the impact of a moth feeding on the studied physiological processes was not mediated through alterations in intercellular CO_2 concentration.

Biochemical response of *Populus* to the moths

Three distinct patterns of phenolic compound production were observed in the moth-infested leaves, where the concentration of different phenolic compounds changed over time in three different ways (Figure 5) when compared to the control group:

1 The first group (Figure 5A) consisting of procyanidin B1, kaempferol, catechin, epigallocatechin, chlorogenic acid, and rutin increased its concentration several times higher after 5 min of chewing than in the control group. The standard

10.3389/ffgc.2024.1376465

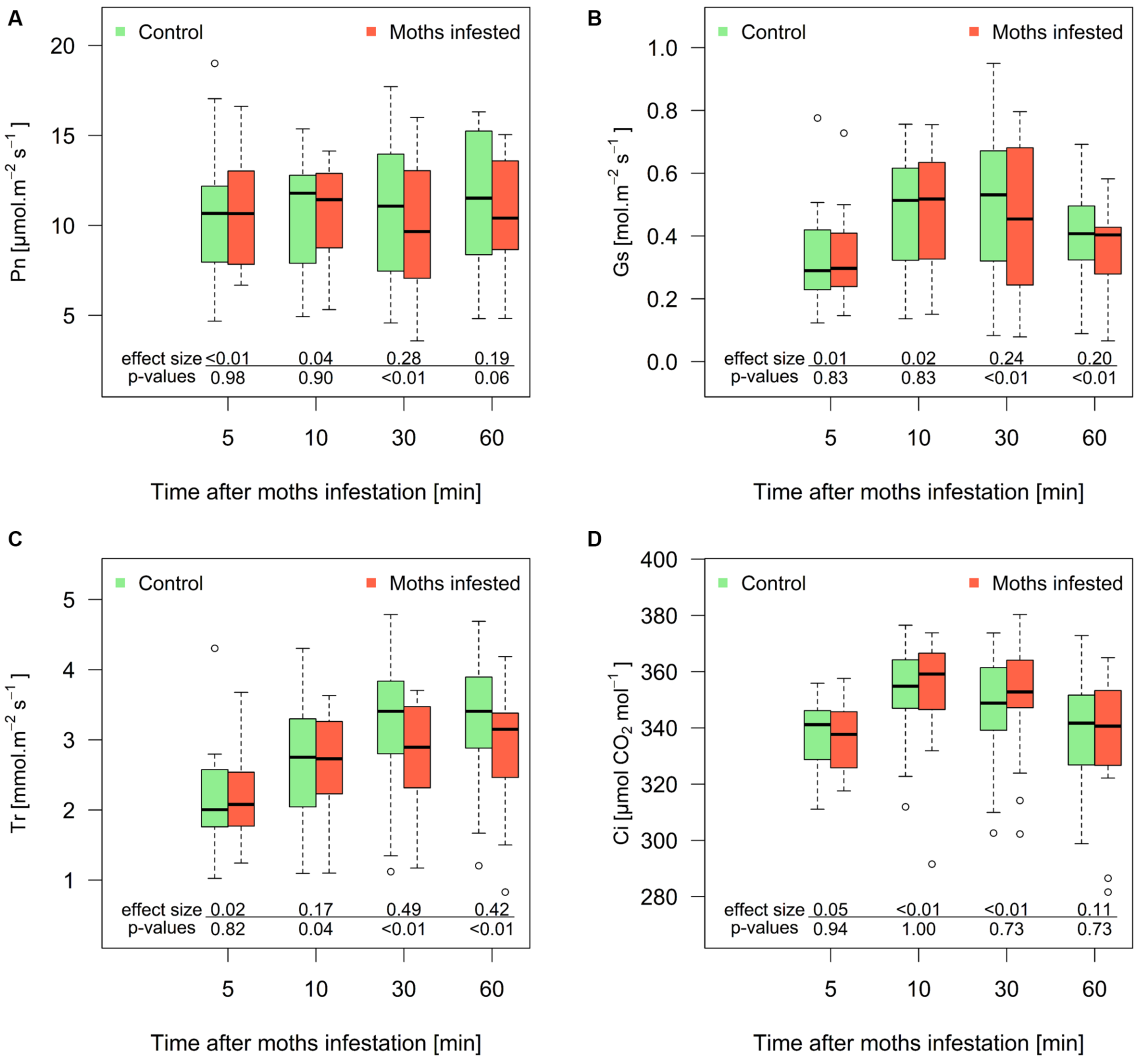

FIGURE 4
Course of net photosynthesis **(A)**, stomatal conductance **(B)**, transpiration **(C)**, and intracellular CO_2 concentration **(D)** in poplar leaves obtained after 5, 10, 30, and 60 min of spongy moth chewing. Values of the Y axis represent the relative shift from the control group. Thick line in the box represents median values, the box range represents lower and upper quartile value, whiskers minimum and maximum values, and circles extreme values. The effect size is a quantitative measure of the magnitude of the experimental effect (Cohen's *d*).

deviations (e.g., catechin and procyanidin B1) increased almost 10 times compared to their concentration in the moths-infested treatment immediately after 5 min of chewing. There was a significant increase (43%) in chlorogenic acid (639 ± 275 µg/g and 914 ± 275 µg/g) and kaempferol (0.16 ± 0.08 µg/g and 0.28 ± 0.18 µg/g, an increase of 75% when compared to control group). Subsequently, this group of substances began to decrease in concentration from 5 min to 60 min reaching control level. In addition to catechin, chlorogenic acid and procyanidin B1 showed lower concentrations than the control group.

2 The second group (Figure 5B) contained quercetin and ferulic acid; these two phenolic compounds had exactly the inverse course in investigated time than the previous group. After the start of feeding, the concentrations started to decrease, reaching a minimum value at 30 min after the start of feeding. Between 30 and 60 min, increases in the concentration of both these phenolic compounds were recorded, reaching approximately half the concentration compared to the control group (30.7 ± 7.8 µg/g). Concentration of ferulic acid was lower during the whole investigated periods when compared to control group. Significant differences were recorded after 10 min (24.3 ± 7.2 µg/g, a decrease of 20%), 30 min (21.7 ± 6.1 µg/g, a decrease of 42%), and 60 min (23.5 ± 8.1 µg/g, an increase of 8%).

3 The third group (Figure 5C) of analyzed phenolic compounds contains gallic acid and taxifolin; the concentration of these substances was stable and did not show any significant response during investigated time segments.

In Figure 6, we show the resulting chromatogram showing selected phenolic substances. By retention time on the x-axis and response rate in mass spectrometry analysis on the y-axis.

10.3389/ffgc.2024.1376465

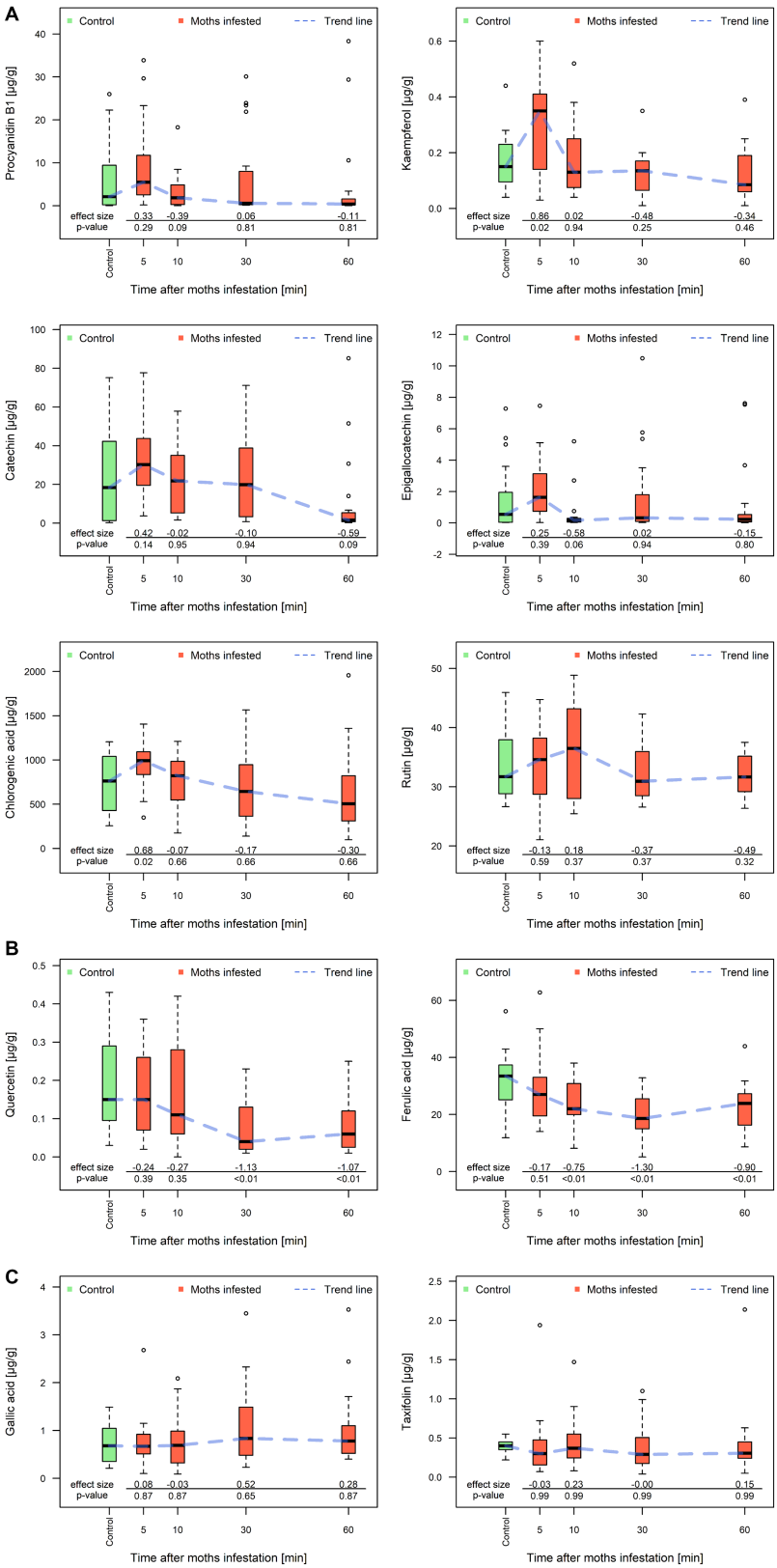

FIGURE 5
Concentration of phenolic compounds of the three groups according to a different patterns of development over time. First group **(A)** procyanidin B1, kaempferol, catechin, epigallocatechin, chlorogenic acid and rutin; second group **(B)** quercetin and ferulic acid; third group **(C)** gallic acid and taxifolin in poplar leaves obtained after 5, 10, 30, and 60 min of chewing by fungus gnats. Y-axis values represent the relative shift from the control group. The thick line in the box represents the median values, the range of the box represents the lower and upper quartile value, the minimum and maximum whisker values, and the circular extreme values. The blue dashed line represents the general trend of compound concentration over time. Effect size is a quantitative measure of the size of an experimental effect (Cohen's *d*).

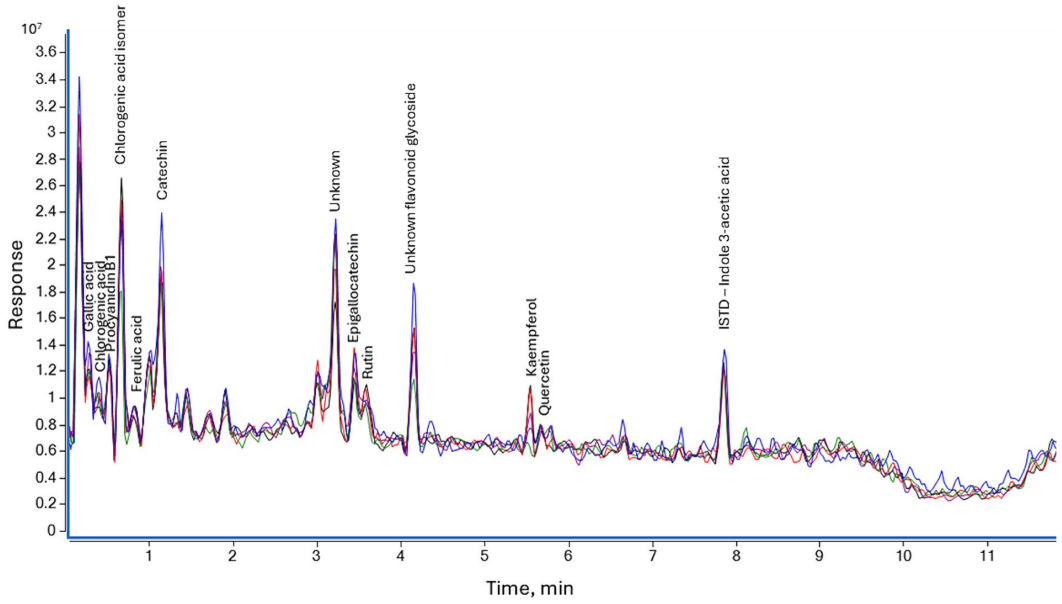

FIGURE 6
Total ion chromatograms of *Populus tremula* polyphenolic compounds: violet – control sample; green – after 5 min; black – after 10 min; red – after 30 min; blue – after 60 min.

Discussion

The current understanding of interactions between plants and insects is potentially vast, as indicated by numerous studies (Arimura, 2021; Mostafa et al., 2022; Wari et al., 2022), and supported by ample data available for meta-analyses (Zebelo and Maffei, 2014; Garcia and Eubanks, 2018; Wallis Ch and Galarneau, 2020). However, it is evident that accurately describing the dynamic relationship between a plant and an insect herbivore is highly complex and constrained. While some attention has been given to the temporal aspect of herbivory events, such as diurnal rhythms and emissions of volatile organic compounds (Kunert et al., 2002), the daily feeding patterns (Doghri et al., 2022), circadian rhythms (Jander, 2012), and early stages of interaction (Maffei et al., 2007), there is a lack of comprehensive studies considering the time perspective in the early phase of insect herbivore attacks.

In this study, we investigated the precise timing of physiological responses and changes in selected secondary metabolites to attacks by sponge moths, resulting in immediate changes in sugars and polyphenols and gasometric parameters. Our findings confirmed previous research by Allison and Schultz (2005) and Schultz et al. (2013) regarding primary metabolite redistribution from roots to damaged leaves in Populus. However, there have been studies documenting the opposite response in other plant species, suggesting that results depend on a variety of factors, including plant condition, resource availability, genetic predisposition, infestation intensity. and the specificity of the plant's defense response (Gómez et al., 2010; Orians et al., 2011). It seems that the well-known law of compensation and growth equilibrium by Saint-Hilaire (1818) generally applies. It says: *"The budget of nature is fixed; but she is free to dispose of particular sums by an appropriation that may please her. In order to spend on one side, she is forced to economize on the other side"* which Schultz et al. (2013) aptly point out in their study.

Taking a closer look at the gasometrical parameter Pn beforehand, the physical damage caused by caterpillar chewing can significantly alter the structure and function of the leaf. The loss of leaf tissue and damage to cell integrity may result in malfunctioning chloroplasts related to photosynthesis, thus reducing the capacity for photosynthetic activity. According to Zhou et al. (2015), a central aspect of any discourse concerning carbon allocation in response to herbivory is photosynthesis, which serves as the primary source of nearly all carbohydrates in green plants. However, the direct effect of leaf biomass disappearance typically does not show a linear correlation with Pn (Bueno et al., 2009). The defensive reactions often incur a cost in terms of reduced photosynthesis, as resources allocated to photosynthetic activities become constrained, leading to lower photosynthetic rates. This shift in energy and resource allocation favors defense mechanisms, as discussed by Arnold et al. (2004) and Gomez et al. (2012), while also restricting carbon fixation.

Physical damage caused by caterpillar feeding results in disruption of the leaf surface. The disruption of the plant tissue thus creates openings, which is usually the explanation for the decrease in transpiration. These physical wounds, when already sealed, serve as barriers, decreasing water vapor's ability to escape from leaf surfaces and lowering transpiration rates (Herms and Mattson, 1992).

At the level of secondary metabolism, trees of the *Salicaceae* family are known to be among the most prolific producers of phenolic compounds (Boeckler et al., 2013). Poplar leaves contain phenolic chemicals with an anti-herbivory function, including procyanidin B1, catechin, chlorogenic acid, quercetin, kaempferol, rutin, taxifolin, and epigallocatechin (Pietarinen et al., 2006; Sobuj et al., 2020). In addition to physiological adjustments, insect bites can induce the production and accumulation of phenolic chemicals in poplar leaves as a defense mechanism. Depending on the extent and duration of insect damage, the concentration of phenolic chemicals can change. The differences in the dynamics of concentration development in our study are in

direct contrast to the studies of Lahtinen et al. (2006). They reported that levels of phenolic compounds tend to rise in response to insect feeding, with higher amounts occurring when damage lasts longer. The activation of defensive signaling pathways causes changes in the amounts of polyphenols in poplar leaves. These signaling molecules can govern the expression of genes related to defense, thereby promoting the creation of defense proteins, protease inhibitors, and various other defensive substances (Walling, 2000). The comparison of our results with the time diagram presented in the study (Maffei et al., 2007) was surprising when we cannot confirm the given values with respect to our results. In particular, metabolic changes (induction of defense substances, allocation of resources) took place in our experiment demonstrably already in the first 5 min of feeding. As part of the results from our other yet unpublished study, the dynamics of changes in gene expression show similar findings. The response of phenolic compounds in *Populus* leaves to spongy moth caterpillars exhibits a notable level of diversity, and the phenolic data exhibited considerable variability even between clones, which is consistent with works (Donaldson et al., 2006; Smith et al., 2011). According to studies, several *Populus* spp. demonstrate diverse patterns of variation in phenolic content in response to caterpillar feeding, with some showing no significant change or even a decrease (Lämke and Unsicker, 2018; Zhang et al., 2020). This significant variation underscores the intricate nature of plant defense strategies and implies that various *Populus* species have developed unique biochemical mechanisms to contend with herbivore assaults. What was particularly noticeable was that this same extensive variability was observed within identical *Populus* clones originating from *in vitro* plant material in the present study.

The majority of prior studies examining the ecological functions of tannins have not specifically investigated individual chemical compounds. Instead, they have relied on general precipitation or colorimetric tests to measure the levels of "total phenolic compounds" or "total hydrolyzable/condensed tannins" (Appel et al., 2001; Boeckler et al., 2013). Given the immense chemical diversity of plant polyphenols, a limiting factor may have been researchers' attempts to pinpoint a singular (primary) effect and define it as the "raison d'être" of the entire class of polyphenols. In fact, it appears more probable that different compounds play distinct roles in plant interactions with their environment (Moctezuma et al., 2014).

Flavan-3-ols, including monomeric catechin and polymeric proanthocyanidins (referred to as condensed tannins), are prevalent phenolics in *Populus* spp. (Ullah et al., 2019; Bandau et al., 2021). Functionally, this group of substances has been shown to induce oxidative stress in the gut of insects (Barbehenn and Constabel, 2011). According to the original work by Feeny (1968), it was generally assumed that higher levels of condensed tannins would reduce the preference of insect herbivores (Forkner et al., 2004). However, studies by Peters and Constabel (2002), Tsai et al. (2006), and Boeckler et al. (2014) suggest that adapted insects, or certain genotypes, may be attracted to higher levels of condensed tannins. The findings of Hjältén and Axelsson (2015) suggest that through coevolution, condensed tannins may even act as stimulants for insect herbivores. Based on the above, the dynamics of tannins appear unclear and inconsistent. When considering the results of our study, which detail the concentration changes of this group of substances after *Lymantria dispar* attack, the situation becomes even more ambiguous.

Quercetin, a key flavonol, is widely distributed in the plant kingdom (Zhang et al., 2020). It plays a complex role in mediating interactions between herbs and insects. It can stimulate insect feeding and promote growth at low concentrations (Rahden-Staron et al., 2001); however, some studies have shown that quercetin may inhibit the activities of antioxidant and detoxification enzymes, resulting in increased mortality of insect herbivores (Gómez et al., 2020). In light of our recorded dynamics, we find agreement with the study by Jing et al. (2024), where a decrease in quercetin and a significant increase in quercetin-3-*O*-glucoside were observed over the course of hours. As noted by Jing et al. (2024), quercetin-3-*O*-glucoside has a crucial negative impact on larval development. and free quercetin had no significant effect on larval growth. Thus, it seems that glucosylation of quercetin should be the subject of further research.

While the antioxidant properties of gallic acid have been observed in other plant species, such as soybean (*Glycine max*), where it has been shown to reduce the level of total ascorbate and glutathione (Ozfidan-Konakci et al., 2019), a contrasting phenomenon is observed in tomato (*Solanum lycopersicum*), where ascorbate content increases (Farghaly et al., 2021). In our study, gallic acid together with taxifolin, belongs to the group of substances with almost no response in the response of *Populus tremula* to *Lepidoptera* attack. Regarding the evolution of gallic acid content, we agree with Zhang et al. (2020), while acknowledging the limited understanding of the impact of this polyphenolic compound on plant resistance to herbivores.

As a crucial factor, hypothetically, along with: plant health vitality, resource availability, genotypes, chemotypes and coevolutionarily given interactions, time appears to be essential for selecting appropriate strategies (and their various combinations) in response to insect herbivory.

Based on our current understanding, there appears to be numerous studies describing the impact of phenolic compounds added to the diet for *Lepidoptera* (Diaz Napal and Palacios, 2015; Su et al., 2017; Wang et al., 2019; Gao et al., 2022); however, no studies focusing on the response of *Populus* spp. mentioning the early metabolic response to *Lepidopteran* attack by phenolic compounds have been found. The general textbook terminology regarding the uncertain classification of plant metabolites into primary and secondary, such as that proposed by Erb and Kliebenstein (2020), appears to shape the thinking and application of approaches. Similarly, this is true according to the results of our study when using the terminology of a strict division into induced defense reaction and tolerant strategy in response to insect herbivory, which may be misleading. It is very common to overlook the dynamic development of the plant's metabolic response. This limitation restricts the characterization of the dynamic trajectory of the metabolic response over time to the identification of a particular response type at a specific point (time) along the developmental curve of the reaction. Based on this, it can be inferred that the approach of many studies (across all taxa) does not define a metabolic strategy but rather a state at specific time - when the samples were collected.

The ability of broadleaves to recover from defoliation and adjust their chemical defense composition according to external conditions is promising in future predictive models shaping forests.

Limitations

Due to the well-documented problems associated with the inherent biological variability of living organisms, various factors were carefully considered in the creation of the experimental design. These factors included the genetic predisposition of the species studied, the potential interplay of temporal effects within individual treatment periods and the cumulative effect of herbivory, the application of multidisciplinary methodologies, and the complexity of elucidating the dynamics of interspecies interactions. Despite careful attention to detail, there is still a chance of inaccuracies or phenomena that are difficult to grasp.

To mitigate these challenges, rigorous measures were implemented: including the use of genetically uniform individuals (*Populus tremula*), setting optimal environmental conditions in growth chambers (especially the elimination of the influence of varying intensity of irradiance), using multiple separate growth chambers to prevent chemical communication between poplars, systematics of manual works, sample collection and laboratory protocols.

Acknowledging the inherent constraints in our study, we believe that our research provides fresh insights into the intricacies of plant-insect interactions. We hope that our findings can spur further investigation in this fascinating field.

Data availability statement

The raw data supporting the conclusions of this article will be made available by the authors, without undue reservation.

Author contributions

FP: Writing – original draft, Writing – review & editing. JČ: Writing – original draft, Writing – review & editing. AK: Writing – original draft, Writing – review & editing. KM: Writing – original draft, Writing – review & editing. JH: Writing – original draft, Writing – review & editing. JB: Writing – original draft, Writing – review & editing. IT: Writing – original draft, Writing – review & editing.

Funding

The author(s) declare that financial support was received for the research, authorship, and/or publication of this article. Supported by grant "EVA4.0," No. CZ.02.1.01/0.0/0.0/16_019/0000803 financed by the OP RDE.

Acknowledgments

The authors are grateful to native speaker Mark Sixmith for language proofreading. The authors are grateful to Karolína Berková for graphical work (KarB.artstudio@gmail.com). KM thankfully acknowledges the Department of Biotechnology, GOI for the Ramalingaswami Re-entry grant (BT/RLF/Re-entry/11/2023).

Conflict of interest

The authors declare that the research was conducted in the absence of any commercial or financial relationships that could be construed as a potential conflict of interest.

Publisher's note

All claims expressed in this article are solely those of the authors and do not necessarily represent those of their affiliated organizations, or those of the publisher, the editors and the reviewers. Any product that may be evaluated in this article, or claim that may be made by its manufacturer, is not guaranteed or endorsed by the publisher.

References

Allison, S. D., and Schultz, J. C. (2005). Biochemical responses of chestnut oak to a galling CYNIPID. *J. Chem. Ecol.* 31, 151–166. doi: 10.1007/s10886-005-0981-5

Anderson, J. T., and Mitchell-Olds, T. (2010). Ecological genetics and genomics of plant defences: evidence and approaches. *Funct. Ecol.* 25, 312–324. doi: 10.1111/j.1365-2435.2010.01785.x

Appel, H. M., Govenor, H. L., D'ascenzo, M., Siska, E., and Schultz, J. C. (2001). Limitations of Folin assays of foliar phenolics in ecological studies. *J. Chem. Ecol.* 27, 761–778. doi: 10.1023/A:1010306103643

Arimura, G. (2021). Making sense of the way plants sense herbivores. *Trends Plant Sci.* 26, 288–298. doi: 10.1016/j.tplants.2020.11.001

Arnold, T., Appel, H., Patel, V., Stocum, E., Kavalier, A., and Schultz, J. (2004). Carbohydrate translocation determines the phenolic content of Populus foliage: a test of the sink-source model of plant defense. *New Phytol.* 164, 157–164. doi: 10.1111/j.1469-8137.2004.01157.x

Bandau, F., Albrectsen, B. R., Robinson, K. M., and Gundale, M. J. (2021). European aspen with high compared to low constitutive tannin defenses grow taller in response to anthropogenic nitrogen enrichment. *For. Ecol. Manag.* 487, 118985–111127. doi: 10.1016/j.foreco.2021.118985

Barbehenn, R. V., and Constabel, C. P. (2011). Tannins in plant–herbivore interactions. *Phytochemistry* 72, 1551–1565. doi: 10.1016/j.phytochem.2011.01.040

Birnbaum, S. S. L., and Abbot, P. (2020). Gene expression and diet breadth in plant-feeding insects: summarizing trends. *Trends Ecol. Evol.* 35, 259–277. doi: 10.1016/j.tree.2019.10.014

Boeckler, G. A., Gershenzon, J., and Unsicker, S. B. (2013). Gypsy moth Caterpillar feeding has only a marginal impact on phenolic compounds in old-growth black poplar. *J. Chem. Ecol.* 39, 1301–1312. doi: 10.1007/s10886-013-0350-8

Boeckler, G. A., Towns, M., Unsicker, S. B., Mellway, R. D., Yip, L., Hilke, I., et al. (2014). Transgenic upregulation of the condensed tannin pathway in poplar leads to a dramatic shift in leaf palatability for two tree-feeding Lepidoptera. *J. Chem. Ecol.* 40, 150–158. doi: 10.1007/s10886-014-0383-7

Bruce, T. J. A., and Pickett, J. A. (2011). Perception of plant volatile blends by herbivorous insects – finding the right mix. *Phytochemistry* 72, 1605–1611. doi: 10.1016/j.phytochem.2011.04.011

Bueno, A. d. F., Bueno, R. C. O. d. F., Nabity, P. D., Higley, L. G., and Fernandes, O. A. (2009). Photosynthetic response of soybean to twospotted spider mite (Acari: Tetranychydae) injury. *Braz. Arch. Biol. Technol.* 52, 825–834. doi: 10.1590/s1516-89132009000400005

Copolovici, L., Pag, A., Kännaste, A., Bodescu, A., Tomescu, D., Copolovici, D., et al. (2017). Disproportionate photosynthetic decline and inverse relationship between constitutive and induced volatile emissions upon feeding of *Quercus robur* leaves by large larvae of gypsy moth (*Lymantria dispar*). Environmental and experimental botany. *Crit. Rev. Plant Sci.* 138, 184–192. doi: 10.1016/j.envexpbot.2017.03.014

Delaney, K. J. (2008). Injured and uninjured leaf photosynthetic responses after mechanical injury on *Nerium oleander* leaves, and *Danaus plexippus* herbivory on

Asclepias curassavica leaves. *Plant Ecol.* 199, 187–200. doi: 10.1007/s11258-008-9423-0

Diaz Napal, G. N., and Palacios, S. M. (2015). Bioinsecticidal effect of the flavonoids pinocembrin and quercetin against *Spodoptera frugiperda*. *J. Pest. Sci.* 88, 629–635. doi: 10.1007/s10340-014-0641-z

Doghri, M., Rodríguez, V. M., Kliebenstein, D. J., and Francisco, M. (2022). Plant responses underlying timely specialized metabolites induction of Brassica crops. *Front. Plant Sci.* 12:807710. doi: 10.3389/fpls.2021.807710

Donaldson, J. R., Stevens, M. T., Barnhill, H. R., and Lindroth, R. L. (2006). Age-related shifts in leaf chemistry of clonal Aspen (*Populus tremuloides*). *J. Chem. Ecol.* 32, 1415–1429. doi: 10.1007/s10886-006-9059-2

Erb, M., and Kliebenstein, D. J. (2020). Plant secondary metabolites as defenses, regulators, and primary metabolites: the blurred functional trichotomy. *Plant Physiol.* 184, 39–52. doi: 10.1104/pp.20.00433

Farghaly, F. A., Salam, H. K., Hamada, A. M., and Radi, A. A. (2021). The role of benzoic acid, gallic acid and salicylic acid in protecting tomato callus cells from excessive boron stress. *Sci. Hortic.* 278:109867. doi: 10.1016/j.scienta.2020.109867

Feeny, P. P. (1968). Effect of oak leaf tannins on larval growth of the winter moth *Operophtera brumata*. *J. Insect Physiol.* 14, 805–817. doi: 10.1016/0022-1910(68)90191-1

Forkner, R. E., Marquis, R. J., and Lill, J. T. (2004). Feeny revisited: condensed tannins as anti-herbivore defences in leaf-chewing herbivore communities of Quercus. *Ecol. Entomol.* 29, 174–187. doi: 10.1111/j.1365-2311.2004.0590.x

Fürstenberg-Hägg, J., Zagrobelny, M., and Bak, S. (2013). Plant Defense against Insect Herbivores. *Int. J. Mol. Sci.* 14, 10242–10297. doi: 10.3390/ijms140510242

Fyllas, N. M., Chrysafi, D., Avtzis, D. N., and Moreira, X. (2022). Photosynthetic and defensive responses of two Mediterranean oaks to insect leaf herbivory. *Tree Physiol.* 42, 2282–2293. doi: 10.1093/treephys/tpac067

Gao, Y. L., Pan, Z. Y., Meng, X., Yuan, Y. F., Li, H. Y., and Chen, M. (2022). The effect of quercetin on the growth, development, nutrition utilization, and detoxification enzymes in *Hyphantria cunea* Drury (Lepidoptera: Arctiidae). *Forests* 13:1945. doi: 10.3390/f13111945

Garcia, L. C., and Eubanks, M. D. (2018). Overcompensation for insect herbivory: a review and meta-analysis of the evidence. *Ecology* 100:e02585. doi: 10.1002/ecy.2585

Gerrienne, P., Gensel, P. G., Strullu-Derrien, C., Lardeux, H., Steemans, P., and Prestianni, C. (2011). A simple type of wood in two early Devonian plants. *Science* 333:837. doi: 10.1126/science.1208882

Gómez, S., Ferrieri, R. A., Schueller, M., and Orians, C. M. (2010). Methyl jasmonate elicits rapid changes in carbon and nitrogen dynamics in tomato. *New Phytol.* 188, 835–844. doi: 10.1111/j.1469-8137.2010.03414.x

Gómez, J. D., Pinheiro, V. J., Silva, J. C., Romero, J. V., Merino-Cabrera, Y., Coutinho, F. S., et al. (2020). Leaf metabolic profiles of two soybean genotypes differentially affect the survival and the digestibility of *Anticarsia gemmatalis* caterpillars. *Plant Physiol. Biochem.* 155, 196–212. doi: 10.1016/j.plaphy.2020.07.010

Gomez, S., Steinbrenner, A. D., Osorio, S., Schueller, M., Ferrieri, R. A., Fernie, A. R., et al. (2012). From shoots to roots: transport and metabolic changes in tomato after simulated feeding by a specialist lepidopteran. *Entomol. Exp. Appl.* 144, 101–111. doi: 10.1111/j.1570-7458.2012.01268.x

Hajek, A. (2001). Larval behavior in *Lymantria dispar* increases risk of fungal infection. *Oecologia* 126, 285–291. doi: 10.1007/s004420000509

Hanik, N., Gómez, S., Best, M., Schueller, M., Orians, C. M., and Ferrieri, R. A. (2010a). Partitioning of new carbon as 11C in *Nicotiana tabacum* reveals insight into methyl jasmonate induced changes in metabolism. *J. Chem. Ecol.* 36, 1058–1067. doi: 10.1007/s10886-010-9835-x

Haruta, M., Pedersen, J. A., and Constabel, C. P. (2001). Polyphenol oxidase and herbivore defense in trembling aspen (*Populus tremuloides*): cDNA cloning, expression, and potential substrates. *Physiol. Plant.* 112, 552–558. doi: 10.1034/j.1399-3054.2001.1120413.x

Herms, D. A., and Mattson, W. J. (1992). The dilemma of plants: to grow or defend. *Q. Rev. Biol.* 67, 283–335. doi: 10.1086/417659

Hjältén, J., and Axelsson, E. P. (2015). GM trees with increased resistance to herbivores: trait efficiency and their potential to promote tree growth. *Front. Plant Sci.* 6:136916. doi: 10.3389/fpls.2015.00279

Holopainen, J. K., and Gershenzon, J. (2010). Multiple stress factors and the emission of plant VOCs. *Trends Plant Sci.* 15, 176–184. doi: 10.1016/j.tplants.2010.01.006

Jander, G. (2012). Timely plant defenses protect against caterpillar herbivory. *Proc. Natl. Acad. Sci.* 109, 4343–4344. doi: 10.1073/pnas.1201443109

Jing, T., Du, W., Qian, X., Wang, K., Luo, L., Zhang, X., et al. (2024). UGT89AC1-mediated quercetin glucosylation is induced upon herbivore damage and enhances *Camellia sinensis* resistance to insect feeding. *Plant Cell Environ.* 47, 682–697. doi: 10.1111/pce.14751

Johnson, M. T. J. (2011). Evolutionary ecology of plant defences against herbivores. *Funct. Ecol.* 25, 305–311. doi: 10.1111/j.1365-2435.2011.01838.x

Khare, S., Singh, N. B., Singh, A., Hussain, I., Niharika, K., Yadav, V., et al. (2020). Plant secondary metabolites synthesis and their regulations under biotic and abiotic constraints. *J. Plant Biol.* 63, 203–216. doi: 10.1007/s12374-020-09245-7

Kunert, M., Biedermann, A., Koch, T., and Boland, W. (2002). Ultrafast sampling and analysis of plant volatiles by a hand-held miniaturised GC with pre-concentration unit: kinetic and quantitative aspects of plant volatile production. *J. Sep. Science* 25, 677–684. doi: 10.1002/1615-9314(20020701)25:10/11<677::AID-JSSC677>3.0.CO;2-5

Labandeira, C. (2007). The origin of herbivory on land: initial patterns of plant tissue consumption by arthropods. *Insect Science* 14, 259–275. doi: 10.1111/j.1744-7917.2007.00141.x-i1

Labandeira, C. (2013). Deep-time patterns of tissue consumption by terrestrial arthropod herbivores. *Naturwissenschaften* 100, 355–364. doi: 10.1007/s00114-013-1035-4

Lahtinen, M., Kapari, L., Haukioja, E., and Pihlaja, K. (2006). Effects of increased content of leaf surface flavonoids on the performance of mountain birch feeding sawflies vary for early and late season species. *Chemoecology* 16, 159–167. doi: 10.1007/s00049-006-0343-y

Lämke, J. S., and Unsicker, S. B. (2018). Phytochemical variation in treetops: causes and consequences for tree-insect herbivore interactions. *Oecologia* 187, 377–388. doi: 10.1007/s00442-018-4087-5

Madsen, S. R., Kunert, G., Reichelt, M., Gershenzon, J., and Halkier, B. A. (2015). Feeding on leaves of the glucosinolate transporter mutant gtr1gtr2 reduces fitness of *Myzus persicae*. *J. Chem. Ecol.* 41, 975–984. doi: 10.1007/s10886-015-0641-3

Maffei, M. E., Mithöfer, A., and Boland, W. (2007). Before gene expression: early events in plant–insect interaction. *Trends Plant Sci.* 12, 310–316. doi: 10.1016/j.tplants.2007.06.001

Medvedev, S. S. (2005). Calcium signaling system in plants Russ. *J. Plant Physiol.* 52, 249–270. doi: 10.1007/s11183-005-0038-1

Moctezuma, C., Hammerbacher, A., Heil, M., Gershenzon, J., Méndez-Alonzo, R., and Oyama, K. (2014). Specific polyphenols and tannins are associated with defense against insect herbivores in the tropical oak Quercus oleoides. *J. Chem. Ecol.* 40, 458–467. doi: 10.1007/s10886-014-0431-3

Mostafa, S., Wang, Y., Zeng, W., and Jin, B. (2022). Plant responses to herbivory, wounding, and infection. *Int. J. Mol. Sci.* 23:7031. doi: 10.3390/ijms23137031

Orians, C. M., Thorn, A., and Gómez, S. (2011). Herbivore-induced resource sequestration in plants: why bother? *Oecologia* 167, 1–9. doi: 10.1007/s00442-011-1968-2

Ozfidan-Konakci, C., Yildiztugay, E., Yildiztugay, A., and Kucukoduk, M. (2019). Cold stress in soybean (*Glycine max* L.) roots: exogenous gallic acid promotes water status and increases antioxidant activities. *Botanica Serbica.* 43, 59–71. doi: 10.2298/BOTSERB1901059O

Pandey, S., Tiwari, S. B., Upadhyaya, K. C., and Sopory, S. K. (2000). Calcium signaling: Linking environmental signals to cellular functions. *Crit. Rev. Plant Sci.* 19, 291–318. doi: 10.1080/07352680091139240

Peters, D. J., and Constabel, C. P. (2002). Molecular analysis of herbivore-induced condensed tannin synthesis: cloning and expression of dihydroflavonol reductase from trembling aspen (*Populus tremuloides*). *Plant J.* 32, 701–712. doi: 10.1046/j.1365-313X.2002.01458.x

Pietarinen, S. P., Willför, S. M., Vikström, F. A., and Holmbom, B. R. (2006). Aspen knots, a rich source of flavonoids. *J. Wood Chem. Technol.* 26, 245–258. doi: 10.1080/02773810601023487

Pilipovič, A., Drekič, M., Orlovič, S., Poljakoviš-Pajnik, L., Nikoliš, N., and Boršev, M. (2015). "Growth and physiological response of different poplar clones on herbivory induced stress," in *Proceedings of the biennial international symposium. Forest and sustainable development*. Braşov, Romania: Transilvania University Press, 121–126.

Poveda, K., Díaz, M. F., and Ramirez, A. (2017). Can overcompensation increase crop production? *Ecology* 99, 270–280. doi: 10.1002/ecy.2088

Poveda, K., Jimenez, M. I. G., and Kessler, A. (2013). The enemy as ally: herbivore-induced increase in crop yield. *Ecol. Appl.* 23, 515–522. doi: 10.1890/09-1726.1

Rahden-Staron, I., Czeczot, H., and Szumilo, M. (2001). Induction of rat liver cytochrome P450 isoenzymes CYP 1A and CYP 2B by different fungicides, nitrofurans, and quercetin. *Mut. Res.* 498, 57–66. doi: 10.1016/S1383-5718(01)00267-4

Rosenkranz, M., and Schnitzler, J. P. (2016). *Plant Volatiles*. Chichester: eLS, John Wiley & Sons, Ltd.

Saint-Hilaire, E. G. (1818). *Philosophie Anatomique*, vol. *2*. Paris: J. B. Bailliere, 566.

Schultz, J. C., Appel, H. M., Ferrieri, A. P., and Arnold, T. M. (2013). Flexible resource allocation during plant defense responses. *Front. Plant Sci.* 4. doi: 10.3389/fpls.2013.00324

Smith, E. (2007). Plant secondary metabolites: occurrence, structure and role in the human diet. *Phytother. Res.* 21:904. doi: 10.1002/ptr.2237

Smith, E. A., Collette, S. B., Boynton, T. A., Lillrose, T., Stevens, M. R., Bekker, M. F., et al. (2011). Developmental contributions to phenotypic variation in functional leaf traits within quaking aspen clones. *Tree Physiol.* 31, 68–77. doi: 10.1093/treephys/tpq100

Sobuj, N., Virjamo, V., Nissinen, K., Sivadasan, U., Mehtätalo, L., Nybakken, L., et al. (2020). Responses in growth and phenolics accumulation to lateral bud removal in male and female saplings of *Populus tremula* (L.) under simulated climate change. *Sci. Total Environ.* 704:135462. doi: 10.1016/j.scitotenv.2019.135462

Stevens, M. T., and Lindroth, R. L. (2005). Induced resistance in the indeterminate growth of aspen (*Populus tremuloides*). *Oecologia* 145, 297–305. doi: 10.1007/s00442-005-0128-y

Su, Q., Zhou, Z., Zhang, J., Shi, C., Zhang, G., Jin, Z., et al. (2017). Effect of plant secondary metabolites on common cutworm, *Spodoptera litura* (Lepidoptera: Noctuidae). *Entomol. Res.* 48, 18–26. doi: 10.1111/1748-5967.12238

Šulc, M., Tomášková, I., Krejzková, A., Samek, M., Diuzheva, A., Hradecký, J., et al. (2021). Trehalose determination in Norway spruce (*Picea abies*) roots. *Analytics Matters. MethodsX* 8:101280. doi: 10.1016/j.mex.2021.101280

Team, R. C. (2021). R: a language and environment for statistical computing. Published online 2020. *Suppl. Inform. Ref. S* 1, 371–378,

Tsai, C. J., Harding, S. A., Tschaplinski, T. J., Lindroth, R. L., and Yuan, Y. (2006). Genome-wide analysis of the structural genes regulating defense phenylpropanoid metabolism in Populus. *New Phytol.* 172, 47–62. doi: 10.1111/j.1469-8137.2006.01798.x

Ullah, C., Unsicker, S. B., Reichelt, M., Gershenzon, J., and Hammerbacher, A. (2019). Accumulation of Catechin and Proanthocyanidins in black poplar stems after infection by Plectosphaerella populi: hormonal regulation, biosynthesis and antifungal activity. *Front. Plant Sci.* 10. doi: 10.3389/fpls.2019.01441

Visakorpi, K., Riutta, T., Malhi, Y., Salminen, J. P., Salinas, N., and Gripenberg, S. (2020). Changes in oak (*Quercus robur*) photosynthesis after winter moth (*Operophtera brumata*) herbivory are not explained by changes in chemical or structural leaf traits. *PLoS One* 15:e0228157. doi: 10.1371/journal.pone.0228157

Vogel, H., Musser, R. O., and de la Paz Celorio-Mancera, M. (2014). Transcriptome responses in herbivorous insects towards host plant and toxin feeding. *Annual Plant Rev.* 47, 197–233. doi: 10.1002/9781118829783.ch6

Walling, L. L. (2000). The myriad plant responses to herbivores. *J. Plant Growth Regul.* 19, 195–216. doi: 10.1007/s003440000026

Wallis Ch, M., and Galarneau, E. R. (2020). Phenolic compound induction in plant-microbe and plant-insect interactions: a Meta-analysis. *Front. Plant Sci.* 11:580753. doi: 10.3389/fpls.2020.580753

Wang, Z., Nur, F. A., Ma, J., Wang, J., and Cao, C. (2019). Effects of poplar secondary metabolites on performance and detoxification enzyme activity of *Lymantria dispar*. *Comp. Biochem. Physiol. Part C* 225:108587. doi: 10.1016/j.cbpc.2019.108587

War, A. R., Paulraj, M. G., Ahmad, T., Buhroo, A. A., Hussain, B., Ignacimuthu, S., et al. (2021). Mechanisms of plant defense against insect herbivores. *Plant Signal. Behav.* 7, 1306–1320. doi: 10.4161/psb.21663

Wari, D., Aboshi, T., Shinya, T., and Galis, I. (2022). Integrated view of plant metabolic defense with particular focus on chewing herbivores. *J. Integr. Plant Biol.* 64, 449–475. doi: 10.1111/jipb.13204

Webster, B., Bruce, T., Pickett, J., and Hardie, J. (2010). Volatiles functioning as host cues in a blend become nonhost cues when presented alone to the black bean aphid. *Anim. Behav.* 79, 451–457. doi: 10.1016/j.anbehav.2009.11.028

Wink, M. (2018). Plant secondary metabolites modulate insect behavior-steps toward addiction? *Front. Physiol.* 9. doi: 10.3389/fphys.2018.00364

Zebelo, S. A., and Maffei, M. E. (2014). Role of early signalling events in plant-insect interactions. *J. Exp. Bot.* 66, 435–448. doi: 10.1093/jxb/eru480

Zhang, W. H., Schmid, B., Liu, L., and Wang, P. (2020). Phenolic responses of Populus species to spongy moth caterpillar herbivory. *J. Plant Ecol.* 13, 1–2. doi: 10.1093/jpe/rtaa009

Zhang, B., Zhou, L., Zhou, X., Bai, Y., Zhan, M., Chen, J., et al. (2022). Differential responses of leaf photosynthesis to insect and pathogen outbreaks: a global synthesis. *Sci. Total Environ.* 832:155052. doi: 10.1016/j.scitotenv.2022.155052

Zhou, S., Lou, Y. R., Tzin, V., and Jander, G. (2015). Alteration of plant primary metabolism in response to insect herbivory. *Plant Physiol.* 169, 01405.2015–01405.1498. doi: 10.1104/pp.15.01405

frontiers | Frontiers in Forests and Global Change

TYPE Original Research
PUBLISHED 14 June 2024
DOI 10.3389/ffgc.2024.1356511

OPEN ACCESS

EDITED BY
Amit Roy,
Czech University of Life Sciences Prague, Czechia

REVIEWED BY
Kanakachari Mogilicherla,
Czech University of Life Sciences Prague, Czechia
Jia-Gang Wang,
Shanxi Agricultural University, China
Xiaoman You,
Chinese Academy of Agricultural Sciences, China

*CORRESPONDENCE
Baojia Gao
✉ baojiagao@163.com

RECEIVED 15 December 2023
ACCEPTED 31 May 2024
PUBLISHED 14 June 2024

CITATION
Sun T, Zhao Y, Zhou G, Gao S, Liu J and Gao B (2024) Defense response to caterpillar feeding stress in wild *Pinus tabuliformis* unveiled by quantitative integrated proteomic and phosphoproteomic analyses. *Front. For. Glob. Change* 7:1356511. doi: 10.3389/ffgc.2024.1356511

Defense response to caterpillar feeding stress in wild *Pinus tabuliformis* unveiled by quantitative integrated proteomic and phosphoproteomic analyses

Tianhua Sun[1], Yanan Zhao[1], Guona Zhou[1], Suhong Gao[2], Junxia Liu[1] and Baojia Gao[1]*

[1]Hebei Key Laboratory for Forest Germplasm Resources and Forest Protection, Hebei Agricultural University, Baoding, China, [2]College of Agronomy and Biotechnology, Hebei Normal University of Science and Technology, Changli, China

Pinus is a genus of great economic and ecological importance, and its members are dominant components of forests throughout the world. During the long evolutionary "arms race," plants have developed complex and diverse systemic defense mechanisms to strategically and intelligently compete with herbivores. To study the alteration pattern and defensive response mechanism triggered by herbivorous feeding stimuli, we firstly built a biological model of the interrelationship between the Chinese pine (*Pinus tabuliformis* Carr.) and the Chinese pine caterpillar (*Dendrolimus tabulaeformis* Tsai et Liu). This model integrated proteomic and phosphoproteomic data, which were then normalized and combined with bioinformatics tools to evaluate and analyze changes in the phosphoproteomic profile in response to the caterpillar's feeding stimulus on pine needles. Systematic identification of differentially significant phosphorylated proteins implicated in the pine's defense mechanism against caterpillar stress was conducted. Furthermore, we predicted upstream kinases of phosphorylation sites and their activities. Through an analysis of Motif patterns of phosphorylated proteins, Mfuzz clustering of phosphorylation sites, and kinase regulatory networks, we explored the functional modules of phosphorylated protein interaction networks in response to stress within pine. In general, our study emphasized the significant role of kinase METK2, PTI12, PGK, as well as At3g59480 for the first time. The identification of these phosphorylated proteins was additionally confirmed through parallel reaction monitoring technology. Furthermore, genes associated with differentially expressed proteins were validated through real-time quantitative polymerase chain reaction detection. This investigation aids in understanding the mechanisms behind resistance formation and regulation of caterpillar feeding incentives in pine. Breeding more resistant pine varieties may benefit from a fuller understanding of these defense strategies in the future.

KEYWORDS

***Pinus tabuliformis* Carr., *Dendrolimus tabulaeformis* Tsai et Liu, proteomic, phosphoproteomics, induced defensive responses**

Introduction

As a representative of coniferous trees, the Chinese pine (*Pinus tabuliformis*) is one of the ecological cornerstone species (Niu et al., 2022). A thorough analysis of the defense mechanisms employed by dominant phytophagous insects in response to biotic stress is crucial for understanding habitat regulation under forest tree species. In this study, our analysis specifically focuses on critical defense mechanisms and habitat regulation in forest tree species, particularly examining how these factors are influenced by herbivore feeding. Proteins are the direct carriers and implementers of functions in plant life activities. Exploring phenomena such as plant biotic stress response and laws utilizing proteins and modified proteins is an essential approach to studying forest ecological protection. The sequence tagging analysis of insect feeding trauma-induced defense genes in hybrid poplar identified two defense proteins: Kunitz trypsin inhibitor and chitinase. Additionally, the genes responsible for the feeding-induced emission of terpene volatiles from hybrid poplar by *Trichoderma harzianum* were cloned and analyzed for their functional characteristics and expression types (Arimura et al., 2009; Cheng et al., 2013; Song et al., 2014). Proteomics and other techniques were used to investigate the molecular characteristics of protein expression in maize in response to insect feeding damage. Additionally, the molecular characteristics of differential expression of resistance proteins in plant-insect co-evolution were examined (Baldwin et al., 2001; Conrath, 2011; Elsayed, 2011; Peng et al., 2011; Wei and Kang, 2011; Smith and Clement, 2012; Cheng et al., 2013). Tobacco lice prick the phloem of tobacco and inject Bt56 protein, which interacts with the transcription factor NTH202 in the phloem to activate the salicylic acid signaling pathway in the plant, which induces the accumulation of salicylic acid in the plant to inhibit jasmonic acid production in the plant and reduce the resistance (Xu et al., 2019). Although these explorations have greatly advanced the study of plant-induced insect resistance, previous studies have also shown that plant-induced defense responses are a complex process. The mechanism of defense response varies from plant to plant and from stimulus to stimulus. As a result, there are many new findings and confusions in the current studies. Here, we investigated for the first time the phosphoproteomics of Chinese pine in response to feeding stimuli of Chinese pine caterpillars under natural conditions. Changes in protein expression levels, protein modifications, identification of functional modules and pathways, and monitoring of resistance-related substances in response to feeding stimuli from Chinese pine caterpillars (*Dendrolimus tabulaeformis*) are involved in the defense process of Chinese pine.

Protein phosphorylation modification, first reported in 1926, has become the most well-known type of post-translational modification (PTM) (Sefton, 1998). The identification of protein phosphorylation modification sites holds significant value for vital biological regulatory processes such as protein phosphorylation, dephosphorylation, alterations in protein structure, changes in enzyme activity, modifications to substrate specificity, and more (Pawson and Scott, 2005). Modified proteomics is a commonly used method to investigate dynamic changes, including plant defense responses, in search of biomarkers, such as stably differentially expressed proteins. PTM is a small but diverse and central regulatory step in the protein mass transition process. PTMs of proteins have a profound impact on protein diversity and molecular function, as they represent highly regulated molecular patterns. Protein phosphorylation modificationomics is significant in plant adaptation mechanisms (Rampitsch, 2017; Fatma et al., 2019). The frequency of proteins involved in the activities of plant life is significant. High-throughput proteomics technology has expanded opportunities for thorough investigations of the protein modifier group (Meier et al., 2020; Demichev et al., 2022).

Phosphorylation modifications are the most prevalent and abundant type of PTMs in proteins. They have a significant impact on the various functions that proteins perform. Additionally, conducting thorough research on the PTM of proteins can provide insights into the mechanisms underlying plant life activities, facilitate the identification of key modification proteins that respond to biotic stress, and enable the identification of specific modification sites. Phosphorylation modifications activate substrates, modulate downstream pathways, and achieve biological significance through cascade amplification effects. Kinases trigger the phosphorylation modification of proteins by transferring phosphate groups to amino acids such as serine, threonine, and tyrosine. This process regulates various functions of target proteins, which in turn impact cellular metabolism, signaling, and other vital life processes. Phosphoproteomics is a crucial method for studying plant processes in response to biotic stresses in great detail. The utilization of phosphoproteomics provides valuable insights into the response mechanisms that trigger resistance in plants during adverse stress conditions (Perazzolli et al., 2016).

Phosphoproteomics unveils the phosphorylation modification between the plant's target of rapamycin (TOR) kinase and the abscisic acid (ABA) receptor-coupled signaling pathways. This illustrates how plants use a conserved phosphorus-regulated feedback mechanism to balance growth, development, and stress responses. When external stressors impact plants, their typical growth activity is hindered by the hormones salicylic acid (SA), jasmonic acid (JA), and ethylene (ET). Instead, this leads to a heightened defense response (Waadt et al., 2022). Proteins undergo phosphorylation when a phosphate kinase transfers a phosphate group to a downstream protein, which may be a kinase or transcription factor. Simultaneously, the upstream kinase stimulates the protein's phosphorylation, resulting in a multistage kinase pattern that facilitates amplification of the signal through cascading. Phosphorylated proteomes can quantify phosphorylated proteins that are significantly expressed in signaling pathways, thereby identifying phenotypically relevant activated signaling pathways and elucidating the associated mechanisms (Liu et al., 2018). The gene set enrichment analysis (GSEA) algorithm predicted the activity of phosphorylated kinases, and the activity did not correlate with their protein expression. Kinase regulation is a "many-to-many" relationship, with multiple phosphorylated kinases regulating one substrate and one phosphorylated kinase regulating multiple substrates. Site modification prediction performs site-by-site clustering analysis, which provides greater differentiation and accuracy than gene clustering analysis (Krug et al., 2019). The level of protein phosphorylation regulated by the protein kinase is correlated to the substrate expression, indicating its regulation state to some extent.

Higher levels of protein phosphorylation are likely to indicate increased protein kinase activity (Hernandez-Armenta et al., 2017).

A proteome-based approach that focuses on phosphorylation was utilized to analyze and identify *Arabidopsis* modification profiles, and to screen conserved sites within a specific amount of phosphorylated peptides and their respective phosphorylation sites. Conservation of function is disrupted through point mutation mimicry, exposing the homeostatic mechanism of TOR kinase and ABA in mediating plant growth, development, and drought stress response (Wang et al., 2018). Phosphorylated proteomic techniques enable the investigation of plant regulation under low-temperature stress conditions (Zhao et al., 2017). Phytosulfokine (PSK) is a plant polypeptide hormone that promotes growth. When PSK signaling is absent, plant growth is inhibited, but disease resistance is increased (Förderer and Chai, 2023). PSK binds to phytosulfokine receptor 1 (PSKR1) and somatic embryogenesis receptor-like kinase (SERK) receptors during plant defense and growth periods, respectively, and induces activation of the calcium-dependent kinase 28 (CPK28) via the phosphorylation pathway. Glutamate synthase 2 (GS2) undergoes serine site phosphorylation at s334 and s360 induced by CPK28 kinase, promoting plant defense responses and regulating nitrogen availability for plant growth, respectively (Ding et al., 2023).

Plant cells utilize intricate signaling pathways in response to intricate biotic stress stimuli. Phosphorylated proteins play a essential role in researching the mechanisms of defense signaling induced by plants (Mukherji, 2005; Rampitsch, 2017). High-throughput phosphoproteomics provides a technological basis for the study of signaling cascades during plant-induced resistance responses, and specific protein-associated signals generated by phosphorylated kinase catalysis. The study of plant protein kinases and phosphorylated proteins has led to the identification of numerous protein modification signaling network components with prominent roles (Bentem and Hirt, 2007; Xing and Laroche, 2011). This creates the possibility of constructing signaling networks such as plant-induced resistance. Reversible protein phosphorylation is important for signal transduction mechanisms and signaling pathways (Rossignol, 2006), advancing the establishment of predictable models of plant protein phosphorylation and the process of plant post-genome integration.

By integrating the proteomic and phosphoproteomic results of Chinese pine caterpillar feeding stimulus-induced defense responses in Chinese pine, we systematically clarify the phosphorylation-modified proteins, kinases, and their defense regulatory functions that are involved in pine's defense response mechanism against caterpillars under natural conditions. To analyze the key phosphorylation modification proteins, core genes and major defense products in the process of Chinese pine resistance induced by caterpillar, and to reveal the expression regulation law and upstream and downstream correlation of the three. A network of interactions and functional modules for phosphorylation-modified proteins of Chinese pine defense response were built. Determining the accuracy of key proteins in the oleander defense response mechanism at the validation level and revealing the specificity of the feeding stimulus in the formation of the oleander defense mechanism.

Materials and methods

Plant and insect materials and growth conditions

The experiment utilized Chinese pine test samples obtained from Huangtuliangzi State-owned Forest Farm in Pingquan City, Chengde City, Hebei Province, and Chinese pine caterpillars collected from Yushulinzi Forest in Pingquan City, Hebei Province, and the border region between Pingquan City and Liaoning Province. Pure Chinese pine forests with identical elevation, slope, aspect, tree thickness, and management level, unaffected by herbivores and disease, were selected for the experiment. Prior to each treatment, a group of sixth–seventh instar mature caterpillar larvae was collected and screened to ensure consistent feeding levels and stress levels on Chinese pine needles. The Chinese pine caterpillars were stored in insect bags to remove any remaining inactive or damaged bodies, including those infested with bacteria, fungi, or other insects, to minimize interference with the experiment. The caterpillars were also deprived of food for at least 12 h prior to testing.

Experimental processing and sample collection

A random sampling method was utilized to select test plants in the forest. Within the test site, sturdy 10-year-old Chinese pine trees with uniform growth, and no herbivores or diseases, were selected and sequentially tagged and labeled. One branch in each of the four cardinal directions was selected, ensuring good size, thickness, and consistent growth from the middle layer of the Chinese pine tree canopy. Wear gloves and gently spread 10 Chinese pine caterpillars (quickly climbing from the bottom of the bag to the opening, representing strong vitality) evenly onto the Chinese pine needles and leaves for each branch. Each branch should have 10 caterpillars. Use identical-sized net covers to wrap around the feeding areas for the Chinese pine caterpillars on each branch, secure the net mouth with a string to prevent the test insects from escaping.

Three treatment groups were established to observe Chinese pine caterpillar feeding at different time points (0 h for control, 2 h, and 8 h). Each group comprised six Chinese pine replicates to ensure reliable results. At each time point, the netting was removed to collect the Chinese pine caterpillars, which were subsequently returned to the insect bags. Three control groups were formed to control leaf-cutting, and the treatment duration was arranged as previously mentioned. For the leaf-cutting procedure, we selected pine needles from a single robust branch positioned in the middle layer of the Chinese pine's canopy, using scissors to make the cuts. Each group had six Chinese pines as biological duplicates.

Controlling each Chinese pine specimen experimentally with identical treatments of pine caterpillar feeding and leaf-cutting, we selected direct-bearing tissue that responded to stress for our sample collection. We ensured that the pine trees were all of equal numbers and vigor. At each of the three intervals in the experimental design, pine needles located 3 cm below the point of injury caused by caterpillar feeding or leaf-cutting were harvested. The specimens were wrapped in aluminum foil, formed into

squares that are smaller than the tank's opening, labeled, and then quickly placed in a liquid nitrogen tank. The specimens were then delivered to the lab and stowed in an ultra-low temperature freezer at −80°C until needed.

The complete experimental procedures for tandem mass tag (TMT) proteomics, including protein ex-traction, trypsin digestion, TMT labeling, high performance liquid chromatography (HPLC) fractionation, liquid chromatography-mass spectrometry/mass spectrometry (LC-MS/MS) analysis, database search, and bioinformatics methods, are elaborated in **Supplementary material**. To compare protein sequences and collect annotation information on homologous proteins, a search was conducted on the Chinese pine transcriptome database.

Bioinformatics analysis

Motif analysis of protein phosphorylation modifications using Motif-x algorithm (MoMo) software V5.0.2. Phosphate kinase family prediction upstream of the phosphate site using Group-based Prediction System (GPS) V5.0 (Wang et al., 2020). Phosphokinase activity prediction using GSEA V4.0.3 (Subramanian et al., 2005; Guo et al., 2019). Phosphokinase activity bar graph using ggplot2 R package4 V3.2.1 (Hadley, 2016). Phosphokinase activity heatmap using heatmap R package V1.0.12. Phosphokinase regulatory network visualization using networkD3 R package V0.4 and Cytoscape5 (Shannon, 2003).

PRM analysis

The materials used for parallel reaction monitoring (PRM) testing included pine needles at 0-, 2-, and 8-h intervals after caterpillar feeding treatments. Each sample was analyzed using three biological replicates for PRM analysis. The complete procedure is presented in **Supplementary material**.

RT-qPCR analysis

Pine needles were collected at 0, 2, and 8 h after feeding and leaf cutting for use as materials in real-time quantitative polymerase chain reaction (RT-qPCR). Comparison of the two treatments with a view to highlighting the specific defense response of Chinese pine to herbivore feeding stimuli. Six replicates were used for each time point treatment, with corresponding sample bags selected randomly. RNA extraction from Chinese pine needles was performed using the Tengen Polysaccharide and Polyphenol Plant Total RNA Extraction Kit DP441 based on its instruction manual. A sample volume of 100 mg of Chinese pine needle tissue was utilized. Thermo Scientific NanoDrop 2000 was employed to determine RNA and cDNA concentrations.

Reverse transcription was performed using the R223-01 Novozymes HiScript II Q RT SuperMix for qRCR (+gDNA wiper) kit. Amplification was conducted with a Thermal Cycler Block 5020, using a 20 μl volume that was incubated at 50°C for 15 min, followed by 85°C for 5 s. Subsequently, we evaluated the concentration of cDNA which passed successfully for the next stage of the experiment.

Primer software was utilized for designing the primers. The NCBI BLAST tool was utilized to screen the primers with the highest specificity. Genewiz synthesized the primers. ACT, also known as actin, served as the reference gene with the primer sequences (5′-3′) F: ATTCTCCTCACCGAAGCACC and R: ATGGGAACTGTGTGGCTGAC. The product size was 188 and the accession number is MN172177. The specific primers for genes are listed in **Supplementary Table 1**.

The primer sequences for RT-qPCR were selected from the Novozymes ChamQ Universal SYBR RT-qPCR Master Mix kit Q711-02/03. The Roche LightCycler 96 instrument was employed for this study. A 20 μl system was used for the RT-qPCR, and mixture configuration can be found in Q711-02/03. In order to enhance the amplification efficiency, the "three-step method" in the kit was employed and the extension time was extended. The specific reaction conditions are as follows: pre-denaturation for 30 s at 95°C was followed by a cycling reaction (40 times) at 95°C for 10 s, 56°C for 30 s, and 72°C for 60 s. Subsequently, a melting curve was run at 95°C for 15 s, 60°C for 60 s, and 95°C for 15 s, with an additional 15 s at 95°C and 60 s at 95°C. The genes' relative expression was analyzed utilizing the $2^{-\Delta\Delta Ct}$ method, and the data underwent statistical analysis using the DPS data processing system (Tang and Zhang, 2013). The experiments were conducted with a minimum of three technical replicates. In addition, at least use three biological replicates along with three technical replicates for RT-qPCR analysis.

Results

The study of Chinese pine phosphorylated proteins generated 143,668 secondary mass spectra, of which 26,056 were valid (18.1% utilization). The findings revealed 10,817 peptides, 9,421 of which were phosphorylated, and 12,848 sites with phosphorylation-modification located on 4,073 proteins. Phosphorylated proteins were detected in pine needles through a T assay with a P-value < 0.05. **Table 1** summarizes the data on phosphorylated proteins and modification sites normalized to the proteomic data. The phosphorylated proteome experiment was performed to analyze the differential proteins and phosphorylation modification sites in the control group (0 h) and the test group (2 and 8 h). Each set of protein abundance values and modification sites were compared, selecting a twofold change, and normalized with the proteome data. From this, the number of differentially expressed proteins was quantitatively determined. Compared to the control group, there were 171 upregulated phosphorylated proteins and 218 phosphorylation-modification sites, as well as 117 downregulated proteins and 147 phosphorylation-modification sites, 2 h after the Chinese pine caterpillar's feeding stimulus. A total of 192 proteins with phosphorylation and 246 sites with upregulated expression of phosphorylation modification were discovered, along with 104 proteins with phosphorylation and 138 sites with downregulated expression of phosphorylation modification, all 8 h following the feeding stimulus. Comparing the phosphorylated proteins and phosphorylation-modified sites at 2 and 8 h after the feeding stimulus revealed that 11 proteins and 12

TABLE 1 Differentially phosphorylated modification sites (phosphorylated protein) summary after normalized.

Compare group	Regulated type	Fold change >1.2	Fold change >1.3	Fold change >1.5	Fold change >2
2 h/0 h	Upregulated	1,033 (597)	870 (524)	578 (387)	218 (171)
	Downregulated	1,703 (896)	1,351 (766)	718 (466)	147 (117)
8 h/0 h	Upregulated	1,115 (652)	964 (590)	656 (443)	246 (192)
	Downregulated	1,578 (841)	1,251 (713)	649 (423)	138 (104)
8 h/2 h	Upregulated	535 (392)	279 (229)	74 (64)	12 (11)
	Downregulated	343 (244)	213 (154)	77 (63)	19 (17)

Filtered with threshold value of expression fold change and P-value < 0.05.

sites had increased expression while 17 proteins and 19 sites had decreased expression.

Motif analysis of protein phosphorylation modifications

The amino acid sequence pattern before and after phosphorylation modification sites, and their role in Chinese pine response to the caterpillar feeding stimulus were obtained and analyzed with statistical precision using MoMo software. The regularity pattern of the amino acid sequence trends in the region containing the phosphorylation modification site was calculated. Therefore, the characteristics of the sequence of phosphorylation modification sites can be determined, enabling the identification or hypothesization of the phosphorylase linked to the response of Chinese pine to the feeding stimulus of the caterpillar. The patterns at the serine and threonine phosphorylation modification sites and their enrichment details, along with the heatmap displaying the amino acid base sequence enrichment upstream and downstream of the phosphorylation modification sites, are presented in **Figure 1**.

Phosphorylated serine has 63 motifs, threonine has 10 motifs and tyrosine has only 5 motifs. Specific information can be found in the latest submitted **Supplementary Table 2**.

Mfuzz clustering analysis of differentially phosphorylated modification sites

Cluster analysis was conducted to study changes in the abundance of phosphorylation modification sites among Chinese pine proteins after caterpillar feeding at different time points (2 h post-treatment, 8 h post-treatment, and 0 h control). A total of 9,629 modification sites were identified using a quantitative histological study of phosphorylation modifications. To eliminate modification sites with significant changes in abundance across 0, 2, and 8 h samples, we initially subjected the relative expression of modification sites to a Log2 logarithmic transformation. Next, we filtered out modification sites with SD (standard deviation) >0.5. The 1,684 modification sites that passed the initial screening were utilized for an expression pattern clustering analysis using the Mfuzz method. The columns in the cluster were labeled by corresponding expression pattern classes, and modification sites in the same cluster displayed similar trends in expression transformation (**Figure 2**). Mfuzz analysis parameters: the number of clusters k is set to six and the degree of cluster fuzzy m is set to two.

To facilitate presentation of all analysis results, the two most significantly enriched entries of GO molecular function.enrich.out (**Supplementary Table 3**), GO cellular component.enrich.out (**Supplementary Table 4**), KEGG.enrich.out (**Supplementary Table 5**), GO biological process.enrich.out (**Supplementary Table 6**), and Domain.enrich.out (**Supplementary Table 7**) enrichment analysis results are displayed on the right side of the corresponding cluster expression pattern clustering graph. Of the 83 phosphorylation sites in cluster 1, the MAPK signaling pathway-plant and pyruvate metabolism showed the highest levels of enrichment in terms of KEGG pathway. Additionally, both nucleic acid binding transcription factor activity and sucrose synthase activity displayed the most significant levels of enrichment for GO molecular function, while GO biological processes showed significant levels of enrichment for nitrogen compound transport and ion transmembrane transport. Among the 263 phosphorylation sites in cluster 2, the KEGG pathway showed the most significant enrichment in photosynthesis and glycolysis/gluconeogenesis. Additionally, the GO cellular composition demonstrated that the photosynthetic membrane was most significantly enriched, while the GO biological processes indicated that monosaccharide metabolic processes were significantly enriched. Of the 107 phosphorylation sites found in cluster 3, the photosynthesis pathway displays the greatest enrichment within the KEGG pathway. Additionally, the GO molecule function shows that nucleic acid binding and organic cyclic compound binding are the most significantly enriched. Similarly, the GO cellular composition demonstrates that intracellular part is the most significantly enriched. As for the GO biological process, RNA metabolic process and RNA processing were significantly enriched. Lastly, the structural domain shows that RNA recognition motif domain is the most significantly enriched. Among the 119 phosphorylation sites in cluster 4, carbon fixation in photosynthetic organisms and starch and sucrose metabolism were found to be significantly enriched KEGG pathways. Meanwhile, lyase activity and catalytic activity were the most significant parts of GO molecule functional enrichment. In terms of structural domains, the ABC-transporter extracellular N-terminal domain and plant PDR ABC transporter associated were the most significantly enriched. The KEGG pathway exhibited the highest level of enrichment for the amino sugar and nucleotide sugar metabolism and MAPK signaling pathway-plant pathways among the 615 phosphorylation sites within cluster 5. Concerning

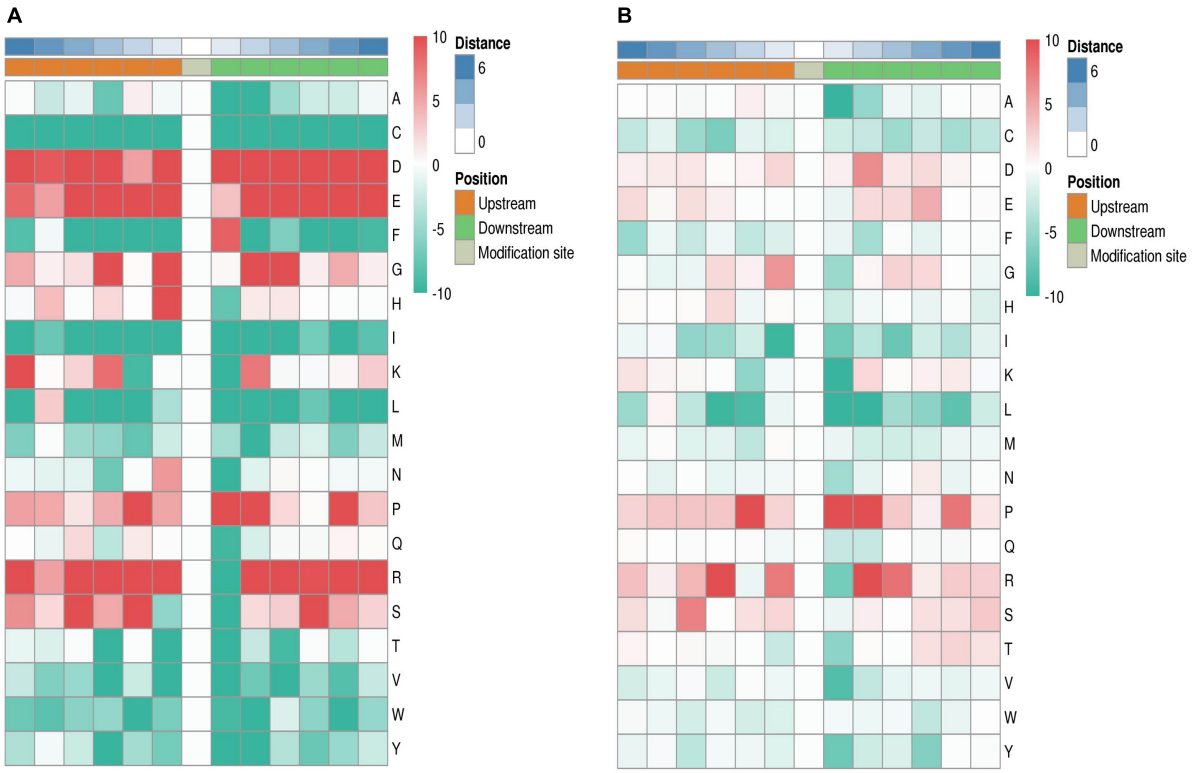

FIGURE 1
Heatmap of serine **(A)** and threonine **(B)** motif enrichment at upstream and downstream of phosphorylation modification sites. The red color in the graph denotes significant amino acid enrichment near the modification site, while the green color signifies a significant reduction in amino acids near the modification site.

GO molecular functions, microtubule binding and cytoskeleton (protein binding) exhibited the most significant enrichment, while the most enriched GO cellular compositions were cell periphery and cytoplasmic part. Additionally, protein binding showed a significant enrichment as a GO molecular function. The 497 sites phosphorylated in cluster 6 showed significant enrichment for endocytosis in KEGG pathway analysis, structural composition of cytoskeleton and protein domain in GO molecular function, and organelle organization and cellular localization in GO biological processes.

Prediction of phosphorylation sites upstream kinases and phosphokinase activity prediction analysis

Phosphokinase prediction upstream of the phosphorylation site was conducted utilizing the GPS 5.0 software. Based on the assumption that analogous short peptide segments may exert comparable biological functions and that akin protein kinases may regulate comparable short linear motifs, it is anticipated that the Chinese pine tree may govern a group of kinase proteins at particular phosphorylation sites prompted by feeding stimuli in caterpillars. The kinase proteins, pertaining to the kinase protein family in this species, were acquired through a comparison with the iEKPD database. Subsequently, protein–protein interaction information (PPI) was used to filter out potential false-positive interactions. A total of 1,736 regulatory connections were foreseen among 413 protein kinases and 780 sites where phosphorylation modification occurred on 485 identified proteins.

The study employed a gene set consisting of the regulatory correlation between phosphokinase and phosphorylation sites. The expression level of phosphosites served as the rank file in the samples, while the relative quantitative ratio value of differentially phosphorylated modification sites served as the rank file in the comparison groups. The kinase activities of the samples and the comparison group were predicted separately using the GSEA method. Fifty-six phosphokinases appeared to be inhibited, and one phosphokinase appeared to be activated in the Chinese pine needles 2 h after being stimulated by the caterpillars' feeding. In the sample collected 8 h after exposure to stress, there was evidence of inhibition in 47 phosphokinases, while only 1 phosphokinase appeared to be activated. Compared to the treatment group, pine needle samples from the control group (0 h) showed inhibition of 15 phosphokinases and activation of 56 phosphokinases (Figure 3A). Phosphorylation of substrate sites can reflect the level of kinase regulation to a certain extent; the higher the protein phosphorylation level influenced by phosphokinase, the greater the kinase activity may be, and vice versa. The trends among the three comparison groups were consistent. In the 2 h vs. 0 h and 8 h vs. 0 h groups, respectively, the number of phosphokinases tending to inhibit was 59 and 57, while the number of phosphokinases tending to activate was 11 and 12. The comparison group at 8 h vs. 2 h had 8 phosphokinases that displayed tendencies toward

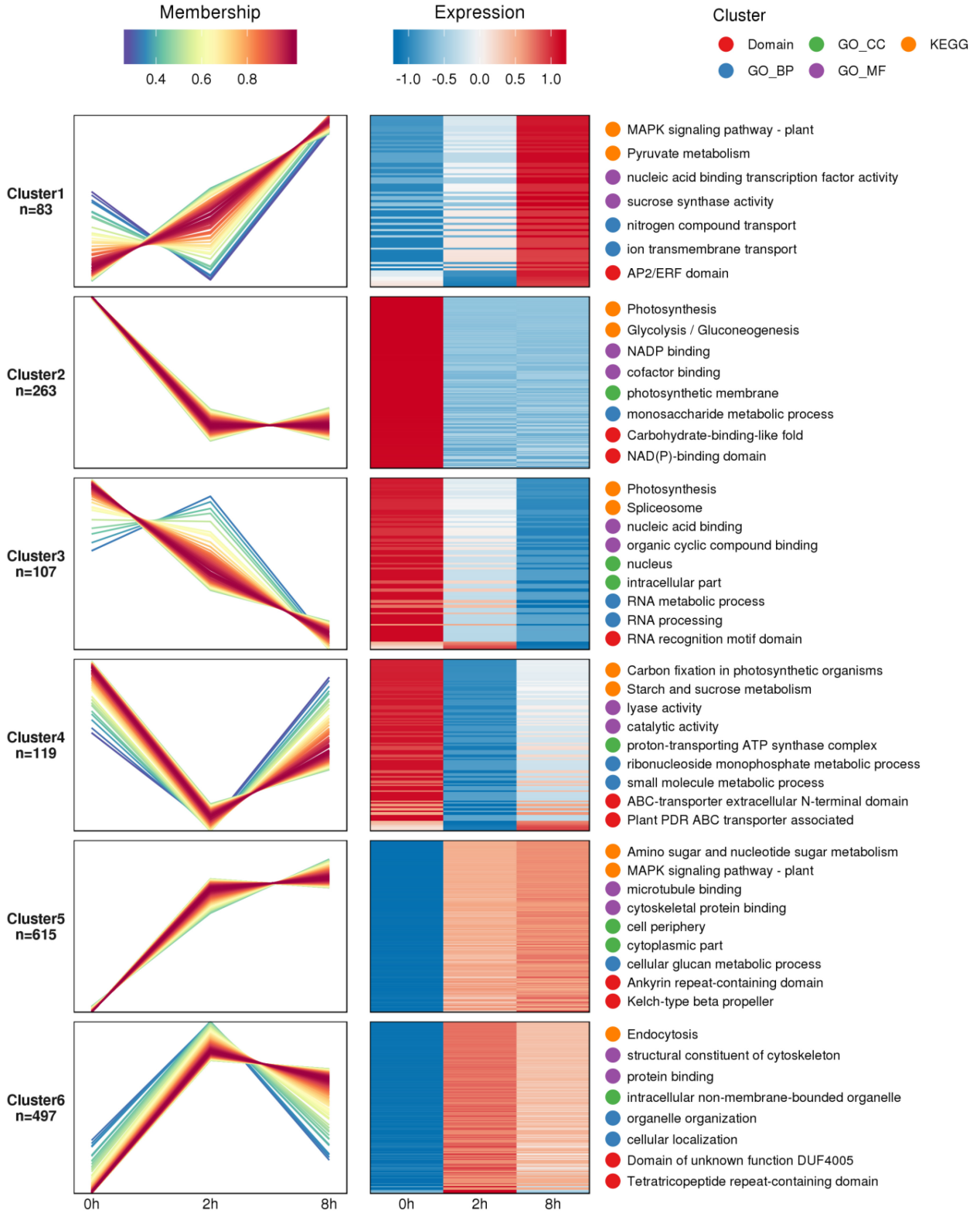

FIGURE 2
Summary graph of cluster analysis of differential phosphorylation site expression patterns. The figure depicts a line graph illustrating the expression of phosphorylation modification sites on the left side, and a heatmap representing the expression on the right side. Each cluster on the graph and map corresponds to a specific modification site. Line graph: the horizontal axis coordinate is the sample, the vertical coordinate is the relative expression of the phosphorylation modification site, a line represents a phosphorylation modification site, and the line color indicates the affiliation of the phosphorylation modification site in the current class. Heatmap: the horizontal axis represents the samples, while the vertical axis displays the different phosphorylation modification sites. The heatmap colors correspond to the relative expression levels of phosphorylation modification sites detected in the samples.

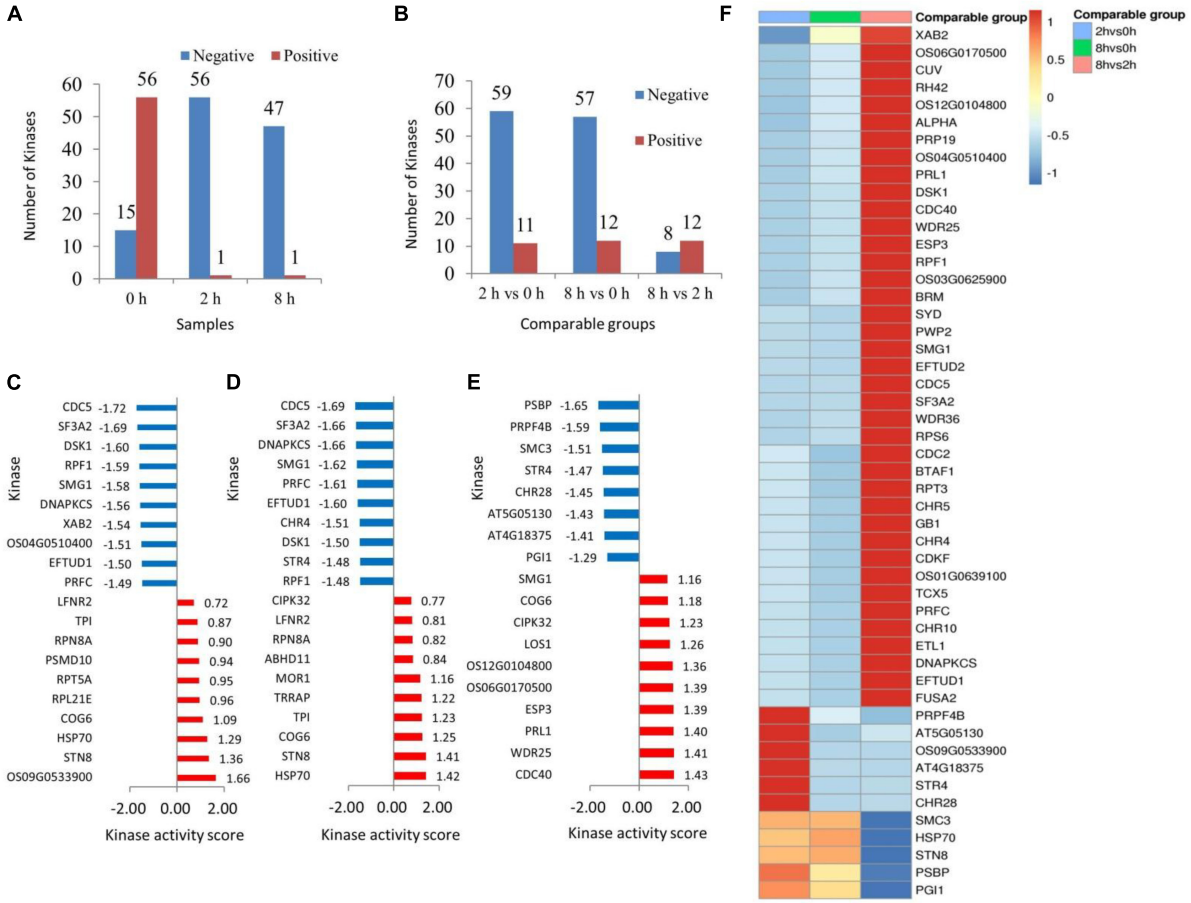

FIGURE 3
Statistical graph of sample **(A)** and comparable groups **(B)** phosphokinase activity. The *x*-axis denotes the sample name while the *y*-axis represents the number of kinases. Red color signifies activation tendency and blue color indicates inhibition tendency. Bar graph of phosphokinase activity scores in 2 h vs. 0 h **(C)**, 8 h vs. 0 h **(D)**, and 8 h vs. 2 h **(E)** comparison group. The enrichment analysis method provided the NES value which served as the kinase activity score. A kinase with a score >0 is typically activated, while a score <0 indicates inhibition. The *x*-axis is the phosphokinase activity score, and the *y*-axis is the top 10 phosphokinases in terms of activity score for the activated or inhibited state, with red representing the activated state and blue representing the inhibited state. Heatmap of phosphokinase activity matrix for the comparison group **(F)**. Columns are sample names, rows are phosphokinases (clustering and *Z*-score normalization transformations on rows).

inhibition and 12 phosphokinases displaying tendencies toward activation. The number of phosphokinases displaying tendencies toward activation was found to be essentially the same throughout all three comparison groups (Figure 3B).

Activity prediction of kinases based on protein phosphorylation expression using GSEA.ES (enrichment score) responds to the extent to which members of the kinase-regulated locus are enriched at either end of the sorted list. Normalization of the enrichment score yields the normalized enrichment score (NES). In the comparison group 2 h vs. 0 h, the phosphokinases OS09G0533900 (endoglucanase 24), STN8 (serine/threonine-protein kinase STN8, chloroplastic) and HSP70 (heat shock 70 kDa protein 17), among others, were in the activated state. Phosphokinase CDC5 (cell division cycle 5-like protein), SF3A2 (splicing factor 3A subunit 2), and DSK1 (protein kinase dsk1), on the other hand, were in an inhibited state (Figure 3C). In the comparison group 8 h vs. 0 h, phosphokinases in activated state included HSP70, STN8, and COG6 (conserved oligomeric Golgi complex subunit 6), among others. Phosphokinases in the inhibited state were CDC5, SF3A2, and DNAPKCS (DNA-dependent protein kinase catalytic subunit) (Figure 3D). The phosphokinase CDC40 (pre-mRNA-processing factor), WDR25 (WD repeat-containing protein25), and PRL1 (protein pleiotropic regulatory locus) were in an activated state in the comparison group at 2 h vs. 8 h. Phosphate kinase PSBP (oxygen-evolving enhancer protein 2, chloroplastic), PRPF4B (serine/threonine-protein kinase PRP4 homolog), and SMC3 (structural maintenance of chromosomes protein 3) were in the inhibited state (Figure 3E).

The Kinase Activity Clustering Heat Map enables observation of kinase activity commonality within the same phenotype or specificity in different phenotypes. This aids exploration of potential relationships between kinase activity and phenotype for further screening of key kinases in Chinese pine in response to caterpillar feeding stimuli. A side-by-side comparison of the significantly enriched phosphokinases in the 2 h vs. 0 h, 8 h vs. 0 h, and 8 h vs. 2 h comparison groups showed that the phosphokinase XAB2 (pre-mRNA-splicing factor SYF1) was in a markedly inhibited state in the 2 h vs. 0 h comparison group, and in a markedly activated state in the 8 h vs. 2 h comparison group.

Nineteen phosphokinases including OS06G0170500 (zinc finger CCCH domain-containing protein 40), CUV (pre-mRNA-splicing factor ATP-dependent RNA helicase DEAH7), and RH42 (DEAD-box ATP-dependent RNA helicase 42), demonstrated inhibition in the 2 h vs. 0 h comparator group, and activation in the 8 h vs. 2 h comparator group. Nineteen phosphokinases, such as SYD (chromatin structure-remodeling complex protein SYD), PWP2 (periodic tryptophan protein 2 homolog), and SMG1 (serine/threonine-protein kinase SMG1), were inhibited further in the comparison group of 8 h vs. 0 h, and were significantly activated in the comparison group of 8 h vs. 2 h. Phosphokinase PRPF4B and AT5G05130 (putative SWI/SNF-related matrix-associated actin-dependent regulator of chromatin subfamily A member 3-like) were activated in both 2 h vs. 0 h comparison groups. PRPF4B was inhibited in the 8 h vs. 0 h comparison group and also in the 8 h vs. 2 h comparison group. On the other hand, AT5G05130 was inhibited in both the 8 h vs. 0 h comparison group and the 8 h vs. 2 h comparison group. Four phosphokinases, including Phosphokinase OS09G0533900, AT4G18375 (KH domain-containing protein), STR4 (rhodanese-like domain-containing protein 4, chloroplastic) and CHR28 (helicase-like transcription factor CHR28), showed activation in the 2 h comparison group when compared to the 0 h group. Additionally, phosphokinase SMC3 was significantly inhibited in the 8 h vs. 2 h comparison group. Both HSP70 and STN8 phosphokinases tended to be activated in the 2 h vs. 0 h comparison group, whereas both phosphokinases PSBP and PGI1 (glucose-6-phosphate isomerase 1, chloroplastic) tended to be activated in the 8 h vs. 0 h comparison group, and were significantly inhibited in the 8 h vs. 2 h comparison group (**Figure 3F**).

Kinase regulatory network analysis

For each comparative group of pine needle samples, we screened for phosphokinases that were significantly activated or inhibited and phosphorylation sites with significantly different expression levels (ratio threshold for fold change in differential expression is 2 and *P*-value threshold for significance of difference is 0.05) in response to insect feeding stress. Construct regulatory networks of kinases, observe regulatory relationships between kinases and substrates, and identify key regulatory kinases within complex networks. The kinases involved in the regulatory network in the control 0 h vs. 2 h post-feeding stimulation comparison groups were RPL21E (60S ribosomal protein L21-2), LOS1 (elongation factor 2), CDC5, SF3A2, and CHR4 (protein CHROMATIN REMODELING 4), and SMG1, DNAPKCS, OS09G0533900, and BTAF1 (TATA-binding protein-associated factor) (**Figure 4A**). The following kinases were involved in the regulatory network for the control 0 h vs. 8 h post-feeding stimulation comparison groups: AT4G18375, DSK1, SMG1, DNAPKCS, and TPI (triosephosphate isomerase, chloroplastic), CHR4, RPL21E, LOS1, BTAF1, and MOR1 (protein MOR1), TRRAP (transformation/transcription domain-associated protein), and STR4 (**Figure 4B**). The 2 and 8 h post-feeding stimulus comparison groups were examined for any inter-kinase associations. However, no such associations were found. Additionally, none of the MCODE score values reached the level of significance, indicating the absence of any clusters.

Analysis of functional modules of differential protein interaction networks

The MCODE add-on in the STRING application was utilized to extract high-connectivity modules in the protein interaction network. Following this, the module proteins underwent analysis for functional enrichment in a bid to identify significant biological processes in which they are involved. The differentially phosphorylated proteome was screened for 14 functional modules, focusing on PGK1 (phosphoglycerate kinase 1)-OS11g0171300 (fructose-bisphosphate aldolase, chloroplastic), and SHM4 (serine hydroxymethyltransferase 4), comparing the 0 and 2 h post-feeding stimulus groups (**Figure 5A**). Comparing the post-feeding stimulus comparison groups at 0 and 8 h, the differentially phosphorylated proteome was analyzed for 12 functional modules. Notably, At2g20050/At2g20040 (protein phosphatase 2C and cyclic nucleotide-binding/kinase domain-containing protein) stood out, followed by MOR1 (**Figure 5B**). No associations were found between differentially phosphorylated proteins in the comparison groups of 2 and 8 h post-feeding stimulus after screening, nor were there any associations of differentially phosphorylated proteins. Furthermore, no MCODE score values reached statistical significance, and consequently, no clusters were labeled.

PRM verification analysis

Parallel reaction monitoring quantification was conducted on four selected target proteins across nine samples (0 h-1, 0 h-2, 0 h-3, 2 h-1, 2 h-2, 2 h-3, 8 h-1, 8 h-2, and 8 h-3). For quantification, our experimental design used more than two distinct peptides per protein, although some proteins were identified with only one peptide due to sensitivity and other factors (**Table 2**). The precision of crucial proteins involved in the defense response mechanism of the Chinese pine was evaluated through protein-level validation. The validated PRM-assayed proteins consist of METK2 (S-adenosylmethionine synthase 2), PTI12 (PTI1-like tyrosine-protein kinase 2), pgk, and At3g59480 (probable fructokinase-4). METK2 plays a vital role in various biotic stresses in plants, and it is involved in the metabolism of cysteine and methionine. The function of PTI12 in plant stress response is focused on cytoskeletal regulation as a tyrosine kinase. pgk, a very conserved family of phosphorylated proteins, regulates senescence death in plant cells. Fructose kinase At3g59480 plays an important defense role in plant resistance pathways.

Real-time fluorescence quantitative PCR analysis

The four genes that correspond to the key phosphorylated proteins, verified through PRM, underwent RT-qPCR analysis. The study examined five groups: 0 h after the treatment (control), 2 h after pine caterpillar feeding stimulation, 2 h after leaf-cutting stimulation, 8 h after feeding stimulation, and 8 h after leaf-cutting stimulation. The trends in the relative expression of these four genes after feeding and leaf-cutting stimulation were as follows:

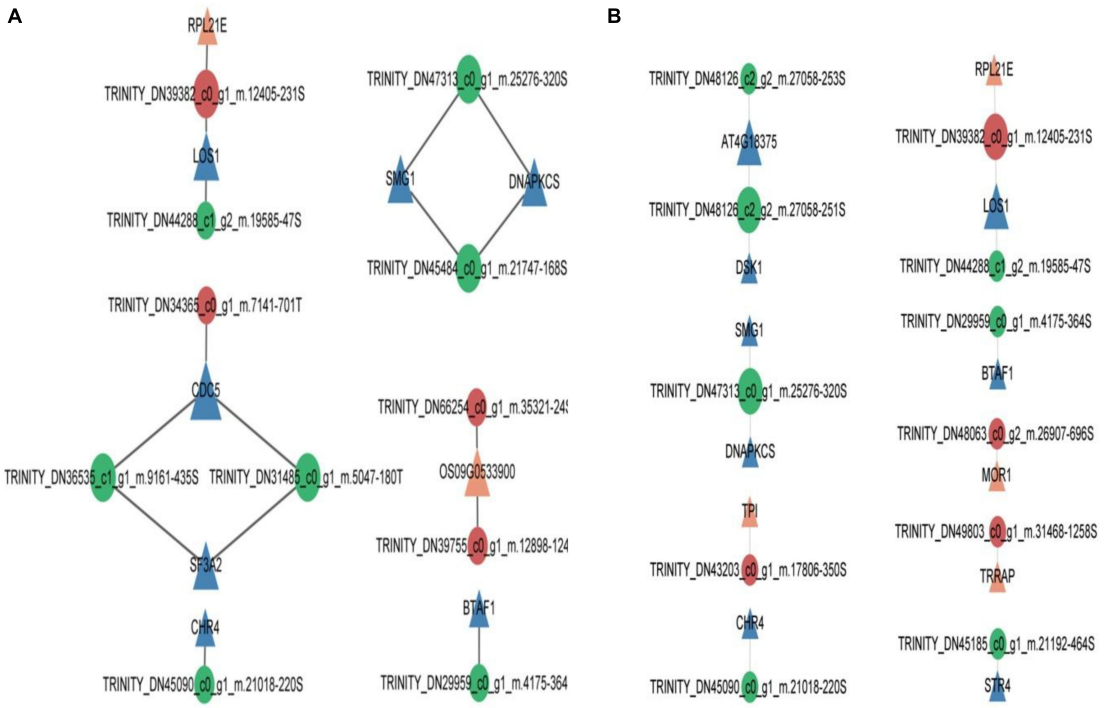

FIGURE 4
Comparison group of 0 h vs. 2 h **(A)** and 0 h vs. 8 h **(B)** kinase regulatory networks. Orange triangles indicate activated kinases while blue triangles indicate inhibited kinases. Red circles denote phosphorylation sites that are upregulated differentially, and green circles suggest phosphorylation sites that are downregulated differentially.

The expression levels of the *METK2* gene (Figure 6A) initially decreased before increasing and remained lower than those of the control at two particular time points post-treatment. The expression of the *METK2* gene showed a statistically significant ($P < 0.01$) decrease 2 h after feeding stimulation. There was also a significant ($P < 0.05$) difference in *METK2* expression 2 h after treatment with leaf-cutting stimulation. *METK2* expression was higher at 8 h compared to 2 h post-feeding, but this difference was not statistically significant. After cutting the leaves, the expression of *METK2* increased after 8 h. The relative expression of METK2 was lower at 8 h after leaf-cutting compared to 2 h after leaf-cutting. Additionally, the differential relative expression of METK2 was lower at 8 h after leaf-cutting with stimulation compared to 8 h after leaf-cutting, but the difference was not significant.

PTI12 (Figure 6B) demonstrated a pattern of increasing and subsequently decreasing relative expression following feeding. The expression of *PTI12* showed a significant increase ($P < 0.01$) 2 h after feeding, followed by a highly significant decrease ($P < 0.01$) 8 h after feeding. The expression level of *PTI12* decreased 2 h after leaf-cutting stimulation. However, it was highly significantly elevated ($P < 0.01$) at 8 h after leaf-cutting in comparison to the expression level observed at 2 h after leaf-cutting. The expression level of *PTI12* was significantly higher ($P < 0.01$) 2 h post-feeding stimulation compared to 2 h post-leaf-cutting stimulation. It is worth mentioning that the relative expression of *PTI12* was lower than that of leaf-cutting stimulation at 8 h after feeding stimulation and reached the level of a highly significant difference ($P < 0.01$).

The relative expression of *pgk* at 2 h after feeding and leaf-cutting was barely different from that of the control at 0 h and was not significant. From 2 to 8 h after treatment, the relative expression of genes increased with both feeding and leaf-cutting stimuli. However, only the difference in the relative expression of *pgk* under feeding stimuli reached a significant ($P < 0.05$) level. Gene expression was higher 8 h after feeding compared to 8 h after leaf-cutting, but there was no significant difference between the two (Figure 6C).

The relative expression of *At3g59480* (Figure 6D) was lower than that of the control and leaf-cutting treatments at both 2 and 8 h under feeding stimuli. This was shown by a notable reduction ($P < 0.01$) in the relative expression of *At3g59480*, 2 h following the feeding stimulus. The expression level of *At3g59480* significantly increased ($P < 0.01$) at 8 h after feeding in contrast to its expression level at 2 h after feeding. Likewise, the gene's expression level also significantly decreased ($P < 0.01$) 2 h after leaf-cutting stimulation. The expression level of *At3g59480* was significantly higher ($P < 0.01$) at 8 h post leaf cutting than at 2 h after leaf cutting. It is worth noting that the relative expression of At3g59480 showed significant differences when comparing 2 h after feeding to 2 h post leaf-cutting, and again when comparing 8 h after feeding to 8 h post leaf-cutting ($P < 0.01$).

Discussion

Exposing plants to external stressors triggers a cascade of resistant defensive processes. Extensive data indicates that

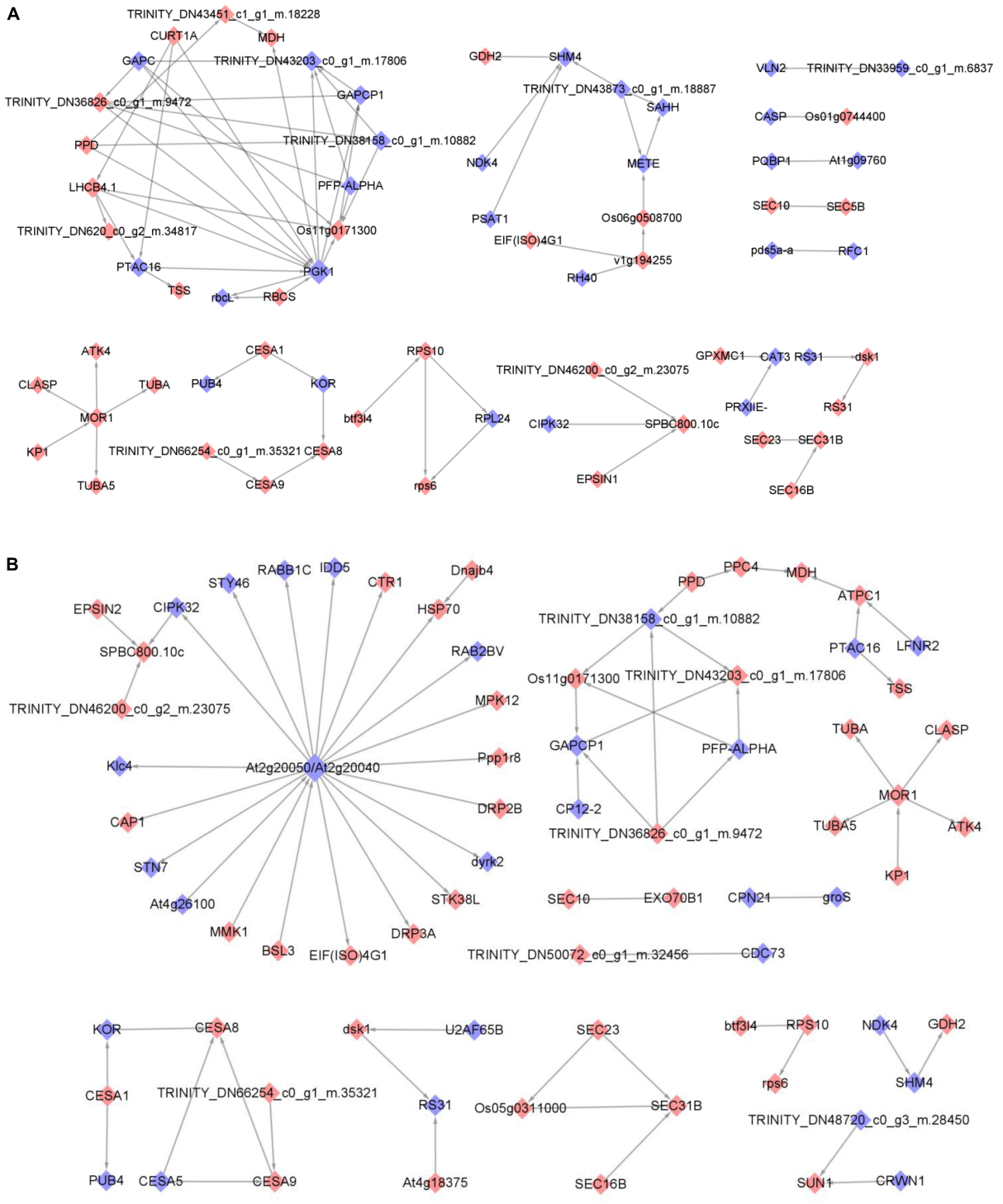

FIGURE 5
Protein Interaction Network Functional Module of 0 h vs. 2 h **(A)** and 0 h vs. 8 h **(B)** significantly different phosphorylated proteins. Phosphorylated protein database numbers or sequences from the comparison group based on a fold difference of 2.0 were compared with the STRING (v.11.0) protein interaction network database. The cytoscape tool was employed to visualize the differential phosphorylated protein interactions. The color scheme distinguished between upregulated proteins (red) and downregulated proteins (blue), with darker colors indicating greater differential folds in expression.

stress responses in plants, induced by various stress factors and extracellular signals, are closely linked to changes in the phosphorylation status of proteins. This phosphorylation status is considered an important aspect of plant immunity. Stress response reactions, including mitotic initiation, isoprene synthesis, cytoplasmic streaming, and sucrose phosphate synthase activity, are regulated by intracellular processes of protein kinase and protein phosphatase. Tyrosine kinases play a crucial role in regulating

TABLE 2 Parallel reaction monitoring phosphorylation-related protein quantification results.

Protein accession	Protein gene	2 h/0 h ratio	8 h/0 h ratio	8 h/2 h ratio
TRINITY_DN44630_c2_g2_m.20172	METK2	5.78	4.63	0.80
TRINITY_DN43176_c1_g1_m.17759	PTI12	3.30	2.94	0.89
TRINITY_DN49631_c0_g1_m.30899	pgk	10.05	6.36	0.63
TRINITY_DN41637_c0_g1_m.15403	At3g59480	43.70	35.22	0.81

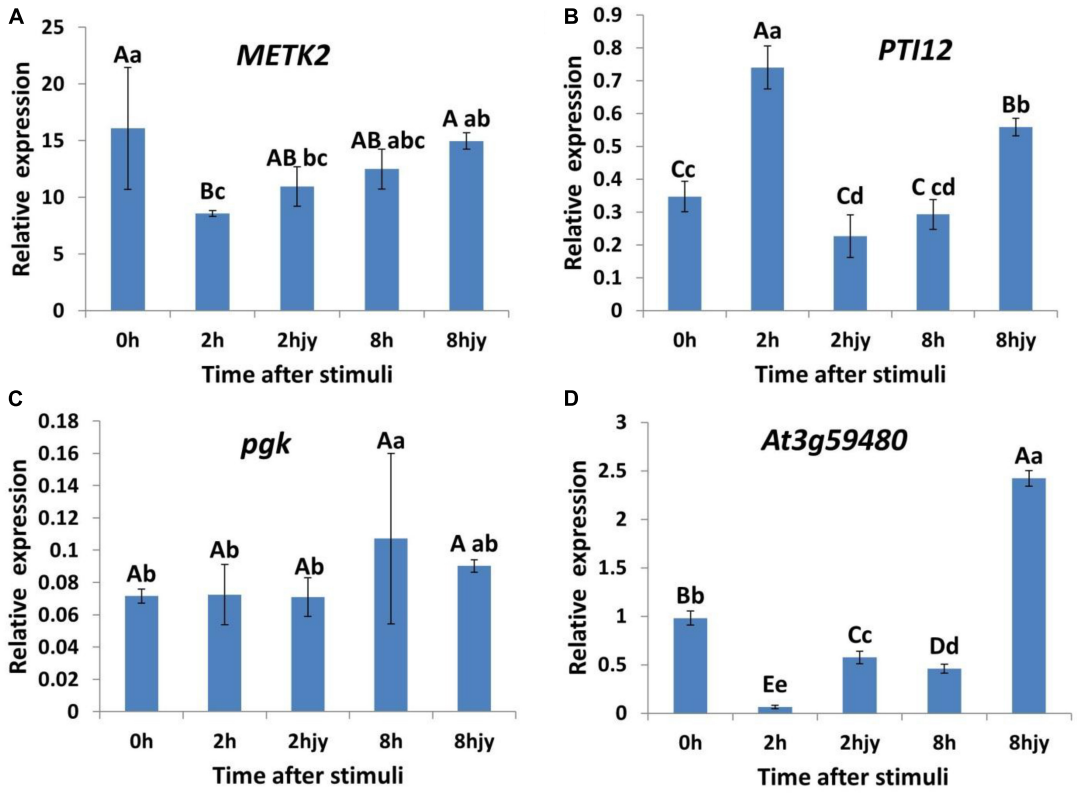

FIGURE 6
Real-time RT-PCR analysis of key phosphorylation-related protein upstream genes. Different letters represent significant differences, capital letters represent extremely significant differences ($P < 0.01$), lowercase letters represent significant differences ($P < 0.05$). **(A)** Relative expression of METK2 gene at 0 h in the control, 2 and 8 h after feeding stimulation and leaf cutting stimulation (2hjy and 8hjy). **(B)** Relative expression of PTI12 gene. **(C)** Relative expression of pgk gene. **(D)** Relative expression of At3g594800 gene.

plants' response to stress, particularly in relation to the cytoskeleton (Samofalova et al., 2020). This study found that the expression of PTI12, a tyrosine-like protein kinase in Chinese pine, increased significantly at 2 and 8 h after caterpillar feeding. However, the expression level at 8 h was lower than at 2 h. Our results confirm that phosphorylated proteins play a critical role in regulating plant defense mechanisms against phytophagous insect feeding in Chinese pine. This is achieved through protein phosphorylation modifications in response to caterpillar feeding, demonstrating an involvement of phosphorylated proteins in regulating plant resistance. The expression level of tyrosine kinase experienced a significant decrease, which regulates a notable increase in the expression level of the heat shock protein Heat Shock 70 kDa Protein 6 (HSP70B). Its molecular chaperone function helps minimize protein aggregation, while also aiding in the repair and protection of cellular proteins from stress damage (Lyu et al., 2019). Tyrosine protein kinase is implicated in the upregulation of 12-oxophytodienoate reductase 3 (OPR3), a vital enzyme in the JA synthesis pathway, which may lead to enhanced resistance of rice against phytophagous insects (Guo et al., 2015).

METK2 participated in the metabolic process of cysteine and methionine following feeding stimulation by the Chinese pine caterpillar. METK2 expression displayed a significant increase at 2 and 8 h compared to 0 h but exhibited higher expression at the onset of stress. These findings suggest that METK2 plays a continuous role in resistance-related processes. METK2 is responsible for catalyzing the conversion of methionine into S-adenosyl-L-methionine. Adenosine homocysteine lyase is an enzyme that utilizes S-adenosyl-L-methionine as a substrate to produce homocysteine (HCY). Bioinformatics analysis of differentially expressed proteins in this study shows that there is an interaction between these two enzymes. *METK2* is an upstream gene of S-adenosylmethionine synthase (SAM), SAM is

an essential element in the induced defense of *Arabidopsis* and plays a direct role in the defense response (Zhang et al., 2010). ET regulates defense transduction signals, while *SAM* is responsible for the involvement of ET biosynthesis (Reymond et al., 2004). The defense gene *SAM* is activated by the two-spotted leaf mite infestation in lima bean leaves, which catalyzes the biosynthesis of ET and induces a resistance response (Arimura et al., 2002). The *SAM* gene improves plants' defense against peach aphids. Technical term abbreviations will be explained upon their first use. Cloning and introducing the maize S-adenosylmethionine synthase (BtSAMS) gene into *Arabidopsis thaliana* reduced the number of peach aphids feeding on BtSAMS plants by over 50% compared to the control. Additionally, the number of neonate wakame on BtSAMS plants was less than 50% of the control (Yang et al., 2023). The expression of *GmSAMS1*, linked to defense response, underwent upregulation following phosphorylation modification in the Genetically Modified Calcium-dependent Protein Kinase 38 (*GmCDPK38)* soybean mutant. This modification ultimately intensified soybean resistance to *Spodoptera litura* (Li et al., 2022). Our results suggest a possible link between the expression of the *METK2* gene and the phosphorylation modification of resistance proteins in response to the ingestion of Chinese pine needles by the Chinese pine caterpillar. This activation or enhancement of resistance function in Chinese pine against caterpillar feeding is likely to occur.

At3g59480 (probable fructokinase-4) participates in the defense response of coconut trees to *Rhynchophorus ferrugineus* stress. Specifically, fructokinase plays a defensive role in the resistance pathway linked to sugar metabolism after 5 and 20 days of *R. ferrugineus*' feeding (Liu et al., 2023). This could explain why the expression of At3g59480 significantly increased in Chinese pine 2 and 8 h after feeding stimulation. It is hypothesized that At3g59480 plays a role in sugar metabolism related to Chinese pine's resistance response to caterpillar feeding stimulation.

Key phosphorylated proteins that are upregulated in response to caterpillar feeding stimuli in Chinese pine include MOR1, MDH, RPS6A, and the chloroplast antibody AT4G01150. The phosphorylated protein MOR1 in pine plays a central role in functional protein modules related to plant microtubule structure, both 2 and 8 h after being exposed to caterpillar stress. MOR1 encodes a protein associated with the microtubule cytoskeleton structure in *A. thaliana*. Microtubule-binding proteins regulate transduction signals inside and outside of plant cells to facilitate the plant's regulatory mechanisms in response to environmental changes. MOR1 is an essential component in the dynamic regulation of microtubules, as highlighted by Chen et al. (2022). The findings of this study suggest that the expression of MOR1 is closely associated with the defense response against resistance in Chinese pine.

Malate dehydrogenase (MDH) had a highly connected position in the interaction network of differentially significant phosphorylated proteins in oil pine, both at 2 and 8 h after insect infestation. This indicates that MDH is involved in the response process of Chinese pine against herbivore stress induced by caterpillar infestation. Previous research indicates that MDH plays a role in abiotic stress processes in plants. Specifically, the expression of genes in the MDH gene family of rice, such as OsMDH8.1, has been observed to have a significant correlation with the response of rice to salt stress (Zhang et al., 2022).

RPS6A is a downstream target gene within the *Arabidopsis* TOR signaling network (Kim et al., 2014). RPS6A's primary functions include the regulation of protein synthesis and total RNA production (Jansen, 2017). Plant lifespan is strongly linked to nutrition and photosynthesis. According to Ren et al. (2012), *Arabidopsis* plants with RPS6A mutations have a longer lifespan, while plants overexpressing TOR ribosomal proteins have a shortened lifespan and accelerated life cycle. In this study, RPS6A was primarily present in the interaction network of phosphorylated Chinese pine resistance proteins 2 h after caterpillar feeding and was mildly less associated with herbivore stress after 8 h. This indicates that Chinese pine caterpillar stress activates the protective mechanism of RPS6A, and further research is required to investigate the specific nutritional and photosynthetic pathways involved, along with their regulatory mechanisms.

Novel chloroplast proteins have been identified in plant genomic and proteomic studies. At4g01150 is the only one of the 33 plastid goblet (PGs) proteins with a predicted transmembrane structural domain. It is localized in the chloroplast-like vesicle membrane (Friso et al., 2004; Peltier et al., 2004). Intense light stress caused a threefold rise in the relative accumulation of At4g01150 in plastid microspheres (Ytterberg et al., 2006). At4g01150 was more abundant in de-yellowed *Arabidopsis* cotyledons than the other three CURT1 family genes (Liang et al., 2021). Genes with unknown function in tobacco, which are homologous to *Arabidopsis* At4g01150, display higher expression levels in plants with high nitrogen application and topping for leaf retention (Lei et al., 2022). *Arabidopsis* chloroplast protein At4g01150 is significantly expressed during the heat stress response (Paul et al., 2020). During the analysis of the interaction network of phosphorylated proteins that are differentially and significantly upregulated in Chinese pine after a feeding boost from caterpillars, it was discovered that At4g01150 holds a prominent position and is linked to multiple proteins. It suggests that At4g01150 may be involved in the core mechanism of the Chinese pine's response toward the feeding stimulus of caterpillars. This result holds significant importance in enhancing the functionality of novel chloroplast proteins.

Key phosphorylated proteins whose expression is reduced in response to insect-feeding stimuli in Chinese pine comprise PGK1, chloroplast antibody AT2G20050, GAPC1, RPL24, and PTAC16. Phosphoglycerate kinase PGK is a highly conserved protein family involved in carbon fixation and metabolic processes in the cytoplasm *in vivo* (Li et al., 2019). PGK1 is localized in the cytoplasm, while its homolog PGK2 is found in chloroplasts. PGK2 regulates programmed cell death in plant cells and performs functions that are comparable to those of the hypersensitive response, such as leaf yellowing, activation of PR genes, and accumulation of hydrogen peroxide (Huang and Zhao, 2017). PGK plays a critical role in regulating the conversion of ATP and ADP in plants. It is involved in various cellular activities such as glycolysis, gluconeogenesis, and the Calvin cycle. The study suggests that PGK is located within the cytoplasm and functions as an ATP generator while also acting as a transferase by transferring phosphate groups to related reactions. PGK participates in the first step of cellular respiration in the cytoplasm, and increased PGK expression suggests an improvement in plant respiration. Troncoso-Ponce et al. (2012) have extensively studied the biochemical profile of PGK isozymes during sunflower development. Pine needle

PGK kinase exhibited the most significant downregulation of phosphorylation among proteins after caterpillar feeding for 2 h. The protein interactions that were differentially significant were centered around it. The decrease in Chinese pine PGK kinase activity, caused by caterpillar feeding, is believed to be a result of pine needle defense regulation and harmful substances in the insect's saliva. Further investigation is required to determine the specifics.

The AT2G20050 chloroplast antibody is central to the phosphorylated protein interaction network of the oil pine caterpillar 8 h after feeding. During the 2–8-h feeding period, the Chinese pine's damage focus shifted from PGK to AT2G20050, as evidenced by changes in pine phosphokinase activity. Many signaling kinases, receptor kinases, and phosphatases have close relationships with AT2G20050 (Mattei et al., 2016). These connections suggest potential functional roles for AT2G20050 in cellular signaling pathways. AT2G20050 negatively regulates protein kinase pathways involved in plant stress response, growth, and development (Kuhn et al., 2006). Chinese pine suppresses the expression of AT2G20050 kinase, triggering a complete defense response mechanism.

The plant's cytoplasmic glyceraldehyde triphosphate dehydrogenase (GAPC) is believed to play a role in the mechanism of drought tolerance in wheat (Zhai, 2017), as well as in responding to iron deficiency stress (Li, 2000). GAPC1 is also recognized as a redox switch overexpressed in plants to improve *Arabidopsis*' response to heat stress (Kim et al., 2020). GAPC1 also contributes to the defense response against reactive oxygen species (ROS) (Schneider et al., 2018). GAPC1 plays a crucial role in initiating resistance through a network of distinct, phosphorylated protein interactions. This process occurs 2 h after exposure to herbivore stimuli in Chinese pine. It is hypothesized that GAPC1 may be involved in the redox reaction process, including the clearance of reactive oxygen stress in Chinese pine. Further investigation is required to identify the specific resistance mechanism. The *Arabidopsis* transcription factor RPL acts as a resistance mechanism by regulating the conversion of energy needed for plant growth and development into a response against pathogen infestation. Its function is similar to that of a "switch" that turns on the defense system. This process involves the inhibition of the expression and transportation of pathogenic bacterial effector proteins, which play a role in the accumulation of flavonoids (Xu et al., 2022).

The expression of RPL24 in Chinese pine needles decreased 2 h after caterpillar feeding stimulation. It is hypothesized that the defense mechanism regulated by RPL24 may be gradually inhibited by insect pest stress, which could involve the regulation of flavonoids and related resistance products. The mechanism of action requires further and in-depth study. Eggermont et al. (2018) proposed that PTAC16 could be linked to the defense response against salt stress in *Arabidopsis*. Additionally, the PTAC16 protein is responsible for regulating the anchoring of the nucleoid membrane (Ingelsson and Vener, 2012). The plastid transcriptionally active kinase, PTAC16, exhibited high connectivity in the interaction network of differentially significant phosphorylated proteins in Chinese pine after 2 and 8 h of insect infestation, indicating a potential role of PTAC16 in the pine response to herbivore stress induced by caterpillars. Pest stress is believed to cause a notable decrease in the expression of PTAC16 kinase, leading to disruptions in signal recognition and plastid transcription in Chinese pine. Further investigation into the underlying mechanism is necessary to understand the phenomenon fully.

Overall, our study first established the interrelationship between wild Chinese pine and Chinese pine caterpillar under natural conditions. Additionally, our study also analyzed motif patterns of phosphorylated proteins and constructed a modification map for phosphorylated proteomics (**Supplementary Table 2**). Furthermore, the study emphasizes the significant role of kinase PTI12 At3g59480, as well as METK2. Additionally, MOR1, MDH, RPS6A, AT4G01150 PGK1, AT2G20050, GAPC1, RPL24, and PTAC16 are involved in Mfuzz clustering, kinase regulatory networks, and functional modules of phosphorylated proteins in the pine response to caterpillar stimuli. Our results advance our understanding of the mechanisms underlying Chinese pine resistance to Chinese pine caterpillar feeding and also PTM in plant immunity. The specific mechanisms by which phosphorylation regulate Chinese pine resistance to caterpillar remain to be investigated in the future.

Data availability statement

The original contributions presented in this study are included in this article/**Supplementary material**, further inquiries can be directed to the corresponding author.

Author contributions

TS: Conceptualization, Data curation, Formal analysis, Funding acquisition, Investigation, Methodology, Project administration, Software, Validation, Visualization, Writing – original draft, Writing – review & editing. YZ: Writing – original draft. GZ: Writing – original draft. SG: Writing – original draft. JL: Writing – review & editing. BG: Writing – review & editing.

Funding

The author(s) declare financial support was received for the research, authorship, and/or publication of this article. This research received funding from the Science and Technology Development Program at Hebei Agricultural University for Research on Molecular Mechanisms of Forest Plant-Insect Interactions. It also received support from Research on Molecular Mechanisms of Population Differentiation and Adaptation of Forest Pests and Insects under Environmental Stress (No. 30771739) and Forest Pests and Diseases (No. 1528003).

Acknowledgments

We express our gratitude to the Huangtuliangzi State forest farm for providing a test plot of natural, pure Chinese Pine forest.

Conflict of interest

The authors declare that the research was conducted in the absence of any commercial or financial relationships that could be construed as a potential conflict of interest.

Publisher's note

All claims expressed in this article are solely those of the authors and do not necessarily represent those of their affiliated organizations, or those of the publisher, the editors and the reviewers. Any product that may be evaluated in this article, or claim that may be made by its manufacturer, is not guaranteed or endorsed by the publisher.

Supplementary material

The Supplementary Material for this article can be found online at: https://www.frontiersin.org/articles/10.3389/ffgc.2024.1356511/full#supplementary-material

References

Arimura, G., Matsui, K., and Takabayashi, J. (2009). Chemical and molecular ecology of herbivore-induced plant volatiles: Proximate factors and their ultimate functions. *Plant Cell Physiol.* 50, 911–923. doi: 10.1093/pcp/pcp030

Arimura, G., Ozawa, R., Nishioka, T., Boland, W., Koch, T., Kühnemann, F., et al. (2002). Herbivore-induced volatiles induce the emission of ethylene in neighboring lima bean plants. *Plant J.* 29, 87–98. doi: 10.1046/j.1365-313x.2002.01198.x

Baldwin, I. T., Halitschke, R., Kessler, A., and Schittko, U. (2001). Merging molecular and ecological approaches in plant–insect interactions. *Curr. Opin. Plant Biol.* 4, 351–358. doi: 10.1016/s1369-5266(00)00184-9

Bentem, S. D., and Hirt, H. (2007). Using phosphoproteomics to reveal signalling dynamics in plants. *Trends Plant Sci.* 12:411.

Chen, Y., Liu, X., Zhang, W., Li, J., Liu, H., Yang, L., et al. (2022). MOR1/MAP215 acts synergistically with katanin to control cell division and anisotropic cell elongation in Arabidopsis. *Plant Cell* 34, 3006–3027.

Cheng, X., Zhu, L., and He, G. (2013). Towards understanding of molecular interactions between rice and the brown planthopper. *Mol. Plant* 6, 621–634.

Conrath, U. (2011). Molecular aspects of defence priming. *Trends Plant Sci.* 16, 524–531.

Demichev, V., Szyrwiel, L., Yu, F., Teo, G. C., Rosenberger, G., Niewienda, A., et al. (2022). dia-PASEF data analysis using FragPipe and DIA-NN for deep proteomics of low sample amounts. *Nat. Commun.* 13:3944. doi: 10.1038/s41467-022-31492-0

Ding, S., Lv, J., Hu, Z., Wang, J., Wang, P., Yu, J., et al. (2023). Phytosulfokine peptide optimizes plant growth and defense via glutamine synthetase GS2 phosphorylation in tomato. *EMBO J.* 42:e111858. doi: 10.15252/embj.2022111858

Eggermont, L., Stefanowicz, K., and Van Damme, E. J. (2018). Nictaba homologs from Arabidopsis thaliana are involved in plant stress responses. *Front. Plant Sci.* 8:2218. doi: 10.3389/fpls.2017.02218

Elsayed, G. (2011). Plant secondary substances and insects behaviour. *Arch. Phytopathol. Plant Protect.* 44, 1534–1549.

Fatma, B., Katrin, F. O., and Wilfried, S. (2019). Phosphorylation-dependent ribonuclease activity of Fra a 1 proteins. *J. Plant Physiol.* 233, 1–11. doi: 10.1016/j.jplph.2018.12.002

Förderer, A., and Chai, J. (2023). Die another day: Phytosulfokine at the molecular trade-off between growth and defense in plants. *EMBO J.* 42:113540. doi: 10.15252/embj.2023113540

Friso, G., Giacomelli, L., Ytterberg, A., Peltier, J.-B., Rudella, A., Sun, Q., et al. (2004). In-depth analysis of the thylakoid membrane proteome of Arabidopsis thaliana chloroplasts: New proteins, new functions, and a plastid proteome database. *Plant Cell* 16, 478–499. doi: 10.1105/tpc.017814

Guo, H. M., Sun, S. C., and Zhang, F. M. (2015). Identification of genes potentially related to herbivore resistance in OPR3 overexpression rice by microarray analysis. *Physiol. Mol. Plant Pathol.* 92, 166–174.

Guo, Y., Peng, D., Zhou, J., Lin, S., Wang, C., Ning, W., et al. (2019). iEKPD 2.0: An update with rich annotations for eukaryotic protein kinases, protein phosphatases and proteins containing phosphoprotein-binding domains. *Nucleic Acids Res.* 47, D344–D350. doi: 10.1093/nar/gky1063

Hadley, W. (2016). *ggplot2: Elegant graphics for data analysis*. New York, NY: Springer-Verlag.

Hernandez-Armenta, C., Ochoa, D., Gonçalves, E., Saez-Rodriguez, J., and Beltrao, P. (2017). Benchmarking substrate-based kinase activity inference using phosphoproteomic data. *Bioinformatics* 33, 1845–1851. doi: 10.1093/bioinformatics/btx082

Huang, X. Z., and Zhao, Y. C. (2017). Functional analysis of PGK gene family in Arabidopsis. *J. Mountain Agric. Biol.* 36:7.

Ingelsson, B., and Vener, A. V. (2012). Phosphoproteomics of Arabidopsis chloroplasts reveals involvement of the STN7 kinase in phosphorylation of nucleoid protein pTAC16. *FEBS Lett.* 586, 1265–1271. doi: 10.1016/j.febslet.2012.03.061

Jansen, W. M. (2017). *Regulatory circuits linking energy status to growth*. Utrecht: Utrecht University.

Kim, S. C., Guo, L., and Wang, X. (2020). Nuclear moonlighting of cytosolic glyceraldehyde-3-phosphate dehydrogenase regulates Arabidopsis response to heat stress. *Nat. Commun.* 11:3439. doi: 10.1038/s41467-020-17311-4

Kim, Y.-K., Kim, S., Shin, Y., Hur, Y. S., Kim, W.-Y., Lee, M.-S., et al. (2014). Ribosomal protein S6, a target of rapamycin, is involved in the regulation of rRNA genes by possible epigenetic changes in Arabidopsis. *J. Biol. Chem.* 289, 3901–3912. doi: 10.1074/jbc.M113.515015

Krug, K., Mertins, P., Zhang, B., Hornbeck, P., Raju, R., Ahmad, R., et al. (2019). A Curated Resource for Phosphosite-specific Signature Analysis. *Mol. Cell. Proteomics* 18, 576–593. doi: 10.1074/mcp.TIR118.000943

Kuhn, J. M., Boisson-Dernier, A., Dizon, M. B., Maktabi, M. H., and Schroeder, J. I. (2006). The protein phosphatase AtPP2CA negatively regulates abscisic acid signal transduction in *Arabidopsis*, and effects of abh1 on AtPP2CA mRNA. *Plant Physiol.* 140, 127–139. doi: 10.1104/pp.105.070318

Lei, B., Chang, W., Zhao, H., Zhang, K., Yu, J., Yu, S., et al. (2022). Nitrogen application and differences in leaf number retained after topping affect the tobacco (*Nicotiana tabacum*) transcriptome and metabolome. *BMC Plant Biol.* 22:38. doi: 10.1186/s12870-022-03426-x

Li, J. (2000). *The cloning of the cytosolic glyceradehyde-3-phosphate dehydrogenase (GADPH) gene (TaGapC1) and its expression and sequence analysis in iron-deficient stress in wheat*. Beijing: Capital Normal University.

Li, R., Qiu, Z., Wang, X., Gong, P., Xu, Q., Yu, Q.-B., et al. (2019). Pooled CRISPR/Cas9 reveals redundant roles of plastidial phosphoglycerate kinases in carbon fixation and metabolism. *Plant J.* 98, 1078–1089. doi: 10.1111/tpj.14303

Li, X., Hu, D., Cai, L., Wang, H., Liu, X., Du, H., et al. (2022). CALCIUM-DEPENDENT PROTEIN KINASE38 regulates flowering time and common cutworm resistance in soybean. *Plant Physiol.* 190, 480–499. doi: 10.1093/plphys/kiac260

Liang, Z., Yeung, W. T., and Ki Mai, K. K. (2021). CURT1A and CURT1C mediate distinct stages of plastid conversion in *Arabidopsis*. *bioRxiv* [Preprint]. bioRxiv 2021.12.01.470752.

Liu, J. J., Sharma, Ki, Zangrandi, L., Chen, C., Humphrey, S. J., Chiu, Y.-T., et al. (2018). In vivo brain GPCR signaling elucidated by phosphoproteomics. *Science* 360:eaao4927. doi: 10.1126/science.aao4927

Liu, L., Yan, W., and Liu, B. (2023). Transcriptome sequencing of Cocos nucifera leaves in response to *Rhynchophorus ferrugineus* infestation. *Front. Genet.* 14:1115392. doi: 10.3389/fgene.2023.1115392

Lyu, K., Gu, L., Wang, H., Zhu, X. X., Zhang, L., Sun, Y. F., et al. (2019). Transcriptomic analysis dissects the mechanistic insight into the Daphnia clonal variation in tolerance to toxic microcystis. *Limnol. Oceanogr.* 64, 272–283.

Mattei, B., Spinelli, F., Pontiggia, D., and Lorenzo, G. (2016). Comprehensive analysis of the membrane phosphoproteome regulated by oligogalacturonides in *Arabidopsis thaliana*. *Front. Plant Sci.* 7:1107. doi: 10.3389/fpls.2016.01107

Meier, F., Brunner, A.-D., Frank, M., Ha, A., Bludau, I., Voytik, E., et al. (2020). diaPASEF: Parallel accumulation–serial fragmentation combined with data-independent acquisition. *Nat. Methods* 17, 1229–1236.

Mukherji, M. (2005). Phophosproteomics in analyzing signaling pathways. *Expert Rev. Proteomics* 2, 117–128.

Niu, S., Li, J., Bo, W., Yang, W., Zuccolo, A., Giacomello, S., et al. (2022). The Chinese pine genome and methylome unveil key features of conifer evolution. *Cell* 185, 204–217. doi: 10.1016/j.cell.2021.12.006

Paul, P., Mesihovic, A., Chaturvedi, P., Ghatak, A., Weckwerth, W., Böhmer, M., et al. (2020). Structural and functional heat stress responses of chloroplasts of *Arabidopsis thaliana*. *Genes* 11:650. doi: 10.3390/genes11060650

Pawson, T., and Scott, J. D. (2005). Protein phosphorylation in signaling–50 years and counting. *Trends Biochem Sci.* 30, 286–290. doi: 10.1016/j.tibs.2005.04.013

Peltier, J.-B., Ytterberg, A. J., Sun, Q., and Wijk, K. J. (2004). New functions of the thylakoid membrane proteome of *Arabidopsis thaliana* revealed by a simple, fast, and versatile fractionation strategy. *J. Biol. Chem.* 279, 49367–49383. doi: 10.1074/jbc.M406763200

Peng, J., Loon, J. J. A., Zheng, S., and Dicke, M. (2011). Herbivore-induced volatiles of cabbage (*Brassica oleracea*) prime defence responses in neighbouring intact plants. *Plant Biol.* 13, 276–284. doi: 10.1111/j.1438-8677.2010.00364.x

Perazzolli, M., Palmieri, M. C., Matafora, V., Bachi, A., and Pertot, I. (2016). Phosphoproteomic analysis of induced resistance reveals activation of signal transduction processes by beneficial and pathogenic interaction in grapevine. *J. Plant Physiol.* 195, 59–72. doi: 10.1016/j.jplph.2016.03.007

Rampitsch, C. (2017). Phosphoproteomics analysis for probing plant stress tolerance. *Methods Mol. Biol.* 2017, 181–193. doi: 10.1007/978-1-4939-7136-7_11

Ren, M., Venglat, P., Qiu, S., Feng, Li, Cao, Y., Wang, E., et al. (2012). Target of rapamycin signaling regulates metabolism, growth, and life span in Arabidopsis. *Plant Cell* 24, 4850–4874. doi: 10.1105/tpc.112.107144

Reymond, P., Bodenhausen, N., Poecke, R. M. P., Krishnamurthy, V., Dicke, M., and Farmer, E. E. (2004). A conserved transcript pattern in response to a specialist and a generalist herbivore. *Plant Cell* 16, 3132–3147. doi: 10.1105/tpc.104.026120

Rossignol, M. (2006). Proteomic analysis of phosphorylated proteins. *Curr. Opin. Plant Biol.* 9, 538–543.

Samofalova, D. O., Karpov, P. A., Raevsky, A. V., and Blume, Y. B. (2020). "Interplay of protein phosphatases with cytoskeleton signaling in response to stress factors in plants," in *Protein phosphatases and stress management in plants: Functional genomic perspective*, ed. G. K. Pandey (Cham: Springer), 261–287.

Schneider, M., Knuesting, J., Birkholz, O., Heinisch, J. J., and Scheibe, R. (2018). Cytosolic GAPDH as a redox-dependent regulator of energy metabolism. *BMC Plant Biol.* 18, 1–14.

Sefton, B. M. (1998). Overview of protein phosphorylation. *Curr. Protoc. Cell Biol.* 1:14.

Shannon, P. (2003). Cytoscape: A software environment for integrated models of biomolecular interaction networks. *Genome Res.* 13, 2498–2504. doi: 10.1101/gr.1239303

Smith, C. M., and Clement, S. L. (2012). Molecular bases of plant resistance to arthropods. *Annu. Rev. Entomol.* 57, 309–328.

Song, S., Huang, H., Gao, H., Wang, J., Wu, D., Liu, X., et al. (2014). Interaction between MYC2 and ETHYLENE INSENSITIVE3 modulates antagonism between jasmonate and ethylene signaling in *Arabidopsis*. *Plant Cell* 26, 263–279. doi: 10.1105/tpc.113.120394

Subramanian, A., Tamayo, P., Mootha, V. K., Mukherjee, S., Ebert, B. L., Gillette, M. A., et al. (2005). Gene set enrichment analysis: A knowledge-based approach for interpreting genome-wide expression profiles. *Proc. Natl. Acad. Sci. U.S.A.* 102, 15545–15550.

Tang, Q. Y., and Zhang, C. X. (2013). Data processing system (DPS) software with experimental design, statistical analysis and data mining developed for use in entomological research. *Insect Sci.* 20, 254–260. doi: 10.1111/j.1744-7917.2012.01519.x

Troncoso-Ponce, M. A., Rivoal, J., Venegas-Calerón, M., Dorion, S., Sánchez, R., Cejudo, F. J., et al. (2012). Molecular cloning and biochemical characterization of three phosphoglycerate kinase isoforms from developing sunflower (*Helianthus annuus* L.) seeds. *Phytochemistry* 79, 27–38. doi: 10.1016/j.phytochem.2012.04.001

Waadt, R., Seller, C. A., Hsu, P.-K., Takahashi, Y., Munemasa, S., and Schroeder, J. I. (2022). Plant hormone regulation of abiotic stress responses. *Nat. Rev. Mol. Cell Biol.* 23, 680–694.

Wang, C., Xu, H., Lin, S., Deng, W., Zhou, J., Zhang, Y., et al. (2020). GPS 5.0: An update on the prediction of kinase-specific phosphorylation sites in proteins. *Genom. Proteomics Bioinform.* 18, 72–80. doi: 10.1016/j.gpb.2020.01.001

Wang, P., Zhao, Y., Li, Z., Hsu, C. C., Liu, X., Fu, L., et al. (2018). Reciprocal regulation of the TOR kinase and ABA receptor balances plant growth and stress response. *Mol. Cell* 69:100–112.e6. doi: 10.1016/j.molcel.2017.12.002

Wei, J., and Kang, L. (2011). Roles of (Z)-3-hexenol in plant-insect interactions. *Plant Signal. Behav.* 6, 369–371.

Xing, T., and Laroche, A. (2011). Revealing plant defense signaling: Getting more sophisticated with phosphoproteomics. *Plant Signal. Behav.* 6, 1469–1474. doi: 10.4161/psb.6.10.17345

Xu, H.-X., Qian, L.-X., Wang, X.-W., Shao, R. X., Hong, Y., Liu, S., et al. (2019). A salivary effector enables whitefly to feed on host plants by eliciting salicylic acid-signaling pathway. *Proc. Natl. Acad. Sci. U.S.A.* 116, 490–495. doi: 10.1073/pnas.1714990116

Xu, M., Wang, X., Liu, J., Jia, A., Xu, C., Deng, X. W., et al. (2022). Natural variation in the transcription factor REPLUMLESS contributes to both disease resistance and plant growth in *Arabidopsis*. *Plant Commun.* 3:100351. doi: 10.1016/j.xplc.2022.100351

Yang, L., Yang, X., and Gao, Y. (2023). S-adenosylmethionine synthase (BtSAMS) from Balsas teosinte confers resistance to peach aphids in Arabidopsis. *Ann. Appl. Biol.* 183, 15–22.

Ytterberg, A. J., Peltier, J. B., and Van Wijk, K. J. (2006). Protein profiling of plastoglobules in chloroplasts and chromoplasts. A surprising site for differential accumulation of metabolic enzymes. *Plant Physiol.* 140, 984–997. doi: 10.1104/pp.105.076083

Zhai, Q. H. (2017). *Screening proteins interacting with cytosolic TAGAPC1 from wheat by yeast two hybrid*. Xianyang: Northwest A&F University.

Zhang, J. H., Sun, L. W., Liu, L. L., Lian, J., An, S. L., Wang, X., et al. (2010). Proteomic analysis of interactions between the generalist herbivore *Spodoptera exigua* (Lepidoptera: Noctuidae) and *Arabidopsis thaliana*. *Plant Mol. Biol. Rep.* 28, 324–333.

Zhang, Y., Wang, Y., Sun, X., Yuan, J., Zhao, Z., Gao, J., et al. (2022). Genome-wide identification of MDH family genes and their association with salt tolerance in rice. *Plants* 11:1498. doi: 10.3390/plants11111498

Zhao, C., Wang, P., and Si, T. (2017). MAP kinase cascades regulate the cold response by modulating ICE1 protein stability. *Dev. Cell* 43:618–629.e5. doi: 10.1016/j.devcel.2017.09.024

frontiers | Frontiers in Forests and Global Change

TYPE Original Research
PUBLISHED 13 November 2024
DOI 10.3389/ffgc.2024.1458554

OPEN ACCESS

EDITED BY
Louis Bernier,
Laval University, Canada

REVIEWED BY
Laurel Haavik,
Southern Research Station, Forest Service (USDA), United States
David Lázaro Gimeno,
University of Helsinki, Finland

*CORRESPONDENCE
Vivek Vikram Singh
✉ singhv@fld.czu.cz

RECEIVED 02 July 2024
ACCEPTED 17 October 2024
PUBLISHED 13 November 2024

CITATION
Singh VV, Naseer A, Sellamuthu G, Mogilicherla K, Gebauer R, Roy A and Jakuš R (2024) Robust reference gene selection in Norway spruce: essential for real-time quantitative PCR across different tissue, stress and developmental conditions. *Front. For. Glob. Change* 7:1458554. doi: 10.3389/ffgc.2024.1458554

Robust reference gene selection in Norway spruce: essential for real-time quantitative PCR across different tissue, stress and developmental conditions

Vivek Vikram Singh[1]*, Aisha Naseer[1], Gothandapani Sellamuthu[1], Kanakachari Mogilicherla[1,2], Roman Gebauer[3], Amit Roy[1] and Rastislav Jakuš[1,4]

[1]Faculty of Forestry and Wood Sciences, Czech University of Life Sciences Prague, Prague, Czechia, [2]ICAR-Indian Institute of Rice Research (IIRR), Hyderabad, India, [3]Department of Forest Botany, Dendrology and Geobiocoenology, Mendel University in Brno, Brno, Czechia, [4]Institute of Forest Ecology, Slovak Academy of Sciences, Zvolen, Slovakia

Accurate gene expression analysis in Norway spruce (*Picea abies*) under diverse stress conditions requires the identification of stable reference genes for normalization. Notably, the literature lacks reports on suitable reference genes in Norway spruce. Here, we aimed to address this gap by identifying suitable reference genes for quantitative real-time PCR in Norway spruce across various stress conditions (drought, heat, pathogen infection) in seedlings, tissues (needle, phloem, root), and developmental stages (seedlings, mature trees). We evaluated the stability of 15 candidate reference genes and assessed their expression stability using five statistical algorithms (ΔCt, geNorm, NormFinder, BestKeeper, and RefFinder). Our results highlight *ubiquitin-protein ligase* (*SP1*), *conserved oligomeric Golgi complex* (*COG7*), and *tubby-like F-box protein* (*TULP6*) as the most stable reference genes, while *succinate dehydrogenase* (*SDH5*) and *heat shock protein 90 (HSP90)* were the least stable under various experimental conditions. *COG7* and *TULP6* are novel candidate reference genes reported for the first time. The expression stability of the identified reference genes was further validated using dehydrin-like protein 5 (*PaDhn5*) under drought conditions in Norway spruce. Pairwise variation analysis suggests that two reference genes were sufficient to normalize gene expression across all sample sets. This study provides a comprehensive analysis of reference gene stability under different experimental conditions and a catalog of genes for each condition, facilitating future functional genomic research in Norway spruce and related conifers.

KEYWORDS

RT–qPCR, housekeeping genes/reference genes, gene expression, developmental stages and tissues, abiotic and biotic stress

1 Introduction

Norway spruce [*Picea abies* (L.) Karst.] is one of the most ecologically and economically important coniferous tree species in Europe. Adapted to cool and wet conditions, its distribution extends from central and eastern Norway across Fennoscandia, the Baltic states, Belarus, Russia, and Central and Southeastern Europe (Danielsen et al., 2021). Over the past several decades, Norway spruce has been extensively planted in areas beyond its natural

distribution range due to its excellent growth performance and desirable wood properties for commercial forestry (Caudullo et al., 2016; Hlásny et al., 2019). However, planting it outside its niche has led to health and vitality issues, increasing its susceptibility to biotic and abiotic stresses. For instance, Norway spruce forests in the Czech Republic experienced a dramatic increase in mortality in 2019, losing an average of 118 million m^3 due to droughts, heatwaves, and bark beetle outbreaks (Ebner, 2020). Traditional management strategies, such as pheromone-based mass trapping, salvage logging, insecticides, and anti-attractants, have been largely ineffective in controlling mass bark beetle attacks (Dobor et al., 2020; Singh et al., 2024a). Consequently, there has been rapid exploration of functional genomics-based tools to develop effective management strategies. Notably, sequencing of the Norway spruce genome, the first among conifers (Nystedt et al., 2013), has significantly advanced gene expression studies aimed at understanding gene functions and molecular regulation under various stresses. However, the appropriate reference genes required for gene expression normalization in Norway spruce have not yet been comprehensively established. Therefore, identifying reliable reference genes is crucial for improving studies on gene expression profiling, providing novel insights into biological processes, and deepening the understanding of regulatory gene networks that contribute to spruce resistance, resilience, and survival (Wise et al., 2007).

The significance of differential gene expression analysis in understanding gene function and molecular regulation in response to various environmental factors is crucial. Real-time quantitative polymerase chain reaction (RT–qPCR) is a widely used technique for analyzing the expression of target genes owing to its high sensitivity, accuracy, specificity, reproducibility, and rapidity (Bustin, 2002; Gachon et al., 2004; Bustin et al., 2005; Takamori et al., 2017). However, the precision of RT–qPCR is highly dependent on using a reference gene as an internal control. Reference genes, also referred to as housekeeping genes, are consistently expressed in cells and are vital for fundamental cellular functions. These genes encode proteins that play crucial roles in essential cellular activities, including cell cycle regulation, DNA replication, and metabolism. An ideal reference gene maintains consistent expression levels across different experimental conditions and tissues and remains unaffected by developmental stages or the organism's genotype (Han et al., 2012; Lu et al., 2018; Sen et al., 2021).

Several studies have identified and validated reference genes in crops, commercially valuable tree species, and herbs, including *Solanum tuberosum* L. (Nicot et al., 2005), *Arabidopsis thaliana* (L.) Heynh. (Czechowski et al., 2005), *Oryza sativa* L. (Jain et al., 2006), *Triticum aestivum* L. (Paolacci et al., 2009), *Linum usitatissimum* L. (Huis et al., 2010), *Eucalyptus robusta* Sm. (de Oliveira et al., 2012), *Populus euphratica* Oliv. (Wang et al., 2014), *Solanum melongena* L. (Mogilicherla et al., 2016), *Bromus sterilis* L. (Sen et al., 2021), *Melissa officinalis* L. (Bharati et al., 2023), and *Populus tremula* L. (Pastierovič et al., 2024). Recently, efforts have been made to identify and validate reference genes in coniferous species such as Chinese fir (*Cunninghamia lanceolata* (Lamb.) Hook.) and Masson pine (*Pinus massoniana* Lamb.) (Bao et al., 2016; Mo et al., 2019; Chen et al., 2019). However, these studies were limited to specific tissues and treatment conditions. Previous research on internal control genes in *P. abies* was limited to embryogenic cell lines (e.g., Vestman et al., 2011; de Vega-Bartol et al., 2013). In maritime pine (*Pinus pinaster*), genes such as *GADPH, 18S rRNA, UBQ,* and *eIF4AII* were found unsuitable as internal controls during embryo development due to the high variability in gene expression during embryogenesis and the involvement of these genes in both basal metabolism and other functions (Gonçalves et al., 2005). More recently, a study identified *elongation factor 1-gamma, histone H1, GAPDH,* and *α-tubulin* as stable reference genes for somatic embryogenesis tissues in *Liriodendron* hybrids, while *elongation factor 1-gamma* and *actin* were most reliable for germinative organ tissues (Li et al., 2021). These findings suggest that results from embryogenic cell lines may not accurately represent seedlings or mature trees under varying stress conditions. Therefore, establishing a set of stable reference genes for Norway spruce across different developmental stages and stress conditions is crucial for improving the accuracy and reliability of gene expression analysis, enhancing our understanding of its physiological processes and stress responses.

Here, we analyzed the expression profiles of 15 candidate reference genes in different conifer species based on published research and our in-house transcriptome data (de Vega-Bartol et al., 2013; Bao et al., 2016; Mo et al., 2019; Chen et al., 2019). These genes are known for performing conserved cellular functions in gymnosperms and, therefore, are expected to show stable expression across various conditions, developmental stages, and tissues. We evaluated the expression stability of *ribosomal protein L26 (RPL26), serine/threonine-protein phosphatase (PP2A2), ribosomal protein L7Ae (RPL7Ae), ubiquitin-like domain-containing CTD phosphatase (UBCP), F-box protein (SKIP22), heat shock protein (HSP90), vacuolar fusion protein (CCZ1), succinate dehydrogenase (SDH5), 18S rRNA (RID2), putative lysine-specific demethylase (JMJ16), conserved oligomeric Golgi complex (COG7), ribosomal protein S10 (RSP10), ubiquitin-protein ligase (SP1), tubby-like F-box protein (TULP6),* and *actin-related protein (ARP9)* across different tissues (needle, phloem and root), developmental stages (seedlings and mature trees), and under various biotic and abiotic stress conditions (drought, heat stress, and pathogen infection) in Norway spruce seedlings. The present study will enhance the accuracy of future gene expression studies and contribute to a more reliable evaluation of reference gene stability in Norway spruce. These reference genes are also expected to serve as templates for other related conifer species and should be further investigated.

2 Materials and methods

2.1 Plant materials and experimental conditions

2.1.1 Greenhouse experiment

Three-year-old containerized Norway spruce seedlings, approximately 40 cm high, were procured from a local nursery and planted in a moist peat/perlite mixture in May 2022. The seedlings were grown using seed material originating from the Bohemian-Moravian highlands (Czech Republic), characterized by 600–750 mm of annual rainfall and an altitude of 500–600 m above sea level. The seedlings were transferred to a greenhouse with a temperature range of 23 ± 2°C and 16-h/8-h light/dark photoperiod cycles at the Czech University of Life Sciences, Prague. Before any treatment, the plants were irrigated regularly with tap water for acclimation to the greenhouse conditions. A total of 16 plants were used for each treatment. The plants were

grouped into sets of four, which were pooled to form one biological replicate. Consequently, each treatment comprised four biological replicates, with each replicate consisting of four plants. ***Control treatment:*** This group was irrigated regularly and was not subjected to any abiotic or biotic treatment. ***Water deficit treatment:*** One group was subjected to drought stress by gradually interrupting the water supply until the mean plant water potential decreased below −2.1 MPa. A water potential value of −2.1 MPa in Norway spruce is considered low, indicating water stress that may lead to embolism formation and a loss of hydraulic conductivity (Rosner et al., 2019). The degree of drought stress was quantified by measuring the predawn water potential using a Scholander pressure chamber (PMS Instruments, Corvallis, Oregon, United States). ***Heat stress:*** To induce heat stress, the seedlings were placed in a climate chamber (FytoScope FS-SI 3400, PSI, Drásov, Czech Republic) at 35°C for 10 days with a constant relative humidity of 80% and regular irrigation. ***Biotic stress:*** The seedlings were inoculated with the Ophiostomatoid fungus *Ophiostoma flexuosum,* and incubated for 1 month in a controlled climate chamber mentioned above. Throughout the treatment period, the plants were carefully maintained under optimal humidity, light, and nutrient conditions.

Samples were collected from three different tissues (needle, phloem, and roots) from all treatments, including abiotic stress (drought and heat), biotic stress (pathogen infection), and control (well-watered) treatments. Tissue samples were snap-frozen in liquid nitrogen immediately after collection and stored at −80°C for further processing.

2.1.2 Field experiment

In addition to the seedlings, samples from mature trees (90–100 years) were collected from research plots of the Czech University of Life Sciences, managed by the School Forest Enterprise (ŠLP) in Kostelec nad Černými lesy (49.9940° N, 14.8592° E) in the eastern district of the Central Bohemian region of the Czech Republic (Singh et al., 2023). The climate in this region is dry and warm in summer, with a vegetation season lasting 150–160 days and an average annual temperature and precipitation of 7–7.5°C and 600 mm, respectively. Norway spruce tissue samples (needle, phloem, and root) were collected from 16 trees in August 2022. The needle samples were collected by shooting branches with a shotgun (Burnett et al., 2021), while phloem and root samples were obtained using a 5 mm cork borer. The phloem samples were collected from the trunk at a height of 2 m. The cork borer was used to extract tissue cores that included both the phloem and cambium layers (Mao et al., 2019). For the root samples, lateral roots were selected from the same trees approximately 1 m from the trunk base (Kalyniukova et al., 2024). After carefully removing layers of soil and moss, the roots were exposed and sampled at 15 cm depth using the same 5 mm cork borer. All tissue samples were snap-frozen in liquid nitrogen immediately after collection and stored at −80°C for further processing. Similar to the greenhouse experiment, four biological replicates were used for each tissue type, with each replicate composed of four individual samples pooled together to reduce individual heterogenicity. The experimental design is schematically represented in Figure 1.

2.2 Selection of candidate reference genes for evaluation

A total of 15 candidate internal control genes, *RPL26, PP2A2, RPL7Ae, UBCP, SKIP22, HSP90, CCZ1, SDH5, RID2, JMJ16, COG7, RPS10, SP1, TULP6,* and *ARP9* were selected for identifying the most suitable reference genes in Norway spruce (Table 1). The selected candidate genes were previously identified in other conifer species (de Vega-Bartol et al., 2013; Bao et al., 2016; Chen et al., 2019; Mo et al., 2019) and showed consistent expression in our in-house transcriptome data (*Unpublished data*). Primers for selected genes were designed through the PrimerQuest™ Tool (Integrated DNA Technologies, United States), and their primer efficiency and correlation coefficients (R^2) were calculated (Table 1). The sequence used to design primers is provided in Supplementary material S1.

2.3 Total RNA extraction, cDNA synthesis, primer design, and quantitative RT–qPCR analysis

Total RNA from all three tissues (needle, phloem, and root) was isolated using a modified cetyltrimethylammonium bromide (CTAB) protocol described by Singh et al. (2024b). Briefly, 100 mg of homogenized tissue was added to the CTAB extraction buffer, followed by the addition of an equal amount of Chloroform:isoamyl alcohol (24:1) and subsequent centrifugation. The top aqueous layer was transferred to a new tube, and 0.5 volume of 5 M lithium chloride was added and incubated for 1 h at −20°C. Then, the mixture was centrifuged at 12,000 rpm for 10 min at 4°C, and the supernatant was discarded. The resulting RNA pellet was washed twice with 70% ethanol. The dried RNA pellet was eluted in 50 µL RNase-free water. The isolated RNA was further treated with the TURBO DNase Kit (Invitrogen, United States) to remove any genomic DNA contamination. RNA integrity and purity (260/280 and 260/230 nm absorbance ratios) were verified by electrophoresis on a 1.2% agarose gel and NanoDrop spectrophotometer (Thermo Scientific™, USA), respectively. Complementary DNA (cDNA) was synthesized from 1 µg of RNA using a High-Capacity cDNA Reverse Transcription Kit (Applied Biosystems, USA) according to the manufacturer's protocol and stored at −20°C.

Before performing RT–qPCR, the cDNA samples were diluted by a factor of five. The RT–qPCR reaction mixture consisted of 5.0 µL of SYBR® Green PCR Master Mix (Applied Biosystems, United States), 1.0 µL of cDNA from fivefold dilutions, 10 µM of forward and reverse primers, and 3.0 µL of RNase-free water (Invitrogen, USA) to make up a total volume of 10.0 µL. Amplification was conducted with initial denaturation at 95°C for 10 min, followed by 40 cycles of 95°C for 15 s and 60°C for 1 min. The reactions were carried out using an Applied Biosystems™ StepOne™ Real-Time PCR System (Applied Biosystems, United States). To verify primer specificity, melting curve analysis was performed, ensuring gene-specific amplification with a gradual increase in temperature from 60 to 95°C. All RT–qPCR assays were conducted with four biological replicates per treatment and tissue, each including four technical replicates.

2.4 Statistical analyses

Five different algorithms and tools, i.e., geNorm, NormFinder, BestKeeper, ΔCt, and RefFinder were used to evaluate the gene expression stability of 15 candidate reference genes in Norway spruce. The comprehensive expression stability of candidate reference genes was evaluated using RefFinder, a web-based tool that combines the

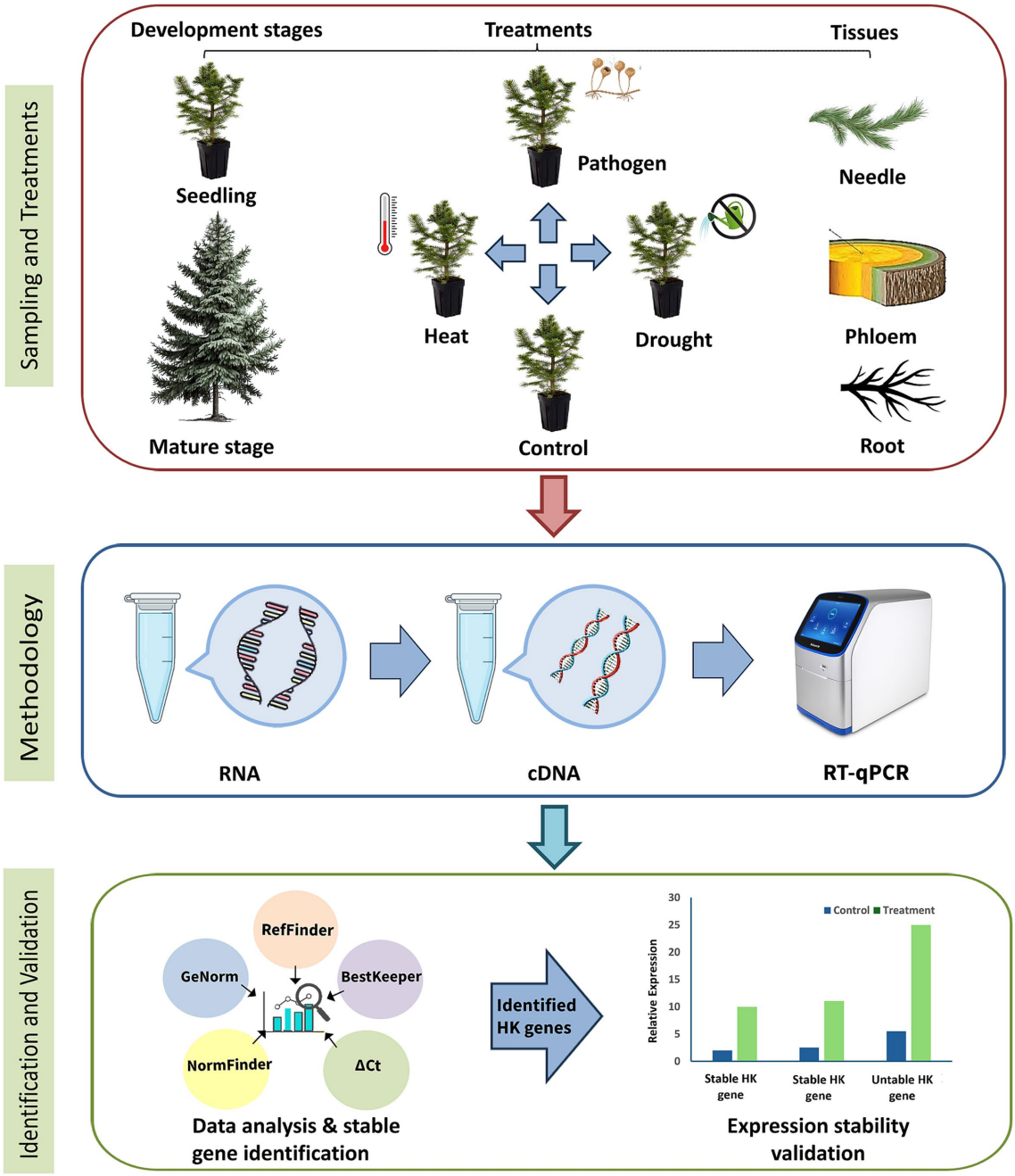

FIGURE 1
Schematic representation of the experimental design used to identify suitable reference genes in Norway spruce.

outputs of the former four algorithms. The geNorm algorithm calculates the expression stability value (M) and conducts pairwise variation (V) comparisons, where the lowest M value suggests the most stable expression (Vandesompele et al., 2002). NormFinder ranks reference genes based on their expression stability within a given set of samples (Andersen et al., 2004). BestKeeper, another freely available algorithm, assesses the standard deviation and correlation coefficient using the Cq (quantification cycle) values of all reference genes (Pfaffl et al., 2004). The ΔCt method directly evaluates the relative expression of gene pairs within each sample (Silver et al., 2006). The mean Cq values of each reference gene from each experiment served as input data and were processed using RefFinder, which combines widely used reference gene screening programs (geNorm, NormFinder, BestKeeper, and the ΔCt method) to calculate the geometric mean of their ranking values to provide an overall comprehensive ranking.

The optimum number of reference genes required under each experimental condition was determined by pairwise variation (V) analysis by calculating the variable value Vn/n + 1 based on the average expression stability (M) with a cutoff of 0.15 using the geNorm algorithm. The Vn/Vn + 1 value indicates the pairwise variation between two consecutive normalization factors. When the value falls below this threshold, adding the n + 1 reference gene becomes redundant.

TABLE 1 Primer information of the reference genes and target genes used in the study.

Gene symbol	Gene name	Primer sequence (5′-3′)		Amplicon length (bp)	PCR efficiency	Regression coefficient
RPL26	Ribosomal protein L26	F:	CATCTAGTGTGCGGCGTATT	114	96.72	0.999
		R:	CTCGTACCACCTGAACTTCATC			
PP2A2	Serine/threonine-protein phosphatase PP2A-2	F:	GGCCTATGTGTGATCTACTGTG	113	96.99	0.997
		R:	GTGATTGAATTGGGCTGCTATG			
RPL7Ae	Ribosomal protein L7Ae	F:	CCACTGTTGGCTGAGGATAAG	119	100.47	0.996
		R:	CCCTCATTGGTTGTCACAGAA			
UBCP	Ubiquitin-like domain-containing CTD phosphatase	F:	CCACAGAATGGGCTTGTGATA	126	96.96	0.999
		R:	GTGGCTCAGATCATCCAGTTC			
SKIP22	F-box protein	F:	TTCCCACAGAGCTCAAACTG	134	91.19	0.995
		R:	CTCAGCCGCATACTTCTTCTT			
HSP90	Heat shock protein	F:	GGCGATCAAGATGAAGCAAAG	138	111.92	0.991
		R:	AAGCACACATGGCGAAGA			
CCZ1	Vacuolar fusion protein	F:	CAAACAGCAATAGCAGTGAAGG	133	93.88	0.999
		R:	ACAGAGAGCTGGCTAGTAAGA			
SDH5	Succinate dehydrogenase	F:	GCTCTACGGGCTGCATATAAA	119	106.87	0.879
		R:	ACCAACAGCGTCACTAACC			
RID2	18S rRNA	F:	GAGGAGCACGAGCTGTATTG	104	93.72	0.987
		R:	CACAACCAGACCACCTGAAA			
JMJ16	Putative lysine-specific demethylase	F:	AGCAGATGTGGAGACTAGGA	122	93.88	0.993
		R:	GGAGCCGTGCAATGTTATTTAG			
COG7	Conserved oligomeric Golgi complex	F:	CCTCGGCTGAAGAAGACAAT	135	103.63	0.997
		R:	TTGTCCCAGCACCCAATAC			
RPS10	ribosomal protein S10	F:	CCTCGATTTGGTGACAGAGATG	110	96.72	0.999
		R:	GCCCTAAATTGAGGCTGGTATT			
SP1	ubiquitin-protein ligase SP1	F:	GGCACTACTCTGACTGTTGT	117	114.86	0.999
		R:	GGCAGATCCTAGCCGTTTC			
TULP6	Tubby-like F-box protein	F:	CCTGAGCCTAATCCATCAGTTT	104	94.79	0.999
		R:	AGTGGGTAGCGATAATCCATTG			
ARP9	Actin-related protein 9	F:	CCTGGAAAGGTGGTGCTATT	120	93.65	0.999
		R:	AATCTCTGTACTTTCGACCACTC			
Target gene						
PaDhn5	Dehydrin like protein	F:	ATCAATGTGCGGGTGAAG	122	120.48	0.951
		R:	ACTCCCACACTGATCTGAA			

2.5 Reference gene validation

Dehydrins are a part of the group 2 late embryogenesis abundant (LEA) protein family that protects conifers against osmotic stress in response to cold and drought conditions (Stival Sena et al., 2018; Čepl et al., 2020; Krokene et al., 2023). To validate the selected reference genes, the relative expression levels of the dehydrin gene *PaDhn5* were analyzed according to the $2^{-\Delta\Delta Ct}$ method (Livak and Schmittgen, 2001) using the most and the least stable reference genes. The data was checked for normality using the Kolmogorov–Smirnov test, and mRNA expression levels of target genes were assessed via single factor ANOVA using XLSTAT cloud (ver. 1.0), and a significance level of $\alpha = 0.05$ was used as the cutoff to indicate significant differences among the control and treatment groups.

3 Results

3.1 Amplification efficiency and specificity of candidate reference genes

Each primer pair produced a single amplicon with an expected amplicon length, as shown by agarose gel electrophoresis (Supplementary material S2). Melting curve analysis revealed a single peak, indicating no primer dimer was present (Supplementary material S3). The amplification efficiency of each primer pair ranged from 91.19 to 114.86%, and the correlation coefficient (R^2) values were greater than or equal to 0.879 (Table 1 and Supplementary material S4). The average cycle threshold (Ct) value was 28.14 (Supplementary material S5), while *SDH5, SP1, RID2,* and *ARP9* showed the highest transcript abundance across most

experimental conditions. In contrast, *RPL7Ae* and *RPL26* were the least expressed reference genes. The remaining nine reference genes exhibited moderate expression levels.

3.2 Expression stability of candidate reference genes

3.2.1 Tissuewise stability

In needle tissues, the three most stable genes were *SP1*, *JMJ16,* and *RID2* according to the comprehensive ranking by RefFinder and by ΔCt, while *UBCP, HSP90,* and *SDH5* were the least stable genes (Table 2). The BestKeeper and NormFinder rankings were inconsistent with those of RefFinder and ΔCt, suggesting that *PP2A2* and *UBCP* are the most stable genes, respectively. The geNorm ranking suggested a combination of *RID2/ TUPL6* as the most stable gene (Supplementary material S6).

For phloem tissues, *RID2, SP1,* and *PP2A2* were the most stable genes according to RefFinder, while the least stable genes were *SKIP22, HSP90,* and *SDH5*. This ranking was consistent with that of the ΔCt method, except that ΔCt ranked *COG7* as the third most stable gene. The BestKeeper and NormFinder algorithms ranked *PP2A2* as the most stable gene in phloem tissues. According to geNorm, the combination of *RPL26/RPS10* was the most stable gene in phloem tissues (Supplementary material S6).

In root tissues, the BestKeeper, ΔCt, and NormFinder rankings for the three most stable genes were not consistent with those of RefFinder. *UBCP, RPL7Ae,* and *SP1* were suggested to be the three most stable genes based on the comprehensive rankings of RefFinder (Table 2). A combination of *COG7/TULP6* was the most stable reference gene in root tissues according to geNorm (Supplementary material S6). The least stable reference genes by the RefFinder comprehensive ranking were *SDH5, HSP90,* and *RID2.*

3.2.2 Treatmentwise stability

3.2.2.1 Control conditions

According to the comprehensive rankings of RefFinder, the three most stable genes under control conditions were *RPS10, RPL26,* and *SP1,* while *CCZ1, SDH5,* and *HSP90* were the least stable (Table 3). BestKeeper ranked *RID2* as the most stable gene, whereas NormFinder ranked *COG7* as the most stable gene. The ΔCt value indicated that *RPS10* was the most stable gene, which is consistent with the RefFinder ranking. The best combination of reference genes according to geNorm was *PP2A2/ TULP6* under control conditions (Supplementary material S7). The *HSP90* gene was the least stable, as determined by geNorm analysis and the other four algorithms.

3.2.2.2 Drought stress conditions

Under drought conditions, *RID2, SP1,* and *COG7* were identified as the three most stable reference genes by the RefFinder algorithm, while a combination of *UBCP/SP1* was the most stable as per geNorm (Supplementary material S7). BestKeeper and NormFinder identified *PP2A2* and *RPL26* as the most stable genes, respectively. Both geNorm and other algorithms (ΔCt, BestKeeper, NormFinder, and RefFinder) identified *SDH5* as the least stable reference gene under drought conditions.

3.2.2.3 Heat stress conditions

For studies under heat stress conditions, *RID2, SP1*, and *RPL26* were identified as the most stable genes by comprehensive ranking by the RefFinder program, whereas BestKeeper and NormFinder ranked *PP2A2* and *RPL26* as the most stable genes, respectively. A combination of *RPL26/ARP9* was ranked as the most stable gene according to geNorm (Supplementary material S7). Unanimously, *SDH5* was suggested as the least stable gene under heat stress conditions by geNorm and other algorithms.

3.2.2.4 Pathogen infection conditions

The topmost three stable genes after Ophiostomatoid fungus inoculation were *SP1, COG7,* and *RPL26* based on the rankings of the RefFinder algorithm, whereas the combination of *PP2A2/ RPL7Ae* was the most stable according to geNorm (Table 2; Supplementary material S7). BestKeeper and NormFinder ranked *PP2A2* and *RPL26* as the most stable genes, respectively, which was not consistent with ΔCt and RefFinder rankings. The gene *SDH5* was the least stable reference gene after fungal inoculation as per four algorithms, and geNorm ranked *RID2* as the least stable reference gene.

3.2.2.5 Mature tree

In mature tree samples, the comprehensive ranking algorithm RefFinder identified *SP1, COG7,* and *TULP6* as the most stable reference genes and *SDH5* as the least stable gene. Similar to previous observations, the BestKeeper and NormFinder rankings were not consistent with that of RefFinder. BestKeeper and NormFinder ranked *PP2A2* and *HSP90*, respectively, as the most stable genes. In contrast, a combination of *RPL26/ARP9* was suggested to be the most stable gene and *COG7* as the least stable reference gene by geNorm analysis (Supplementary material S7).

3.3 Optimal reference gene selection for normalization

To achieve more accurate and reliable gene expression results, it is often recommended to use multiple reference genes. According to Vandesompele et al. (2002), if the Vn/Vn + 1 value is below 0.15, the addition of an additional reference gene (n + 1) is deemed unnecessary, suggesting that the initial reference gene is sufficient for normalizing target gene expression. Using the geNorm algorithm, we determined the optimal number of reference genes for each condition. Our analysis revealed that at least two reference genes were necessary for accurate normalization in (mature trees and combined conditions), as indicated by the pairwise comparison values (Figure 2).

3.4 Validation of reference gene selection

Based on the RefFinder comprehensive analysis, *SP1* and *COG7* were identified as the most stable genes, whereas *SDH5* was identified as the least stable gene for gene expression studies in Norway spruce samples under drought conditions. To validate the reliability of the candidate reference genes, the relative expression of the target gene *PaDhn5* under drought stress was normalized with the most stable reference genes (*SP1* and *COG7*) and the least stable reference gene

TABLE 2 Tissue-wise rankings of candidate reference genes based on stability value calculated by ΔCt, BestKeeper, NormFinder, and RefFinder. Each tissue group represent 4 biological replicates, each individually consisting of 4 plants pooled together.

Conditions	Gene names	Methods										Recommended gene
		geNorm		ΔCt		BestKeeper		NormFinder		RefFinder		
		Stability value	Ranking	Avg. of STDEV	Ranking	Stability value	Ranking	Stability value	Ranking	Stability value	Ranking	
Needle	*SP1*	0.265	2	0.71	1	0.77	3	0.150	2	1.32	1	*SP1, JMJ16, RID2*
	JMJ16	0.328	4	0.71	2	0.85	6	0.234	10	2.21	2	
	RID2	0.231	1	0.74	3	0.77	4	0.208	5	3.66	3	
	TULP6	0.231	1	0.76	4	0.94	9	0.225	9	4.56	4	
	RPL7Ae	0.443	8	0.77	6	0.72	2	0.236	12	4.92	5	
	PP2A2	0.516	12	0.94	10	0.59	1	0.316	13	5.62	6	
	COG7	0.370	6	0.77	5	0.97	11	0.210	6	5.76	7	
	CCZ1	0.349	5	0.78	7	0.86	7	0.190	4	6.48	8	
	ARP9	0.486	11	0.82	8	0.79	5	0.224	8	7.11	9	
	RPS10	0.418	7	0.83	9	0.94	8	0.215	7	8.74	10	
	RPL26	0.477	10	1.03	11	0.97	10	0.163	3	10.98	11	
	SKIP22	0.300	3	1.03	12	1.17	13	0.236	11	11.98	12	
	UBCP	0.463	9	1.12	13	1.02	12	0.146	1	12.74	13	
	HSP90	0.567	13	1.60	14	1.54	15	0.318	14	14.24	14	
	SDH5	0.684	14	1.89	15	1.31	14	0.475	15	14.74	15	
Phloem	*RID2*	0.633	8	0.85	1	0.61	7	0.164	9	1.63	1	*RID2, SP1, PP2A2*
	SP1	0.710	10	0.86	2	0.62	8	0.180	10	2.38	2	
	PP2A2	0.478	3	0.94	6	0.42	1	0.075	1	3.22	3	
	RPS10	0.316	1	0.91	4	0.46	2	0.137	6	3.56	4	
	COG7	0.796	12	0.91	3	0.64	9	0.226	12	4.82	5	
	TULP6	0.601	7	0.92	5	0.56	6	0.149	8	5.33	6	
	ARP9	0.504	4	0.98	7	0.46	3	0.137	7	5.86	7	
	RPL26	0.316	1	0.98	8	0.46	4	0.097	2	6.51	8	
	RPL7Ae	0.560	6	1.00	10	0.51	5	0.127	3	7.21	9	
	JMJ16	0670	9	0.98	9	0.78	10	0.199	11	9.74	10	
	CCZ1	0.887	14	1.13	11	0.79	11	0.246	13	11.47	11	
	UBCP	0.532	5	1.17	13	0.88	12	0.129	4	12.22	12	
	SKIP22	0.841	13	1.17	12	0.98	13	0.265	15	12.24	13	
	HSP90	0.753	11	2.28	14	1.51	14	0.249	14	14	14	
	SDH5	0.413	2	2.70	15	2.09	15	0.135	5	15	15	

(Continued)

10.3389/ffgc.2024.1458554

TABLE 2 (Continued)

Conditions	Gene names	Methods										Recommended gene
		geNorm		ΔCt		BestKeeper		NormFinder		RefFinder		
		Stability value	Ranking	Avg. of STDEV	Ranking	Stability value	Ranking	Stability value	Ranking	Stability value	Ranking	
Root	*UBCP*	0.449	4	1.06	3	1.30	6	0.197	1	3.22	1	*UBCP, RPL7Ae, SP1*
	RPL7Ae	0.529	6	1.12	5	1.20	5	0.321	10	3.34	2	
	SP1	0.343	2	1.01	1	1.43	9	0.215	2	3.46	3	
	PP2A2	0.562	7	1.13	6	1.02	1	0.321	9	3.46	4	
	RPS10	0.492	5	1.14	7	1.18	4	0.304	7	3.74	5	
	COG7	0.330	1	1.04	2	1.38	8	0.218	3	4.56	6	
	RPL26	0.583	8	1.21	9	1.08	3	0.266	5	5.05	7	
	TULP6	0.330	1	1.07	4	1.30	7	0.242	4	5.29	8	
	ARP9	0.593	9	1.28	11	1.05	2	0.311	8	5.76	9	
	SKIP22	0.622	10	1.20	8	1.50	10	0.387	12	9.21	10	
	JMJ16	0.639	11	1.26	10	1.62	13	0.372	11	11.20	11	
	CCZ1	0.722	13	1.51	12	1.60	12	0.525	14	12.00	12	
	RID2	0.871	14	1.65	13	1.51	11	0.683	15	12.47	13	
	HSP90	0.391	3	1.92	14	1.93	14	0.270	6	14.00	14	
	SDH5	0.677	12	2.75	15	2.18	15	0.410	13	15.00	15	

10.3389/ffgc.2024.1458554

TABLE 3 Expression stability rankings of the reference genes, calculated by ΔCt, BestKeeper, NormFinder, and RefFinder across various treatment conditions in seedlings and untreated mature trees. Each treatment group represents 4 biological replicates, each individually consisting of 4 plants pooled together.

Conditions	Gene names	Methods										Recommended gene
		geNorm		ΔCt		BestKeeper		NormFinder		RefFinder		
		Stability value	Ranking	Avg. of STDEV	Ranking	Stability value	Ranking	Stability value	Ranking	Stability value	Ranking	
Control	*RPS10*	0.158	2	0.45	1	0.31	5	0.100	3	1.78	1	*RPS10*, *RPL26*, *SP1*
	RPL26	0.209	8	0.45	2	0.27	4	0.112	5	2.38	2	
	SP1	0.168	3	0.46	4	0.35	8	0.121	6	3.56	3	
	PP2A2	0.136	1	0.48	6	0.23	2	0.129	7	3.83	4	
	JMJ16	0.195	6	0.46	3	0.31	7	0.167	10	4.21	5	
	RID2	0.183	4	0.50	7	0.23	1	0.176	12	4.30	6	
	COG7	0.189	5	0.48	5	0.31	6	0.089	1	5.18	7	
	TULP6	0.136	1	0.56	9	0.26	3	0.145	8	6.98	8	
	RPL7Ae	0.258	11	0.56	8	0.54	12	0.175	11	9.12	9	
	SKIP22	0.240	10	0.57	10	0.49	10	0.163	9	10.00	10	
	ARP9	0.201	7	0.60	11	0.59	13	0.094	2	10.91	11	
	UBCP	0.217	9	0.68	13	0.40	9	0.101	4	11.62	12	
	CCZ1	0.309	12	0.67	12	0.51	11	0.202	13	11.98	13	
	SDH5	0.389	13	0.97	14	0.72	14	0.358	14	14.00	14	
	HSP90	0.471	14	1.32	15	1.04	15	0.361	15	15.00	15	
Drought	*RID2*	0.274	7	0.85	1	0.79	5	0.102	9	2.11	1	*RID2*, *SP1*, *COG7*
	SP1	0.169	1	0.86	2	0.80	7	0.080	4	2.30	2	
	COG7	0.211	2	0.89	3	0.88	9	0.081	5	4.49	3	
	ARP9	0.305	9	0.95	7	0.74	3	0.097	8	4.74	4	
	RPL26	0.221	3	0.93	5	0.77	4	0.063	1	4.86	5	
	JMJ16	0.322	10	0.95	8	0.96	10	0.130	11	5.32	6	
	PP2A2	0.265	6	1.02	10	0.55	1	0.092	7	5.48	7	
	RPL7Ae	0.357	12	0.97	9	0.70	2	0.137	13	5.58	8	
	RPS10	0.342	11	0.93	4	0.79	6	0.138	14	5.63	9	
	TULP6	0.232	4	0.93	6	0.85	8	0.077	2	6.62	10	
	SKIP22	0.293	8	1.05	11	1.06	13	0.120	10	11.47	11	
	UBCP	0.169	1	1.13	13	1.00	11	0.084	6	12.22	12	
	CCZ1	0.253	5	1.13	12	1.01	12	0.080	3	12.24	13	
	HSP90	0.370	13	1.94	14	1.46	14	0.137	12	14.00	14	
	SDH5	0.384	14	3.07	15	2.46	15	0.150	15	15.00	15	

(Continued)

10.3389/ffgc.2024.1458554

TABLE 3 (Continued)

Conditions	Gene names	Methods										Recommended gene
		geNorm		ΔCt		BestKeeper		NormFinder		RefFinder		
		Stability value	Ranking	Avg. of STDEV	Ranking	Stability value	Ranking	Stability value	Ranking	Stability value	Ranking	
Heat	*RID2*	0.816	7	0.92	1	1.06	6	0.249	6	1.57	1	*RID2, SP1, RPL26*
	SP1	0.978	11	0.94	2	1.07	7	0.264	8	3.60	2	
	RPL26	0.320	1	1.00	4	0.98	4	0.181	1	3.72	3	
	TULP6	0.767	6	1.00	5	1.17	8	0.205	2	4.23	4	
	COG7	0.891	9	0.96	3	1.19	9	0.290	9	4.24	5	
	ARP9	0.320	1	1.03	7	0.94	3	0.206	4	5.38	6	
	PP2A2	0.679	5	1.14	10	0.65	1	0.326	10	5.61	7	
	RPL7Ae	0.582	4	1.06	9	0.82	2	0.261	7	5.80	8	
	RPS10	0.370	2	1.02	6	1.03	5	0.244	5	5.96	9	
	JMJ16	0.853	8	1.04	8	1.26	10	0.339	11	7.95	10	
	SKIP22	0.936	10	1.16	11	1.40	12	0.384	13	10.98	11	
	UBCP	0.484	3	1.27	12	1.29	11	0.206	3	11.98	12	
	CCZ1	1.107	13	1.29	13	1.41	13	0.495	14	12.74	13	
	HSP90	1.022	12	2.29	14	2.01	14	0.384	12	14.00	14	
	SDH5	1.216	14	3.01	15	2.73	15	0.496	15	15.00	15	
Pathogen infection	*SP1*	0.430	4	0.89	1	0.87	5	0.258	2	1.50	1	*SP1, COG7, RPL26*
	COG7	0.583	9	0.93	2	0.93	9	0.293	6	3.22	2	
	RPL26	0.616	12	0.97	4	0.85	3	0.311	7	3.83	3	
	PP2A2	0.320	1	1.01	7	0.66	1	0.260	4	4.14	4	
	JMJ16	0.479	5	0.98	5	0.95	10	0.389	9	4.47	5	
	RPL7Ae	0.320	1	1.01	8	0.79	2	0.087	1	5.03	6	
	TULP6	0.583	10	0.96	3	0.90	8	0.436	12	5.09	7	
	RPS10	0.512	6	0.98	6	0.89	7	0.262	5	5.38	8	
	ARP9	0.645	13	1.05	9	0.85	4	0.455	14	7.35	9	
	RID2	0.850	14	1.23	13	0.89	6	0.963	15	10.72	10	
	SKIP22	0.596	11	1.07	10	1.07	13	0.417	11	10.94	11	
	UBCP	0.364	2	1.11	11	1.02	12	0.258	3	10.98	12	
	CCZ1	0.536	7	1.15	12	0.95	11	0.407	10	11.74	13	
	HSP90	0.563	8	2.13	14	1.79	14	0.442	13	14.00	14	
	SDH5	0.368	3	2.71	15	2.08	15	0.328	8	15.00	15	

(Continued)

10.3389/ffgc.2024.1458554

TABLE 3 (Continued)

Conditions	Gene names	Methods										Recommended gene
		geNorm		ΔCt		BestKeeper		NormFinder		RefFinder		
		Stability value	Ranking	Avg. of STDEV	Ranking	Stability value	Ranking	Stability value	Ranking	Stability value	Ranking	
Mature trees	*SP1*	0.688	9	0.91	1	0.96	7	0.192	3	1.63	1	*SP1*, *COG7*, *TULP6*
	COG7	0.851	14	0.94	2	1.02	9	0.355	14	2.45	2	
	TULP6	0.638	7	0.98	3	0.96	6	0.189	2	3.57	3	
	PP2A2	0.443	2	1.03	6	0.67	1	0.312	10	3.66	4	
	RPL7Ae	0.531	4	1.02	5	0.83	3	0.334	11	4.36	5	
	RPS10	0.473	3	1.02	4	0.89	5	0.278	7	4.47	6	
	ARP9	0.333	1	1.13	9	0.83	2	0.344	12	6.00	7	
	RPL26	0.333	1	1.10	8	0.86	4	0.245	6	6.51	8	
	JMJ16	0.754	11	1.07	7	1.13	12	0.312	9	8.53	9	
	UBCP	0.552	5	1.16	11	1.08	10	0.230	5	10.24	10	
	SKIP22	0.816	13	1.15	10	1.20	13	0.355	15	11.20	11	
	RID2	0.728	10	1.21	13	0.97	8	0.296	8	11.29	12	
	CCZ1	0.780	12	1.20	12	1.12	11	0.347	13	11.98	13	
	HSP90	0.603	6	1.95	14	1.63	14	0.168	1	14.00	14	
	SDH5	0.670	8	2.45	15	1.87	15	0.203	4	15.00	15	

10.3389/ffgc.2024.1458554

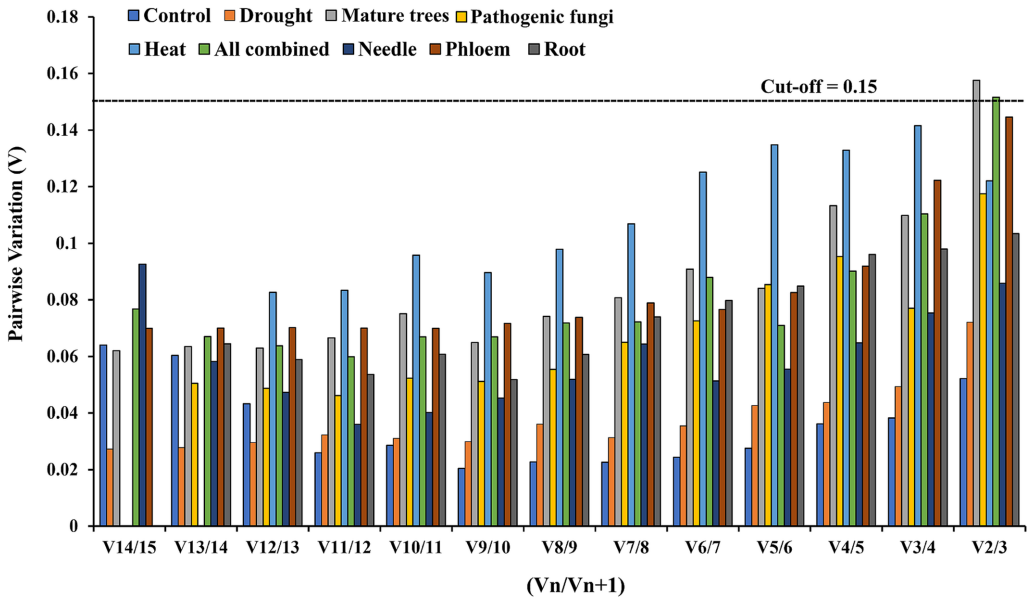

FIGURE 2
Pairwise variation analysis to determine the optimal number of reference genes required for normalization. The recommended cutoff value is 0.15, under which another gene is not required for normalization.

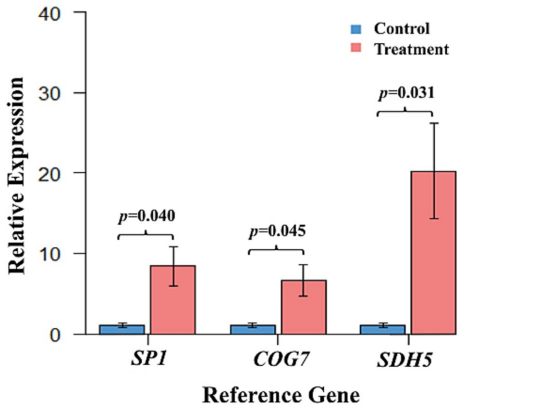

FIGURE 3
Relative expression levels of the target gene *PaDhn5* in drought-treated and control phloem samples after normalization with the most stable and the least stable gene. Normalization was performed using the most stable genes, *SP1* and *COG7*, and the least stable gene, *SDH5*, under drought conditions. The data represent the mean ± SD values of four biological replicates. Single-factor ANOVA was performed to compare the control and treatment groups of each gene to statistically analyze the relative expression of *PaDhn5*. *p*-values for each were generated as 0.04, 0.045, and 0.031 for the expression of *PaDhn5* when calculated against reference genes *SP1*, *COG7*, and *SDH5*, respectively.

(*SDH5*). The results indicated that the expression levels of *PaDhn5* in drought-treated samples increased by 8-fold and 6-fold (*p*-values = 0.040 and 0.045), respectively, when normalized with the stable reference genes *SP1* and *COG7*, compared to the control. In contrast, normalization with the least stable reference gene *SDH5* resulted in an almost 20-fold increase ($p = 0.031$) in expression (Figure 3).

4 Discussion

In recent years, forests worldwide have experienced climate change-driven droughts, storms, windthrows, and high-temperature disturbances, leading to extensive tree mortality. In Europe, one of the most economically important forest tree species is Norway spruce, which was widely planted outside its natural distribution area during the eighteenth and nineteenth centuries. Nevertheless, recent climatic conditions have led to a decline in its vitality, increasing susceptibility to stress and rendering the species particularly vulnerable to the tree-killing spruce bark beetle, *Ips typographus* and other *Ips* beetles (Biedermann et al., 2019; Singh et al., 2024a). These factors underscore the importance of understanding the molecular responses of Norway spruce to both abiotic and biotic stresses.

RT–qPCR is a highly effective and dependable technique for quantitatively studying the relative abundance of target genes. This method is widely employed to investigate plant-pathogen interactions and uncover underlying molecular mechanisms (Vijayakumar and Sakuntala, 2024). RT–qPCR is a relatively less expensive and faster method for exploring target genes under specific conditions. Despite its frequent use, there are concerns that researchers may not always adhere to recommended protocols, which can lead to misleading results (Bustin et al., 2009). Housekeeping genes, commonly referred to as reference genes, are a group of genes that are consistently expressed in cells and are crucial for fundamental cellular functions. They are stable throughout a species irrespective of treatments but can be specific to a particular tissue or developmental stage (Lin and Lai, 2010; Li et al., 2021). For accurate measurement of relative gene expression, it is crucial to use multiple reference genes with stable expression under specific biological conditions (Dai et al., 2018; Wang et al., 2021). While RT–qPCR is effective and reliable

for quantifying mRNA levels across different experimental conditions, several factors, such as RNA extraction, cDNA synthesis, primer design, and material handling, can impact the results (Schmittgen and Zakrajsek, 2000; Bustin et al., 2005; Huggett et al., 2005). Reliable reference genes help mitigate these variations, necessitating the evaluation of the stability of reference genes for each experimental condition to ensure precise and reliable data interpretation. Recent studies have evaluated reference genes in various coniferous species (e.g., Bao et al., 2016; Mo et al., 2019; Chen et al., 2019); however still, such studies on Norway spruce are limited to the embryogenic developmental stages (e.g., Vestman et al., 2011; de Vega-Bartol et al., 2013).

Among the 15 evaluated candidates, *SP1, COG7,* and *TULP6* were the most stable reference genes, making them suitable for gene expression normalization in Norway spruce. The *SP1* ubiquitin-protein ligase plays a crucial role in regulating chloroplast protein import, essential for plant development (Ling and Jarvis, 2015). It interacts with the translocon at the outer envelope membrane of chloroplasts (TOC) to recognize and import client proteins. *SP1* ubiquitin-protein ligase associates with TOC complexes and mediates the ubiquitination of TOC components, leading to their degradation through the ubiquitin-proteasome system (UPS) and reorganization of the TOC machinery. Ubiquitin-protein ligase (ubiquitin-conjugating enzyme) genes have been identified as suitable reference genes in various tissues of Brazilian rubber trees (*Hevea brasiliensis*) (Li et al., 2011), in alfalfa (*Medicago sativa*) cultivars under different stress conditions (Castonguay et al., 2015), in *Arabidopsis thaliana* (Czechowski et al., 2005), *Brachypodium distachyton* (Hong et al., 2008), *Vernicia fordii* (Han et al., 2012), *Capsicum annuum* (Wan et al., 2011) and *Brachiaria brizantha* (Silveira et al., 2009). Our findings are in accordance with these studies, showing stable expression of *SP1* in various tissue types and under various environmental conditions (Tables 2–4). Nevertheless, not all ubiquitin conjugating enzymes can be used as internal controls for normalization (Wan et al., 2011).

Conserved oligomeric Golgi complex subunit 7 (*COG7*) is a crucial component of the COG complex and is essential for maintaining the normal morphology and function of the Golgi apparatus (Klink et al., 2022). Specifically, *COG7* is part of lobe B of the COG complex, which contains COGs5-8 (Ungar et al., 2002; Blackburn et al., 2019). This protein plays a vital role in various developmental processes, including embryo development, pigmentation, cell and organ expansion, and the formation of the organized shoot apical meristem (Ishikawa et al., 2008; Vukašinović et al., 2017; Rui et al., 2020, 2021). Despite its unstable expression across different tissue types, *COG7* was ranked second in overall expression stability after *SP1,* according to RefFinder analysis. This implies that *COG7* could be a viable reference gene for gene expression normalization, particularly in experiments investigating mechanisms of resistance to drought and pathogens (Tables 3, 4). To our knowledge, no previous studies have considered *COG7* as a candidate reference gene.

Tubby-like F-box proteins (TULPs) were first discovered in mice and are highly conserved across a wide range of organisms. In plants, these Tubby-like proteins play a role in stress signaling pathways (Lai et al., 2004; Reitz et al., 2013). To date, 11 Tubby genes have been identified in *Arabidopsis*, 14 in rice, and 11 in poplar (Yang et al., 2008; Hong et al., 2015). Most plant TULPs possess a conserved F-box domain at the N-terminus and a Tubby domain at the C-terminus (Yang et al., 2008). Although TULPs are believed to function as transcription factors, their exact mechanisms of action remain largely unknown (Yulong et al., 2016). TULP6, while exhibiting variable expression across treatments, was the third most stable gene after *SP1* and *COG7* according to RefFinder analysis, indicating its potential as a reference gene for normalizing gene expression, especially in studies involving developmental stages (Tables 3, 4). Notably, TULPs have not been previously considered as reference genes.

To validate the identified reference genes, we evaluated the expression of dehydrin-like protein 5 (*PaDhn5*), a stress-responsive protein, across various Norway spruce tissues, developmental stages, and stress conditions. Dehydrins, part of the late embryogenesis abundant (LEA) family, accumulate in response to abiotic stresses and play a role in cryoprotection and membrane protection from reactive oxygen species (Close, 1997; Nylander et al., 2001; Rorat et al., 2006; Sun et al., 2021). Our results revealed that using the least stable reference gene (*SDH5*) led to erroneous data, showing a 20-fold increase in *PaDhn5* expression under stress conditions. In contrast, the most stable reference genes, *SP1* and *COG7*, resulted in more consistent *PaDhn5* expression levels, with an 8-fold and 6-fold increase, respectively (Figure 3). The significant discrepancy between the most and least stable reference genes highlights the importance of using stable reference genes to prevent bias in RT-qPCR normalization. Based on our findings, we recommend using the identified stable reference genes and their combinations (Figure 4) for accurate normalization in RT-qPCR analyses of gene expression in Norway spruce, which will improve the sensitivity and reproducibility of the results.

5 Conclusion

This study provides a catalog of genes that have been reported in various conifer species and validated for Norway spruce for the first time. We evaluated 15 candidate reference genes in various tissues and developmental stages under different environmental conditions using RT–qPCR and systematically assessed their expression stability to identify the most suitable reference gene for each condition. The study identified *ubiquitin-protein ligase (SP1), conserved oligomeric Golgi complex (COG7),* and *tubby-like F-box protein (TULP6)* as the most suitable candidate reference genes, while *succinate dehydrogenase (SDH5)* was found to be the least stable. Notably, this is the first report testing *COG7* and *TULP6* as candidates for reference genes and confirming their stable expression. In addition, normalizing RT–qPCR data with both stably and unstably expressed genes showed that *PaDhn5* expression aligns with the current knowledge of Norway spruce physiology. The fluctuations in gene expression between stable and unstable gene normalizations emphasize the need for validating reference genes for reliable RT–qPCR results. In summary, the identified and recommended reference genes and their combinations for normalizing gene expression in Norway

TABLE 4 Overall expression stability rankings of the reference genes throughout the tissues across all stress treatments, tissue types, and developmental stages as calculated by geNorm, ΔCt, BestKeeper, NormFinder, and RefFinder.

Conditions	Gene names	Methods										Recommended gene
		geNorm		ΔCt		BestKeeper		NormFinder		RefFinder		
		Stability value	Ranking	Avg. of STDEV	Ranking	Stability value	Ranking	Stability value	Ranking	Stability value	Ranking	
Overall	*SP1*	0.567	6	0.91	1	0.96	7	0.195	2	1.63	1	*SP1*, *COG7*, and *TULP6*
	COG7	0.633	8	0.94	2	1.02	9	0.243	5	2.45	2	
	TULP6	0.597	7	0.98	3	0.96	6	0.215	4	3.57	3	
	PP2A2	0.487	3	1.03	6	0.67	1	0.244	7	3.66	4	
	RPL7Ae	0.507	4	1.02	5	0.83	3	0.265	8	4.36	5	
	RPS10	0.459	2	1.02	4	0.89	5	0.243	6	4.47	6	
	ARP9	0.389	1	1.13	9	0.83	2	0.265	9	6.00	7	
	RPL26	0.389	1	1.10	8	0.86	4	0.192	1	6.51	8	
	JMJ16	0.663	9	1.07	7	1.13	12	0.285	10	8.53	9	
	UBCP	0.515	5	1.16	11	1.08	10	0.202	3	10.24	10	
	SKIP22	0.698	10	1.15	10	1.20	13	0.322	12	11.20	11	
	RID2	0.869	14	1.21	13	0.97	8	0.347	15	11.29	12	
	CCZ1	0.762	12	1.20	12	1.12	11	0.330	13	11.98	13	
	HSP90	0.725	11	1.95	14	1.63	14	0.307	11	14.00	14	
	SDH5	0.806	13	2.45	15	1.87	15	0.340	14	15.00	15	

10.3389/ffgc.2024.1458554

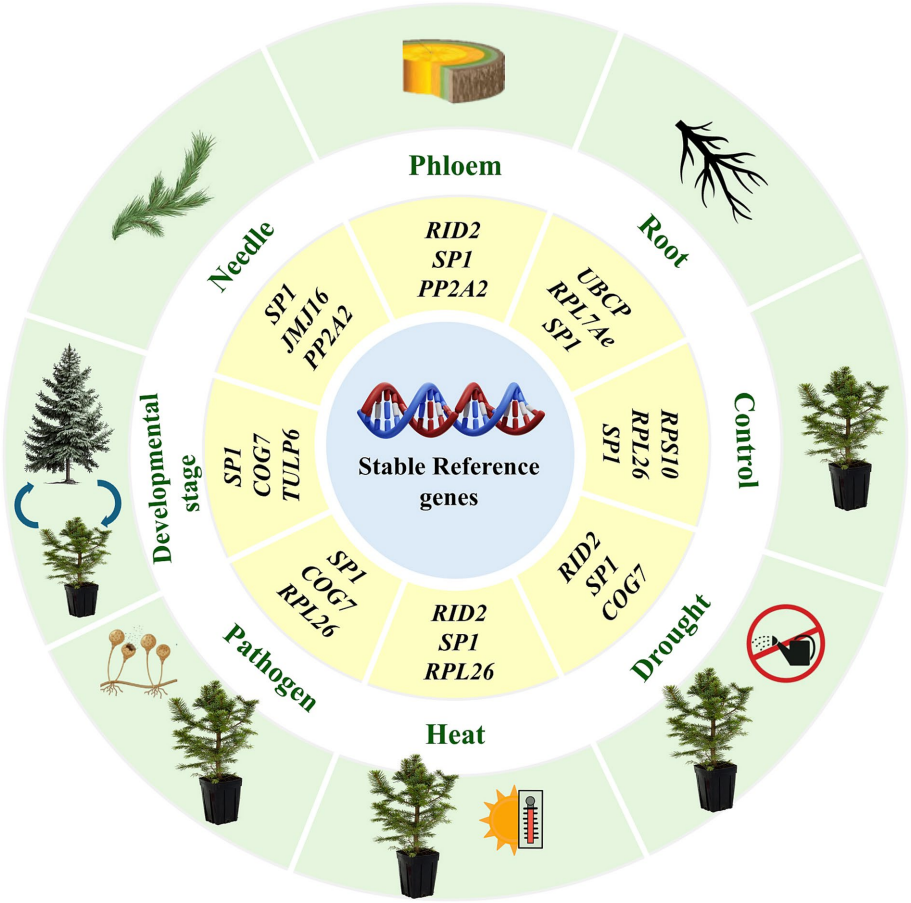

FIGURE 4
Recommended reference genes under different experimental conditions, tissues, and developmental stages.

spruce under various experimental conditions will benefit future gene expression and functional genomics studies in Norway spruce and related conifer species.

Data availability statement

The original contributions presented in the study are included in the article/Supplementary material, further inquiries can be directed to the corresponding author.

Author contributions

VVS: Conceptualization, Methodology, Data curation, Formal analysis, Visualization, Resources, Project administration, Funding acquisition, Writing – original draft, Writing – review & editing. AN: Methodology, Data curation, Formal analysis, and Writing – review & editing. GS: Methodology, Data curation, Formal analysis, Writing – review & editing. KM: Methodology, Writing – review & editing. RG: Methodology, Writing – review & editing. AR: Methodology, Resources, Writing – review & editing. RJ: Writing – review & editing.

Funding

The author(s) declare that financial support was received for the research, authorship, and/or publication of this article. This work was funded by the Internal Grant Agency (IGA; grant no. 43950/1312/3123 awarded to VVS) at the Faculty of Forestry and Wood Sciences, Czech University of Life Sciences, Prague, Czech Republic and the Ministry of Education, Youth and Sports of the Czech Republic (grant INTER-TRANSFER LTT20017).

Acknowledgments

AN, GS, and AR acknowledge support by Excellent Team Grants from the Faculty of Forestry and Wood Sciences, Czech University of Life Sciences, Prague, Czech Republic. KM acknowledges the Ramalingaswami Re-entry Fellowship (BT/RLF/Re-entry/11/2023) from the Department of Biotechnology, Government of India. The authors thank Dr. Ivana Tomášková and Dr. Kateřina Hamouzová for providing supporting facilities, and Dr. Madhab Kumar Sen for his assistance and consultations. The authors also thank the editor and reviewers for their helpful suggestions, which improved the quality of this work.

Conflict of interest

The authors declare that the research was conducted in the absence of any commercial or financial relationships that could be construed as a potential conflict of interest.

Publisher's note

All claims expressed in this article are solely those of the authors and do not necessarily represent those of their affiliated organizations, or those of the publisher, the editors and the reviewers. Any product that may be evaluated in this article, or claim that may be made by its manufacturer, is not guaranteed or endorsed by the publisher.

Supplementary material

The Supplementary material for this article can be found online at: https://www.frontiersin.org/articles/10.3389/ffgc.2024.1458554/full#supplementary-material

References

Andersen, C. L., Jensen, J. L., and Orntoft, T. F. (2004). Normalization of real-time quantitative reverse transcription-PCR data: a model-based variance estimation approach to identify genes suited for normalization, applied to bladder and colon cancer data sets. *Cancer Res.* 64, 5245–5250. doi: 10.1158/0008-5472.can-04-0496

Bao, W., Qu, Y., Shan, X., and Wan, Y. (2016). Screening and validation of housekeeping genes of the root and cotyledon of *Cunninghamia lanceolata* under abiotic stresses by using quantitative real-time PCR. *Int. J. Mol. Sci.* 17:1198. doi: 10.3390/ijms17081198

Bharati, R., Sen, M. K., Kumar, R., Gupta, A., Žiarovská, J., Fernández-Cusimamani, E., et al. (2023). Systematic identification of suitable reference genes for quantitative real-time PCR analysis in *Melissa officinalis* L. *Plants* 12:470. doi: 10.3390/plants12030470

Biedermann, P. H., Müller, J., Grégoire, J. C., Gruppe, A., Hagge, J., Hammerbacher, A., et al. (2019). Bark beetle population dynamics in the Anthropocene: challenges and solutions. *Trends Ecol. Evol.* 34, 914–924. doi: 10.1016/j.tree.2019.06.002

Blackburn, J. B., D'Souza, Z., and Lupashin, V. V. (2019). Maintaining order: COG complex controls Golgi trafficking, processing, and sorting. *FEBS Lett.* 593, 2466–2487. doi: 10.1002/1873-3468.13570

Burnett, A. C., Serbin, S. P., Lamour, J., Anderson, J., Davidson, K. J., Yang, D., et al. (2021). Seasonal trends in photosynthesis and leaf traits in scarlet oak. *Tree Physiol.* 41, 1413–1424. doi: 10.1093/treephys/tpab015

Bustin, S. A. (2002). Quantification of mRNA using real-time reverse transcription PCR (RT-PCR): trends and problems. *J. Mol. Endocrinol.* 29, 23–39. doi: 10.1677/jme.0.0290023

Bustin, S. A., Benes, V., Garson, J. A., Hellemans, J., Huggett, J., Kubista, M., et al. (2009). The MIQE guidelines: minimum information for publication of quantitative real-time PCR experiments. *Clin. Chem.* 55, 611–622. doi: 10.1373/clinchem.2008.112797

Bustin, S. A., Benes, V., Nolan, T., and Pfaffl, M. W. (2005). Quantitative real-time RT-PCR–a perspective. *J. Mol. Endocrinol.* 34, 597–601. doi: 10.1677/jme.1.01755

Castonguay, Y., Michaud, J., and Dubé, M. P. (2015). Reference genes for RT-qPCR analysis of environmentally and developmentally regulated gene expression in alfalfa. *Am. J. Plant Sci.* 6, 132–143. doi: 10.4236/ajps.2015.61015

Caudullo, G., Tinner, W., and de Rigo, D. (2016). "*Picea abies* in Europe: distribution, habitat, usage and threats" in European atlas of forest tree species. eds. J. San-Miguel-Ayanz, D. de Rigo, G. Caudullo, T. Houston Durrant and A. Mauri (Luxembourg: Publication Office of the European Union), 114–116.

Čepl, J., Stejskal, J., Korecký, J., Hejtmánek, J., Faltinová, Z., Lstibůrek, M., et al. (2020). The dehydrins gene expression differs across ecotypes in Norway spruce and relates to weather fluctuations. *Sci. Rep.* 10:20789. doi: 10.1038/s41598-020-76900-x

Chen, R., Chen, W., Tigabu, M., Zhong, W., Li, Y., Ma, X., et al. (2019). Screening and evaluation of stable reference genes for quantitative real-time polymerase chain reaction (qRT-PCR) analysis in Chinese fir roots under water, phosphorus, and nitrogen stresses. *Forests* 10:1087. doi: 10.3390/f10121087

Close, T. J. (1997). Dehydrins: a commonalty in the response of plants to dehydration and low temperature. *Physiol. Plant.* 100, 291–296. doi: 10.1111/j.1399-3054.1997.tb04785.x

Czechowski, T., Stitt, M., Altmann, T., Udvardi, M. K., and Scheible, W. R. (2005). Genome-wide identification and testing of superior reference genes for transcript normalization in arabidopsis. *Plant Physiol.* 139, 5–17. doi: 10.1104/pp.105.063743

Dai, F., Zhao, X., Tang, C., Wang, Z., Kuang, Z., Li, Z., et al. (2018). Identification and validation of reference genes for qRT-PCR analysis in mulberry (*Morus alba* L.). *PLoS One* 13:e0194129. doi: 10.1371/journal.pone.0194129

Danielsen, J. S., Morgado, L., Mundra, S., Nybakken, L., Davey, M., and Kauserud, H. (2021). Establishment of spruce plantations in native birch forests reduces soil fungal diversity. *FEMS Microbiol. Ecol.* 97:fiab074. doi: 10.1093/femsec/fiab074

de Oliveira, L. A., Breton, M. C., Bastolla, F. M., Camargo, S. D., Margis, R., Frazzon, J., et al. (2012). Reference genes for the normalization of gene expression in *Eucalyptus* species. *Plant Cell Physiol.* 53, 405–422. doi: 10.1093/pcp/pcr187

de Vega-Bartol, J. J., Santos, R. R., Simões, M., and Miguel, C. M. (2013). Normalizing gene expression by quantitative PCR during somatic embryogenesis in two representative conifer species: *Pinus pinaster* and *Picea abies*. *Plant Cell Rep.* 32, 715–729. doi: 10.1007/s00299-013-1407-4

Dobor, L., Hlásny, T., and Zimová, S. (2020). Contrasting vulnerability of monospecific and species-diverse forests to wind and bark beetle disturbance: the role of management. *Ecol. Evol.* 10, 12233–12245. doi: 10.1002/ece3.6854

Ebner, G. (2020). Significantly more damaged wood in 2019. Available at: https://www.timberonline.net/log_wood/2020/02/significantly-more-damagedwood-in-2019.html (Accessed May 12, 2024).

Gachon, C., Mingam, A., and Charrier, B. (2004). Real-time PCR: what relevance to plant studies? *J. Exp. Bot.* 55, 1445–1454. doi: 10.1093/jxb/erh181

Gonçalves, S., Cairney, J., Maroco, J., Oliveira, M. M., and Miguel, C. (2005). Evaluation of control transcripts in real-time RT-PCR expression analysis during maritime pine embryogenesis. *Planta* 222, 556–563. doi: 10.1007/s00425-005-1562-0

Han, X., Lu, M., Chen, Y., Zhan, Z., Cui, Q., and Wang, Y. (2012). Selection of reliable reference genes for gene expression studies using real-time PCR in tung tree during seed development. *PLoS One* 7:e43084. doi: 10.1371/journal.pone.0043084

Hlásny, T., Krokene, P., Liebhold, A., Montagné-Huck, C., Müller, J., Qin, H., et al. (2019). Living with bark beetles: Impacts, outlook and management options. Joensuu: European Forest Institute.

Hong, M. J., Kim, D. Y., and Seo, Y. W. (2015). Interactions between wheat tubby-like and SKP1-like proteins. *Genes Genet. Syst.* 90, 293–304. doi: 10.1266/ggs.14-00084

Hong, S. Y., Seo, P. J., Yang, M. S., Xiang, F., and Park, C. M. (2008). Exploring valid reference genes for gene expression studies in *Brachypodium distachyon* by real-time PCR. *BMC Plant Biol.* 8, 1–11. doi: 10.1186/1471-2229-8-112

Huggett, J., Dheda, K., Bustin, S., and Zumla, A. (2005). Real-time RT-PCR normalisation; strategies and considerations. *Genes Immun.* 6, 279–284. doi: 10.1038/sj.gene.6364190

Huis, R., Hawkins, S., and Neutelings, G. (2010). Selection of reference genes for quantitative gene expression normalization in flax (*Linum usitatissimum* L.). *BMC Plant Biol.* 10:71. doi: 10.1186/1471-2229-10-71

Ishikawa, T., Machida, C., Yoshioka, Y., Ueda, T., Nakano, A., and Machida, Y. (2008). EMBRYO YELLOW gene, encoding a subunit of the conserved oligomeric Golgi complex, is required for appropriate cell expansion and meristem organization in *Arabidopsis thaliana*. *Genes Cells* 13, 521–535. doi: 10.1111/j.1365-2443.2008.01186.x

Jain, M., Nijhawan, A., Tyagi, A. K., and Khurana, J. P. (2006). Validation of housekeeping genes as internal control for studying gene expression in rice by quantitative real-time PCR. *Biochem. Biophys. Res. Commun.* 345, 646–651. doi: 10.1016/j.bbrc.2006.04.140

Kalyniukova, A., Várfalvyová, A., Płotka-Wasylka, J., Majchrzak, T., Makoś-Chełstowska, P., Tomášková, I., et al. (2024). Deep eutectic solvent-based shaking-assisted extraction for determination of bioactive compounds from Norway spruce roots. *Front. Chem.* 12:1385844. doi: 10.3389/fchem.2024.1385844

Klink, V. P., Lawaju, B. R., Niraula, P. M., Sharma, K., McNeece, B. T., Pant, S. R., et al. (2022). The conserved oligomeric Golgi (COG) complex, a window into plant-pathogen interactions. *J. Plant Interact.* 17, 344–360. doi: 10.1080/17429145.2022.2041743

Krokene, P., Børja, I., Carneros, E., Eldhuset, T. D., Nagy, N. E., Volařík, D., et al. (2023). Effects of combined drought and pathogen stress on growth, resistance and gene expression in young Norway spruce trees. *Tree Physiol.* 43, 1603–1618. doi: 10.1093/treephys/tpad062

Lai, C. P., Lee, C. L., Chen, P. H., Wu, S. H., Yang, C. C., and Shaw, J. F. (2004). Molecular analyses of the *Arabidopsis* TUBBY-like protein gene family. *Plant Physiol.* 134, 1586–1597. doi: 10.1104/pp.103.037820

Li, H., Qin, Y., Xiao, X., and Tang, C. (2011). Screening of valid reference genes for real-time RT-PCR data normalization in *Hevea brasiliensis* and expression validation of a sucrose transporter gene HbSUT3. *Plant Sci.* 181, 132–139. doi: 10.1016/j.plantsci.2011.04.014

Li, T., Yuan, W., Qiu, S., and Shi, J. (2021). Selection of reference genes for gene expression analysis in *Liriodendron* hybrids' somatic embryogenesis and germinative tissues. *Sci. Rep.* 11:4957. doi: 10.1038/s41598-021-84518-w

Lin, Y. L., and Lai, Z. X. (2010). Reference gene selection for qPCR analysis during somatic embryogenesis in longan tree. *Plant Sci.* 178, 359–365. doi: 10.1016/j.plantsci.2010.02.005

Ling, Q., and Jarvis, P. (2015). Regulation of chloroplast protein import by the ubiquitin E3 ligase SP1 is important for stress tolerance in plants. *Curr. Biol.* 25, 2527–2534. doi: 10.1016/j.cub.2015.08.015

Livak, K. J., and Schmittgen, T. D. (2001). Analysis of relative gene expression data using real-time quantitative PCR and the $2^{-\Delta\Delta CT}$ method. *Methods* 25, 402–408. doi: 10.1006/meth.2001.1262

Lu, J., Yang, C., Zhang, Y., and Pan, H. (2018). Selection of reference genes for the normalization of RT-qPCR data in gene expression studies in insects: a systematic review. *Front. Physiol.* 9:1560. doi: 10.3389/fphys.2018.01560

Mao, J., He, Z., Hao, J., Liu, T., Chen, J., and Huang, S. (2019). Identification, expression, and phylogenetic analyses of terpenoid biosynthesis-related genes in secondary xylem of loblolly pine (*Pinus taeda* L.) based on transcriptome analyses. *PeerJ* 7:e6124. doi: 10.7717/peerj.6124

Mo, J., Xu, J., Jin, W., Yang, L., Yin, T., and Shi, J. (2019). Identification of reference genes for quantitative gene expression studies in *Pinus massoniana* and its introgression hybrid. *Forests* 10:787. doi: 10.3390/f10090787

Mogilicherla, K., Solanke, A. U., Prabhakaran, N., Ahmad, I., Dhandapani, G., Jayabalan, N., et al. (2016). Evaluation of suitable reference genes for normalization of qPCR gene expression studies in brinjal (*Solanum melongena* L.) during fruit developmental stages. *Appl. Biochem. Biotechnol.* 178, 433–450. doi: 10.1007/s12010-015-1884-8

Nicot, N., Hausman, J. F., Hoffmann, L., and Evers, D. (2005). Housekeeping gene selection for real-time RT-PCR normalization in potato during biotic and abiotic stress. *J. Exp. Bot.* 56, 2907–2914. doi: 10.1093/jxb/eri285

Nylander, M., Svensson, J., Palva, E. T., and Welin, B. V. (2001). Stress-induced accumulation and tissue-specific localization of dehydrins in *Arabidopsis thaliana*. *Plant Mol. Biol.* 45, 263–279. doi: 10.1023/A:1006469128280

Nystedt, B., Street, N. R., Wetterbom, A., Zuccolo, A., Lin, Y. C., Scofield, D. G., et al. (2013). The Norway spruce genome sequence and conifer genome evolution. *Nature* 497, 579–584. doi: 10.1038/nature12211

Paolacci, A. R., Tanzarella, O. A., Porceddu, E., and Ciaffi, M. (2009). Identification and validation of reference genes for quantitative RT-PCR normalization in wheat. *BMC Mol. Biol.* 10:11. doi: 10.1186/1471-2199-10-11

Pastierovič, F., Mogilicherla, K., Hradecký, J., Kalyniukova, A., Dvořák, O., Roy, A., et al. (2024). Genome-wide transcriptomic and metabolomic analyses unveiling the defence mechanisms of *Populus tremula* against sucking and chewing insect herbivores. *Int. J. Mol. Sci.* 25:6124. doi: 10.3390/ijms25116124

Pfaffl, M. W., Tichopad, A., Prgomet, C., and Neuvians, T. P. (2004). Determination of stable housekeeping genes, differentially regulated target genes and sample integrity: BestKeeper-excel-based tool using pairwise correlations. *Biotechnol. Lett.* 26, 509–515. doi: 10.1023/b:bile.0000019559.84305.47

Reitz, M., Pai, S., Imani, J., and Schafer, P. (2013). New insights into the subcellular localization of tubby-like proteins and their participation in the *Arabidopsis-Piriformospora indica* interaction. *Plant Signal. Behav.* 8:e25198. doi: 10.4161/psb.25198

Rorat, T., Szabala, B. M., Grygorowicz, W. J., Wojtowicz, B., Yin, Z., and Rey, P. (2006). Expression of SK3-type dehydrin in transporting organs is associated with cold acclimation in Solanum species. *Planta* 224, 205–221. doi: 10.1007/s00425-005-0200-1

Rosner, S., Johnson, D. M., Voggeneder, K., and Domec, J. C. (2019). The conifer-curve: fast prediction of hydraulic conductivity loss and vulnerability to cavitation. *Ann. For. Sci.* 76:82. doi: 10.1007/s13595-019-0868-1

Rui, Q., Tan, X., Liu, F., Li, Y., Liu, X., Li, B., et al. (2021). Syntaxin of plants31 (SYP31) and SYP32 is essential for Golgi morphology maintenance and pollen development. *Plant Physiol.* 186, 330–343. doi: 10.1093/plphys/kiab049

Rui, Q., Wang, J., Li, Y., Tan, X., and Bao, Y. (2020). Arabidopsis COG6 is essential for pollen tube growth and Golgi structure maintenance. *Biochem. Biophys. Res. Commun.* 528, 447–452. doi: 10.1016/j.bbrc.2020.05.189

Schmittgen, T. D., and Zakrajsek, B. A. (2000). Effect of experimental treatment on housekeeping gene expression: validation by real-time, quantitative RT-PCR. *J. Biochem. Biophys. Methods* 46, 69–81. doi: 10.1016/S0165-022X(00)00129-9

Sen, M. K., Hamouzová, K., Košnarová, P., Roy, A., and Soukup, J. (2021). Identification of the most suitable reference gene for gene expression studies with development and abiotic stress response in *Bromus sterilis*. *Sci. Rep.* 11:13393. doi: 10.1038/s41598-021-92780-1

Silveira, É. D., Alves-Ferreira, M., Guimarães, L. A., da Silva, F. R., and Carneiro, V. T. D. C. (2009). Selection of reference genes for quantitative real-time PCR expression studies in the apomictic and sexual grass *Brachiaria brizantha*. *BMC Plant Biol.* 9:84. doi: 10.1186/1471-2229-9-84

Silver, N., Best, S., Jiang, J., and Thein, S. L. (2006). Selection of housekeeping genes for gene expression studies in human reticulocytes using real-time PCR. *BMC Mol. Biol.* 7:33. doi: 10.1186/1471-2199-7-33

Singh, V. V., Naseer, A., Mogilicherla, K., Trubin, A., Zabihi, K., Roy, A., et al. (2024a). Understanding bark beetle outbreaks: exploring the impact of changing temperature regimes, droughts, forest structure, and prospects for future forest pest management. *Rev. Environ. Sci. Biotechnol.* 23, 257–290. doi: 10.1007/s11157-024-09692-5

Singh, V. V., Naseer, A., Sellamuthu, G., and Jakuš, R. (2024b). An optimized and cost-effective RNA extraction method for secondary metabolite-enriched tissues of Norway spruce (*Picea abies*). *Plants* 13:389. doi: 10.3390/plants13030389

Singh, V. V., Zabihi, K., Trubin, A., Cudlín, P., Korolyova, N., Jakuš, R., et al. (2023). Effect of diurnal solar radiation regime and tree density on sap flow of Norway spruce (*Picea abies* [L.] karst.) in fragmented stands. Preprint. Available online: https://www.researchsquare.com/article/rs-3262723/v1

Stival Sena, J., Giguère, I., Rigault, P., Bousquet, J., and Mackay, J. (2018). Expansion of the dehydrin gene family in the Pinaceae is associated with considerable structural diversity and drought-responsive expression. *Tree Physiol.* 38, 442–456. doi: 10.1093/treephys/tpx125

Sun, Z., Li, S., Chen, W., Zhang, J., Zhang, L., Sun, W., et al. (2021). Plant dehydrins: expression, regulatory networks, and protective roles in plants challenged by abiotic stress. *Int. J. Mol. Sci.* 22:12619. doi: 10.3390/ijms222312619

Takamori, L. M., Pereira, A. V. C., Maia Souza, G., Vieira, L. G. E., and Ferreira Ribas, A. (2017). Identification of endogenous reference genes for RT-qPCR expression analysis in *Urochloa brizantha* under abiotic stresses. *Sci. Rep.* 7:8502. doi: 10.1038/s41598-017-09156-7

Ungar, D., Oka, T., Brittle, E. E., Vasile, E., Lupashin, V. V., Chatterton, J. E., et al. (2002). Characterization of a mammalian Golgi-localized protein complex, COG, that is required for normal Golgi morphology and function. *J. Cell Biol.* 157, 405–415. doi: 10.1083/jcb.200202016

Vandesompele, J., De Preter, K., Pattyn, F., Poppe, B., Van Roy, N., De Paepe, A., et al. (2002). Accurate normalization of real-time quantitative RT-PCR data by geometric averaging of multiple internal control genes. *Genome Biol.* 3, RESEARCH0034–RESEARCH0012. doi: 10.1186/gb-2002-3-7-research0034

Vestman, D., Larsson, E., Uddenberg, D., Cairney, J., Clapham, D., Sundberg, E., et al. (2011). Important processes during differentiation and early development of somatic embryos of Norway spruce as revealed by changes in global gene expression. *Tree Genet. Genomes* 7, 347–362. doi: 10.1007/s11295-010-0336-4

Vijayakumar, S., and Sakuntala, M. (2024). Validation of reference gene stability for normalization of RT-qPCR in *Phytophthora capsici* Leonian during its interaction with *Piper nigrum* L. *Sci. Rep.* 14:7331. doi: 10.1038/s41598-024-58139-y

Vukašinović, N., Oda, Y., Pejchar, P., Synek, L., Pečenková, T., Rawat, A., et al. (2017). Microtubule-dependent targeting of the exocyst complex is necessary for xylem development in Arabidopsis. *New Phytol.* 213, 1052–1067. doi: 10.1111/nph.14267

Wan, H., Yuan, W., Ruan, M., Ye, Q., Wang, R., Li, Z., et al. (2011). Identification of reference genes for reverse transcription quantitative real-time PCR normalization in pepper (*Capsicum annuum* L.). *Biochem. Biophys. Res. Commun.* 416, 24–30. doi: 10.1016/j.bbrc.2011.10.105

Wang, H. L., Chen, J., Tian, Q., Wang, S., Xia, X., and Yin, W. (2014). Identification and validation of reference genes for *Populus euphratica* gene expression analysis during abiotic stresses by quantitative real-time PCR. *Physiol. Plant.* 152, 529–545. doi: 10.1111/ppl.12206

Wang, W., Hu, S., Cao, Y., Chen, R., Wang, Z., and Cao, X. (2021). Selection and evaluation of reference genes for qRT-PCR of *Scutellaria baicalensis* Georgi under different experimental conditions. *Mol. Biol. Rep.* 48, 1115–1126. doi: 10.1007/s11033-021-06153-y

Wise, R. P., Moscou, M. J., Bogdanove, A. J., and Whitham, S. A. (2007). Transcript profiling in host-pathogen interactions. *Annu. Rev. Phytopathol.* 45, 329–369. doi: 10.1146/annurev.phyto.45.011107.143944

Yang, Z., Zhou, Y., Wang, X., Gu, S., Yu, J., Liang, G., et al. (2008). Genomewide comparative phylogenetic and molecular evolutionary analysis of tubby-like protein family in *Arabidopsis*, rice, and poplar. *Genomics* 92, 246–253. doi: 10.1016/j.ygeno.2008.06.001

Yulong, C., Wei, D., Baoming, S., Yang, Z., and Qing, M. (2016). Genome-wide identification and comparative analysis of the TUBBY-like protein gene family in maize. *Genes Genom* 38, 25–36. doi: 10.1007/s13258-015-0338-6

Frontiers in
Forests and Global Change

Informs and promotes sustainable management of the world's forests

An innovative journal that places forests at the forefront of attention for scientists, policy makers and the public. It advances our understanding of how forests 'work', spanning from molecules to ecosystems to the biosphere.

Discover the latest Research Topics

See more →

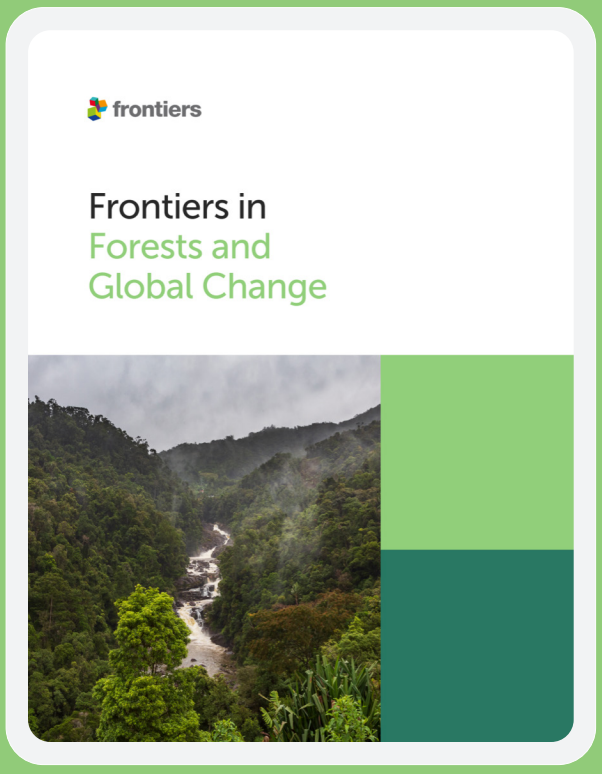

Frontiers

Avenue du Tribunal-Fédéral 34
1005 Lausanne, Switzerland
frontiersin.org

Contact us

+41 (0)21 510 17 00
frontiersin.org/about/contact